Novel insights into the interaction of the Calcium Sensing Receptor with the Receptor Activity Modifying Proteins

---

PhD

Aditya Jwalant Desai
Department of Human Metabolism

November 2012

Acknowledgements:

It is very easy to name all the people who helped me get through this, though it is equally difficult to thank them adequately. First and foremost, I would like to extend my deepest gratitude to my supervisor, Prof.Tim Skerry for giving me an opportunity to work with him. Without his constant support, encouragement, optimism and teaching; this thesis would not have been possible. I thank him for believing in me especially during the "downs" of the project. He taught me that scientific research is the disinterested reporting of observations, which I shall always follow. I would like to thank Dr.Gareth Richards from the bottom of my heart for perusing my thesis, for being an excellent mentor and a very good friend. I thank him for being supportive after my project got changed near the end of the first year and helping me in framing the current project. He made me understand science clearly and simply by ignoring my endless mistakes and has played an instrumental role in my training. I am also deeply grateful to Dr.Dave Roberts for his invaluable and enduring training, guidance and support. He taught me techniques like molecular cloning, FRET and SPA used in this project. I also thank him for kindly providing me with the constructs used in this project. The discussions, encouragement and critiques made by Gareth and Dave were of immense significance to the progress of this work. I would like to thank Dr. Peter Grabowski for his excellent suggestions and insights during my PhD. I thank Dr.Stephen Brown from the RNAi facility for letting me use the plate-reader for Ca^{2+} imaging. I thank Dr.Colin Gray for helping me with microscopy. I am grateful to Dr.Paul Heath and Dr.Clive Buckle for allowing me to use the Nanodrop machine. I would like to thank Lan Zhu for being a great student and efficiently performing the GPRC6A work during her MSc project under my supervision. My cordial Thanks to Brindha, Susana and Suruchi for a friendly support in and out of the lab. I would like to thank my friends Karan, Marc, Ning, Ruchika, Akash, Ankita, Nick, Hannah, Robin, Shikha and Yogi for the 'good-times' and making life in Sheffield really enjoyable. I would also like to thank my friends in India- Kunal, Heeral, Hiral and the rest of the troop for always being there for me. Last but by no way the least, I am deeply indebted to my family and Baba who have fostered me lovingly and encouraged me in all my endeavors. They have always been my strength. I dedicate my thesis to my parents for their unending love and support.

Abstract:

Calcium (Ca^{2+}) homeostasis is a tightly controlled mechanism by which adequate Ca^{2+} levels are maintained in the body. A G-protein coupled receptor known as the Calcium Sensing Receptor (CaSR) plays crucial role in Ca^{2+} homeostasis by sensing minute changes in extracellular Ca^{2+} and modulating the secretion of calciotropic hormones. It was shown that a group of accessory proteins known as Receptor Activity Modifying Proteins (RAMPs), specifically RAMP1 and 3 are responsible for cell-surface trafficking of the CaSR. Based on this, it was hypothesised that CaSR and RAMPs traffic to the cell-surface as high-order oligomers. FRET-based stoichiometry revealed equal abilities of RAMP1 and 3 to chaperone CaSR to the cell surface, even though RAMP3 interacted more efficiently. Furthermore, a higher fraction of RAMP3 than RAMP1 was observed in the CaSR-complex on the cell-surface, suggesting a higher-order oligomer. Next, it was hypothesised that CaSR and RAMPs associate in an endogenous expression system and that RAMPs play a role in CaSR signalling. In medullary thyroid carcinoma TT cells, an attenuation of CaSR signalling by RAMP1 knock-down suggested an association between them. Also, blocking of RAMP1 using antibodies significantly attenuated CaSR-mediated signalling in these cells; consequently demonstrating its role in CaSR signalling. Finally it was hypothesised that RAMP expression is regulated by agents of Ca^{2+} homeostasis. However, no changes in RAMP mRNA expression were observed upon treatment with Ca^{2+} and calcitriol in TT cells; and with Ca^{2+} in human osteosarcoma cells.

Furthermore, it was shown using FRET that RAMP1 associated and caused cell-surface trafficking of GPRC6A, a GPCR closely related to the CaSR.

Taken together, it is demonstrated for the first time that RAMP plays a role in CaSR signalling and further research could establish the importance of RAMPs in Ca^{2+} homeostasis and subsequently as important drug targets against the pathologies of the CaSR.

Table of Contents

List of figures

List of tables

List of Abbreviations

FGF-2	Fibroblast Growth Factor 2
˚C	degree Celsius
µF	micro farads
µl	Micro-litre
5' UTR	5' Untranslated Region
5-HT	5-Hydroxytryptophan
A/bis A	Acrylamide/Bis-Acrylamide
aa	Amino acid
Ab	antibody
Actβ	Beta actin
ADH	Autosomal Dominant Hypocalcaemia
Ala	alanine
ALP	Alkaline Phosphatase
AM	Adrenomedullin
AM ester	Acetoxymethyl ester
AMBP1	Adrenomedullin Binding Protein 1
AMR1	Adrenomedullin receptor type-1
AMR2	Adrenomedullin receptor type- 2
AMR3	Adrenomedullin receptor type-3
AMY	Amylin
AMYR1	Amylin receptor type 1
AMYR2	Amylin receptor type 2
AMYR3	Amylin receptor type 3
ANOVA	Analysis of Variance
APS	Ammonium per sulfate
ATP	Adenosine triphosphate
BCA	Bicinchoninic acid
BLAST	Basic local Alignment Search Tool
Bmax	Binding maximum
BMM	Bone marrow macrophages
bp	base pair
BRET	Bioluminsecence Resonance Energy Transfer
BSA	Bovine serum albumin
$Ca_{[i]}$	intracellular Ca^{2+} concentration
cAMP	Cyclic adenosine monophosphate
CaSR	Ca^{2+} Sensing Receptor
cDNA	complimentary deoxyribonucleic acid
Cer	Cerulean
CFP	Cyan Fluorescent Protein
CGRP	Calcitonin Gene Related Peptide
CHO cells	Chinese Hamster Ovary cells

Cit	Citrine
CLR	Calcitonin Like Receptor
CMV	Cytomegalovirus
CO_2	Carbon dioxide
CPM	Counts-per-minute
Ct	Threshold cycle
CT	Calcitonin
C-tail	Carboxy-terminal tail
CTR	Calcitonin receptor
Cys	Cysteine
DAG	Diacylglycerol
DEPC	Diethyl Pyrocarbonate
DMEM	Dulbecco's Modified Eagle Medium
DNA	Deoxyribonucleic acid
dNTP	Deoxynucleotide Triphosphate
DTT	Dithiothreitol
Ec	Characteristic FRET efficiency
Ec50	Half maximal effective concentration
ECD	Extracellular domain
ECL	Enhanced chemi- luminescent
EDTA	Ethylenediaminetetraacetic Acid
EGFR	Epidermal growth factor receptor
EGTA	Ethylene glycol tetra acetic acid
ER	Endoplasmic reticulum
ERE	Oestrogen responsive elements
ERK	Extracellular signal-regulated kinase
ESTs	Expressed sequence tags
Fa	Fraction of acceptor in FRET complex
FACS	Fluorescence-activated cell sorting
FCS	Foetal Calf Serum
Fd	Fraction of donor in FRET complex
fg	femto-gram
FHH	Familial Hypocalciuric Hypercalcaemia
fM	femto molar
FRET	Förster Resonance Energy Transfer
g	Gram
$G_{12/13}$	G-protein subtype 12/13
GABA	gamma-Aminobutyric acid
GAPDH	Glyceraldehyde 3-phosphate dehydrogenase
Gd^{3+}	Gadolinium ion
GDP	Guanosine diphosphate
GFP	Green fluorescent protein

GHRH	Growth hormone-releasing hormone
GLP	Glucagon-like peptide
Gluc	Glucagon
GPCR	Guanine Nucleotide-binding protein-Coupled Receptor
G-protein	Guanine nucleotide-binding protein
GRE	Glucorticoid responsive elements
GRK	GPCR kinase
GTP	Guanosine-5'-triphosphate
$GTP\gamma^S$	Guanosine-5'-O-[gamma-thio]triphosphate
HCl	Hydrochloric acid
HEK-293	Human Embryonic Kidney 293
HPRT1	Hypoxanthine phosphoribosyltransferase 1
hr	Hour
I_A	Intensity of acceptor channel
Ic_{50}	half maximal inhibitory concentration
I_D	Intensity of donor channel
I_F	Intensity of FRET channel
IGF	Insulin-like growth factor
IGF-1R	Insulin-like growth factor type-1 receptor
IgG	Immunoglobulin
IL	Interleukin
IP3	Inositol triphosphate
JNK	c-Jun NH(2)-terminal kinase
Kbp	Kilo base pairs
K_d	Dissociation constant
KDa	Kilo Dalton
Ki	inhibition constant
KO	Knock out
kV	Kilovolt
LB	Luria broth
LPS	Lipopolysaccharide
LRP	lipoprotein receptor related peptides
Lys	Lysine
M3 receptor	Muscarinic receptor type 3
mAb	monoclonal antibody
MAPK	Mitogen activated protein kinase
MCSF	Macrophage colony stimulating factor
mg	Milligram
mGluR	Metabotropic glutamate receptor
min	minute(s)
ml	Milliliter

mM	milli molar
mm	Millimeter
mRNA	messenger ribonucleic acid
ng	nano-gram
NHERF	Na^+/ H^+ exchanger regulatory factor -1
nm	nano meter
nM	nano molar
NSF	N-ethylmaleimide sensitive factor
NSHPT	Neonatal Severe Hyperparathyroidism
N-terminal	Amino-terminal
OD	Optical density
PBS	Phosphate buffered saline
PCR	Polymerase chain reaction
PDGF	Platelet-derived growth factor
pg	pico-gram
PI	Phosphoinositol
PKA	Protein kinase A
PKC	Protein kinase C
PLA_2	Phospholipase A
PLC	Phospholipase C
PLD	Phospholipase D
pM	pico molar
Pro	Proline
PT	Parathyroid
PTH	Parathyroid hormone
PTH 1R	Parathyroid hormone receptor type 1
PTH2R	Parathyroid hormone receptor type 2
PTHrP	Parathyroid hormone-related peptide
PVDF	polyvinylidene chloride
qPCR	quantitative polymerase chain reaction
R (in FRET)	The molar ratio of acceptor to donor
RAMP	Receptor Activity Modifying Protein
RANKL	Receptor Activator for Nuclear Factor κ B Ligand
RCP	CGRP-receptor component protein
RhoGEFs	Ras homology guanine nucleotide exchange factors
RNA	Ribonucleic acid
ROI	Region of interest
rpm	revolutions per minute
RT PCR	Reverse transciptase polymerase chain reaction
SD	Standard deviation
SDS	Sodium dodecyl sulfate
SDS-PAGE	Sodium dodecyl sulfate polyacrylamide gel electrophoresis

sec	second(s)
SEM	standard error of mean
Ser-Lys	Serine-Lysine
siRNA	small interfering RNA
SNPs	Single-nucleotide polymorphism
SPA	Scintillation Proximity Assay
$t_{1/2}$	Half-life
TBS	Tris-buffered saline
TEMED	N,N,N',N'-Tetramethylethylenediamine
T_m	Melting temperature
TM	Trans-membrane
TRPV	Transient receptor potential cation channel subfamily V
Tyr	Tyrosine
v/v	volume per volume
VIP	Vasoactive Intestinal Peptide
VPAC1R	Vasoactive Pituitary Adenylate Cyclase–activating peptide receptor type-1
w/v	weight per volume
xg	centrifugal acceleration relative to g.
YFP	Yellow fluorescence protein
α	Proportionality constant relating acceptor fluorescence at the acceptor excitation to the donor excitation
β	Proportionality constant relating donor fluorescence detected at the acceptor emission relative to that detected at the donor emission
γ	Ratio of the extinction coefficient of the acceptor to the donor at the donor excitation.
µg	micro-gram
µl	micro-litre
µM	micro-molar
ξ	Proportionality constant relating the sensitized acceptor emission to the decrease in donor fluorescence due to FRET

CHAPTER 1: GENERAL INTRODUCTION

1.1. Calcium homeostasis:

Calcium (Ca^{2+}) is an extremely important element involved in numerous physiological processes. It also acts as an intracellular messenger as well as a co-factor for enzymes inside the cell [1]. Free intracellular Ca^{2+} concentrations in the cytoplasm is usually ~100nM which can go up to 1µM upon release from intracellular stores or influx of extracellular Ca^{2+} through channels [1], whereas extracellular Ca^{2+} concentrations are usually ~10,000 fold higher and are usually maintained at 2.2-2.6mM total and 1.1-1.4mM ionized concentration through a tightly regulated mechanism called Ca^{2+} homeostasis [1, 2].

The parathyroid gland is the most important organ involved in Ca^{2+} homeostasis. Parathyroid chief cells sense minute decreases in extracellular Ca^{2+} concentration from the natural set point of 1-1.3mM, and subsequently cause rapid transient release of parathyroid hormone PTH (typically 2-3% decrease in extracellular Ca^{2+} can lead to 150-200 fold increase of serum PTH levels) [2, 3]. This mobilizes Ca^{2+} from the reserves by enhancing renal reabsorption of Ca^{2+} and excretion of phosphate as well as promoting bone resorption [2]; and so is classified as a hypercalcaemic hormone. Conversely, an increase in extracellular Ca^{2+} inhibits PTH release and its consequent actions [2, 3].

Increase in serum Ca^{2+} levels also cause an increase in secretion of the hypocalcaemic hormone calcitonin from thyroid C-cells [2]. Calcitonin is a peptide hormone which potently lowers serum Ca^{2+} by decreasing osteoclastic bone resorption and increasing Ca^{2+} urinary secretion [4, 5]. The third calciotropic hormone involved in Ca^{2+} homeostasis is the active form of vitamin D-1,25$(OH)_2$D (calcitriol), which is converted into mature form in the kidney by the effects of decreased Ca^{2+} as well as increased PTH levels [6]. Calcitriol increases intestinal Ca^{2+} absorption from dietary sources [2], enhances bone resorption [7], facilitates Ca^{2+} reabsorption in the kidneys [8] as well as inhibits the synthesis of PTH mRNA, thus completing the endocrine feedback loop [9].

So, as shown in the Figure 1.1 these hormones coordinate to facilitate the operation of Ca^{2+} homeostasis.

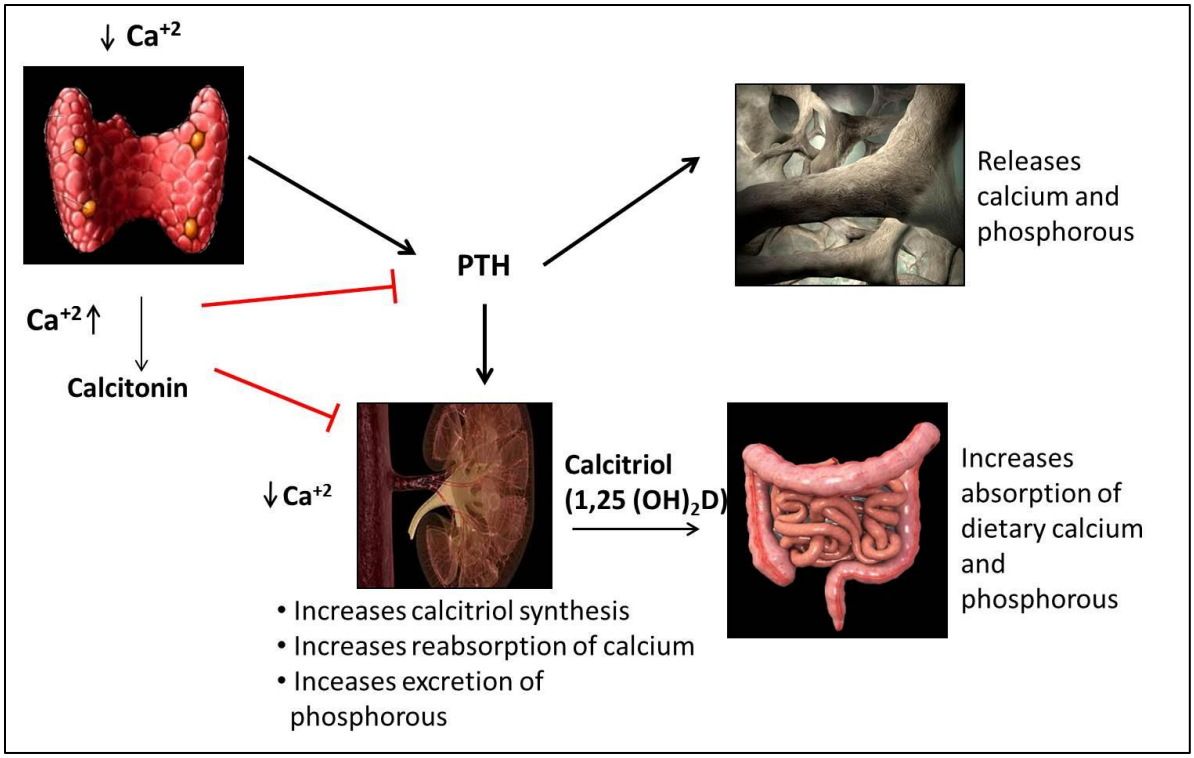

Figure 1.1: Schematic representation of Ca^{2+} homeostasis:
A decrease in extracellular Ca^{2+} stimulates PTH production and secretion from the parathyroid glands, which acts on kidneys to enhance renal reabsorption of Ca^{2+} and stimulates the synthesis of vitamin D_3 into its active form (calcitriol) in case of a prolonged hypocalcaemia (few hours). It also enhances bone resorption causing release of Ca^{2+} and phosphorous. Calcitriol increases intestinal Ca^{2+} absorption and increases bone turnover. PTH also prevents retention of phosphate mobilized from bone and intestinal absorption. The consequent increased serum Ca^{2+} levels cause the normalization of the natural set point (1-1.3mM of free Ca^{2+} in mammals) and returns the secretion of PTH to basal. Hypocalcaemic hormone, calcitonin is secreted from the thyroid when Ca^{2+} levels are above the threshold which counteracts the action of the hypercalcaemic hormones.

This robust mechanism can only be tightly regulated due to the ability of the cells to "sense Ca^{2+}" in their environment. This function is rendered by a cell-surface receptor which is present on the cells involved in Ca^{2+} homeostasis like the parathyroid, kidney and bone cells. Accordingly, this receptor is called the Ca^{2+} Sensing Receptor (CaSR) and it belongs to the family of receptors known as the G-protein coupled receptors (GPCRs). CaSR was first isolated as a Ca^{2+}-sensor from the bovine parathyroid cells, where it inhibited PTH secretion upon activation [10]. Before moving into the details on the Ca^{2+} sensing receptor, a brief introduction about the GPCR family is necessary.

1.2. G-protein coupled receptors (GPCRs):

The GPCR family is one of the largest families of cell-surface receptors in mammals (around 800-1000 GPCRs in human genome, consisting of >2% of protein coding genome) [11]. They bind to a variety of targets and mediate their signaling through a pathway involving guanosine nucleotide-binding proteins (G proteins). They are involved in numerous vital functions like taste, odor, memory, response to light, action of hormones and neurotransmitters [11].

GPCRs are characterized by seven hydrophobic stretches of amino acids (aa) that form 7 transmembrane (TM) segments, connected by alternating extracellular and intracellular loops which form the N-terminal extracellular domain and C-terminal intracellular domain respectively (Figure 1.2). The first crystal structure of a GPCR was of bovine rhodopsin by Palczewski *et al* [12]. Recently the crystal structures of other GPCRs have also been discovered such as the β-adrenergic receptor [13-15], opioid receptor [16, 17], M3 muscarinic acetylcholine receptor [18] and nociception receptor [19]. These crystal structures have provided important structural information regarding the conformational changes in the structure of few GPCRs caused by their activation by ligands. It has been shown that this phenomenon involves an outward or inward movements of the TM segments three, five, six and seven which consequently facilitates G protein coupling to the receptor[20-22].

G-proteins are at the top in hierarchy of multiple signalling components activated by a GPCR. G-proteins bind to specific regions on the C-tail or parts of trans-membrane loops in the cytoplasm upon activation of the receptor; consequently leading to rapid changes in the concentration of intracellular signaling molecules like cyclic AMP (cAMP), cyclic GMP (cGMP), inositol phosphates, diacylglycerol (DAG), arachidonic acid and cytosolic ions [23]. Apart from the G proteins, GPCRs can also couple to β-arrestins and GRKs which modify the phosphorylation status of the receptor (uncouple the G proteins) and thereby acting as safety mechanism to prevent overstimulation of GPCRs. In addition to this, β-arrestins can also couple GPCRs to kinase pathways [24].

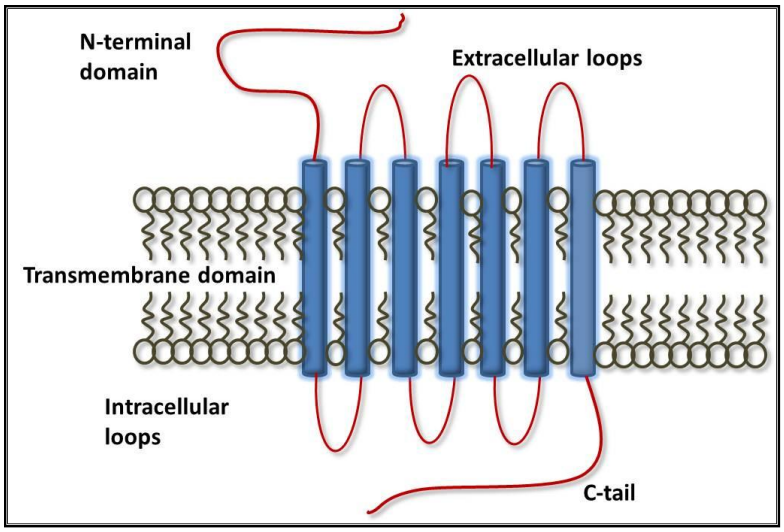

Figure 1.2: Structure of a GPCR:
There are 7 trans-membrane (TM) domains connected by alternating extracellular and intracellular loops which form the extracellular and C-terminal intracellular domains respectively.

G-proteins are hetero-trimeric composed of α, β and γ sub-units. The β and γ sub-units are tightly associated and can be regarded as a single functional sub-unit [23]. In an inactivated state of the receptor, GDP is bound to Gα subunit, which is replaced by GTP upon activation of the receptor. Binding of GTP causes dissociation of G-protein from the receptor into active α (GTP bound) and βγ sub-units. These activated sub-units stimulate different secondary messenger proteins [23]. This mechanism is described in detail in chapter 4, section 4.1.1. G proteins are divided into four families based on the similarities in their α-subunits as shown in table 1.1.

G-protein family	Subtype	Function
G_s	$G_{\alpha s}$ $G_{\alpha olf}$	Increases the activity of adenylate cyclase (AC).
G_i	$G_{\alpha i1}$ $G_{\alpha i2}$ $G_{\alpha i3}$ $G_{\alpha oA}$ $G_{\alpha oB}$ $G_{\alpha z}$ $G_{\alpha t1}$ $G_{\alpha t2}$ $G_{\alpha g}$	Decreases AC activity, Involved in phospholipase C (PLC), ERK activation Involved in Ca^{2+} & K^+ channels Increases cGMP dependant phosphodiesterase activity
G_q	$G_{\alpha q}$ $G_{\alpha 11}$ $G_{\alpha 14}$ $G_{\alpha 15 \text{ or } 16}$	Activates PLC
G_{12}	$G_{\alpha 12}$, $G_{\alpha 13}$	Regulates Ras homology guanine nucleotide exchange factors (RhoGEFs)

Table 1.1: G-protein families, their subtypes and respective functions
as reviewed in [23].

GPCRs are classified into different families in humans based on their structure and ligands [25, 26]:

Family A receptors (Rhodopsin family):

The rhodopsin family constitutes the largest number of GPCRs present in the human genome. The members of this family possess several characteristics such as the Asn-Ser-X-X-Asn-Pro-X-X-Tyr motif in the TM segment 7 of the receptor. This motif is involved in maintaining receptors in an inactive conformation. These receptors also possess the Asp/Glu-Arg-Tyr/Phe motif at the

interface of TM segment 3 and intracellular loop 2 that is involved in activation of G-proteins. Generally, the ligands to this family of receptors bind either to the extracellular domain or extracellular loops of the TM domain. The family is further classified into following groups:

- Receptors for retinals, odorants, adenosines, etc. The ligand binding site is localized in the 7 TM domains.
- Receptors for peptides, cytokines, thrombin, etc. The ligand binds to either to the extracellular loops or to the upper parts of the TM domain.
- Receptors for glycoprotein hormones. Receptors have large extracellular domain where the ligands bind [25, 26].

Family B receptors (Secretin receptor family):

The N-terminus of family B receptors is ~60-80 aa long and contains conserved Cys residues which are particularly responsible for ligand binding. The ligands for this family are peptides. The receptors include secretin receptor, calcitonin receptor, calcitonin receptor like receptor, parathyroid hormone releasing receptor, vasoactive intestinal peptide receptor and others [25, 26].

Frizzled/ Taste-2 receptor family:

This family contains two groups of receptors clustered together to form a single family.

- Frizzled receptors contain a 200 aa N-terminus with conserved Cys residues participating in ligand binding. They bind to a glycoprotein called Wnt as their ligand and require accessory proteins know as lipoprotein receptor related peptides (LRPs) for Wnt binding and signaling.
- Taste-2 receptors have a very short N-terminal and the ligand binds to 7-TM domain. They are expressed in the tongue and palate epithelium and function as bitter taste receptors [25, 26].

Family C receptors (Metabotropic glutamate receptor family):

The N-terminus of these receptors is ~280 to 580 aa long which contains the ligand recognition domain. Family C receptors include 8 metabotropic glutamate receptors, 2 GABA receptors, CaSR, GPRC6A and 5 taste receptors [27]. The N-terminus forms two distinct lobes, separated by a cavity in which ligand binds, causing the lobes to close and thus form a "Venus fly trap" model (Figure 1.3). This two-lobed structure is separated from 7-TM domain by conserved cysteine residues that play multiple roles like maintaining receptor conformation and functional activation of receptor following stimulation by agonist. [25, 26].

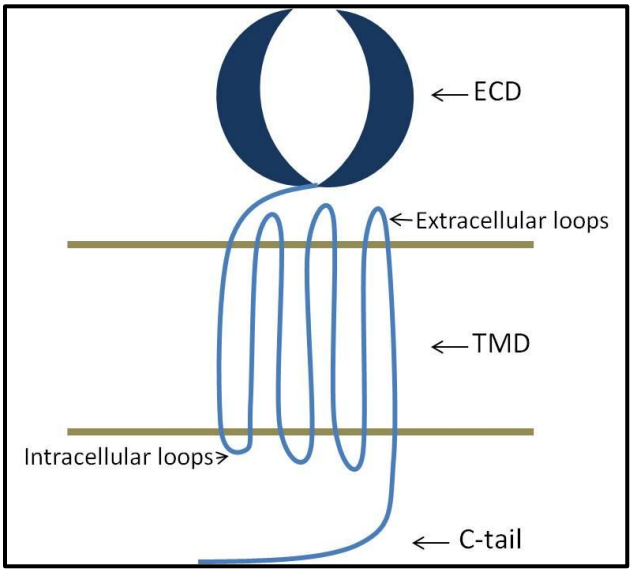

Figure 1.3: Schematic representation of structure of Family C GPCR.
Two Family C GPCRs, CaSR and its closely related receptor GPRC6A were studied in this project.

1.3. CaSR and its role in Ca^{2+} homeostasis:

As mentioned earlier, CaSR is a GPCR which binds to Ca^{2+} and so the discovery of CaSR provided a link between changes in extracellular Ca^{2+} levels and changes in PTH secretion [10]. Pathologies related to the inherited mutations of CaSR have established that it is as an important regulator of systemic Ca^{2+} homeostasis, which will be described later in section 1.4. CaSR is a widely distributed cell-surface receptor and its role in Ca^{2+} homeostasis should be understood by studying its expression in the tissues involved in the mechanism.

1.3.1. Parathyroid cells:

CaSR is very highly expressed in the parathyroid glands on the chief cells, where it senses increases in the levels of extracellular Ca^{2+} and inhibits the secretion of PTH to prevent its hypercalcaemic actions [10, 28, 29]. It also reduces the expression of PTH mRNA [30], and proliferation of parathyroid cells in culture [31] through an array of second messenger signalling. Recently, it has been shown that inhibition of PTH secretion is not a robust response to check against hypercalcaemia as mice lacking the PTH gene could defend against induced hypercalcaemia similar to wild type mice; whereas mice lacking both CaSR and PTH gene failed to do so [32]. This means that hypercalcemia can be defended by other mechanisms. So, the PTH secretion from chief cells to defend against hypocalcaemia is probably the primary but not robust function of parathyroid glands in Ca^{2+} homeostasis.

1.3.2. Thyroid:

CaSR is expressed on the thyroid parafollicular C-cells where upon sensing increase in serum Ca^{2+} levels, it facilitates the secretion of the hypocalcaemic calcitonin [33]. Accordingly, mice with a heterozygous mutation of CaSR have decreased secreted calcitonin levels under Ca^{2+} challenge, compared to wild-type mice and consequently exhibit a compromised response to hypercalcaemia, indicating the role of CaSR in calcitonin secretion [34]. The importance of calcitonin in Ca^{2+} homeostasis is demonstrated by a study where mice with a functional CaSR but lacking the PTH gene, defended against hypercalcaemia by secreting more calcitonin and increasing renal Ca^{2+} clearance compared to the double knock-out (*Casr*$^{-/-}$. *Pth*$^{-/-}$) mice [32].

1.3.3. Kidney:

Kidney regulates the excretion/reabsorption of nutrients including divalent ions and hence plays an important role in divalent ion homeostasis. CaSR is widely expressed in different parts of kidney, where it facilitates the excretion of Ca^{2+} and reabsorption of phosphorus upon activation [32, 35-37]. Role of CaSR in renal Ca^{2+} homeostasis has been conclusively demonstrated and is shown to be independent of PTH regulation. It was shown that mice lacking both CaSR and PTH genes could not defend against hypercalcaemia as compared to wild type because of their reduced renal Ca^{2+} clearance [32, 35], and compromised calcitonin secretion [32]. In order to check whether these effects were due to the absence of PTH, mice

with a functional CaSR but lacking PTH gene were also tested under same hypercalcaemic challenges and it was found that they could defend similar to wild type. This shows the importance of renal Ca^{2+} homeostasis governed by CaSR. Accordingly, renal Ca^{2+} clearance along with the actions of hypocalcaemic calcitonin serves as a 'ceiling' to limit hypercalcaemia [32].

Ca^{2+} reabsorption in the kidneys is caused by the action of $Na^{2+}/K^{+}/Cl^{-}$ co-transporter (NKCC2) and the K^{+} channel Kir 1.1. The actions of these channels cause reabsorption of NaCl, which creates a difference in the membrane potential favoring Ca^{2+} reabsorption [38]. It was shown that CaSR inhibits the action of Kir1.1 channel under hypercalcemia [38]. So, it is suggested that activation of CaSR leads to failure in generating membrane potential favorable for Ca^{2+} reabsorption. [38]. Further to this, 1,25-dihydroxyvitaminD_3 also facilitates direct Ca^{2+} reabsorption in kidneys [8]. Activation of CaSR also inhibits the PTH mediated maturation of 25-hydroxycholecalciferol to calcitriol as shown by experiments in the human proximal tubule cell line HKC-8 [39]. *In vivo* studies on *Casr*$^{-/-}$ mice have shown that CaSR dampens the response to 1,25-dihydroxyvitaminD_3 independently of PTH actions [40]. Thus CaSR exerts a tight control on circulating 1,25-dihydroxyvitaminD_3 both at the level of its synthesis and in modulating its effects.

1.3.4. Bone:

Bone is the largest reservoir of Ca^{2+} in the body and so is also intimately involved in systemic Ca^{2+} homeostasis. Bone constantly undergoes formation and break-down leading to changes in local Ca^{2+} concentrations. Sensing such changes becomes important to orchestrate the activity of different bone cells. CaSR is present in bone and plays a role in sensing local changes in Ca^{2+} concentrations. CaSR is expressed in bone cells such as osteoblasts [41, 42], chondrocytes [43], and osteoclasts [44-46]. Targeted deletion of CaSR (lacking exon 7 which codes for TM domain and intracellular loops) in osteoblasts in mice using type-1 collagen promoter resulted in significant reduction in body weight and severe under-mineralization of skull, ribs and long bones [43]. There was marked reduction in bone volume, bone mineral density and thickness of trabecular and cortical bone and increased apoptosis of osteoblasts [43]. There was an increase

in osteoclast numbers and osteoclast function promoting NF-κB signalling [47]. Also, expression of IGF-1 (anabolic in bone) was reduced [43]. Using a different promoter- osterix which is more specific for osteoblasts, similar results were obtained [43]. Co-cultures of osteoblasts and osteoclasts derived from these mice *ex vivo* exhibited delayed differentiation and reduced mineralization of osteoblasts and increased osteoclastogenesis, supporting the *in vivo* observations [47]. These results are also supported by *in vitro* studies which show that CaSR promotes primary osteoblast proliferation, expression of differentiation markers and mineralized nodule formation upon increase in concentration of extracellular Ca^{2+} via extracellular signal-regulated kinase 1/2 (ERK1/2), Akt or c-Jun NH(2)-terminal kinase (JNK) pathways [41, 42]. These results show a direct role of CaSR in bone and the pathology of the knock-out models is related to defective mineralization and paracrine Ca^{2+} sensing leading to imbalance in bone turnover [47].

CaSR deletion in chondrocytes in mouse model using type-2 collagen promoter caused embryonic lethality before E13 due to inhibition of early cartilage and bone mineralization [43]. Using tamoxifen inducible knockout, CaSR deletion after E13 resulted into viable litters but with severe defects in cartilage and bone mineralization and significant reductions in IGF-1 and IGF-1R expression in growth plate [43]. This shows a definitive role of CaSR in cartilage.

In the case of osteoclasts, CaSR, upon activation exhibits a regulatory role [44, 45]. In cultured rabbit osteoclasts, CaSR is responsible for regulation of osteoclast activity as measured by pit formation on dentine slices [44]. Decreased osteoclastogenesis was seen in immature osteoclasts (RAW 264.7 cells) expressing dominant negative CaSR mutant; and in osteoclasts derived from *Casr*$^{-/-}$ mice [45]. Also, CaSR activation by 20mM Ca^{2+} caused PLC-NF-κB dependent apoptosis of normal cultured rabbit osteoclasts [45]. This shows that CaSR plays an inhibitory role in osteoclast function.

Taken together, CaSR plays a role in bone by sensing changes local Ca^{2+} concentrations within the bone microenvironment and possibly by orchestrating the function of bone cells, as shown in figure 1.4 below

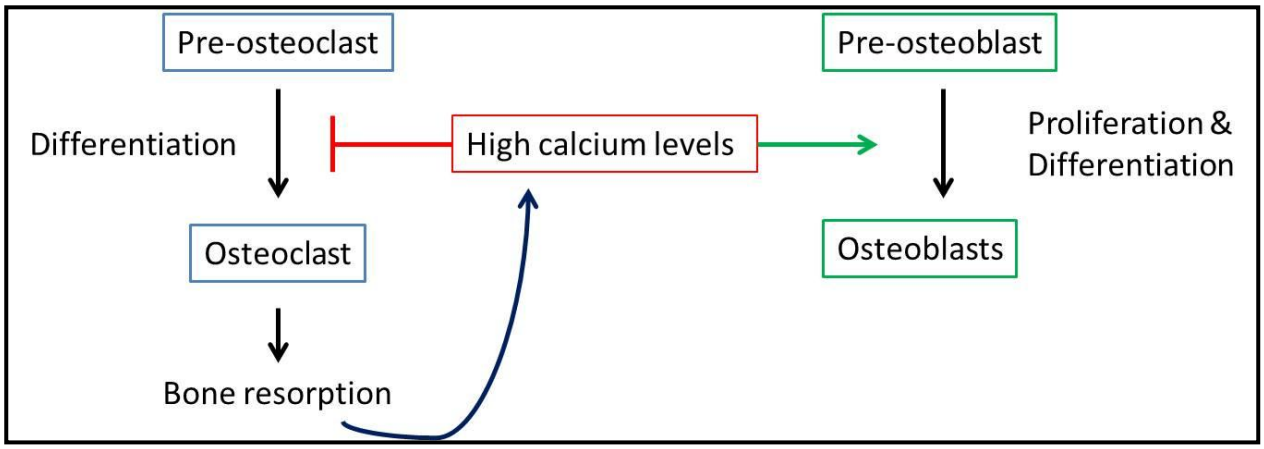

Figure 1.4: Schematic model for the role of CaSR in bone remodelling, based on the evidence from in vitro studies:

CaSR on pre-osteoclasts sense high local Ca^{2+} levels upon bone resorption causing decreased osteoclastogenesis and increased apoptosis, whereas CaSR on pre-osteoblasts is activated promoting proliferation and differentiation of osteoblasts. Adapted from [48].

1.3.5. Gut:

Food digestion and nutrient absorption including that of Ca^{2+}, takes place in the gut. CaSR expression has been established all along the gastrointestinal tract namely, the stomach [49], small intestine [50] and colon [50, 51]. Although it is known that calcitriol increases intestinal Ca^{2+} absorption from dietary sources [2] as a part of Ca^{2+} homoeostasis, a direct link between the role of CaSR and intestinal Ca^{2+} transport is yet to be identified. However, the expression of CaSR in the gut has been linked to facilitation of food digestion and nutrient sensing. CaSR is shown to be activated by aromatic L-aa *in vitro* in the presence of extracellular Ca^{2+} [52]. So, the aa serve as allosteric activators of CaSR. Indeed, it was shown that CaSR caused secretion of CCK upon activation by L-aa from intestinal mucosal cells isolated from mice, an effect which was blocked by CaSR antagonist [53]. Also, it was shown that in the G-cells of stomach, activation of CaSR leads to gastrin release, with a concurrent rise in intracellular Ca^{2+} [49]. This aids in further digestion of food and consequent increase in nutrient absorption. It has been hypothesised that as the demand for more Ca^{2+} rises, the level of extracellular Ca^{2+} in the stomach possibly modulates CaSR to cause more gastrin secretion, which causes more ionization of Ca^{2+} from food and consequently its absorption in the intestine [54].

Thus, CaSR is essential for Ca^{2+} homeostasis and acts like a 'thermostat' by modulating the hyper and hypo calcaemic activities of hormones involved in the mechanism.

1.4. Pathological mutations and knock-out models of CaSR:

The importance of CaSR in Ca^{2+} homeostasis is supported by the pathological conditions caused by its inactivating and activating mutations, as well as by the phenotypes of the knock-out mice models.

Heterozygous inactivating mutations of CaSR cause Familial Hypocalciuric Hypercalcaemia (FHH), which is an autosomal dominant disorder characterized by mild, long and asymptomatic hypercalcaemia (serum Ca^{2+} concentration from ~2.75 to ~3.5 mmol/l), that significantly reduces the rates of urinary Ca^{2+} excretion [55]. Hypercalcaemia is caused due to the decrease in sensitivity for the extracellular Ca^{2+} because of loss-of-function mutations and consequently increased PTH levels [56]. Apart from the inactivating mutations, it has been reported in the clinical studies that in some patients with normal functioning CaSR, production of auto-antibodies against the N-terminal of CaSR cause an acquired FHH like disorder [57, 58].

Homozygous loss-of-function mutations of CaSR cause life threatening- Neonatal Severe Hyperparathyroidism (NSPHT) [55, 59]. Accordingly, total parathyroidectomy must be performed in very early stage of life to prevent death. NSHPT is characterized by severe hypercalcaemia (~3-3.5mmol/l to 6.25-7.5mmol/l total Ca^{2+} levels), hyperparathyroidism, skeletal defects such as fractures of long bones and ribs that cause respiratory distress [60].

In both cases defective CaSR results in impaired Ca^{2+} perception, and consequently leading to an increase in the Ca^{2+} sensing set point [61]. Accordingly, the parathyroid gland perceives the Ca^{2+} levels in the serum as low even though they are higher than normal, and continues to secrete PTH causing hypercalcaemia. Also, the Ca^{2+} levels in the kidneys are detected as low and so the excretion of Ca^{2+} is prevented by increasing renal reabsorption, causing hypercalcaemia.

On the other hand, activating mutations of CaSR cause Autosomal Dominant Hypocalcaemia (ADH), in which the Ca^{2+}-set point is lowered by over-sensitive CaSR and consequently PTH secretion is inhibited and Ca^{2+} excretion is elevated even at low levels of Ca^{2+} [62].

Approximately, a total of 253 mutations of CaSR have been associated with FHH, NSHPT and ADH according to the information on the Ca^{2+} Sensing Receptor database (http://www.casrdb.mcgill.ca/?Topic=MutationSearch&v=new&s=d); which includes missense, nonsense, deletion and or insertion, silent and splice variant mutations with a majority of them within the N-terminal domain of the receptor suggesting its importance.

Evidence from CaSR knock-out animal studies also demonstrated the vital role of CaSR in systemic Ca^{2+} homeostasis. CaSR knock-out mouse model with targeted disruption of exon 5 (which codes for the residues 460-536 of the N-terminal domain) exhibited similar phenotype to FHH and NSHPT in humans corresponding to heterozygous and homozygous deletions [63]. These exon 5-deficient *Casr*$^{-/-}$ mice exhibited impaired growth from post-natal day 2 compared to the wild type or *Casr*$^{+/-}$ mice. Also a high rate of mortality of the knock-out mice within day 7 post-birth was observed [63]. The knock-out mice exhibited increased Ca^{2+} and PTH levels, modest increase in magnesium levels, parathyroid hyperplasia, impaired renal Ca^{2+} excretion and bone abnormalities [63]. However, this phenotype could be rescued by deleting the PTH gene [35], or the gene responsible for the development of parathyroid glands known as Gcm-2 (where the mice fail to develop parathyroid glands) [64]. These results indicate that the phenotype observed in exon-5 deficient *Casr*$^{-/-}$ mice was mainly due to hyperparathyroidism and a definitive role of CaSR in individual organs like bone could not be established. However, it was found that exon-5 CaSR knock-out is a hypomorph, which meant that the spliced receptor lacking 77 aa in the N-terminal domain was partially functional and could compensate for the absence of full length CaSR in cultured mouse keratinocyte [65], growth plate chondrocytes [66] and lungs [67]. Accordingly, an alternative CaSR knock-out murine model has been established with targeted deletions of exon 7 (codes for 7 TM domain and 4 intracellular loops) in specific tissues like parathyroid glands, bone or cartilage, as described earlier in 1.3.4 [43]. Accordingly, this model has shown that mice lacking CaSR in parathyroid glands have severe

hyperparathyroidism, growth and bone defects [43]. The above evidences from the clinical and animal model studies thus demonstrate an essential role of CaSR in Ca^{2+} homeostasis.

1.5. Ligands of CaSR:

CaSR is a highly promiscuous receptor which binds a variety of natural and synthetic ligands. Although the primary ligand is considered to be Ca^{2+}, many functional studies have helped to understand the affinities of various ligands activating the CaSR, which point its important role in physiology in different systems. Due to the absence of high affinity ligands of CaSR, the potencies of ligands have been determined using functional assays for signal transduction pathways, rather than the usual radioligand binding assay used for other GPCRs.

1.5.1. Cations:

CaSR was discovered as a Ca^{2+}-sensor from the bovine parathyroid cells, where it inhibited PTH secretion upon activation [10]. The pharmacology of Ca^{2+} binding to the CaSR has been further understood by expressing CaSR in various cell systems and measuring the increases in intracellular Ca^{2+} concentrations and IP_3 and PI-PLC activation. Accordingly, over-expressing the recombinant CaSR in various cell systems like *Xenopus laevis* oocytes [10], HEK-293 [28][68] have reported the potency for Ca^{2+} (Ec_{50} value) between 3-4 mM. The binding of Ca^{2+} to the CaSR is a highly synergistic event, where binding of one molecule facilitates the binding of more molecules, as indicated by the Hill's co-efficient of ~3-4 [69-71]; suggesting multiple Ca^{2+} binding sites. This property enables the receptor to sense minute changes in extracellular Ca^{2+} levels, even though the Ec_{50} is between 3-4 mM.

Apart from Ca^{2+}, Mg^{2+} is also an agonist of the CaSR with an Ec_{50} of 4-7 mM depending on the concentration of extracellular Ca^{2+} [10, 72, 73]. Mg^{2+} is also considered to be a partial agonist of CaSR, with a Hill's co-efficient of around 1 and eliciting 50-60% of maximum response compared to Ca^{2+} in IP activation [30], suggesting that at *in vivo* concentrations Ca^{2+} and Mg^{2+} might activate CaSR in additive fashion.

Other cations with a higher potency than the above stated ligands as measured by CaSR-mediated Ca^{2+} mobilization, IP_3 activation; or PLA_2 activation and pERK phosphorylation in CaSR

transfected cells, include: Gd^{3+} (~2.2 µM) [73-76], Zn^{2+} (~132µM), Ni^{2+} (~120µM) [77], Pb^{2+} (~140µM), Co^{2+} (~400µM) and Fe^{2+} (5mM elicits response, Ec_{50} not determined) [74]. Other divalent inorganic ion ligands of CaSR with potency in millimolar range like Ca^{2+} and Mg^{2+} include Ba^{2+} (<2 mM) and Mn^{2+} (2.8mM) [30] and Al^{3+} [75, 78]. While most of the divalent ions may be thought to be present in the body as co-factors for enzymes or for other purposes, their physiological concentration is much lower than that required to activate the CaSR and are unlikely to represent as physiological agonists of CaSR under normal conditions [74, 77]. However, they may contribute to heavy metal toxicity in the body like in the kidneys or liver, especially since they activate CaSR additively with Ca^{2+} and Mg^{2+} and bind at a high affinity [74, 77].

It is shown that strontium ranelate which is used as an anti-osteoporotic drug, exerts its effects on osteoblasts and osteoclasts via the CaSR [79, 80]. In rat primary osteoblasts, Sr^{2+} stimulated the proliferation of the cells by activating the CaSR [59], whereas in osteoclast Sr^{2+} induced apoptosis via CaSR-mediated PKCβ2-DAG pathway [80]. Its potency to activate the CaSR is positively related to the extracellualr Ca^{2+} concentrations. This effect of strontium ranelate on the CaSR in osteoblasts and osteoclasts may be directly implicated to its antiresorptive action *in vivo*.

1.5.2. Polyamines:

CaSR is allosterically activated by spermine (Ec_{50} ~500µM) and spermidine (Ec_{50} ~4mM) in the presence of 0.5mM extracellular Ca^{2+} concentration in CaSR-transfected HEK-293 cells [71]. The potencies of the polyamines are directly related to the number of positive charges on the molecule (spermine has 4 positive charges and spermidine has 2 positive charges), as well as to the extracellular Ca^{2+} concentration. The binding of polyamines is highly co-operative with a Hill's co-efficient of >3 [71].

1.5.3. Aminoglycoside antibiotics:

In cell systems like oocytes and HEK-293 overexpressing the CaSR, its has been shown that neomycin (Ec_{50} ~50µM) activates the CaSR [76, 81, 82]. In opossum kidney cells endogenously expressing CaSR other aminoglycoside antibiotics in addition to the neomycin, such as

gentamycin (Ec_{50} ~258μM) and tobramycin (Ec_{50} ~170μM) increased CaSR-mediated intracellular Ca^{2+} levels and ERK-1,2 phosphorylation through PIP_2-PLC dependent pathway [81]. The rank order of potencies of these antibiotics is directly proportional to the number of amino group present in their structures [82]. In transfected HEK-293 cells, the sensitivity of CaSR for aminoglycosides was shown to be pH mediated [82]. Accordingly lowering the extracellular pH from 7.4 to 6.9 to mimic the conditions in the proximal tubule enhanced the sensitivity of the CaSR towards the aminoglycoside antibiotics (left-shift in potency) without any change in the maximal response. This effect is thus related to the increase in ionization of the antibiotic [82]. Since the major site of aminoglycoside antibiotic toxicity is kidney, these studies suggested CaSR activation by the antibiotics could probably be the mode of action of this phenomenon [81, 82].

1.5.4. Amino-acids and polypeptides:

CaSR has been demonstrated to be a stereo-selective receptor for the L-aromatic aa. It was shown that L-phenylalanine (Ec_{50} ~2.2mM) and L-tryptophan function in an allosteric manner, in the presence of >1 mM extracellular Ca^{2+} to activate CaSR in transfected HEK-293 cells [52]. Furthermore, a mixture of L-aa at a concentration emulating the fasting serum levels activated the CaSR by increasing its sensitivity to Ca^{2+} by 20-40% compared to individual aa [52]. So it was hypothesised that in physiology, CaSR could also act as a nutrient-sensing receptor in the gut where differences in the levels of L-aa can modulate its sensitivity leading to changes in digestion responses [52]. Furthermore since CaSR is also expressed in the neurons, it is hypothesised to contribute towards the neurotoxicity caused by high phenylalanine levels in phenylketonuria [52].

Using CaSR transfected HEK-293 cells and cultured rat hippocampal pyramidal neurons lacking CaSR, it was demonstrated that amyloid β-peptide activated the CaSR at 1μM concentration, consequently eliciting $Ca_{[i]}$ responses via non-selective cation channel [83]. However, this effect at normal physiological levels has not been verified yet [83].

1.5.5. Phenylalkylamine derivatives

Phenylalkylamine derivatives are small molecule, orally active compounds that modify the affinity of the CaSR for Ca^{2+}. The compounds that increase the affinity of CaSR for Ca^{2+} are known as calcimimetics, whereas those inhibiting the activity of CaSR are known as calcilytics.

Calcimimetics function only in the presence of extracellular Ca^{2+} (minimum 0.5 mM) and hence are positive allosteric modulators [29]. The first generation calcimimetics were NPS-467 and NPS-568 which increased the sensitivity of CaSR for Ca^{2+} in CaSR transfected HEK-293 cells and concurrently decreased the secretion of PTH in cultured bovine parathyroid cells [29]. NPS-568 was tested for use in humans against secondary hyperparathyroidism (HPT) caused by end-stage renal disease [84, 85]. The compound decreased the serum PTH concentrations, increased calcitonin secretion from thyroid C-cells and lowered ionized Ca^{2+} in the serum [84, 85].

However, NPS-568 was superseded by a second generation calcimimetic called Cinacalcet (NPS 1493, AMG 073, Sensipar®) which has better bioavailability and pharmacodynamics [86, 87]. Cinacalcet is the first calcimimetic available as an FDA-approved drug for the treatment of secondary HPT and it efficiently reduces serum PTH, Ca^{2+} and Ca^{2+}-phosphorous levels [88-91].

Interestingly, it has been shown that calcimimetic NPS-568 can act as a small-molecule chaperone for CaSR. CaSR like all GPCRs, exhibits a secretory pathway for cell-surface trafficking. Typically for GPCRs after synthesis the polypeptide is directed to the ER, where the receptor gets folded, anchored in the ER membrane and is core-glycosylated. It is here that a chaperone if any, couples to the receptor. Next, the receptor is transported to the Golgi apparatus where it is terminally glycosylated before delivery to the plasma membrane. It was observed in a study that overnight incubation with NPS-568 under normal cellular Ca^{2+} levels, rescued the loss-of function CaSR mutants from ER retention and increased their expression on the cell membrane in transfected HEK-293 cells [92]. Using ^{35}[S]cysteine labeling strategy to mark the newly synthesized ^{35}[S]CaSR, it was discovered that NPS-568 increased the plasma membrane CaSR population by inducing an active conformation of the CaSR which increased its co-translational stability and also increased the entry of maturely glycosylated CaSR into the

secretory pathway from ER to cell membrane [93]. This shows a conformational check point in the ER as a part of CaSR biosynthesis [93].

NPS 2143 (Ic_{50} ~43nM) was the first calcilytic reported to inhibit the function of CaSR in transfected HEK-293 cells and increase the secretion of PTH in cultured bovine parathyroid cells [94]. However, its long half-life resulted into chronic PTH elevations causing increased bone turnover, but no change in the bone mineral density [95]. This study led to a novel approach for the development of treatment for osteoporosis, whereby short increases in endogenous PTH levels can result in bone formation [95].

SB-423557, a calcilytic derived from NPS 2143, demonstrated 2-3 fold transient increase in PTH levels leading to increased bone mineral density along with normal tolerance in healthy human volunteers [96]. With recent advances other calcilytics with promising initial results in animals have been developed like compound 7h and 11m by Novartis and JTT-305 [97, 98] but their potency, efficacy and safety in clinical trials have not been reported yet.

1.6. Structure-functional relationships of the CaSR:

Brown *et al* were the first to clone the CaSR by functional screening of the *Xenopus laevis* oocytes transfected with bovine parathyroid-gland RNA library [10]. As described earlier, CaSR belongs to the Family C of GPRCs. The topological structure predicted from its nucleotide sequence consists of three main structural domains: (1) a large extracellular amino terminal domain (ECD) which is also called as the “Venus-flytrap” (VFT) domain of ~600 aa (2) a ~250 a.a TM domain and (3) ~200 aa C-terminal tail [10].

1.6.1. The extracellular domain (ECD):

The large ECD of the Family C GPCRs shares a common topology of a bilobed “Venus-flytrap” structure. The structure of the ECD of Class C receptors was first identified by 3D modeling of the ligand binding ECD of the metabotropic glutamate receptor1, based on its homology with bacterial periplasmic binding protein observed by sequence identity analysis [99]. In the case of CaSR, structural homology using the solved crystal structures of the extracellular ligand-binding domains of mGluR1 [100], mGluR3 and mGluR7 [101], demonstrated that CaSR shares the bi-

lobed Venus-flytrap (VFT) (~600 aa) domain followed by 62 residue of cysteine-rich domain [102].

The N-terminal domain of the CaSR extends from the residues 20 to 536 and has 11 glycosylation sites [10, 103]. N-linked glycosylation is shown to be important for the effective cell-surface delivery of CaSR [104]. Site-directed mutagenesis revealed that out of the 11 putative N-glycosylation sites, 8 are effectively glycosylated and the glycosylation of at least three sites is critical for cell-surface expression of the receptor [105].

ECD is the binding site for Ca^{2+} as was demonstrated by chimeric receptor approach using ECD of the CaSR and TM domain and C-tail of mGluR1 to measure PI-PLC responses to Ca^{2+}. It was shown that the mutant receptor was not compromised for its Ca^{2+}-sensing ability and could activate PI-PLC effectively, thus indicating that Ca^{2+} bound to the ECD [106, 107]. Recent studies by Huang *et al* have mapped at least 5 important separate residues on lobes 1 and 2 of the ECD and the hinge region connecting them as putative Ca^{2+} binding [108]. Here the ECD was divided and cloned into three functional subdomains containing putative Ca^{2+} binding sites predicted using homology modeling with mGluR1. The divalent binding characteristics of these proposed sites were tested using terbium-luminescence transfer analysis and intracellular Ca^{2+} increases. (Here, terbium ion- Tb^{3+}, is used as a trivalent-analogue for Ca^{2+} as it has same ionic radius and it produces luminescence due to energy transfer from the aromatic residues in the binding pocket, and hence is used to probe Ca^{2+} sites. Additionally, terbium binding is competed with increasing concentration of Ca^{2+}). Based on the results obtained, a two-state CaSR activation model was proposed [108] (Fig 1.5); according to which, under normal physiological Ca^{2+} levels (1.1-1.3mM), the receptor exists in a partially active form due to Ca^{2+} binding to only one high affinity site (site 1 shown in figure 1.5) and is responsible for sensing and maintenance of this balance (basal activity). At lower Ca^{2+} levels than 1.1-1.3mM, the conformation of the receptor changes to inactive form due to dissociation of Ca^{2+} from the high-affinity site 1. Such a change would facilitate secretion of PTH, which in turn elevates extracellular levels of Ca^{2+}. On the contrary, under very high Ca^{2+} levels, the receptor changes to an active conformation, due to Ca^{2+} docking at all the binding sites; which in turn leads to inhibition of PTH secretion [108]. The

study also identified the known loss and gain-of-function mutations related to FHH and ADH respectively within the identified Ca^{2+} binding sites, which not only supports the results obtained, but also gives a physiological significance to them [108].

Also, the binding site for neomycin is localized to the ECD as reported by a study where a chimeric receptor, containing ECD of mGluR1 and TM domain and C-tail of CaSR, could not be activated by neomycin, whereas the reverse configuration of the chimeric receptor responded to neomycin [107].

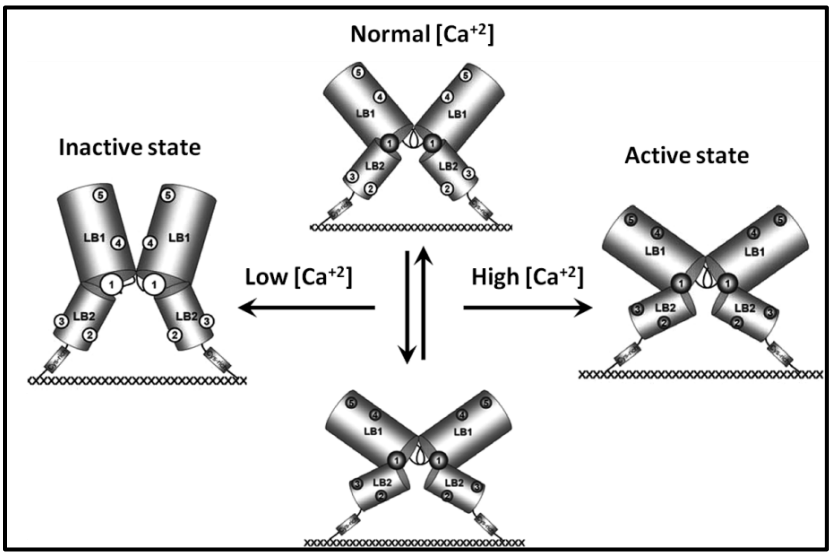

Figure 1.5: Hypothesised two-state working model of CaSR:
White circles represent empty sites and grey circles represent Ca^{2+} docked sites. LB=lobe. The active and inactive forms are in equilibrium, and the state of the receptor's activity varies in response to the association or dissociation of Ca^{2+} ions in the predicted binding sites. High-affinity site 1 senses the normal range of extracellular Ca^{2+} levels (1.1-1.3mM). Under low-Ca^{2+} conditions, the Ca^{2+} binding sites are empty, and the CaSR exists in an inactive conformation. Under high-extracellular Ca^{2+} conditions, the binding of Ca^{2+} to all sites leads to conformational changes that favor activation of the receptor. Thus, deviation from the state of homeostasis can be restored by the sensing of extracellular Ca^{2+} by these putative Ca^{2+}-binding sites and the resultant reversible conformational changes [108]. "Reprinted with kind permission from [108]. Copyright (2009) American Chemical Society".

In addition to the role as an orthosteric ligand binding domain, the ECD is also involved in CaSR dimer formation by harboring Cys-Cys covalent bond site [109], which is discussed further in section 1.6.4.

A separate cysteine-rich domain is attached to the end of ECD by non-covalent interactions [110], that consists of 9 highly conserved Cys residues which is responsible in activating the TM domain by the conformational changes due to agonist binding to the ECD [102].

1.6.2. The trans-membrane domain:

The seven trans-membrane helices of the CaSR along with the extra and intracellular loops are involved in non-redundant roles such as processing and cell-surface trafficking of the receptor [111], maintaining normal conformation of the receptor [68, 112], binding of phenylalkamine-derived allosteric modulators [113] and G-protein coupling [114].

CaSR requires all the seven trans-membrane domains for core glycosylation and cell-surface expression of the receptor. It was shown that CaSR mutants with three or five trans-membrane domains expressed in HEK-293 cells were not core-glycosylated, failed to traffic to the cell-surface and hence showed no activity in response to extracellular Ca^{2+} [111]. This can be due to improper folding and ER retention or faster degradation of these mutant receptors when compared to the wild-type receptors [111]. It has been shown that five important acidic residues (Glu-755, Glu-757, Asp-758, Glu-759 and Glu-767) on the extracellular loop 2 are responsible for cell-surface trafficking and response to Ca^{2+} [112].

In addition to this, the TM domain contains residues that prevent an increase in the sensitivity of the receptor towards ligand without changing its cell-surface trafficking. Alanine-substitution of three residues of TM domain which are conserved among the family C members (Asp-758, Glu-759 and Glu-767), increased the sensitivity of CaSR for Ca^{2+}, leading to a speculation that these residues impose conformational limitations to the CaSR to reduce its basal activation [112]. Indeed the physiological importance of this is demonstrated by the presence of activating mutations of CaSR causing ADH, in the TM domain. Residues between Ile-819 and Glu-837 present at the junction of TM helices 6 and 7 (includes extracellular loop 3) harbor these activating mutations, which increase the sensitivity of the receptor for Ca^{2+}, without change in cell-surface expression levels in context to wild-type receptor [68]. This ‘hot-spot’ for ADH mutations was discovered by creating CaSR mutants using systematic alanine mutagenesis of these residues and measuring responses to Ca^{2+} in HEK-293 cells [68]. Also, an important

residue Pro-823 on TM6 of CaSR is responsible for switching of the receptor from an inactive to an active (functional) state upon Ca^{2+} binding. [68].

TM domain of the CaSR is also responsible for binding of its positive and negative allosteric modulators. A study using chimeric receptor approach with the amino-terminus of the rhodopsin receptor and the TM domain and C-tail of the CaSR demonstrated that the mutant receptor still retained biological activity towards NPS-568, an allosteric positive modulator [113]. Different approaches have been used to map the residues within the TM domain responsible for binding the allosteric modulators. These include using ECD deleted CaSR mutants [48]; mutation of specific residues of the TM domain [48][94]; using a homology model of CaSR TM domain made by sequence alignment with the rhodopsin receptor backbone [115]; as well as a three-dimensional model of the CaSR TM domain built via sequence alignment method based on the conserved residues obtained by using the crystal structure of bovine rhodopsin receptor as a template [116]. The results obtained by these studies have revealed overlapping and separate binding residues for NPS-568 (calcimimetic) and NPS 2143 (calcilytic) on the TM helices 2, 3, 5, 6 and 7 *(double-lined and bold circles in figure 1.6)* [68, 112, 115-117] (TM domain 3 and 5 residues- exclusively bind calcilytic; TM helices 6 and 7 shared residues for both). This suggests that the binding pockets of the positive and negative allosteric regulators are partially overlapping, but not identical.

Also, using chimeric receptor containing ECD of mGluR1 and TM domain and C-tail of the CaSR, it was observed that Gd^{3+} could activate the mutant receptor transfected in *Xenopus laevis* oocytes, indicating the presence of its possible binding site in TM domain of the CaSR [107].

The intracellular loops of CaSR are important for interaction of the receptor with $G_{q/11}$ proteins *(broken circles in figure 1.6)*, which were discovered by testing the effect of alanine scanning mutagenesis on signalling of the bovine CaSR [114]. CaSR also couples to other G-proteins as described later but the mechanism by which it couples to other G-proteins is still unknown.

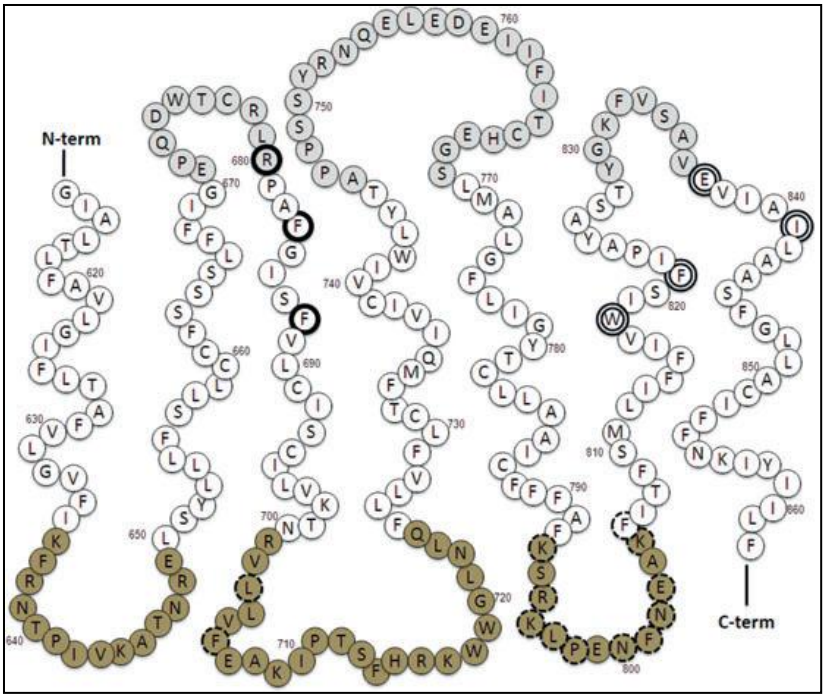

Figure 1.6: Schematic representation of CaSR TM domain:
7 TM domains of CaSR are shown with alternating extracellular loops are shown in light grey and intracellular loops are shown in dark grey. *Double-lined residues* represent interacting sites for both calcimimetics and calcilytics. *Bold circles* are residues interacting with calcilytics only. *Broken circles* on intracellular loop 2 and 3 represent residues affecting $G_{q/11}$ mediated PI-PLC activation. Reprinted from [118] with kind permission from John Wiley and Sons. License number- 2777650617213.

1.6.3. The C-terminal domain:

C-terminal tail of the human CaSR is 216 aa long and is composed of residues 863-1078 [28]. Functional importance of the C-tail of CaSR is rendered by stretches of residues from 865-898 which are shown to be involved in cell-surface trafficking and/or signalling of the receptor [69, 93, 111].

In the case of residues important for receptor trafficking, CaSR C–tail substitution or deletion mutants revealed that residues between 865-874 *(double circles in figure 1.7)* promoted cell-surface receptor expression [111]. Recently, it has been demonstrated that residues between 868 to 898 are responsible for ER retention, a property of the CaSR which acts as a quality control checkpoint [93]. They used ^{35}[S]cysteine labeling pulse chase to monitor receptor synthesis and trafficking of wild type vs C-tail truncation CaSR mutants [93].

For normal signal transduction of the CaSR, residues 865-888 *(grey circles in figure 1.7)* are essential for PI-PLC activation [111]. Also, the residues between 868-886 *(region indicated by broken line in figure 1.7)*, especially the residue 876; appears to be important for the Ca^{2+} sensitive activation of G_q-proteins [69].

Activation of the CaSR can cause phosphorylation of protein kinase C (PKC), which disrupts the signalling of the receptor. PKC mediated phosphorylation of active CaSR causes inhibition of most of the PI-PLC mediated signalling [119, 120]. The CaSR C-tail as well as intracellular loops of the TM, contain five PKC phosphorylation sites, out of which T888 is the major site *(inverted black triangle in figure 1.7)* [119]. Hence, PKC-mediated CaSR phosphorylation serves as a negative feedback mechanism leading to oscillations of $Ca_{[i]}$ instead of constant elevated $Ca_{[i]}$ and thus protecting against the cytotoxic effects of the latter [120].

There is evidence suggesting an involvement of GRK (GPCR kinase, regulating the activity of the receptor) and β-arrestins in PKC-mediated inhibition of CaSR signalling in HEK-293 cells over-expressing GRK, PKC, β-arrestin and CaSR. It was initially reported that over-expressing GRK-2, GRK-4 and β-arrestin-2 in HEK 293-CaSR transfected cells caused agonist dependent inhibition of CaSR signalling via GRK-mediated PKC phosphorylation of the receptor and subsequent translocation of β-arrestin to the C-tail of the CaSR [121]. However, a more recent study using HEK-293 cells modified for stronger anchorage has suggested that an agonist dependent CaSR phosphorylation by PKC leads to β-arrestin mediated inactivation and desensitization; whereas GRK-2 and not 4 leads to agonist dependent CaSR inactivation and desensitization by inhibiting the $G_{\alpha q}$ proteins and not by PKC activation as previously reported [122]. In addition to these *in vitro* studies, β-arrestin-2 null-mouse exhibited increased sensitivity to Ca^{2+} [121]. This was demonstrated by lower PTH levels under normal conditions compared to the wild-type mice, and an attenuation of increase in PTH secretion in response to forced hypocalcaemia, hence further suggesting a possible role of β-arrestin in CaSR desensitization [121].

Slower desensitization following agonist stimulation is an important feature of CaSR in physiology which is attributed to the C-terminal tail. It was shown that the residues between 868-886 *(region indicated by broken line in figure 1.7)*, especially 876, was responsible for CaSR

desensitization [69]. This was done by measuring Ca^{2+} activation of various CaSR C-tail truncated-GFP fused mutants and then studying their desensitization by visualizing for GFP to assess their location and expression levels (post-activation) [69].

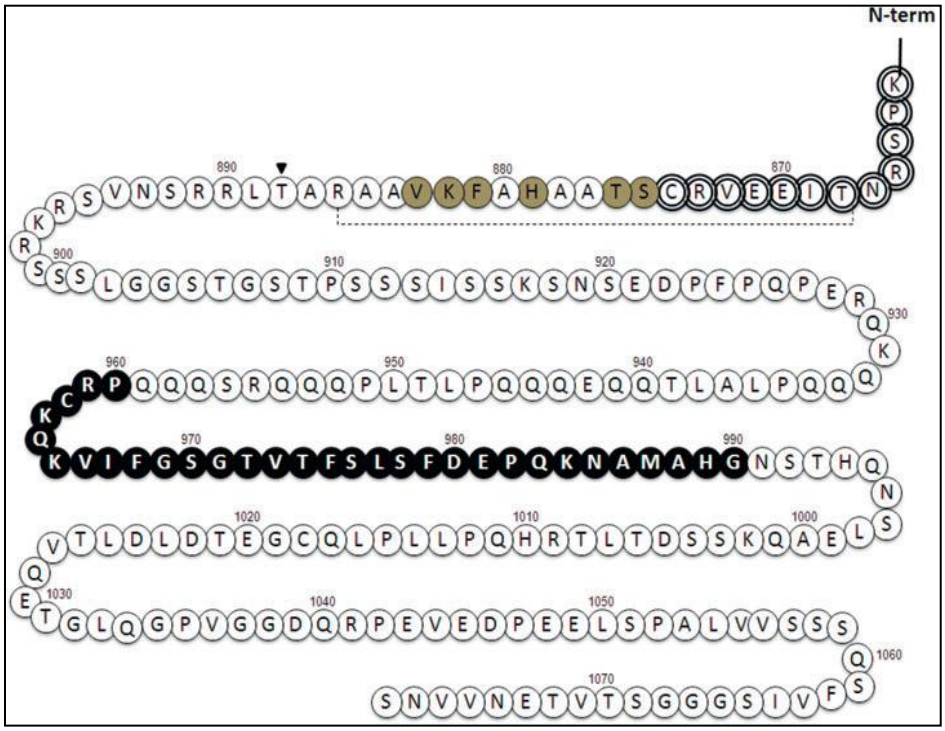

Figure 1.7: Schematic representation of CaSR C-tail:
Double circles: Residues 863-874 supporting receptor expression and signal transduction. *Grey circles*: Residues responsible for PI-PLC signal transduction alone. *Broken line circles*: Responsible for co-operativity and decreasing rate of de-sensitization. *Inverted black triangle*: T-888 PLC phosphorylation site. *Black circles*: Residues 960-990 binding site for filamin A (discussed in section 1.8.3). Reprinted from [118] with kind permission from John Wiley and Sons. License number- 2777650617213.

1.6.4. Homo-dimerization of CaSR:

Oligodimerization is a commonly observed phenomenon amongst GPCRs, especially with Family C receptors where it is a characteristic feature [123, 124]. CaSR exists as a homo-dimer on the cell-surface and it is shown that its glycosylation is essential for the formation of a dimer [109, 125]. CaSR dimerization was discovered by reducing SDS-PAGE electrophoresis where shift in the pattern of bands compared to non-reducing conditions were observed [125]. It was shown

in transfected HEK-293 cells that the CaSR could exist in immature form being glycosylated with carbohydrates with high mannose content (130-140kDa immune-reactive band) which is present only intracellularly. On the cell-surface, it was present only in a mature state of glycosylation (150-160kDa immune-reactive band) [70, 104].

CaSR was shown to mainly exists as a dimer on the cell-surface, at a size greater than 200kDa observed by non-reducing SDS-PAGE using HEK-293 CaSR-transfected cell sample. It was further shown that a proportion of 200kDa product got converted into a 160kDa band under reducing conditions. This shows that only the mature glycosylated disulphide-linked dimeric CaSR is present on the cell-surface [125]. These results were confirmed by co-immunoprecipitation experiments by transfecting separately-tagged CaSR monomers into HEK-293 cells [126]. Also, it was reported that cross-linking of the cell-surface proteins before SDS-PAGE produced bands for CaSR at a size greater than 280KDa suggesting its existence as a high-order oligomer on the cell-surface [125].

The site for dimerization of CaSR has been mapped on the ECD of the receptor. It was shown using site-directed mutagenesis approach that Cys-129 and Cys-131 located within the region protruding from one lobe of the Venus fly-trap domain, are essential for forming covalent disulphide linkage for the dimer formation [109]. However, it was observed in a later study that mutating these residues could still facilitate the formation of a functional CaSR-dimer, via non-covalent bonds between unrecognized residues possibly present in the TM domain [126].

The importance of CaSR dimerization was demonstrated by co-expression of two CaSR mutants- one with a subunit unable to bind the agonist (mutation in ECD) and another with subunit deficient for G-protein activation (mutation in intracellular loop). It was observed that both the mutants could still form dimers that led to signaling, thus uncovering the significance of dimerization of the CaSR to form a functional receptor unit [127]. This result also shows that the ECD and the COOH are two important functional domains for the activity of the CaSR, which may have compensatory role when either one of them is mutated [127].

1.7. Signalling of CaSR:

Following the activation of CaSR, downstream signalling is complex and cell-type dependent. CaSR has been shown to activate various signalling pathways (figure 1.8) depending on the agonist or the cell type. Signalling of the CaSR is discussed in more detail in section 4.1.2 of chapter 4.

1.7.1. Pleiotropic G-protein coupling and activation of phospholipases:

CaSR is shown to couple to more than one G-protein by experiments in different cell types [128-131]. The most characterized response upon activation of CaSR is increase in intracellular Ca^{2+} levels mediated via $G_{q/11}$ activated PLC-IP_3 pathway, in both CaSR transfected HEK-293 and cell types endogenously expressing CaSR including bovine parathyroid cells. [132-135]. In CaSR transfected HEK-293 cells other phospholipases are also activated via $G_{q/11}$ pathway such as PLA_2 which activates arachidonic acid and PLD which forms phosphatidic acid [132]

Apart from $G_{q/11}$, CaSR can also couple to $G_{\alpha i}$ which inhibits adenylate cyclase activity by reducing cAMP stimulation [129]. In transfected canine kidney cells stably expressing CaSR, it was shown that CaSR signals via $G_{12/13}$ proteins [130]. Interestingly, it has been shown that CaSR which couples to $G_{\alpha i}$ in normal breast epithelial cells, changes its G-protein preference to $G_{\alpha s}$ in two breast cancer cell lines, with a potential significance for pathogenesis of cancer via PTHrP secretion [131]. The mechanism for this is still unknown.

1.7.2. Protein Kinases:

CaSR activation has also been associated with activation of various MAPKs to induce mitogenic effects of extracellular Ca^{2+} on cells such as osteoblasts [136], ovarian surface epithelial cells [137], fibroblasts [138], opossum kidney and ovarian surface epithelial cells [81, 139, 140].

ERK1/2 activation following $G_{q/11}$ and G_i activated PLC-PKC activation by CaSR has been demonstrated in transfected HEK-293 cells and cultured human parathyroid cells [141, 142]. ERK 1/2 activation has also been attributed to PI3-K-Akt pathway in various cell types such as opossum kidney and ovarian surface epithelial cells [81, 139, 140]. How these pathways are chosen or interact to cause ERK1/2 activation is not yet established.

Others MAPK activated by CaSR are p38 in HEK-293 transfected cells, murine osteoblasts like cells and Leydig cells [143-145] and JNK in H-500 Leydig cells and canine kidney cells line MDCK [145, 146]. However, the significance of activation of different MAPKs by CaSR is not fully understood in terms of its different biological actions via different ligands. Also, how various signal transduction pathways (i.e. different G-proteins to phospholipases to different MAPK activation) synchronize dependently, or chosen exclusively based on agonist/cell type is poorly understood.

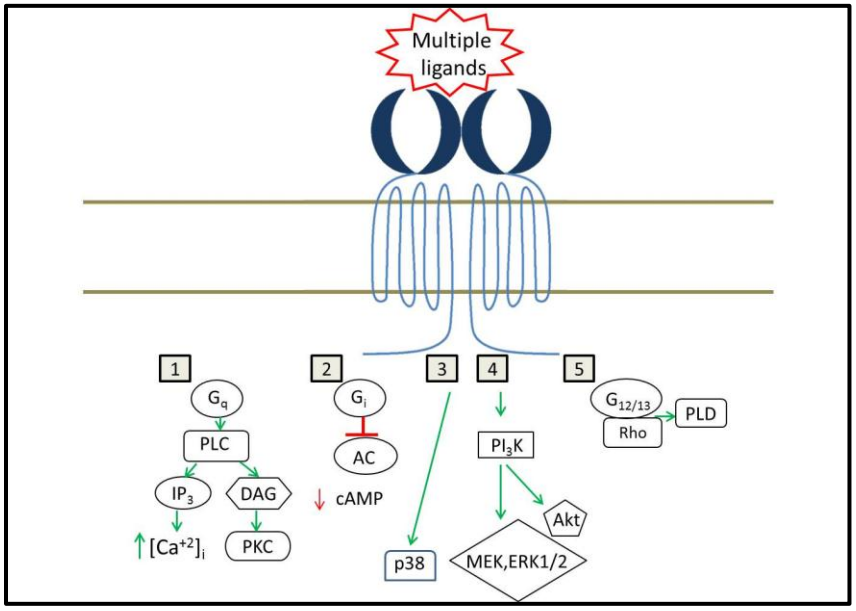

Figure 1.8: Schematic overview of signalling pathways activated by the CaSR.

1.8. Interaction of CaSR with other receptors and proteins:

1.8.1. Family C GPCRs:

Family-C GPCRs have a characteristic feature of forming homodimers or heterodimers. As already discussed, CaSR exists as homo-dimer on the cell-surface. Other family C receptors like GABA receptors are shown to form obligatory functional hetero-dimers containing GABA(B1) and GABA(B2) sub-units [147]. Also, it has been shown that Family C GPCRs can form high-order oligomers/hetero-dimers amongst themselves. CaSR and mGluR1α were co-immunoprecipitated from bovine brain and co-localized in hippocampal and cerebellar regions [148]. This interaction was confirmed in transfected HEK-293 cells where CaSR and mGluR1α or

mGluR5 formed disulphide linked dimers. Furthermore, CaSR and mGluR1α or mGluR5 heterodimer complex, exhibited glutamate sensitivity and glutamate induced internalization, as well as enhanced cell-surface expression when co-transfected with mGluR binding partner homer 1c [148].

In cultured growth plate chondrocytes, CaSR forms heterodimers with GABA(B) receptor, as shown by co-immunoprecipitation [149]. Knock-down of GABA(B) blunted high Ca^{2+} mediated PLC and ERK1/2 activation, suppressed cell proliferation and increased apoptosis, suggesting a role of CaSR-GABA(B) heterodimer for Ca^{2+} sensitivity and normal functioning of growth plate chondrocytes [149]. In another study, CaSR+GABA(B1) and CaSR+GABA(B2) heterodimer was co-immunoprecipitated from co-transfected HEK 293 cells as well as from mouse whole brain and hippocampal neurons [150]. Although CaSR could traffic to the cell-surface on its own in transfected HEK-293 cells, GABA(B2) seemed to enhance the cell-surface population of CaSR as well as PLC activation following activation by Ca^{2+}, an effect which was not observed with GABA(B1) [150]. It is noteworthy that in transfected HEK 293 cells, CaSR facilitated cell-surface expression of GABA (B1) subunit, which on its own was restricted inside the ER [150].

1.8.2. Caveolae:

Caveolae are microdomains present on the plasma-membrane, where multiple signaling molecules are concentrated. CaSR is found co-localized with caveolae, which contains $G_{\alpha q/11}$, nitric oxide synthase and several PKC isoforms in bovine parathyroid cells [151]. Caveolin-1 is phosphorylated upon activation of the CaSR [151]. In addition to bovine parathyroid cells, caveolin-1 is also co-localized in human parathyroid cells in culture, where it negatively regulates the activity of ERK1/2 [152]. This was shown by observations where the localization of phosphorylated ERK1/2 was found in caveolin-1 in normal cultured bovine and human parathyroid cells. On the contrary, in parathyroid cells cultured from adenomas, decrease in caveolin-1 expression was co-related to hyperactivity of ERK1/2 localized in perinuclear and nuclear regions. This resulted in increased cell proliferation and reduced Ca^{2+} sensitivity [152]. This suggests a role of caveolae in normal functioning of Ca^{2+} sensing of parathyroid cells.

1.8.3. Filamin A:

Filamin acts as a scaffolding protein that crosslinks actin and can directly link the cell-surface receptors to the cytoskeleton. CaSR has been shown to interact with the scaffolding protein filamin A in transfected HEK-293 and melanoma cells; and bovine parathyroid cells [153-155]. Using yeast-two hybrid system and co-immunoprecipitation method, it was shown that the residues 907-997 *(shown by black circles in figure 1.6)* of CaSR C-tail are responsible for its interaction with filamin A [153, 154]. In absence of filamin A, CaSR failed to activate ERK1/2 in CaSR-transfected melanoma and HEK-293 cells [153, 154]. However, in a different study it was demonstrated that although the CaSR C-tail truncation mutants from 962-997 failed to establish high affinity interaction with filamin A, they could still activate ERK1/2 signalling [155]. The same mutants failed to activate ERK1/2 pathway in cells lacking filamin A, implying its presence but not necessarily high affinity interaction with CaSR, a prerequisite for ERK1/2 signalling [155]. This was further explained by the evidence in transfected HEK-293 cells showing that the essential residues for ERK1/2 activation lie between 868-879 of CaSR, which were still intact in the mutants [155]. The researchers suggested that the role of filamin A is to enhance cell-surface expression of the CaSR by decreasing its degradation rate [155] (it is interesting to note that in the same study some CaSR reached the cell-surface in absence of filamin A, suggesting an alternate mechanism). Additionally, it binds and organizes components of MAPK signalling cascade [153-155].

1.8.4. Receptor Activity Modifying Proteins (RAMPs):

RAMPs are type-1 TM accessory proteins with a single TM domain, originally discovered to confer ligand binding specificity to the family B Calcitonin-like receptor (CLR) [156]. There are three isoforms of RAMPs (RAMP 1, 2 and 3) in humans [156]. It was shown that RAMP1 and 3 interact with CaSR in transfected cells to traffic the receptor to the cell-surface [157]. On studying the trafficking and surface expression of pH-sensitive green fluorescent-protein variant super ecliptic pHfluorin (SEP)-CaSR, it was observed that this phenomenon differed markedly in transfected HEK-293 cells and COS-7 cells. In COS-7 cells the SEP-CaSR could not exit ER where it was trapped in immature core glycosylated form, whereas it displayed robust expression on

plasma membrane in HEK-293 cells. Using immunocytochemistry, co-immunoprecipitation and siRNA approaches, it was discovered that in HEK-293 cells the endogenously expressed RAMP1 facilitated the cell-surface trafficking of the CaSR [157]. It was subsequently discovered RAMP3 was also a partner of CaSR with the same functional consequence [157]. On the other hand, expressing RAMP1 or 3 in RAMP-negative COS-7 cells, facilitate the cell–surface expression of the otherwise ER-trapped CaSR. So, interaction of CaSR with RAMP1 and RAMP3 but not RAMP2 is essential for its cell-surface trafficking in HEK-293 and co-transfected COS-7 cells [157]. It was shown that RAMPs facilitated glycosylation of CaSR, thereby trafficking it to the plasma membrane [157]. However, other functional consequences like signalling were not tested in this study. The proposed working model of this interaction is shown in the figure 1.9 below:

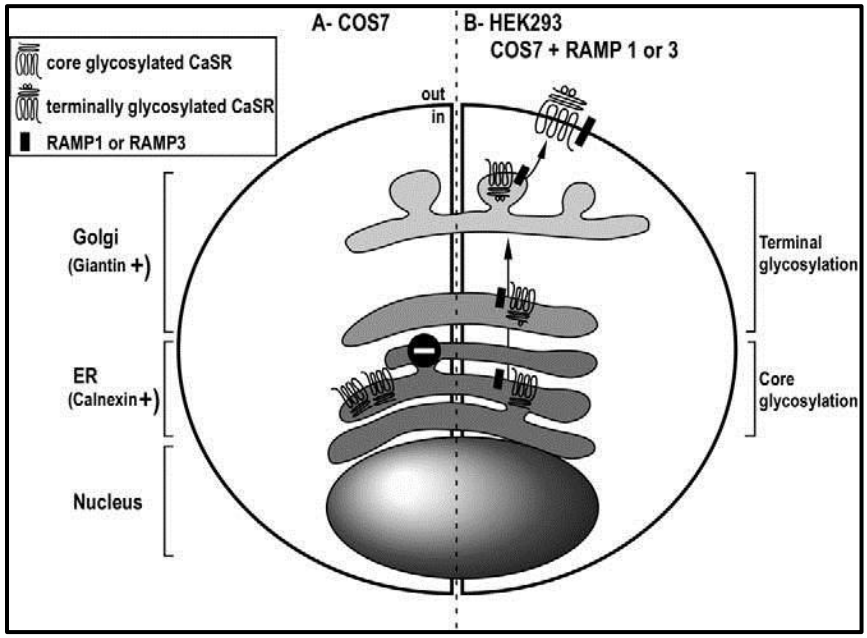

Figure 1.9: Proposed model for RAMP regulation of CaSR trafficking:
(A) In absence of RAMP1/3, CaSR is retained inside the ER in core-glycosylated form in COS-7 cells; whereas (B) in HEK-293 cells, expressing RAMP1 endogenously, or in COS-7 cells transfected with RAMP1/3, their association with CaSR bypasses the ER retention and reaches Golgi apparatus where it is terminally glycosylated, followed by cell-surface delivery of the receptor complex. Image reproduced/adapted with permission of "Journal of Cell Science" from the paper [157].

Another family C GPCR known as the GPCR6A also showed a similar failure of cell-surface expression when transfected alone [158, 159]. Given below is the background information on the receptor.

1.9. GPRC6A and its role in physiology:

GPRC6A was identified using homology searches of all known family C GPCRs [158]. cDNA cloning using human kidney cDNA library revealed three isoforms of the receptor containing 6 exons. Isoform 1 is 926 aa in size with 7 TM domains and a large 590 aa N-terminal domain, whereas isoforms 2 and 3 are smaller and naturally occurring splice variants of the receptor [158]. GPRC6A has 34% aa sequence identity to the CaSR, 28% aa identity to the taste receptor 1, 24% aa identity to mGluR1 and 45% identity with odorant goldfish receptor 5.24 [158].

It has been observed using c-myc tagged hGPRC6A that the receptor is poorly expressed on the cell-surface of transfected HEK 293 cells when compared to $GABA_BR$, whereas there is no cell-surface expression of the receptor in CHO and COS-7 cells [158, 159]. However, it has been reported that the mouse-GPRC6A trafficked to the cell-surface more efficiently than the human-GPRC6A in transfected HEK-293 cells [159].

GPRC6A is highly expressed in kidneys, heart, liver, skeletal muscle, testis, spleen, leucocytes and at comparatively lower levels in brain, pancreas, bone, calvaria, placenta and lung, suggesting its role in various physiological processes [158, 160, 161].

Nutrient sensing

The role of GPRC6A in nutrient sensing has mainly been related to its promiscuity to sense L-aa and its expression in gut [159, 160]. GPRC6A along with CaSR have been localized in rat gastric somatostatin-secreting D cells [162]; and in the rat gastric antrum which contains gastrin secreting cells [163]. It was observed that mouse GPRC6A transfected in oocytes elicited inward current for intracellular Ca^{2+} activation on exposure to L-aa such as arginine, lysine, serine, alanine, glycine , ornithine, cysteine and histidine in the presence of 0.5mM extracellular Ca^{2+} [159, 160]. Similar results were obtained when a chimeric receptor containing human-GPRC6A ECD and TM domain and C-tail of closely related odorant receptor 5.24 from fish was expressed

in oocytes [159], which also indicate that the ECD of GPRC6A is sufficient for nutrient sensing. GPRC6A has also been reported to be present in type 1 taste cells along with CaSR in murine taste tissue; however the role of GPRC6A in taste perception is not yet elucidated [164].

Bone and bone-pancreas endocrine loop

Apart from being an L-aa sensing receptor, GPRC6A also responds to cations including Ca^{2+}; leading to speculations of it being an alternative CaSR [165]. It was shown in HEK-293 cells overexpressing GPRC6A that Ca^{2+}, magnesium, gadolinium, aluminium and NPS-R568 (an allosteric activator of CaSR) caused ERK phosphorylation via a $G_{\alpha q}$ and $G_{\alpha i}$-mediated pathway [165]. Furthermore, alignment of CaSR with GPRC6A has shown that the Ca^{2+} and NPS-R568 binding sites are conserved in GPRC6A [165]. However, differences in affinities of these shared agonists exist between GPRC6A and CaSR. For example higher levels of extracellular Ca^{2+} were required to activate GPRC6A as observed by increased ERK phosphorylation (minimum 5mM) and intracellular Ca^{2+} (40mM), in comparison to ~3mM for CaSR. This strongly suggests lower affinity of GPRC6A for Ca^{2+}, which is much higher than its circulating levels [165]. The role of GPRC6A in bone biology has been shown by deletion of the gene in mice. It was observed by Pi *et al* that *Gprc6a*$^{-/-}$ mice lacking exon 2 (codes for ECD) exhibit osteopenia and decreased bone mineral density (BMD), due to impaired bone mineralization [161, 166]. This is associated with reduced expression of osteoblast function markers like osteocalcin, alkaline phosphatase (ALP), Runx2 and osteoprotegerin [166]. *Ex vivo* cultures of the primary osteoblasts and bone marrow stromal cells derived from these *Gprc6a*$^{-/-}$ mice, displayed an attenuated response to extracellular Ca^{2+}-stimulated ERK activation, diminished ALP expression and impaired mineralization [166]. On the contrary, an earlier study by another group (Wellendorph *et al*) using TM domain and C-tail lacking *Gprc6a*$^{-/-}$ mice of the same strain, showed that there was no difference in bone phenotype between knock-out and wild type mice; consequently not suggesting a role of mGPRC6A in osteoblasts [167]. Although the reasons for these contrasting observations are currently unknown, the effects of different mutant mGPRC6A forms (TM+C-tail deletion vs ECD deletion) might vary [166].

In addition to the abnormal bone phenotype, the exon-2 lacking *Gprc6a*$^{-/-}$ mice also exhibit metabolic disorders such as hepatic steatosis (fatty liver), hyperglycaemia, glucose intolerance and insulin resistance as well as increased renal Ca^{2+} and phosphorous excretion [161]. These defects were linked to malfunctions in energy metabolism caused by aberrant osteocalcin function, which is a ligand of GPRC6A [161, 168]. Osteocalcin is an osteoblast-specific secreted molecule, which has been shown to be involved in the bone-pancreas endocrine loop. Insulin signalling in osteoblasts promotes osteocalcin production as well as maturation [169]. The matured osteocalcin acts on the β-cells of pancreas where it increases insulin secretion and consequently insulin sensitivity, thus forming a feed-forward loop integrating bone function and energy metabolism [169]. Recently it has been shown both *in vitro* and *in vivo* that osteocalcin activated mGPRC6A-mediated ERK activation in β cells of pancreas leading to increased insulin secretion [168]. Accordingly, the metabolic disorders in the exon-2 lacking *Gprc6a*$^{-/-}$ mice are largely associated with the disrupted osteocalcin-endocrine loop [161, 168].

Testosterone mediated physiological functions:

GPRC6A is also linked to functions of testosterone as shown by *in vitro* and *in vivo* studies [161, 170, 171]. The exon-2 lacking *Gprc6a*$^{-/-}$ male mice show decreased lean body mass, increased mammary pad fat mass, decreased weight and size of testes and seminal vesicles, increased circulating levels of estradiol and reduced levels of testosterone [161]. These mice exhibited decreased ERK activation in bone marrow and testis in response to testosterone [170].

These effects are supported by *in vitro* studies where hGPRC6A transfected in HEK-293 cells and natively expressing in mouse prostate cancer cell line 22Rv1, showed increased ERK phosphorylation and enhanced 22Rv1 cell proliferation in response to permeable and impermeable form of testosterone [170]. This effect was attenuated by GPRC6A siRNA-mediated knock-down [170].

Taken together it is suggested that, GPRC6A might coordinate the anabolic responses of various tissues through the sensing of extracellular aa, osteocalcin, divalent cations and androgen [161].

1.10. RAMPs and their interacting partners:

RAMPs were discovered to engender ligand-binding specificity to a previously thought orphan Family B GPCR for Calcitonin Gene Related Peptide (CGRP) known as the Calcitonin Like Receptor (CLR) [156]. Three RAMPs – RAMP1, 2 and 3 have been discovered. RAMP1 was discovered first by measuring CGRP responses in oocytes transfected with cDNA of human neuroblastoma cell line- SK-N-MC. It was shown that when CLR interacted with RAMP1, it formed a functional receptor complex for CGRP. Subsequent database searches for RAMP1 ESTs discovered RAMP2 and 3 [156]. However, when CLR interacted with RAMP2 or RAMP3, it formed two pharmacologically distinct receptor phenotypes for another peptide hormone belonging to the calcitonin family known as Adrenomedullin (AM) [156]. RAMPs 1-3 are responsible for trafficking of CLR to the cell-surface, altering ligand binding specificity and signal transduction following receptor activation [156].

In addition to CLR, RAMPs are shown to associate with other GPCRs. Interacting partners of RAMPs discovered so far are summarized in the table below:

GPCR	RAMP	Consequence
CLR	RAMP 1, 2, 3	CLR+RAMP1= functional CGRP receptor CLR+RAMP2/3 = functional AM receptor
CTR	RAMP1,2,3	Each RAMP form distinct amylin receptors
VPAC1	RAMP 1,2,3	VPAC1+RAMP2 show enhanced PI hydrolysis
PTH1R	RAMP2	unknown
PTH2R	RAMP3	unknown
GlucR	RAMP2	unknown
Secretin	RAMP3	No change in signalling and internalization of the receptor.
CaSR	RAMP1,3	Essential for cell-surface trafficking of the receptor.

Table 1.2: GPCR interacting partners of RAMPs

RAMPs associate with another Family-B GPCR known as Calcitonin receptor (CTR) and completely change the receptor phenotype to a receptor binding the hormone amylin [172]. Accordingly, RAMP 1-3 interact with CTR and bind amylin, giving rise to different amylin receptor phenotypes [172, 173]. Also, receptor derived by RAMP1 and 3 and CTR interaction

also shows moderate affinity for CGRP. However, binding of CT does not require association of CTR with any RAMPs [172, 173].

Other interacting partners of RAMPs from family B GPCRs have also been discovered using immunocytochemistry technique on overexpressed tagged RAMPs and receptors in COS-7 and HEK 293 cells [174]. It was found that Vasoactive Intestinal peptide/ Pituitary Adenylate Cyclase–activating peptide (VPAC-1) receptor interacts with all three RAMPs [174]. VPAC-1R/RAMP2 complex displays enhanced agonist mediated PI hydrolysis without any change in cAMP stimulation compared with VPAC-1R alone, indicating alteration of signaling pathway by RAMP2 [174]. Parathyroid hormone -1 receptor (PTH 1R) and glucagon receptor interact only with RAMP-2, while PTH 2R with RAMP3, however functional consequences these interactions were not studied [174]. The same study also showed that VPAC2R, growth hormone releasing hormone (GHRH), glucagon-like peptide 1 (GLP1) and GLP2 receptors do not interact with RAMPs [174].

Another study has shown using bioluminescence resonance energy transfer (BRET) that secretin receptor interacts specifically with RAMP3 via the TM6 and TM7 domain of the receptor and not RAMP1 and 2 in COS-7 and CHO cells [175]. Functionally, there was no change in signalling or internalization of the secretin receptor in presence of RAMP3 [175]. Also, RAMP3 could rescue a mutant secretin receptor that is normally trapped inside the cell, showing a chaperone role of RAMP3. The study also reported that increasing secretin receptor levels in cells already expressing RAMP3 and CLR (AM2 receptor), decreased functional AM2 receptors and increasing secretin-RAMP3 interaction, demonstrating the competition for RAMP by GPCRs to form other functional molecular interactions [175].

In the case of family C GPCRs, only CaSR has been identified as a receptor partner of RAMP1 and RAMP3 [157] as discussed before in section 1.8.4.

Since RAMPs are more widely distributed in the body than their known interacting partners (see section 1.14), there is a strong possibility that there are yet unidentified GPCR partners of RAMPs.

1.11. Structure of RAMPs:

RAMPs are type-1 trans-membrane proteins and share 30% similarity in their primary aa sequence [156]. RAMP1 and 3 are 148 aa long while RAMP2 is 175 aa long [156] (Figure 1.10). Each RAMP has a short C-terminal domain of ~10 aa and a single TM domain of ~20 aa. The rest of the protein consists of an ECD with a signal peptide [176] . RAMP1 and RAMP3 have six conserved cysteine residues, four of which are common to RAMP2 [177] (Figure 1.10). In 2008, the crystal structure of RAMP1 ECD (figure 1.11) was reported, which suggested that RAMP1 ECD consists of three α helices stabilized by 3 disulphide linkages formed by six cysteine residues [178] which is similar to recently reported ECD of RAMP2, which has 2 disulphide linkages instead [179]. There are consensus sites for N-glycosylation in RAMP-2 (one site) and RAMP-3 (three sites) which are glycosylated, whereas RAMP1 is unglycosylated [180, 181](Figure 1.10).

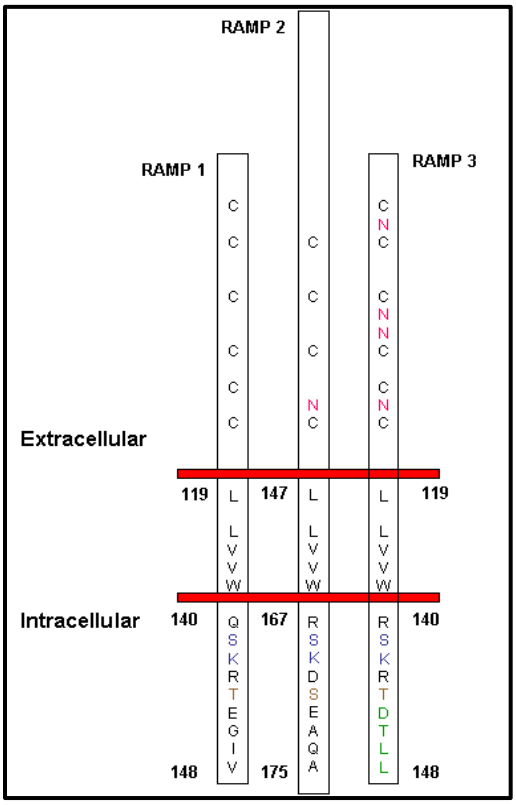

Figure 1.10: Structural comparison of RAMPs:

RAMP 2 is the least conserved and is 26aa longer than RAMP1 and RAMP3. The conserved cysteine residues (C) in the extracellular domain are shown. N-terminal glycosylation sites (N) is shown in pink colour. Amino acids in trans-membrane domain are conserved. Conserved Ser-Lys (S,K;blue) are shown in intracellular region. Putative phosphorylation sites (threonine in RAMP 1 and 3, and serine in RAMP2)

are shown in brown; PDZ binding motif in RAMP3 is shown in green. Adapted from [176] and re-drawn by self.

Various structural features of RAMPs contribute towards their specific functions. Majority of findings explaining molecular mechanisms of function of RAMPs are based on studies with the CLR and CTR.

1.12. Interspecies variance:

RAMP genes have been cloned and sequenced from the mouse, rat and human genomes [182, 183]. Amino-acid sequence identity observed between mouse and human RAMP1, RAMP2 and RAMP3 is 70%, 68% and 84% respectively [182]. Mouse RAMPs show 90% sequence identity with their counterparts in rats.

The effect of sequence differences between RAMPs was demonstrated using pharmacological studies on receptor complexes formed by RAMPs from one species and receptor from another and comparing the results with same-species combinations. It was shown that human RAMP2/rat CLR had a lower affinity for CGRP antagonist ($CGRP_{8-37}$) and AM antagonist (AM_{22-52}); than all-rat and all-human RAMP2/CLR complex, as measured by cAMP responses [184]. It was shown that hRAMP1 had a higher affinity to form complex with rCLR compared to hRAMP2 [185]. This was shown when a AM binding to AM receptor formed by co-transfected hRAMP2 and rCLR in rat osteoblasts UMR 106-06 cells, was reduced by 50% on co-transfection with hRAMP1 with a parallel increase in CGRP binding [185].

In the case of mouse RAMPs, there is discrepancy between the affinity of RAMP3 compared to RAMP1/2 to form complex receptor with rCLR [182]. Co-expression of mRAMP1 and 2 with rCLR revealed distinct CGRP or AM receptors, with a similar level of interaction with rCLR. This suggests that structural difference does not have an effect on the functions of RAMP1 and 2 in mouse [182, 183]. Co-transfection of RAMP1 and 3 or RAMP2 and 3 into COS-7 cells with rCLR, led to similar levels of ligand binding as RAMP3 alone (with rCLR); suggesting that in these cells, RAMP3 has a greater affinity than other RAMPs to form a receptor-complex with the rCLR [182]. The physiological significance of these pharmacological differences due to species

variation of RAMPs is not explained yet. Detailed information regarding the differences in pharmacological profiles between human CGRP, RAMP and AMY receptors is given later.

1.13. Molecular mechanisms of RAMP function:

1.13.1. Receptor chaperones:

As described earlier, RAMPs are essential for cell-surface trafficking of CLR in order to form CGRP receptor or AM1 and AM2 receptors as discovered by visualizing the internalization of tagged receptors following agonist treatment as well as performing signalling studies in transfected cells [156, 186]. The cell-surface trafficking property of RAMPs is related to the conserved cysteine residues on their N-terminal domain [181, 187]. The conserved cysteine residues of RAMPs are shown to form disulphide linkages suggesting common secondary structures of 3 helices like the crystal structure of RAMP1 ECD as mentioned earlier (Figure 1.11). Mutational analyses have shown that loss of four conserved cysteine residues on RAMPs significantly compromised the cell-surface trafficking of the CLR [181, 187]. Further loss of two cysteine residues in RAMP1 which are conserved in RAMP3 but not RAMP2 do not affect the cell-surface trafficking efficiency of RAMP1 [188], whereas no study has been done to understand the loss of all the cysteine residues of RAMP3. Also, substitution of histidine residues 124 and 127 of RAMP2 with alanine, impaired the cell-surface delivery of CLR [189]. It was shown by studies in transfected HEK-239T cells, that RAMPs promoted fully-matured glycosylation of CLR that represented the functional CGRP/AM receptors on the cell-surface and which selectively bound their respective ligands; whereas the core-immature glycosylated forms were not ligand-bound [190].

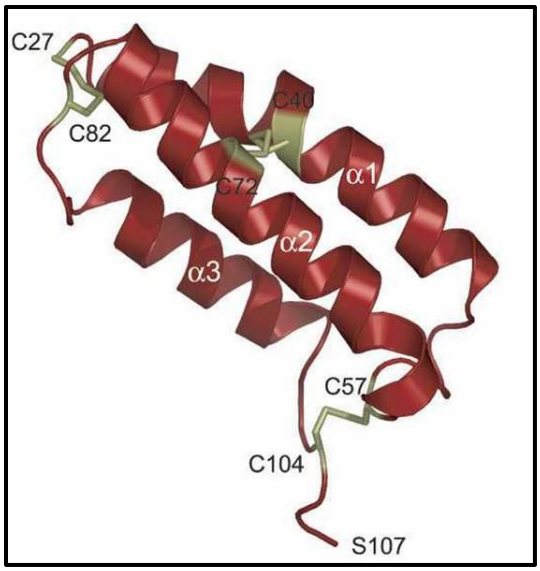

Figure 1.11: 3D ribbon structure of RAMP1 ECD:
3 α helices (α1, α2 and α3) are shown in red and the disulphide linkages (C: cysteine residues) are shown in yellow [178]. Taken with permission from "John Wiley and Sons". License number 2785851499230.

In addition to the essential requirement of the N-terminal domain of RAMPs, studies have also shown the importance of C-tail in the function of receptor trafficking. It has been suggested using HEK-293 cells transfected with tagged RAMPs, that the C-tail of RAMP2 is important for cell-surface expression of CLR, as deletion of C-tail of RAMP2 (last 9 aa) led to disruption of CLR trafficking to the cell-surface and consequently receptor function, whereas the deletion of RAMP1 or 3 C-tail did not disrupt the trafficking of the CLR [191]. Interestingly exchanging the C-tails of RAMP2 and 3 with each other did not cause any change in cell-surface expression and agonist mediated internalization of the CLR RAMP complex indicating the importance of the conserved Ser-Lys residues present in the C-tail of RAMPs (figure 1.10), in cell-surface trafficking of the two AM receptors [191]. In stark contrast to this, another study showed that untagged-RAMP2 C-tail deletion mutant lacking last 8 aa, showed responses similar to wild type RAMP2 to AM when co-transfected with CLR in COS7 cells; whereas there was a slight decrease in efficacy for the same in HEK 293 cells. This indicates the differential behavior of RAMPs due to different cell backgrounds and possibly due to the number of aa deleted (9 vs 8) [192].

Furthermore, cell-surface trafficking of RAMPs alone without any presence of a GPCR partner also varies amongst different isoforms [156, 193]. It has been shown that RAMP1 cannot traffic to the cell-surface on its own [156, 193], whereas RAMP2 and 3 can, with RAMP3 showing greater cell-surface expression levels [174, 180]. RAMP1 is present as a disulphide-linked homodimer inside the ER and the Golgi bodies in absence of an interacting receptor [156, 193]. RAMP1 contains QSKRT sequence adjacent to the TM domain which acts as an intracellular retention signal and prevents GPCR-independent cell-surface trafficking, as shown by co-immunoprecipitation and immune-fluorescence techniques on tagged deletion mutants of RAMP1 [194]. Accordingly, it was shown that the deletion of last 8 aa of the C-tail of RAMP1 containing the retention sequence increased receptor-independent cell-surface expression of c-myc RAMP1 in HEK 293 cells compared to the wild-type RAMP1 [192].

Mutational analyses have shown that N-glycosylation status of RAMP2 and 3 is responsible for their GPCR-independent trafficking [180]. It was also shown that by the introduction of N-glycosylation sites in RAMP1 (which natively lacks any), caused its GPCR-independent cell surface expression, a characteristic which is not seen in wild type RAMP1 [180]. Studies using N-tagged RAMP2 and 3 have shown their GPCR independent cell-surface expression, however the effect of the tag towards the phenomenon has not been addressed [174, 180]. It is not known yet whether RAMPs are able to form heterodimers. If they do, there can be an additional possible explanation to the differences in the pharmacology CLR receptor phenotypes resulting from RAMPs from different species, as discussed earlier (section 1.12). Accordingly, the difference in affinities to form complex receptors amongst RAMPs that is observed might not due to competition of the RAMP interaction with CLR, but competition of the interaction between the RAMPs themselves.

1.13.2. Modulating receptor-ligand binding specificity and affinity:

RAMPs are known to engender distinct pharmacological profiles to CLR or CTR on the basis of functional interaction of their different isoforms [156]. Thus, they provide a novel mechanism for modulating receptor specificity which is completely different from the classical one-receptor-one ligand understanding.

Pharmacology of recombinant GPCR/RAMP receptor complexes:

The receptor phenotypes formed by RAMPs are able to bind different ligands with varying affinities and potencies. This shows that RAMPs not only form distinct functional receptors, but also modulate their pharmacology. When RAMP1 associates with CLR it binds CGRP, whereas RAMP2 or 3 on association with CLR, form two distinct receptors for AM with similar potencies to activate cAMP (AMR1 and AMR2) [184][165]. Interestingly, AMR1 has ~100 fold higher affinity for AM than CGRP and so is specifically selective for AM binding only; whereas AMR2 has a higher affinity for CGRP than AMR1 (by ~180% [165]) and so it binds AM preferentially. However, the pharmacology of these receptors does differ depending on the species and isoforms of CGRP (α and β) [184].

The decreasing order of relative binding affinities for CGRP, AM and AMY for their respective receptor types, as determined using competitive inhibition experiments for radiolabelled-ligand binding in various studies, is shown in the table below: [156, 195]:

Receptor subtype	Receptor composition	Pharmacology	References
CGRP	CLR+RAMP1	βCGRP ≥ αCGRP > αCGRP $_{(8-37)}$ (antagonist) > AM >> AM $_{(22-52)}$ (antagonist)	[156, 195]
AMR1	CLR+RAMP2	AM > AM$_{(22-52)}$ > αCGRP$_{(8-37)}$ ≥ βCGRP > αCGRP	[156, 195, 196]
AMR2	CLR+RAMP3	AM> AM$_{(22-52)}$ = αCGRP$_{(8-37)}$ = βCGRP > αCGRP	[164, 165]
AMYR1	CTR+RAMP1	AMY > βCGRP > αCGRP > CT > AM	[172, 173, 197]
AMYR2	CTR+RAMP2	AMY = CT > αCGRP	[172, 173]
AMYR3	CTR+RAMP3	AMY > βCGRP > αCGRP > CT =AM	[172, 173, 197]

Table 1.3: Decreasing order of relative binding affinities of ligands at different receptor complexes formed by RAMPs.

In the case of AMY receptors, AMYR1 and AMYR3 have a higher affinity for amylin than AMYR2 (~3.5 fold vs AMYR1; ~4.6 fold vs AMYR3) [172, 197]. Human AMR1 has a higher affinity for αCGRP than βCGRP, whereas AM3R exhibits equal affinities [187]. However, it has been recently shown that rat AMR1 has a higher affinity towards αCGRP than βCGRP compared to human AMR1 and rat AMR3 has a higher affinity for α and β CGRP than CT compared to human AMR2 [198]. Also, rat AMR3 exhibits higher affinity towards $\alpha CGRP_{(8-37)}$ than rat AMR1 [198]. This shows that species variation exist amongst AMY receptor phenotypes and so it is important not to assume that there will always be a direct translation of observations between different species.

The molecular mechanisms for all the above stated interactions has not been deciphered yet, although there is more information on CGRP and AM binding to their receptors, through the recent advances in RAMP biology.

Structural features of RAMPs responsible for ligand binding:

Many studies have determined that the extracellular N-terminal domain of RAMPs is essential for ligand binding of the CLR [190, 196, 199]. In fact, recent studies have deciphered the crystal structures of RAMP1/2 ECD in complex with CLR ECD, hence giving a very detailed information about the residues important in forming the ligand binding pocket as described later [179, 200].

Initial work using immunoprecipitation of tagged CLR+RAMP complexes which were cross-linked to their respective radio-labeled ligands showed that the radiolabelled CGRP was incorporated into RAMP1 whereas radiolabelled AM was incorporated into RAMP2 or RAMP3. This suggested that the RAMPs form or lie in close proximity of the ligand binding pocket in complex with CLR [190]. Further ligand binding and deglycosylation experiments using wild type and chimeric RAMP (N-terminal RAMP1/TM domain, C-tail RAMP2 and vice versa) constructs showed that the N-terminus of RAMPs, engendered specific ligand selectivity of CLR by modulating its glycosylation status from immature to mature glycosylated form [196].

The importance of the ECD for ligand binding for RAMP1 was shown using chimeric receptor approaches, where the N-terminal domain of RAMP1 attached with the TM domain and C-tails

of PDGF receptor could form stable receptor complex with CLR and respond to cAMP upon stimulation with CGRP [201]. The cell-surface expression levels of CLR with this RAMP1 mutant were ~30% less than with the wild-type RAMP1; whereas they were decreased by 50% when expressed with RAMP ECD alone (with 21 aa removal containing TM domain and C-tail and no PDGF TM domain and C-tail attached) [201]. However, the affinity and potency of these chimeric mutants for CGRP binding were compromised significantly (~10 fold vs WT in the case of RAMP1-ECD+PDGF; and 4000 fold for RAMP1 ECD alone vs WT), suggesting that the ECD with the TM domain alone or with the C-tail is responsible for achieving full biological affinity and potency of CGRP binding [201]. These results were in contrast to an earlier report where deletion of 20 aa out of the total 22 aa of the TM domain along with the C-tail rendered non-functional CGRP receptor [194]. Although the discrepancy between both results is not known, it was hypothesised that difference in sizes (shorter by one aa than in [201]) of mutant RAMP1 constructs between both studies could have been the cause [201].

Subsequent studies using RAMP1 mutants with deletions in the ECD, identified regions 91-94, 96-100 or 101-103 (in the α helix 3 according to the crystal structure) likely to be important for CGRP binding [199]. However, individual residue substitution with alanine did not effect CGRP binding indicating that these residues are not directly involved in CGRP binding but might contribute to forming ligand binding pocket [199]. Similar studies using deletion mutants of RAMP2 and RAMP3 identified aa 86-92 of RAMP2 and 59-65 of RAMP3 responsible for AM binding, without affecting cell-surface trafficking [202]. However, individual substitution of these aa in RAMP2 did not cause any change in AM binding and cAMP stimulation indicating that AM does not bind directly to these residues and so it is speculated that in both RAMP2 and RAMP3; these aa are conserved and might contribute in forming ligand binding pocket [202].

Recently, the crystal structure of RAMP1 ECD in complex with CLR ECD has been reported [200]. Accordingly, the α2 and α3 helices of RAMP1 form a complex with αC_1 of CLR through electrostatic and hydrophobic interactions and this interaction does not cause a significant conformational change in the arrangement of the CLR ECD (figure 1.12 A) [200, 203]. It has been shown that out of the residues responsible for interaction between RAMP1 and CLR,

alanine substitutions of Y66, F93 and H97 residues of RAMP1 resulted in decreased CLR trafficking, whereas, F101 caused reduction in potency of CGRP, indicating that these residues are important in forming CGRP receptor [203]. It has also been demonstrated that the CGRP receptor antagonists olcegepant (BIBN4096BS) and telcagepant, form hydrophobic interactions with Trp 74 of α helix-2 of RAMP1, and Thr 122 and Trp 72 of CLR ECD, thus showing that the binding pocket is formed of shared residues from both RAMP1 and CLR (figure 1.12 B). [200].

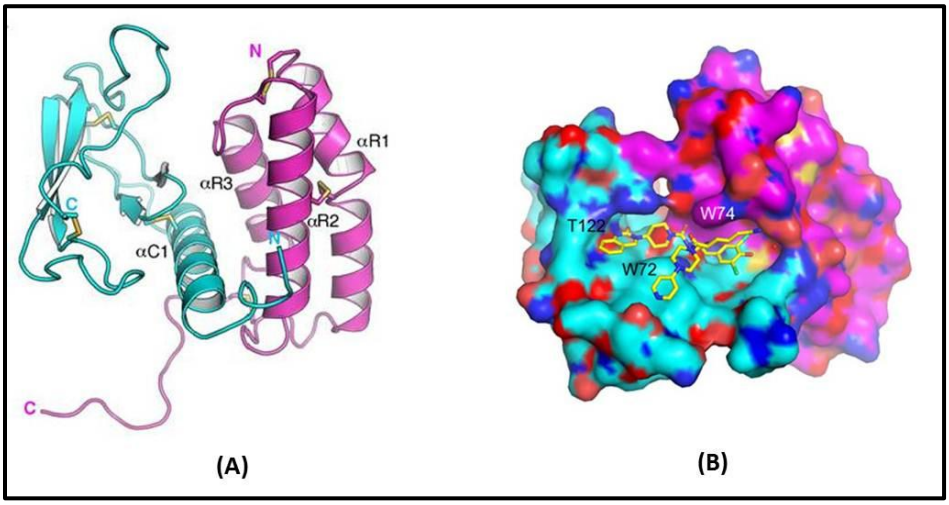

Figure 1.12: 3D ribbon structure of CLR/RAMP1 ECD complex:
(A)CLR is shown in cyan and its single α helix is labeled as αC1. RAMP1 is shown in purple and the three α helices are labeled αR1, αR2 and αR3. Disulphide linkages are shown in yellow. (B) Binding of olcegepant (BIBN4096BS) (yellow) in the bonding pocket on CLR RAMP interface with residues Trp 74 on RAMP1 (purple) and Thr 122 and Trp 72 of CLR (cyan). Taken from [200]. License numbers: 2844920493600 (A) & 2844930605496 (B).

Precise information is now available for ligand binding pocket in case of CLR+RAMP2 receptor complex as well [179]. Crystal structure of CLR+RAMP2 ECD has shown that RAMP2 α2 and α3 helices interact with CLR α1 helix through a number of hydrophobic interactions. Residues Trp72, Phe92 and Trp121 on CLR (loops 2, 3 and 5 respectively) interact with RAMP2 specific residues Glu101, Leu109 and Phe111 located on α2 helix and form pocket, not observed in RAMP1 (shown by dotted line in fig 1.13) and are likely to form ligand binding pocket for AM. So, due to this difference of interacting aa on the CLR and RAMP2 interface compared to

RAMP1; there is a change in shape of the ligand binding pocket due to RAMP2 specific residues which engenders ligand specificity [179].

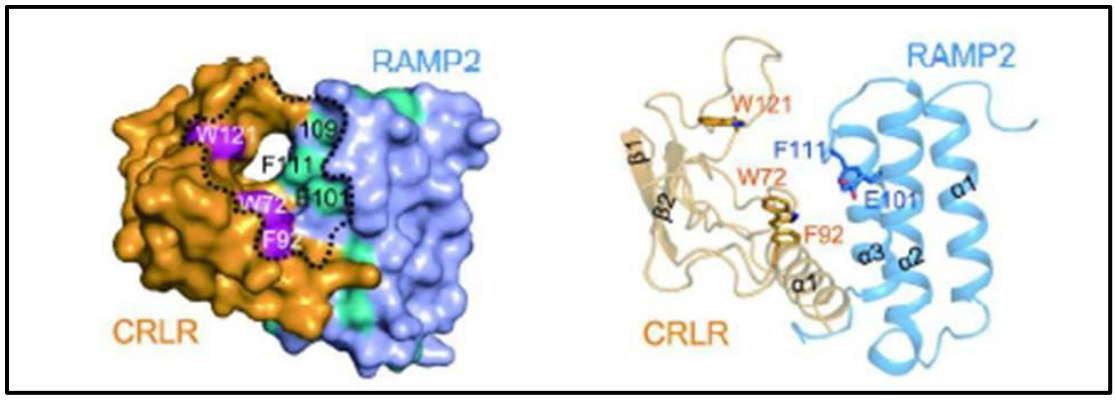

Figure 1.13: Putative AM ligand binding pocket on CLR+RAMP2 ECD:
Molecular surface (L) and ribbon structure (R) representation of putative CLR+RAMP2 ligand binding pocket [179]. License number 2797640916031.

Taken together, from both the crystal structures (CLR+RAMP1/2 ECD), a two domain model where both CLR and RAMP residues are involved applies for ligand binding specificity.

It is interesting to note that the residue Trp 74 in RAMP1 is not involved in βCGRP binding as shown by substitution mutagenesis [204, 205]. On the other hand, the substitution increased the potency of the CLR+RAMP1 receptor for AM by about ~10 fold [204, 206]. Substitution of the corresponding conserved residue on RAMP3 Glu74 to Trp caused an attenuation of AM potency at AMR2 by ~9-10 fold without any change in βCGRP potency [204-206]. It has been explained that the Glu at this position in RAMP3 has a higher negative charge which probably creates favorable electrostatic or hydrogen interactions with AM, enhancing its binding [206]. Mutagenesis of the corresponding residue in RAMP2- Glu101 completely abolished the trafficking and consequent AM stimulation of the AMR1 [204]. These results suggested that position 74 in RAMP1 and RAMP3 and 101 in RAMP2 are important determinants of differential AM binding affinities for the CGRP and AM1/AM2 receptors.

The importance of an aromatic residue at the position 84 in RAMP1 and 3 and 111 in RAMP2 is hypothesised to be responsible for the interaction of the RAMP-receptor complex with the peptide-ligand [207, 208]. The aromatic aa Trp located at position 84 on the loop joining α2 and

α3 helices of RAMP1, is shown to be important for the normal potency for cAMP response of CGRP, $CGRP_{(8-37)}$ and non-peptide CGRP antagonists at the CGRP receptor, as discovered using alanine mutagenesis [207]. This residue along with Trp 74 is shown to be a part of the hydrophobic binding pocket on the RAMP1 and CLR ECD interface [204]. This residue is conserved in RAMP3; whereas is replaced by another aromatic aa Phe at position 111 in RAMP2. Archbold *et al*, have hypothesised that these aromatic aa could be important for interaction with the C-terminus of the peptide ligands via pi-pi bonds for all CLR/RAMP receptor complexes [208]. Taken together, small but specific aa differences between different RAMPs might affect peptide affinity possibly by differentially interacting with the C-terminus of the peptide [208].

1.13.3. Role of RAMPs in receptor regulation:

RAMPs play a role in regulation of the receptor complex following agonist stimulation [186, 209]. Initial studies showed that CGRP receptor and AMR1 and 2 internalized with similar kinetics following agonist stimulation as observed by visualization of the tagged CLR co-transfected with different RAMPs in HEK-293 cells using fluorescence microscopy; as well as by performing radiolabelled-ligand binding assays following agonist treatment to check for the number of remaining receptors on the cell-surface [186]. It was further shown that following agonist stimulation, CLR+RAMP complexes were internalized and targeted to lysosome mediated degradation mainly through clathrin-dependent pathway and sufficient recycling of any receptor combination complexes was not observed [186]. A separate study investigating the CLR+RAMP1 complex showed the same result and further reported that the internalization was probably β-arrestin and dynamin dependent [193].

However, RAMP3 is unique in this regards than RAMP1 or 2. It contains a PDZ-binding motif on its C-tail, which can bind to a chaperone called N-ethylmaleimide sensitive factor (NSF); as determined by co-localization and overlay assay [209]. This results in recycling of the AMR2 instead of degradation as measured by the recovery of cAMP generation and ligand binding following an initial drop post agonist stimulation in transfected HEK-293 cells; an effect not observed with AMR1 and CGRP receptors [209]. This effect was also confirmed in rat fibroblast

cells which natively express NSF and RAMPs, where RAMP3 siRNA knock-down or adding NSF-inhibitor, prevented the recycling of the receptor complex [209]. Another such interacting partner to the PDZ-domain of RAMP3 is the Na^+/ H^+ exchanger regulatory factor -1 (NHERF-1), an adaptor protein that prevents the internalization of the receptor complex. It was observed in HEK-293 cells transfected with AMR2 components and NHERF-1, that following agonist stimulation, AMR2 was desensitized as measured by a decrease in cAMP activation; however radioligand binding studies showed that the number of binding sites did not change, which meant that the AMR2 did not undergo internalization [210]. Knock-down of RAMP3 or NHERF-1 in human proximal tubule cells endogenously expressing these proteins, prevented the inhibition of internalization following agonist treatment as observed in the wild-type cells [210]. Such interactions were not observed for RAMP1 or 2 suggesting a functional difference between AM receptor 1 and 2. The C-tail of RAMPs also contains phosphorylation and ubiquitination sites (figure 1.10) but their role in receptor trafficking is not yet known [191].

1.13.4. Role of RAMPs in receptor signalling:

There is increasing evidence showing a role of RAMPs in signalling of some its GPCR partners [174, 192, 211]. The C-tail of RAMPs has been shown to play a significant role in signalling of the AMY receptors by probably involving direct G-protein coupling, as shown by studies COS-7 cells co-transfected with C-tail mutant RAMP and CTR [192, 211]. VPAC1 receptor signalling is also modulated by RAMPs. It was shown that VPAC1 receptor interacts with all RAMPs, however only its association with RAMP2 in COS-7 cells, causes augmentation in efficacy of PI hydrolysis by VIP with no change in efficacy for cAMP generation, ligand binding affinity and potency, when compared to VPAC1 receptor alone [174]. Our group has shown that there is a decrease in efficacy of $G_{\alpha i}$ and not $G_{\alpha q}$ activation when VPAC1 receptor is co-transfected with RAMP2 [Roberts *et al*, unpublished data].

In addition, our group has shown that RAMPs can modulate the G-protein activation profile of the PTH1/2R, VPAC1R and glucagon receptor. Although these receptors are capable of trafficking to the cell-surface and signalling on their own, presence of RAMP2 with PTH1R and

VPAC1R and RAMP3 with glucagon receptor; increased the efficacy of G-protein responses without any significant changes in binding affinities and potencies [Roberts *et al*, unpublished data]. These data show for the first time that RAMPs are involved in direct G-protein coupling of the VPAC1, PTH1/2 and glucagon receptors.

Another intracellular peripheral membrane protein called CGRP-receptor component protein (RCP) has been found to couple with the CGRP and AMR1 and play a role in generating agonist-induced cAMP response [212] by coupling the receptor to the cellular signal transduction pathway.

Taken together, RAMPs play many functions during different stages of life cycle of a receptor which are summarized in the figure 1.14 below:

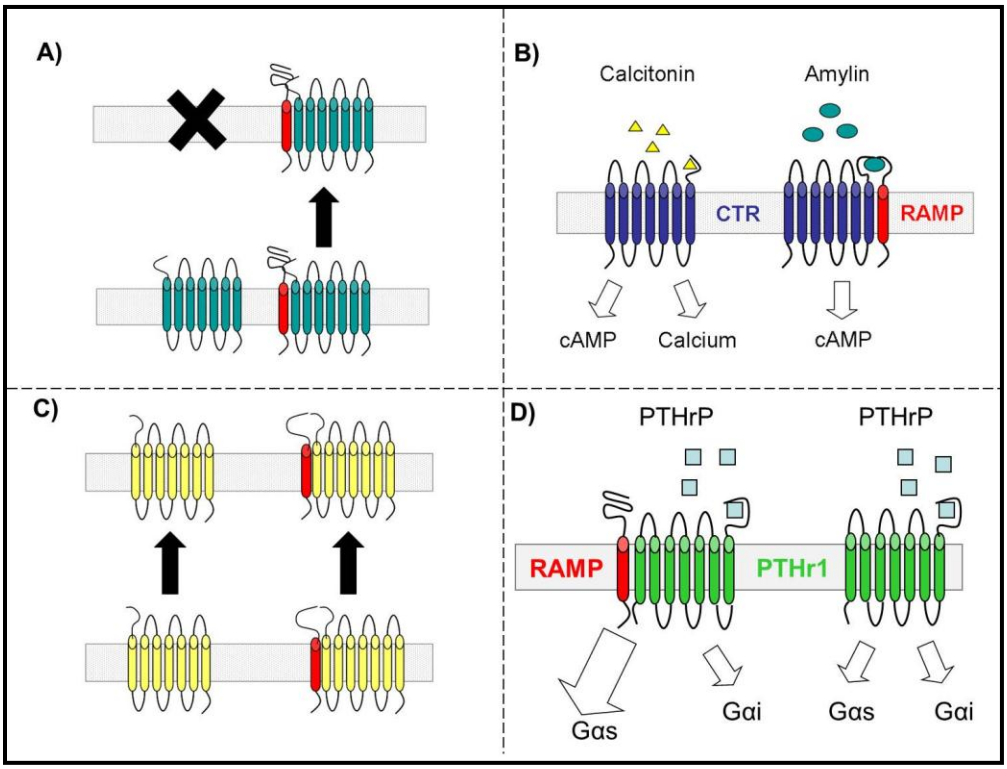

Figure 1.14: Summary of RAMP functions:
(A) Molecular chaperone for trafficking CLR, CaSR to the cell-surface (B) Altering ligand specificity and hence receptor phenotype. Here, expression of RAMP1,2,3 with CTR changes the receptor phenotype to AMY receptor. (C) and (D) although some Family B GPCRs do not require RAMP for trafficking (VPAC1R, PTH1R,Gluc1R), RAMP interaction modulates signalling pattern of G-proteins. In D, we show that PTHrP causes increase in efficacy (big arrow -left) in $G_{\alpha s}$ at PTH1R with RAMP2 compared to receptor alone (smaller arrow-right), with no change in other G-proteins [Roberts *et al*, unpublished data].

1.14. Expression of RAMPs in physiology:

RAMPs are ubiquitously expressed throughout the body (table 1.4) [150][183, 213, 214].which indicates that they facilitate actions of various effectors on their GPCRs, and that more receptor-partners of RAMPs are yet to be discovered. There is also variation in levels of expression of different RAMP isoforms amongst different tissues as shown in the table 1.4, which summarizes the expression of RAMPs in physiology known so-far [183, 213]. RAMP1 gene is expressed in many tissues like the uterus, bladder, brain, pancreas, and gastro-intestinal tract. RAMP2 and RAMP3 show similar distribution pattern but are expressed more strongly in lung, breast, immune system and foetal tissues (table 1.4).Understanding the role of RAMPs in physiology is difficult given the numerous RAMP-receptor partners expressing in the same tissue. Also, most of the data showing expression of RAMPs in different tissues is based on mRNA expression of RAMPs, due to lack of good quality antibodies for RAMPs.

Tissue	**RAMP1**			**RAMP2**			**RAMP3**		
	Rat[a]	**Mouse**[b]	**Human**[c]	**Rat**	**Mouse**	**Human**	**Rat**	**Mouse**	**Human**
Adult brain	***	****	**	*	*	*	**	****	**
Embryo brain	ND	***	ND	ND	*	ND	ND	****	ND
Adult lung	**	**	(-)	*** *	****	**	**	*	***
Embryo lung	ND	***	ND	ND	****	ND	ND	*	ND
Adult heart	*	*	***	**	**	***	*	*	****
Adult atria	(-)	ND	ND	**	ND	ND	(+/-)	ND	ND
Adult ventricle	(-)	ND	ND	**	ND	ND	(-)	ND	ND
Adult kidney	(+/-)	(+/-)	(-)	*	*	(+/-)	***	**	***
Adult liver	*	*	(-)	*	*	(-)	(-)	(+/-)	**
Embryo liver	ND	**	ND	ND	*	ND	ND	(+/-)	ND
Adult spleen	***	(+/-)	ND	***	***	ND	*	(+/-)	ND
Adult thymus	****	***	ND	*	(-)	ND	*	ND	ND
Adult aorta	***	ND	ND	**	ND	ND	(-)	ND	ND
Adult stomach	*	*	ND	*	**	ND	ND	**	ND
Embryo gut	ND	**	ND	ND	**	ND	ND	**	ND

Adult skeletal muscle	***	***	***	**	*	**	(+/-)	(+/-)	***
Adult testis	***	*	ND	*	*	ND	*	***	ND
Adult fat	****	ND	ND	***	ND	ND	**	ND	ND
Adult vas deferens	***	ND	ND	***	ND	ND	**	ND	ND
Placenta	ND	ND	(-)	ND	ND	***	ND	ND	***
Pancreas	ND	***	****	ND	*	**	ND	ND	***

* indicates the level of expression in arbitrary units. on the relative density of bands in each of the reviewed articles. ND indicates not determined. [a] compiled from [215] and [183]. [b] compiled from [182] and [214]. [c] compiled from [156].

Table 1.4: Tissue distribution of RAMP mRNA expression

Adapted from [213]

The expression patterns of RAMPs change in various pathological conditions. This may be to alter the function of AM, CGRP or other ligands of receptor-partner of RAMPs that may be upregulated or downregulated during those particular conditions. Most of the information on expression of RAMPs in physiology and its regulation by different interventions/pathophysiological conditions is based on work done on calcitonin family of receptors/peptides which is discussed in detail in section 5.1.2 of chapter 5.

1.15. Animal models lacking RAMP gene:

The importance of RAMPs in physiology is shown by the phenotype of the mice models lacking specific RAMP gene.

RAMP1 and 3 genes have three exons and RAMP2 has four exons. In each RAMP gene, first exon codes the 5' UTR sequence and a signal peptide, while exon 3 in RAMP1, 3 and exon 4 in RAMP-2 encodes all of the C-terminal and TM domain and the distal 464 aa of N-terminal domain. *Ramp1*$^{-/-}$ mice were generated by targeted deletion of exon 2 (ECD) [216] on the C57/BL6 strain. *Ramp1*$^{-/-}$ mice, showed hypertension with no changes in heart rate as vascular relaxant activity of both CGRP isoforms was suppressed in them [216]. This indicates that RAMP1 mediated CGRP signalling is essential for vasorelaxation and hence regulation of blood pressure. Additionally in these mice, LPS induced inflammatory responses increased serum levels of CGRP and proinflammatory cytokines, compared to wild-type mice [216]. This shows that CGRP signalling through RAMP1 is also responsible in regulation of proinflammatory

cytokines upon invasion of pathogens [216]. Serum levels of Ca^{2+}, PTH, bone formation or resorption markers were not studied.

Ramp2$^{-/-}$ mice were generated by deleting the 5'UTR along with exons 1 and 2 (coding for ECD), while *Ramp3*$^{-/-}$ were generated by deleting exons 2 and 3 (coding for ECD and TM domain and C-tail respectively) on the 129S6/SVEV strain [217]. In both the models, there was no measurable compensatory effect by other RAMP due to the absence of one. It was shown that out of RAMP2 and 3, RAMP2 was essential during embryonic development. It was shown that *Ramp2*$^{-/-}$ mice died during mid-gestation due to extreme *hydrops foetalis* and severe cardiovascular defects [217], which is linked to the defective AM signalling as shown by a similar phenotype in the *Am*$^{-/-}$ and *Clr*$^{-/-}$ mice [218, 219]. However, *Ramp3*$^{-/-}$ mice appear normal in their development until old age, where in comparison to the wild-type mice, they failed to increase body weight associated with increase in age. Thus, RAMP2 and RAMP3 gene has independent functions *in vivo* which cannot be compensated by the other [217].

Recently, a sex-dependent, cardio-protective role of RAMP3 in the setting of chronic hypertension was demonstrated [220]. In order to understand the role of RAMP3 in cardiovascular diseases, *Ramp3*$^{-/-}$ mice were cross-bred with an angiotensin 2-mediated chronic hypertension murine model called as RenTgMK. It was observed that compared to that in RenTgMK:*Ramp3*$^{-/-}$ mice, RAMP3 was upregulated in RenTgMK mice and more strongly so in the females. To this effect, male RenTgMK had increased cardiac hypertrophy, pathological remodeling, and decreased survival compared to female RenTgMK mice or wild-type controls. In addition to this, in the male RenTgMK:*Ramp3*$^{-/-}$ mice there were increased measures of heart failure and cardiac apopotosis; a phenotype that was absent in female RenTgMK:*Ramp3*$^{-/-}$ mice. This study, for the first time showed sexually dimorphic cardioprotective role of RAMP3 [220].

In *Ramp2*$^{+/-}$ female mice, fertility is reduced compared to wild type, *Clr*$^{+/-}$ and *Ramp3*$^{-/-}$ mice as indicated by a decrease in the litter size, foetal growth restriction, foetal demise and postnatal lethality, showing the importance of RAMP2 in fertility [217, 221]. Role of RAMP2 in endocrine homeostasis has also been demonstrated recently using *Ramp2*$^{+/-}$ female mice. *Ramp2*$^{+/-}$ female mice have hyperplastic anterior pituitary gland, accelerated mammary gland

development and exhibit hyperprolactinemia during pregnancy and in basal conditions [221]. These results suggests that signalling through RAMP2-receptor complexes formed by already identified and still unknown GPCRs is important for reproductive and endocrine functions [221].

It has been reported that *Ramp2*$^{+/-}$ mice show decreased bone mineral density and bone mineral content, indicating a role of RAMP2 in bone development [221]. Since, *Ramp2*$^{-/-}$ mice die during mid-gestation, it is only possible to study *Ramp2*$^{+/-}$ mice [218]. Preliminary data from our group suggests that RAMP3 KO mice show increased trabecular bone thickness and increased cortical bone thickness (Unpublished data, Pacharne *et al)*. These results suggest that RAMPs play an important role in regulating bone formation by regulating the role of hormones like AM, PTH, AMY and others on bone.

These diverse effects due to the absence of RAMPs in physiology cannot be linked only to the actions of the calcitonin family of peptides. Since RAMPs have a broader tissue distribution than CLR, it indicates that additional GPCRs require the RAMPs for their function. This idea is supported by the history of RAMP biology itself, where since their discovery as associating proteins to CLR [156], other GPCRs such as CTR [172], PTH1 and 2R, VPAC1R, GlucR [174], secretin [175] and CaSR [157] have been shown to associate with RAMPs, although the functional consequences for all are not completely elucidated yet. Because a large proportion of clinically available drugs target GPCRs [13], there is great interest in understanding pharmacological and biochemical properties of the RAMPs with the ultimate goal of manipulating the GPCR/RAMP interface for treatment of human disease.

1.16. Hypotheses for the project:

The project was based on the following hypotheses:

Hypothesis 1: RAMP1 and 3 differentially interact with the CaSR in higher order RAMP/CaSR complexes on the cell-surface.

Hypothesis 2: RAMPs interact with GPRC6A and are responsible for its cell-surface trafficking in transfected COS-7 cells which can be measured by FRET-based stoichiometry.

These hypotheses were tested using FRET-based stoichiometry analysis in transfected COS-7 cells as described in detail in chapter 3.

Hypothesis 3: RAMPs are involved in CaSR signalling and alter ligand induced CaSR signalling.

This was tested in overexpressing system using antibody-capture SPA and in endogenous expression system using live-cell Ca^{2+} imaging, as described in detail in chapter 4.

Hypothesis 4: RAMP mRNA is differentially regulated in human medullary thyroid carcinoma and human osteosarcoma cell line by agents involved in Ca^{2+} homeostasis.

This hypothesis was tested by measuring the changes in mRNA expression levels of RAMPs upon different treatments using real-time quantitative PCR, as described in detail in chapter 5.

CHAPTER 2: GENERAL METHODS

2.1. Maintainence of cell lines:

Cell line	Name of the culture medium used
COS-7 (African Green Monkey Fibroblast like kidney cells)	DMEM complete medium containing 4.5g/L glucose, Glutamax^{TM} (GIBCO)
HEK-293 (Human embryonic kidney cells)	DMEM complete medium containing 4.5g/L glucose, Glutamax^{TM} (GIBCO)
TT (Human medullary thyroid carcinoma cells)	F-12K (Kaighn's modification) complete medium containing (GIBCO)
MG63 (Human osteosarcoma cells)	DMEM complete medium containing containing 4.5g/L glucose, Glutamax^{TM} (GIBCO)
SAOS-2 (Human osteosarcoma cells)	DMEM complete medium containing containing 4.5g/L glucose, Glutamax^{TM} (GIBCO)
TE85 (Human osteosarcoma cells)	DMEM complete medium containing containing 4.5g/L glucose, Glutamax^{TM} (GIBCO)

Table 2.1: List of cell lines and their respective culture medium used.

Cell lines were maintained in T-175 cm^2 flasks (Nunclon, Thermo scientific) in their respective media as shown in the table 2.1) at 37˚C in 5% CO2 incubator. The complete medium contained 10% heat inactivated Foetal Calf Serum (FCS, GIBCO Paisley), 1mM Sodium Pyruvate (Sigma-Aldrich) and 1% penicillin and streptomycin (Sigma-Aldrich. Thereafter, the media was changed twice a week until the cells were confluent. The cells were used in exponential growth phase.

2.2: Passage of cells:

To passage cells, they were washed twice with sterile Phosphate buffered saline (PBS, GIBCO) before addition of 10% trypsin solution (Sigma-Aldrich) and incubated for 5 to 10 minutes at 37˚C in order to detach the cells from the bottom surface of the flask. The cells were pelleted by centrifuging at 170 xg for 5 minutes and were added to new flask with complete DMEM media in a ratio of 1:25 or 1:10 depending upon their requirement. These cells were maintained at 37˚C at 5% CO_2 and the media was changed twice a week until they were confluent.

2.3: Cell counting using haemocytometer:

Cells were detached and collected as a pellet as described in the previous section. 1ml of medium was added to the cells and then the cell suspension was further diluted 1:10 using PBS and mixed thoroughly. 10µl of cell suspension was added onto a haemocytometer and cells in the four large corner squares were counted. The total number of cells counted was divided by four and the number of cells per ml was calculated by the given formula:

Number of cells/ml= Average number of cells counted x 10^4 x dilution factor.

2.4: Trizol RNA extraction:

RNA extraction from cells was performed using Trizol reagent (Invitrogen). Cells in monolayers were harvested in 1ml of Trizol reagent and incubated for 5 minutes at room temperature. 0.2ml of chloroform was added and the tubes were shaken vigorously for 15 sec and incubated for 3 minutes at room temperature. Following centrifugation at 12,000xg for 15 min at 4˚C, the upper aqueous phase was transferred into a sterile RNase free tube. 0.5ml of isopropyl alcohol was added and the samples were incubated at room temperature for 20 min followed by centrifugation at 12,000xg for 10 minutes at 4˚C. The supernatant was removed and the pellet was washed twice with 1ml of 75% ethanol, followed by centrifuging at 12,000g for 5 min at 4^{o}C after every wash. The pellet was then air dried and resuspended in DEPC-treated water. RNA was quantified using Nanodrop® spectrophotometer.

2.5: DNase 1 treatment:

For the RT-PCR, RNA samples were treated with TURBO DNase (Ambion) enzyme to remove any contaminating DNA. 1µl TURBO DNase (2U) was used for up to 5µg of RNA in a 50µl reaction and incubated at 37^{o}C for 20min. 0.1 volume of DNase inactivation reagent was added and the reaction was further incubated for 5 min at RT, flicking the tube 2-3 times during the incubation. The tubes were then centrifuged at 10,000g for 2 min and the supernatant containing the RNA was carefully transferred into a fresh RNase free tube and quantified using Nanodrop® spectrophotometer.

2.6 Complimentary DNA (cDNA) synthesis:

Post DNase treatment, cDNA was synthesized from RNA using high capacity RNA-to-cDNA kit (Applied Biosystems). The bench and pipettes were cleaned using RNase zap solution (Ambion) before starting cDNA synthesis. Autoclaved, UV sterilized 0.2ml tubes were used. 2µg of RNA was used for a 20µl reaction containing 10µl 2X RT buffer, 1µl 20x enzyme mix and nuclease-free water to adjust the volume. For RT- controls, the enzyme mix was not added. The tubes were briefly centrifuged to spin down the contents and to eliminate any air bubbles and the

reaction was incubated at 37°C for 60min in a thermocycler (Mastercycler, Eppendorf). The cDNA synthesized was aliquoted into sterile 0.5ml tube (Eppendorf) and stored at -20˚C.

2.7: Reverse transciptase (RT) PCR:

To establish the expression of RAMPs in COS-7 cells, RT PCR was performed. RNA was extracted using Trizol reagent (Invitrogen) followed by DNase1 treatment and cDNA synthesis as described in the described before. 0.2ml PCR tubes were autoclaved and the bench and pipettes were cleaned using RNAse zap solution (Ambion). RT-PCR was performed on the cDNA, according to the recipe given in the table 2.2 using Go Taq Flexi DNA polymerase (Promega) for a 50µl reaction:

Component	Final concentration
5X Green flexi buffer	1X
25mM $MgCl_2$	2.5mM
dNTPs 10mM each	0.2mM each
Upstream primer	2µM
Downstream primer	2µM
Go Taq polymerase	1.25 units

Table 2.2: Recipe for PCR reaction using Go Taq polymerase.

The sequence of primers (Eurofins, MWG Operon) is given in the table 2.3 below:

Gene	Sequence 5' to 3'	Length	T_m (°C)	Annealing Temp (°C)
RAMP1	F: GAGACGCTGTGGTGTGACTG R: TCGGCTACTCTGGACTCCTG	20 20	60.53 60.55	55°C
RAMP 2	F: GGACGGTGAAGAACTATGAG R: TCATGGCCAGGAGTACAT	20 18	57.3 56.7	51.5°C
RAMP 3	F: AAGGTGGACGTCTGGAAGTG R: TAGTCCAAGCAGGGCCTAGA	21 21	59.35 59.35	54.0
HPRT1	F: TGTAATGACCAGTCAACAGGG R: TGGCTTATATCCAACACTTCG	21 21	57.87 55.92	51.0

Table 2.3: Sequences of primers for RAMP1,2,3 and HPRT1

The reaction was run in a thermocycler (Mastercycler, Eppendorf) in the following cycle:

Step 1: 94˚C for 3 min

Step 2: 94˚C for 30 sec

Step 3: x˚C for 30 sec

Step 4: 62˚C for 1 min

Repeat steps 2 to 4 for 35 cycles

2.8: Agarose gel electrophoresis:

To separate and visualize the PCR products, agarose gel electrophoresis was performed. 1% agarose gel was prepared by dissolving 1g of agarose powder (Sigma Aldrich) in 100ml 1× TBE buffer (Fisher scientific) in a conical flask (Pyrex ®, Fisher) and dissolved in a microwave for 2.5 min. 2µl of ethidium bromide (Sigma Aldrich, 500µg/ml) was added to the gel and the gel was poured into a gel-cast with a comb and was allowed to solidify for 20 min. The gel was placed in a tank containing 1x TBE buffer. The RT-PCR products were loaded into the wells after diluting with sample loading buffer, along with 10µl of DNA standards (Norgen). The gel was run at 150V for 30 minutes. The separated DNA was visualized under UV light using a Molecular Imager Gel Doc™ × RT with Image Lab™ software (Bio-RAD), and the gel was photographed with a gel-Doc-It system.

2.9: Real time PCR:

To determine the relative amount of cDNA in the samples, quantitative real-time PCR analysis was performed using ABi 7900HT sequence detection system (Applied biosystems). Before starting each experiment, pipettes, tips, 384-well plate (Greiner bio one), plate sealer and DEPC treated water (Sigma Aldrich) were sterilized under UV light for 20 min in a PCR hood. A reaction was performed in a single well of a 384 well plate, containing 2µl cDNA diluted in 1:2 ratio with DEPC treated water, 5µl of TaqMan® universal PCR master mix (Applied biosystems), 0.5µl of Gene specific TaqMan® inventoried assay (Applied biosystems)(accession mumbers given in the appendix) and 2.5µl of DEPC-treated water to a final volume of 10µl. Each reaction was performed in duplicates at following conditions:

Step 1: 50˚C for 2 min

Step 2: 95˚C for 10 min

Step 3: 95°C for 15sec

Step 4: 60˚C for 1 min

Step 3 and 4 were repeated for 40 cycles.

Actβ and HPRT1 were used as an endogenous control for normalizing the expression of target genes. Average threshold cycle (C_t) values were used for relative expression analysis. According to the ABi manual, a Ct value of more than 35 could be inaccurate and so the limit for analysis for this study was restricted to the Ct value of 34. $2^{-\Delta Ct}$ method was used for relative quantitation, where the C_t value of test gene was normalized to C_t value of Actβ in the same sample (eg C_t RAMP-C_t Actβ) and the value obtained was called the ΔC_t value for that particular test gene. This value was converted into linear form by using the formula: $2^{-\Delta Ct}$. These values were plotted on a graph using GraphPad Prism version 5.00 for Windows (GraphPad Software, San Diego California USA, www.graphpad.com). The data was represented as fold change in expression of the gene of interest, relative expression to the expression of Actβ.

2.10: Protein sample preparation:

Cells were washed with ice cold PBS, scrapped off using a cell scraper and spun at 1500g for 5 min at 4^{o}C. 1ml of ice cold cell lysis buffer was added to the cells and incubated for 1hr on a rotor at 4^{o}C. If substantial amount of insoluble debris remained, it was homogenized using a Dounce homogenizer (Fisher scientific) on ice (20 strokes). The sample was then centrifuged for 10min at 20,000g at 4^{o}C and the supernatant was used for quantification.

2.11: Bicinchoninic acid (BCA) protein assay:

Protein was quantified using BCA assay kit (Pierce). 1mg/ml BSA fraction V (Sigma Aldrich) prepared in cell lysis buffer was used as a standard. 2µl to 20µl of 1mg/ml of BSA and 5µl and 10µl of protein samples were added to 1.0 ml of the working reagent (50:1 bicinchoninic acid: $CuSO_4$) and incubated at 65˚C for 30 minutes. Optical Density (OD) at 562 nm was obtained using a spectrophotometer (Eppendorf) and the concentration of the protein was calculated from the BSA standard curve.

2.12: SDS-PAGE and Western blotting:

2.12.1. SDS-PAGE:

SDS-PAGE gels were cast using 1.5mm width glass spacer plates (Bio-rad). First the spacer plate and the outer glass plate were washed with a detergent, dried and wiped with methanol. Next the separating gel of desired concentration was prepared in a 50ml tube using the recipe given

in the appendix and poured between the glass plates on the casting apparatus, immediately after which distilled water was added on the top. Once the separating gel was set, 5% stacking gel was prepared and poured using the recipe given in the appendix and appropriate sized comb was placed.

After the stacking gel was set on top of the separating gel, it was allowed to equilibrate in 1x running buffer (recipe in appendix) for 45 min. Protein samples were diluted in 6x Laemmli buffer (recipe in appendix) and heated at 42°C for 10 min and the biotinylated protein standard (Cell signalling) was heated at 95°C for 5 min. Desired concentration of protein was carefully loaded using a pipette into the wells along with the biotinylated protein standards. Prestained protein standard (Biorad) was also loaded onto the gel to separate two different types of protein samples and to visualize the transfer of proteins on the PVDF membrane in western blotting. The gel was then electrophoresed at 90V till the samples were settled at the bottom of the stacking gel and then at 150V till the samples reached to the bottom of the separating gel as visualized by the bromophenol blue stained gel front.

2.12.2: Western blotting:

Transfer:

The electrophoresed proteins were transferred to Hybond-P polyvinylidene chloride (PVDF) membrane (Amersham). The PVDF membrane was made permeable by soaking it in 100% methanol before use. The arrangement for transfer was as follows:

The gel was placed on the PVDF (which was kept on cathode side), both of which were sandwiched from both the sides with sponge and 2 blotting papers (presoaked in transfer buffer). A 50ml tube was rolled on top to remove any air bubbles. The electro-blotting was allowed to occur in presence of ice-cold transfer buffer (recipe in appendix) at 100V for 80 min.

Immuno-blotting:

The presence of protein was detected by immuno-blotting. Following the transfer, PVDF membrane was incubated in blocking solution of 5% non-fat milk powder (Marvel) in TBS (recipe in appendix) for 1 hour. Primary antibodies against RAMP1,2,3 raised in goat (sc-8850, sc-8852 and sc-8854 respectively, Santacruz biotechnology, Autogenbioclear) were diluted

1/300 v/v from 0.2µg/µl stock concentration, the CaSR (ab-19347, Abcam) was diluted 1/500 v/v from 1µg/µl stock concentration and G_{α} proteins [$G_{\alpha q}$ (C-19) sc-392, $G_{\alpha s/olf}$ (C-18) sc-383 and $G_{\alpha i\text{-}3}$ (C-10) sc-262, Santacruz biotechnology, Autogenbioclear] were diluted 1/500 v/v from 0.2µg/µl stock concentration in 1% milk solution in TBS and incubated with the PVDF overnight at 4°C on a roller.

The next day, PVDF was washed 3 times for 5 minutes each with 0.05% Tween-20 (Fisher scientific) in TBS and incubated with secondary antibody (anti goat or anti mouse HRP conjugated IgG immunoglobulin, Sigma Aldrich) at 1:10,000 dilution or anti-biotin HRP conjugated antibody (1:1000) dilution in 1% milk solution for 1 hour with gentle agitation. The membrane was washed 5-7 times for 5min each with 0.05% Tween-20 in TBS.

The PVDF was then soaked in Supersignal west dura ECL cocktail (Thermoscientific) for 15-30 seconds and exposed to a chemiluminescence detecting film (Hyperfilm™ ECL, Amersham). The film was developed in the dark room by incubating first in the developer (Agfa), followed by fixer (Agfa) and finally water after which it was air dried.

2.13: Immuno-cytochemistry:

TT cells were seeded on 15x15mm #1 glass coverslips (Menzel-Glaser) which were previously baked for 90 min at 165^{o}C. The cells were washed twice with PBS and fixed for 10min at room temperature using 4% PFA (Sigma Aldrich), 48hr post transfection. If total expression was to be checked, cells were permeabilized using 0.5% Tween-20 (Fisher scientific) for 10 min at room temperature followed by incubation with 10% rabbit serum (Vector labs) with 0.5% BSA (w/v) in PBS for 30min at room temperature in order to block non-specific binding of the secondary antibody. Primary antibodies (RAMP1 sc-8850- Santacruz biotech or Goat IgG- Vector labs) were then incubated overnight at 4^{o}C in 1% rabbit serum with 0.5% BSA (w/v) in PBS at 1:50 v/v dilution of the 0.2µg/µl stock concentration. Next day, the coverslips were washed three to four times with 0.5% BSA (w/v) in PBS and then incubated with secondary antibody (Rabbit anti goat IgG conjugated with FITC, DAKO) for 45min in dark at room temperature in 1% rabbit serum with 0.5% BSA in PBS at 1:400 dilution of 2.5µg/µl stock concentration. Following the incubation, the coverslips were washed four times with 0.5% BSA (w/v) in PBS and incubated

with DAPI counterstain at 1:5000 dilution of 5mg/ml stock concentration for 3 min followed by further three washes with 0.5% BSA (w/v) in PBS. The coverslips were drained to remove excess liquid and mounted on a clean glass slide (VWR international) using Prolong Gold (Invitrogen) and stored in dark at room temperature overnight before imaging.

Imaging conditions:

HCX PL FLUOTAR L 40.0x0.60 dry objective on an Inverted widefield fluorescence microscope LeicaDMI4000B was used to capture images at 8-bit resolution and 1x1 binning at room temperature. Three channels were set each for FITC (exposure 1.5sec, gain 3.5, filter-L5), DAPI (exposure 150ms, gain 3.0, filter A4) and phase contrast (exposure 70ms, gain 2.2) to capture RAMP1 or control IgG staining, nuclear staining and a phase contrast image for TT cells.

2.14: Statistical analysis:

All data presented are either mean± SEM or mean ± SD, as specified in the results section. The graphs were plotted and the statistical analysis was done using GraphPad Prism version 5.00 for Windows (GraphPad Software, San Diego California USA, www.graphpad.com). All the data sets were assessed for Gaussian distribution (normality) using the widely recommended D'Agostino and Pearson omnibus normality test, as it first measures the skewness or asymmetry of the data from the normal distribution and then computes how far each value is from normal distribution. It subsequently creates a single p value from the sum of these discrepancies, and so is easy to interpret. It also works well when several values are identical. Kruskal-Wallis one-way ANOVA test was used to compare the means when two or more experimental groups were involved along with a control group. This test was used as it is a non-parametric test, and hence could be used on the data which were not normally distributed. This was followed by comparing each data set with another, using Dunn's multiple comparison post-test. Two-way ANOVA with Bonferroni post-test was used for multiple comparisons such as differences in FRET within the negative control FRET groups, the negative control vs test groups, and within the test groups (chapter 3), and also to compare the effects of both time and treatment on the mRNA expression levels of RAMPs or CaSR (chapter 5). Since the data were not normally distributed, Mann Whitney test was used as a non-parametric t-test to compare the differences

between two specific groups only, such as fraction of RAMP or GPCR between two specific pairs of combinations (chapter 3), and differences in expression of RAMP/CaSR in specific vs negative control siRNA transfected cells (chapter 4). The statistical tests performed for each particular experiment is mentioned in the relevant results section. $p<0.05$ was considered as statistically significant result.

CHAPTER 3: MEASURING MOLECULAR INTERACTIONS BETWEEN CaSR /GPRC6A AND RAMPs USING FRET BASED STOICHIOMETRIC ANALYSIS

3.1. Introduction

The interaction of RAMPs with CaSR was demonstrated by Bouschet *et al* [157] where they showed that RAMP1 and 3 are responsible for the cell-surface trafficking of the CaSR in transfected COS-7 and HEK-293 cells. There is no information yet regarding the differences in characteristics of interaction between RAMP1 and 3. Accordingly, it was aimed to characterize this molecular interaction in detail using förster resonance energy transfer (FRET) based techniques. Furthermore, the interaction of CaSR with RAMPs led to further hypothesis that, other family C GPCRs could also interact with RAMPs. In view of that, GPRC6A which shares 34% aa sequence identity with the CaSR [158] was chosen as a candidate and its interaction with RAMPs was tested using FRET technique.

3.1.1. Förster Resonance Energy Transfer (FRET):

Techniques such as co-localization by immunofluorescence and co-immunoprecipitation are widely used to study protein-protein interactions inside the cells, however their sensitivity is limited and chemicals used in the technique (eg detergents) might alter the native interactions [222]. Also, the resolution of a fluorescence microscope is several hundred nanometers, so unless robust calculations are carried out using more than one method, its sensitivity cannot be relied upon completely for analysis of co-localization [222]. Alternative approaches such as FRET have been developed which rely on measuring energy transfer between two fluorescent proteins labeled to proteins of interest [222-231].

The principle of FRET relies on non-radiative transfer of energy from a fluorophore in excited state known as donor, to an acceptor fluorophore; thereby exciting it [222]. Successful FRET between two fluorophores can only occur if two essential conditions are met. First, the distance separating them must be less than 10nm; and the emission spectra of the donor fluorophore must overlap with the excitation spectra of the acceptor fluorophore for an efficient energy transfer to occur [222] (Fig 3.1.1).

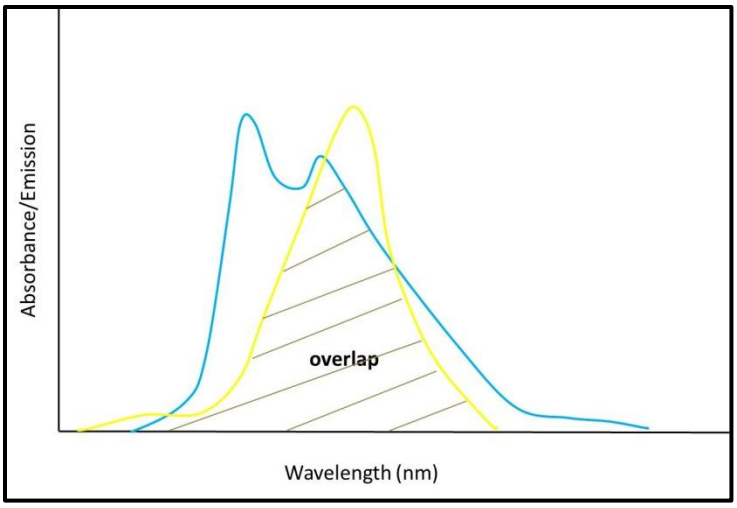

Figure 3.1.1: Spectral overlap between donor and acceptor molecules:
The emission spectrum of the donor (blue) is overlapping with the excitation spectrum of the acceptor (yellow). Adapted from [222].

FRET efficiency is inversely proportional to the sixth power of the distance (R) between two fluorophores [222, 232]:

$$E_{FRET} = \frac{1}{1 + R^6/R_0^6}$$

Here, R_0 is the distance where FRET efficiency is 50%. R_0 is dependent on the angle between the two fluorophores and the extent of spectral overlap between the two fluorophores [222, 232]. Effective R_0 for GFP variants (the most widely used fluorophores in FRET) is limited between 4 and 6nm with a range of up to and below 10nm and most FRET pairs have R_0 of ~5nm [232, 233]. Accordingly, when the distance between two interacting partners is greater than R_0, the FRET efficiency is extremely low and is considered as close to nothing, whereas for distances greater than R_0, FRET efficiency is the highest. Hence FRET can be used as a "molecular ruler" for distance calculation within this range [233]. Due to the steep dependence of FRET efficiency to R_0, FRET can be used to measure accurate changes in protein-protein interaction caused by various factors [222].

Apart from the above stated factors that affect the FRET efficiency, others such as the proportion of intensities of donor and acceptor molecules which depends on their relative

stoichiometry and brightness can limit the usefulness of FRET for certain interactions, as FRET occurring is proportionally very small compared to the very high background of fluorescent labels that are not undergoing FRET [222, 234].

Most commonly used fluorescent proteins are GFP variants CFP and YFP [235] and their mutants Cerulean (Cer) [236] and Citrine (Cit) [237] respectively, because of their overlapping spectra. Development of Cer and citrine had advantages over parental CFP and YFP such as higher extinction coefficient and quantum yield, resistance to acid quenching and prevention of homo and hetero-dimerization of the fluorophores [236-238].

3.1.2. Method of FRET imaging used:

Sensitized emission:

Sensitized emission technique was used in this study to measure the specific interactions between the GPCRs and RAMPs. In this technique the donor fluorophore is excited at a particular wavelength and the energy transferred is measured as the emission of the acceptor [222-224] (Figure 3.1.2). Because of the spectral overlap between the two fluorophores, problem with bleed-through (spillage of donor and acceptor fluorescence into FRET channel detector) and cross-talk (excitation of acceptor at donor excitation wavelength) of fluorescence exists in this method; which requires corrections using appropriate controls [9, 10]. Two-channel based approach using a confocal microscope is better than using a widefield fluorescence microscope, as decreased bleed-through and increased specific excitation of CFP can be achieved by using a laser [9]. However, the need for image processing amplifies the noise that is initially in the images and hence this method is not useful for small FRET signals where it can be difficult to differentiate between background noise and specific FRET signal [222].

Sensitized emission method can also be used to measure stoichiometry of the components involved in FRET which gives a deeper insight into the interaction [224] as explained below.

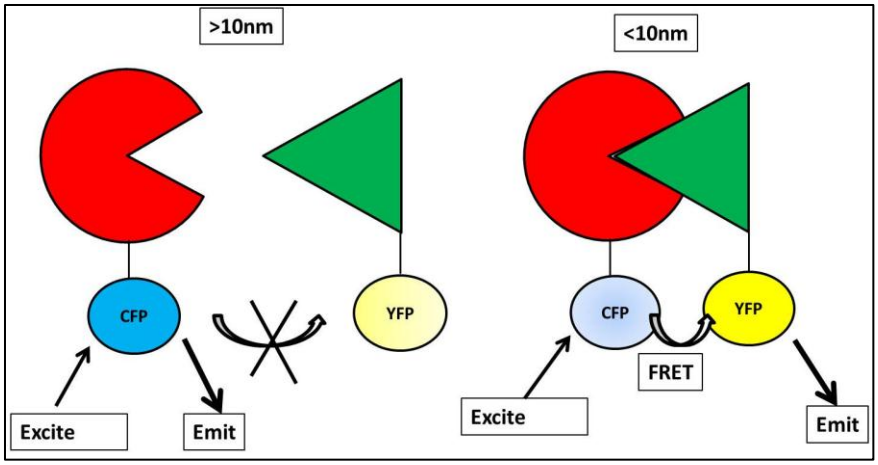

Figure 3.1.2: Principle of sensitized emission:
Two interacting proteins (red and green) are tagged on their C-terminus with donor (CFP) and acceptor (YFP) respectively. When the proteins do not interact, FRET cannot occur, whereas in case of an interaction, the distance between the proteins is within 10nm and so energy is transferred from excited donor to the acceptor thereby exciting it and the emitted fluorescence by the acceptor is measured as the FRET between them.

FRET-based stoichiometry in living cells:

FRET stoichiometry is derived from the concept that the measure of FRET efficiency of a specific donor-acceptor complex, can allow stoichiometric discrimination of interacting components [224]. Basically, in sensitized emission the emission of acceptor due to FRET is influenced by four main components (Figure 3.1.3)- efficiency of energy transfer (E) between donor-acceptor pair, fraction of donor (Fd) involved FRET, fraction of acceptor (Fa) involved in FRET and the ratio of total acceptor to donor (R) (free and complexed). Hoppe *et al* [224] have developed a method of FRET stoichiometry that measures these at each pixel in an image.

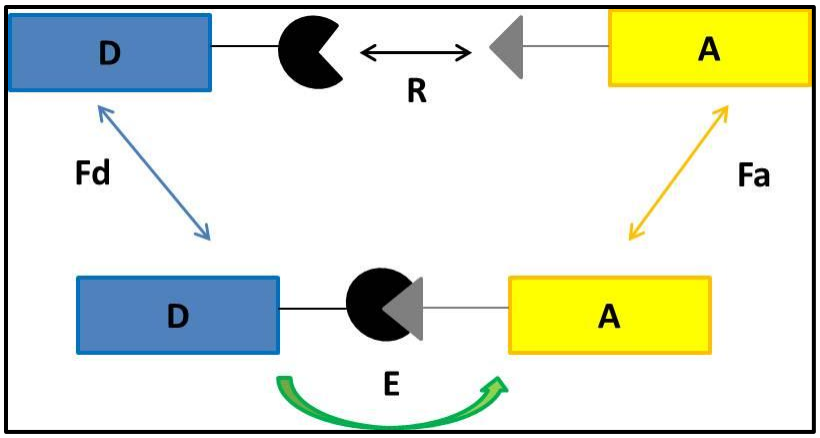

Figure 3.1.3: Principle of FRET stoichiometry:
Donor is shown in blue and acceptor is shown in yellow attached to their respective proteins. Interactions between donor, acceptor and donor-acceptor complexes influence the emission spectrum through four parameters: efficiency of energy transfer (E), fraction of donor (Fd) and acceptor (Fa) in complex and the ratio of total acceptor to donor (R). Adapted from [224].

The fractions of donor and acceptor in FRET complex are calculated based on information in three images namely: the donor image, the acceptor image and FRET image. So, as shown in the figure 3.1.3, the fraction of donor or acceptor in FRET complex is calculated by dividing the concentration of donor-acceptor complex by the total concentration of the donor or acceptor respectively (free plus complexed).

Such measurements are complicated due to the presence of excess non-interacting donor or acceptor molecules which create high background fluorescence; making the specific measurements difficult. These problems are circumvented by using the equations derived by Hoppe *et al* [224], due to the correction factors used. Accordingly, in addition to correcting for bleed-through of donor or acceptor fluorescence into the FRET channel; this method also uses two additional correction factors γ and ξ which help in calculating the fraction of donor or acceptor in FRET complex accurately [224]. γ corrects for the excitation of acceptor at donor's wavelength which is due to the overlapping fluorescent spectra of the fluorophores and helps in calculating Fa; whereas ξ is a proportionality constant used in measuring Fd by accounting for the increase in acceptor emission relative to a corresponding decrease in donor's emission due to FRET. It was shown that this method could distinguish between the excess of donor or acceptor present and could determine correct fractions of the components present in the FRET

complex. This was done by keeping either Fa or Fd constant and varying the other component to measure its fraction in FRET complex. For example, by keeping the concentration of donor constant and increasing the concentration of the acceptor let to a concurrent linear increase in the fraction of acceptor in FRET complex. This shows that the method could distinguish between the excess donor present [224].

Also R, measures the ratio of total concentration of acceptor to donor (free and complexed) present at each pixel of the image. R=1 indicates equal fractions of donors and acceptors in the given image pixel, R>1 or <1 indicate an excess of either acceptor or donor respectively. So, comparing Fa or Fd with R gives an idea about the relative local concentrations of free acceptor or donor molecules that do not participate in FRET [224]. Thus, FRET stoichiometry gives a measure of physical parameters which are transferrable from one molecular interaction to another.

3.1.3. Hypotheses and aims:

It was hypothesised that RAMP1 and 3 differentially interact with the CaSR in higher order RAMP/CaSR complexes on the cell-surface.

It was also hypothesised that RAMPs interact with GPRC6A in COS-7 cells and enable its cell-surface trafficking. The specific aims were:

- To optimize a FRET method to measure sensitized molecular interaction between GPCRs and RAMPs using positive and negative controls.
- To measure FRET efficiency of interaction between CaSR as well as GPCR6A with RAMPs on the cell-surface; and determine the fraction of RAMPs and receptor present in the FRET complex on the cell-surface, using FRET-based stoichiometry analysis.

3.2: Methods and Materials:

3.2.1. cDNA constructs used:

GPCRs were engineered into pcDNA 3.1 Citrine vector such that the citrine was tagged to the C-terminal of the GPCR. RAMPs were engineered into pcDNA 3.1 Cerulean vector such that, that RAMP gene was followed by a linker sequence (at RAMP C-terminal) which was followed by the Cerulean gene.

As a negative control, pcDNA 3.1 Citrine vector alone was used with pcDNA 3.1 RAMP Cerulean vector, whereas, as a positive control, pcDNA3.1 vector containing a fusion construct containing Cerulean cDNA followed by 18 aa linker sequence and then Citrine cDNA was created and will be referred to as Cerulean-citrine fusion.

pcDNA 3.1 CaSR-citrine vector was engineered by me as described below; whereas the pcDNA 3.1 CLR-citrine, pcDNA 3.1 GPRC6A-citrine, pcDNA 3.1 RAMPs-cerulean, pcDNA 3.1 cerulean-citrine fusion, pcDNA 3.1 cerulean and pcDNA 3.1 citrine vectors were a kind gift by Dr. David Roberts of our group. The cloning sites for engineering the constructs used are shown in the table 3.2.1 below:

Construct	Cloning sites
pcDNA 3.1-Citrine/Cerulean	Not-1-Cit-Xho1 into pcDNA 3.1
pcDNA 3.1 –RAMP-Cerulean	Kpn1-RAMP-Not-1-Cerulean
pcDNA 3.1-CaSR-Citrine	HindIII-CaSR-Not1-Citrine
pcDNA 3.1-GPRC6A-Citrine	HindIII-GPRC6A-Not1-Citrine
pcDNA 3.1-CLR-Citrine	HindIII-CLR-Not1-Citrine

Table 3.2.1: Cloning sites for the engineering the constructs used in FRET

3.2.2. Engineering CaSR gene into pcDNA 3.1-Citrine vector:

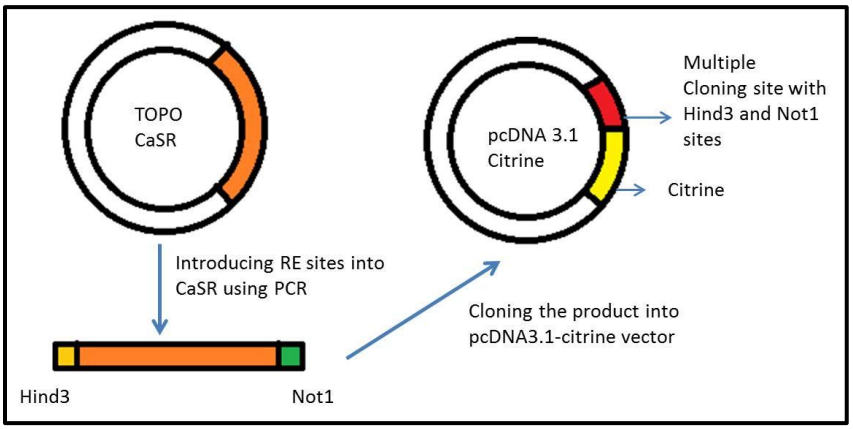

Figure 3.2.1: Cloning strategy of CaSR cDNA from TOPO CaSR into pcDNA3.1-Citrine

CaSR cDNA was cloned from TOPO vector (Geneservice) containing CaSR cDNA into pcDNA 3.1 citrine vector. For this, HindIII and Not1 restriction enzyme recognition sites were introduced into the CaSR gene using PCR as shown in the figure 3.4 above. The amplified PCR product was then cloned into the pcDNA3.1 vector between the HindIII and Not1 sites such that citrine was at the C-terminal of CaSR. A step-by-step protocol is given below:

(a) Culture of TOP10 E.Coli glycerol stocks containing TOPO CaSR or pcDNA3.1-Citrine:

TOP10 E.Coli glycerol stocks containing TOPO CaSR or pcDNA 3.1-citrine vector were cultured in autoclaved LB broth (Sigma Aldrich) containing 0.1mg/ml ampicillin (Sigma Aldrich) at 37^{o}C overnight in a shaking incubator at 200rpm.

(b) Plasmid extraction:

TOPO CaSR and pcDNA 3.1 citrine plasmid DNA were isolated using PureYield^{TM} Plasmid Midiprep System (Promega) according to the manufacturer's protocol. Cells were pelleted by centrifuging at 2000g for 10 min and resuspended in 3ml cell resuspension solution and vortexed thoroughly. 3ml of cell lysis solution was added and the tubes were gently inverted 3-5 times and incubated for 3 min after which 5ml of neutralizing solution was added and mixed gently by inverting 5 times. PureYield^{TM} clearing column was assembled into the top of a PureYield^{TM} binding column and the assembly was placed onto the vacuum manifold (Promega). The lysate was poured into a PureYield^{TM} clearing column and maximum vacuum was applied

till the lysate passed through. The PureYield^{TM} clearing column was removed and 5ml endotoxin removal wash solution was added and vacuum was applied to pull the solution through the column followed by a wash with 20ml of column wash solution. The membrane was dried by applying vacuum for further 60 seconds. PureYield^{TM} clearing column was removed from the vacuum manifold and placed in a clean 50ml tube. 600µl of nuclease-free water was added and the tube was centrifuged at 1500g for 5 min at room temperature to elute the plasmid DNA.

(c) Polymerase chain reaction using TOPO CaSR vector to engineer restriction enzyme sites for cloning:

HindIII and Not1 restriction enzyme sites were engineered on either sides of the CaSR gene in the TOPO vector by using primers with restriction site sequence (table 3.2.3). This amplified the entire CaSR gene from TOPO CaSR, excluding the stop codon, as the citrine was to be engineered to the C-terminal of the CaSR. This was achieved by PCR using KOD hot start DNA polymerase (Novagen). The reaction was set in a 0.2ml PCR tube in a final volume of 100µl using the following receipe:

Component	Final concentration
10x buffer for KOD hot start polymerase	1X
25mM $MgSO_4$	1.5mM
dNTPs 10mM each	0.2mM each
Forward primer	2µM
Reverse primer	2µM
Go Taq polymerase	0.04U/µl
Template cDNA :TOPO CaSR	100ng

Table 3.2.2: Recipe for KOD hot start DNA polymerase PCR

Primer sequences (restriction enzyme recognition site is highlighted)

Gene	Sequence 5' to 3'	Length	Tm (°C)	Annealing Temp (°C)
CaSR	**F(HindIII):**TATCAAGCTTGTCATGGCATTTTATAGC TGCTGCTGGGTCCTC **R(Not1):** TATTCGGAAGCGGCCGCTGAATTCACTACGTT TTCTGTAACAGTGCTGCC	43 50	62.41 67.00	55.0°C

Table 3.2.3: Primer sequences for cloning CaSR in pcDNA 3.1 Citrine vector

The reaction was run in a thermocycler (Mastercycler, Eppendorf) using the following cycling conditions:

Step 1: 95˚C for 2 min
Step 2: 95˚C for 30 sec
Step 3: 55˚C for 30 sec Repeat steps 2 to 4 for 35 cycles
Step 4: 68˚C for 2 min

Following the completion of PCR, 5µl of product was subjected to agarose gel electrophoresis as described in section 2.8 of chapter 2 to check the product length (expected size ~3300bp).

(d) Precipitation of PCR product:

PCR product was precipitated to remove the contents of the PCR reaction and purify the amplified DNA. PCR product was precipitated using isopropanol by adding 2 volumes of isopropanol to the PCR product and the reaction was incubated for 30min at -20^{o}C. The tubes were then centrifuged at 20,000g for 30 min at 4^{o}C and the supernatant was discarded. DNA pellets were allowed to air dry and were resuspended in 30µl nuclease-free water.

(e) Restriction digestion of the CaSR PCR product and pcDNA 3.1 Citrine vector with HindIII and Not1:

In order to clone the purified PCR product between the HindIII and Not1 sites of the pcDNA 3.1 citrine vector; 10µg of PCR product and 10µg of pcDNA 3.1 Citrine vector were digested separately using 20units of HindIII and Not1 restriction enzymes (New England Biolabs) in the

presence of 1x NEbuffer 2 (New England Biolabs) and 1x BSA (10mg/ml stock) in a final volume of 100µl. The reaction was incubated at 37^{o}C overnight. The next day, the restricted DNA were precipitated as described in section 3.2.2 (d) and resuspended into 50µl nuclease-free water.

(f) Dephosphorylation of restricted pcDNA 3.1 Citrine vector:

To prevent the self-ligation of the HindIII and Not1 restricted pcDNA3.1-citrine vector, dephosphorylation was carried out by incubating with 5units of Antarctic phosphatase enzyme (New England Biolabs) in presence of 1x Antarctic phosphatase buffer (New England Biolabs) and nuclease free water at 37^{o}C overnight.

The next day, reaction was stopped by precipitating the DNA as described in section 3.2.2 (d). DNA was quantified using BioPhotometer (Eppendorf) using 1 in 50 dilution in a plastic cuvette (Eppendorf) at 260nm.

(g) Gel extraction of the restricted CaSR insert:

In order to remove the impurities from the restriction enzyme reaction in the form of the salts from the buffer and restriction enzyme, CaSR insert was electrophoresed and the correct sized band was gel extracted. HindIII and Not1 restricted CaSR insert was subjected to agarose gel electrophoresis as described in section 2.8 of chapter 2, but without using ethidium bromide. After the electrophoresis, the gel was stained using 1% crystal violet (w/v) for 20min and then de-stained using distilled water. The band at the correct size was visualized under white light and was cut using a scalpel. The DNA was then extracted using Zymoclean^{TM} gel DNA recovery kit (Zymo research). 3 volumes of ADB reagent were added to the agarose gel excised, and incubated at 37^{o}C until the gel slice was completely dissolved. The molten agarose solution was transferred into zymo-spin^{TM} I column in a collection tube and centrifuged at 10,00g for 30 sec. 200µl of wash buffer was then added and the column was washed by centrifuging at 10,000g for 30 sec. 10µl of nuclease-free water was added directly to the column and the DNA was eluted in a clean 1.5ml tube by centrifuging at 10,000g for 30 sec. DNA was quantified using BioPhotometer as described before in (f).

(h) Ligation of the CaSR insert into the dephosphorylated pcDNA3.1-citrine vector:

1µg of the gel extracted CaSR insert and the dephosphorylated pcDNA 3.1 Citrine vector were ligated using 2000U of T4 DNA ligase enzyme (New England biolabs) in presence of 1x T4 DNA

ligase reaction buffer (New England biolabs) and nuclease-free water in a final volume of 100µl. The reaction was incubated overnight at room temperature.

On the following day, the ligation mixture was precipitated as described in section 3.2.2 (d) and the DNA pellet was resuspended in 50µl of nuclease-free water.

(i) Gel extraction of the ligated product:

In order to use the ligated product-only for the further procedure, it was gel extracted according to the expected band size. The ligated product was subjected to agarose gel electrophoresis without ethidium bromide and stained with 1% crystal violet (w/v) for visualisation at correct size of ~10kbp. The ligated product only was gel extracted as mentioned earlier in section 3.2.2 (g) and resuspended in 20µl nuclease-free water.

(j) PCR for the ligated product and Dpn1 digestion:

At the end of a ligation reaction, there will be presence of unligated insert and empty vector as well as successfully ligated product. In order to selectively obtain the CaSR ligated into the pcDNA3.1-citrine vector, the ligated product was amplified using primers specific for CaSR. For this, PCR was performed as described in section 3.2.2 (c) using KOD hot start DNA polymerase. The primers used were specific to the mid region of the CaSR gene:

Gene	Sequence 5' to 3'	Length	TM (°C)	Annealing Temp (°C)
CaSR	**F:** CCCTTCTCCAACTGCAGCCGAGACTG	26	69.5	60°C
	R: CAGTCTCGGCTGCAGTTGGAGAAGGG	26	69.5	

Table 3.2.4: Primer sequences for amplifying CaSR pcDNA 3.1 Citrine ligated product.

The reaction was run in a thermocycler (Mastercycler, Eppendorf) in the following cycle

Step 1: 95˚C for 2 min
Step 2: 95˚C for 30 sec
Step 3: 60˚C for 30 sec
Step 4: 68˚C for 5 min

Repeat steps 2 to 4 for 20 cycles

After the PCR, the contents of the tube were spun down briefly and incubated overnight at 37^{o}C with 20units of Dpn1 enzyme to cleave any methylated parental strands (to remove the vectors without CaSR insert). The following day, Dpn1 treated PCR product was precipitated as described in section 3.2.2(d) and the pellet was resuspended in 20µl of nuclease-free water.

(k) Transformation of the ligated product into TOP10 E.Coli:

A vial containing 50µl TOP10 chemically competent E.Coli (Invitrogen) was first thawed on ice; and then incubated for further 25min on ice after adding 100ng of the ligated product. TOP10 E.Coli cells were then heat shocked for 40sec at 42^{o}C and immediately transferred to ice and incubated for 2 min. 250µl of S.O.C. medium (Invitrogen) was added to the vial following incubation for 1hr at 37^{o}C at 200rpm in a shaking incubator. After this, TOP10 E.Coli were spread on a pre-warmed LB agar (Sigma Aldrich) plate containing 100µg/ml ampicillin with a cell-spreader and incubated at 37^{o}C overnight.

(l) Colony selection, culture, plasmid isolation:

Colonies were picked and cultured in 2ml LB broth containing 100µg/ml ampicillin overnight at 37^{o}C at 200rpm in a shaking incubator.

Plasmid isolation was performed using Wizard plus SV Minipreps DNA Purification system (Promega) according to the manufacturer's protocol. 1ml of culture medium was pelleted by centrifuging at 10,000g for 5 min and resuspended thoroughly in 250µl cell resuspension solution. 250µl of cell lysis solution was added to each sample and mixed by inverting 4 times. 10µl of alkaline phosphatase was then added, mixed by inverting and incubated for 5 min at room temperature, following which 350µl of neutralization solution was added and mixed. The lysate was then centrifuged at 10,000g for 10 min at room temperature. The cleared lysate was decanted into a spin column- attached to an adapter on vacuum manifold, and passed through the column by applying vacuum. 750µl of wash solution was added and passed through the column by applying vacuum. This step was repeated using 250µl of wash solution. The column was transferred to a collection tube and centrifuged at 10,000g for 2 min in a table top centrifuge to remove any remaining ethanol from the wash solution. Plasmid DNA was eluted

by adding 100µl of nuclease-free water to the spin column and collected into a fresh 1.5ml tube by centrifuging at 10,000g for 1 min at room temperature.

(m) Restriction digestion screening of the pcDNA 3.1 CaSR-citrine clones for presence of CaSR using HindIII and Not1:

The selected colonies were initially screened for the presence of CaSR insert by restriction digestion of the extracted plasmid DNA. 1µg of DNA isolated was subjected to restriction digestion with 10units of HindIII and Not1 as described section 3.2.2 (e) for 1hr at 37^{o}C. The restricted clones were then separated using agarose gel electrophoresis and visualized under UV light for positive clones which showed a band for CaSR at ~3300bp.

(n) Sequencing of positive clones and result analysis:

The positive clones were cultured overnight and plasmid DNA was isolated as described in section 3.2.2 (l) and precipitated section 3.2.2 (d). Plasmid DNA for each positive clone were sequenced using ABi automated sequencer at the Genomics Core Facility in the Medical school, University of Sheffield using the following primers: CaSR engineered into the pcDNA 3.1 citrine was sequenced from bp 380-550and 1150-2850 to confirm the presence of CaSR (data not shown)

Primer name	Sequence 5' to 3'	Length
CMV primer	CGCAAATGGGCGGTAGGCGTG	21
1160+	TTGGCCTCAAACACCAGGAGGACACGGTT	29
1950+	AACTGGCACCTCTCCCCAGAGGATGGCT	28

Table 3.2.5: Primer sequence for CaSR sequencing in positive clones.

The sequencing results were matched to the sequence of CaSR in TOPO CaSR vector using EMBOSS matcher and were also searched using nucleotide BLAST for aligning sequences.

(o) Preparation of bacterial glycerol stock:

30% (v/v) glycerol was added to the culture of bacteria of the positive clone in a 1.5ml tube and was flash frozen using liquid nitrogen. The tube was stored at -80^{o}C for future usage.

3.2.3. Transfection of COS-7 cells with pcDNA 3.1 GPCR-Citrine and pcDNA 3.1 RAMP-Cerulean:

The following protocol was used for FRET analysis of CaSR/GPRC6A with RAMPs. Electroporation technique was used to co-transfect COS-7 cells with tagged GPCR and RAMP or positive and negative control vectors for FRET imaging.

COS-7 cells were grown to confluency, after which they were detached using trypsin and collected as a pellet as described in section 2.2 of chapter 2. The cell pellet was resuspended in 1ml of electroporation buffer (recipe in appendix) and the numbers of cells were counted as described in section 2.3 of chapter 2. The numbers of cells and the amount of DNA optimized for each transfection combination is given below:

Transfection combination	Amount of DNA	Number of COS-7 cells
Citrine alone/Cerulean alone	5µg	0.8 million
Citrine alone+RAMPs-cerulean	3µg+15µg	1.5 million
Citrine-cerulean fusion	5µg	0.8 million
CLR-citrine+RAMPs-cerulean	3µg+3µg	1.5 million
CaSR-citrine and GPRC6A alone	10µg	1.5 million
CaSR-citrine+RAMPs-cerulean	10µg+15µg	2.5 million
GPRC6A-citrine+RAMPs-cerulean	10µg+10µg	2.5 million

Table 3.2.6: Number of COS-7 cells and amount of DNA for FRET transfections

After counting, the required numbers of cells were transferred into a 4mm gap electroporation cuvette (York biosciences) in a final volume of 0.4ml, adjusted using the electroporation buffer, followed by which the required amount of DNA was added. The cells were then electroporated using gene pulser (Biorad) at 960µF, 0.25kV. 1ml of culture medium was added to the cells and incubated for 5 min at room temperature. Cells were then gently seeded using a sterile plastic

dropper into a sterile 35mm glass-bottom plate (Ibidi) and left at room temperature for 20min before transferring into the cell culture incubator at 37^{o}C, 5% CO_2 for 48hr. Fresh medium was replaced the next day to remove the dead cells due to electroporation.

3.2.4. Cell fixation and mounting:

Cells were washed twice with PBS 48hr post-transfection and fixed using 4% paraformaldehyde for 10min at room temperature, followed by 3 washes with PBS. Cells were then mounted by adding 500µl Mowiol mountant (recipe in appendix) and were left overnight before imaging.

3.2.5. FRET Imaging:

Images were captured using a Zeiss Plan apo 63X/1.4 oil immersion lens on a Zeiss LSM 510 inverted laser scanning confocal fluorescence microscope fitted with an argon laser at room temperature. Confocal images of the fluorescent proteins were acquired using an argon laser together with an HFT458/514nm dichroic, a NFT515nm beam splitter, pin hole set to 496µm, detector gain 550 and individually as a separate channel under the following conditions: Cerulean was excited using the 458nm laser line with a 100% laser intensity and a band pass BP480-520 emission filter; Citrine was excited using the 514nm laser line attenuated to 20% laser intensity and a band pass BP535-590 emission filter; FRET was excited using the 458nm laser line with a 100% laser intensity and a BP480-520 emission filter. All fluorescence channels were scanned and the collected together, line by line with a mean of 1.

3.2.6. FRET analysis:

Bleed-through calculations:

Cerulean and Citrine fluorescence bleed-through into the FRET channel were calculated using FRET and co-localization analyzer plugin for ImageJ [239]. pcDNA 3.1 Cerulean or pcDNA 3.1 Citrine COS-7 cell images collected using either the CFP and FRET or YFP or FRET channels were used. At least 10 images were used to calculate the mean values of the bleed through constants β (bleed-through of donor fluorescence in FRET channel) and α (bleed-through of acceptor fluorescence in FRET channel).

Calculating FRET efficiency for sensitized emission (NFRET) using PixFRET:

NFRET calculations for FRET efficiency for sensitized emission were done using pixel-by-pixel analysis by PixFRET plugin for ImageJ [239]. The resulting FRET images generated by the PixFRET plugin were used as representative images for a particular receptor/RAMP combination in the results section. The bleed-through values for CFP (β) and YFP (α) channel obtained from above were entered into the plugin. An ROI was drawn outside the cell, to calculate the background intensity for each channel and the threshold was set to 1.5; so that only pixels with value greater than 1.5 times the background intensity were used for analysis, in order to minimize background noise and mathematical errors. The following equation was selected to calculate FRET efficiency:

$$\mathrm{NFRET} = \frac{\mathrm{FRET}\text{-}[\mathrm{CFP} \times (\mathrm{CFP}_{\mathrm{BT}})]\text{-}[\mathrm{YFP} \times (\mathrm{YFP}_{\mathrm{BT}})]}{\sqrt{(\mathrm{CFP} \times \mathrm{YFP})}}$$

BT= bleed through

The NFRET and FRET of stack images were saved for further analysis of membrane NFRET.

3.2.7. FRET based stoichiometric analysis:

All FRET-based stoichiometric analysis was done as described in [224] using ImageJ software.

Calculation of E_C:

E_c is the maximum achievable FRET between the fluorophores used (cerulean and citrine) using the positive control construct containing fusion of cerulean linked to citrine. E_C was measured using sensitized emission for pcDNA3.1 cerulean-citrine construct transfected COS-7 cell images. First, the background fluorescence for each channel was subtracted from their respective images (CFP, YFP and FRET images). Next, 6-8 ROIs were drawn per image of a cell (avoiding the over-exposed regions) using ImageJ; and the intensities for CFP, FRET and YFP channel images were obtained. The values were used in the equation given above for NFRET and the calculation for mean and SEM for FRET efficiencies was done using Microsoft Excel.

Calculation of γ,ξ:

Once β, α and E_C were calculated, γ and ξ were calculated according to the formulae derived by Hoppe *et al* [224]. γ is the ratio of the extinction coefficient of the acceptor to the donor at the donor excitation. ξ is the proportionality constant relating the sensitized acceptor emission to the decrease in donor fluorescence due to FRET.

$$\gamma = \frac{E_c}{\left[\frac{I_F - \beta I_D}{\alpha I_A} - 1\right]}$$

$$\xi = \frac{\gamma I_D E_c}{(1 - E_C)(I_F - \alpha I_A - \beta I_D)}$$

Here, I_A= intensity of the acceptor channel; I_D= intensity of the donor channel; I_F= intensity of the FRET channel.

Background corrected pcDNA 3.1 cerulean-citrine fusion COS-7 cell images were used for analysis in ImageJ. 6-8 ROIs were drawn per image of cell and the intensities for CFP, FRET and YFP channels were obtained, and used in the above equations to calculate mean and SEM values for γ and ξ using Microsoft Excel.

Image processing and calculation of Fa, Fd and R:

All the images were processed using ImageJ for pixel-by-pixel analysis. Macros were developed for image arithmetic to calculate Fa, Fd and R. First, the background for CFP, FRET and YFP images was calculated using the same ROI. Next, Gaussian blur of 2 was applied to the YFP or the acceptor image and the threshold was applied. This image generated a binary mask image, which was applied to the CFP and the FRET images. The images were inverted and converted into 16-bit format. Next, 1.5x background value for respective channel was subtracted from respective images to generate I_D, I_F and I_A images (I_D, I_A and I_F = Intensity of donor/acceptor/FRET channel). These images were then used to produce FRET stoichiometry images by image arithmetic using the equations [224]:

$$F_A = \gamma\left[\frac{I_F - \beta I_D}{\alpha I_A} - 1\right]\left(\frac{1}{E_C}\right)$$

$$F_D = \left[1 - \frac{I_D}{(I_F - \alpha I_A - \beta I_D)(\xi/\gamma) + I_D}\right]\left(\frac{1}{E_C}\right)$$

$$R = \left(\frac{\xi}{\gamma^2}\right)\frac{\alpha I_A}{(I_F - \alpha I_A - \beta I_D)(\xi/\gamma) + I_D}$$

Calculating NFRET, Fa, Fd and R on the cell membrane:

In order to calculate the FRET efficiency and FRET based stoichiometry on the cell-surface, the raw acceptor image was opened in ImageJ. Using the selection tool, 50-pixel dots were drawn around the cell-surface of the acceptor image as shown in the results section. Each dot was taken as a ROI and the combined ROIs for each image was saved and applied to the NFRET, Fa, Fd and R images to measure the FRET efficiency and FRET based stoichiometry at the cell-surface only. The average and SEM values corresponding to each ROI were calculated for all the images using Microsoft Excel.

3.3: Results

3.3.1. Negative control for FRET:

In order to determine the non-specific FRET occurring due to random interactions between the fluorophores, a negative control was used. Accordingly, citrine only (free in the cytosol) and cerulean-RAMPs were used. COS-7 cells were co-transfected with 5µg of pcDNA 3.1-citrine-and 15µg of RAMPs-cerulean pcDNA 3.1. Figures 3.3.1, 3.3.2 and 3.3.3 show representative images for the expression of cerulean-RAMP (A), free citrine (B) and FRET (D) for different citrine+ cerulean-RAMP1/2/3 combinations respectively. It was observed that majority of citrine was expressed throughout the cell whereas, RAMP1 and 2-cerulean were mainly present in the perinuclear region, whereas RAMP3-cerulean expression could be seen ranging from the perinuclear region to the cell membrane. No FRET can be seen on the cell-surface in any combination (figure 3.3.1-3.3.3 D). Using a 50 pixel cell-surface ROI on the citrine image (C) the NFRET values obtained were 11.58 ± 2.8 for citrine + RAMP1-cerulean, 11.47 ± 2.92 for citrine +RAMP2-cerulean and 12.33 ± 1.6 for citrine + RAMP3-cerulean as shown in Fig 3.3.4 and table 3.3.1. These values were set as threshold for considering NFRET values in calculation for all receptor + RAMP experiments as specific. The NFRET values are represented in all the results as % of the maximum NFRET value calculated using the citrine-cerulean fusion (E_c value), which was used as the positive control for the FRET method. The mean values calculated for the stoichiometric constants β (0.31), α (0.126), γ (0.30) and ξ (0.20); as well as E_c for the Cerulean-citrine fusion positive control (~33%) are given in appendix table 7.1.

Citrine + RAMP1

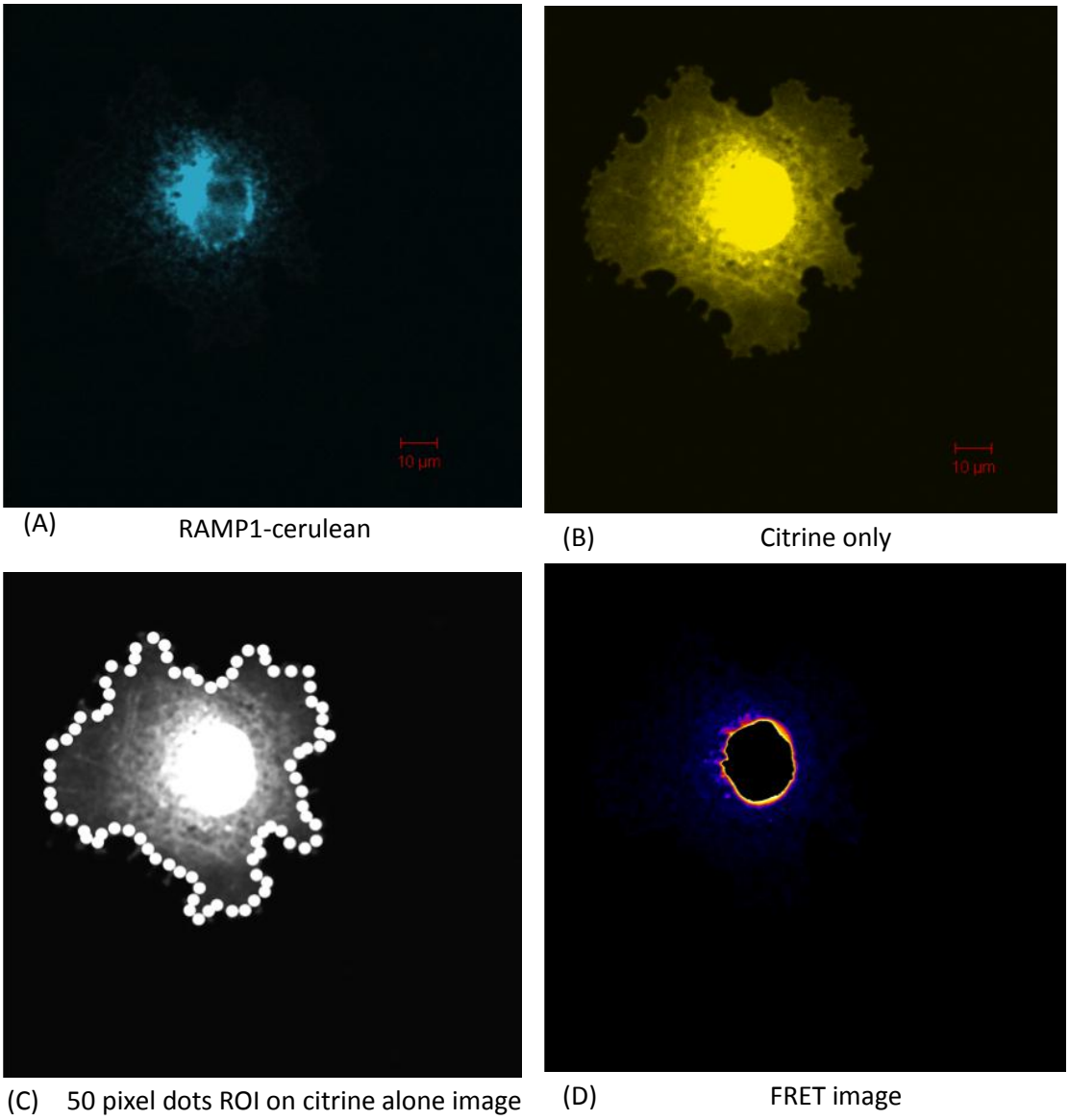

(A) RAMP1-cerulean

(B) Citrine only

(C) 50 pixel dots ROI on citrine alone image

(D) FRET image

Figure 3.3.1: Representative image for FRET between free Citrine and RAMP1-cerulean in COS-7 cells:. COS-7 cells were transfected with 5µg pcDNA 3.1 Citrine and 15µg pcDNA3.1 cerulean-link-RAMP1 and were imaged using the confocal microscope 48hr post transfection. (A) Expression of RAMP1-cerulean (B) Expression of free Citrine (C) 50 pixel dot ROI around the cell membrane of Citrine only image. (D) FRET between citrine and Cer RAMP1. Scale bar 10µm

Citrine + RAMP2

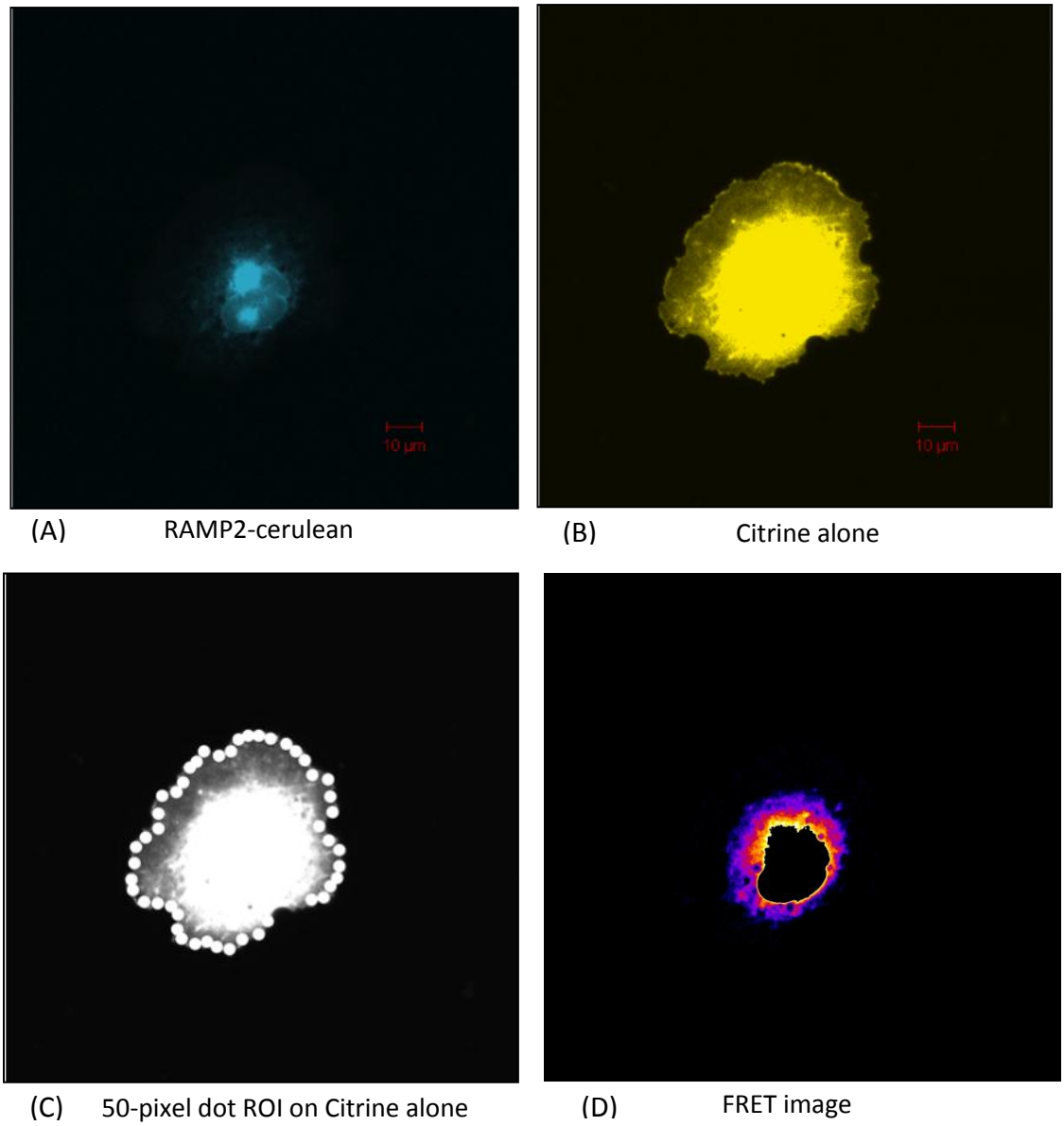

(A) RAMP2-cerulean (B) Citrine alone

(C) 50-pixel dot ROI on Citrine alone (D) FRET image

Figure 3.3.2: Representative image for FRET between free Citrine and RAMP2-cerulean in COS-7 cells: COS-7 cells were transfected with 5µg pcDNA 3.1 Citrine and 15µg pcDNA3.1 cerulean-link-RAMP2 and were imaged using the confocal microscope 48hr post transfection. (A) Expression of RAMP2-cerulean (B) Expression of free Citrine (C) 50 pixel dot ROI around the cell membrane of Citrine only image to measure cell-surface FRET. (D) FRET between citrine and Cer RAMP2. Scale bar 10µm

Citrine + RAMP3

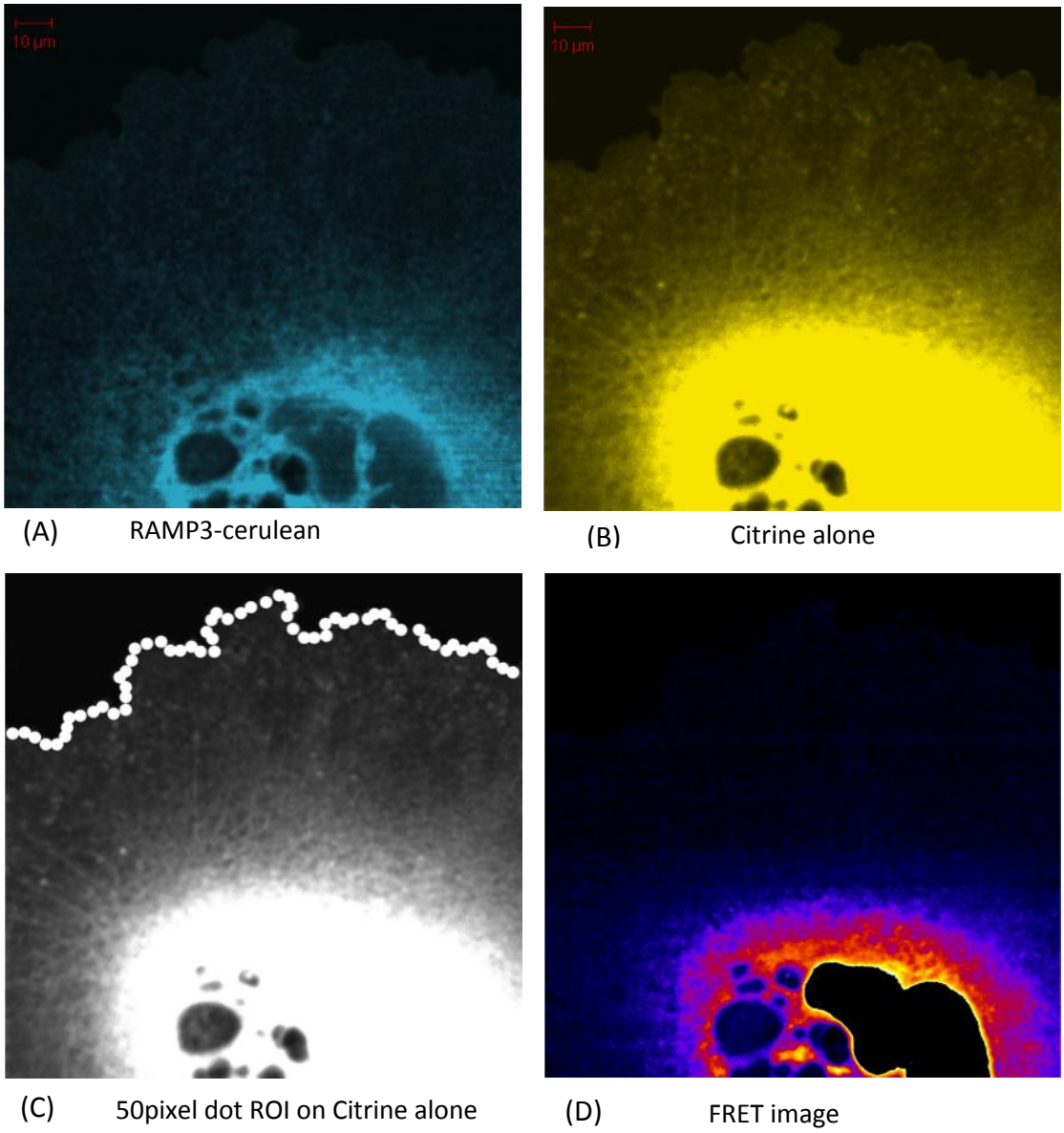

Figure 3.3.3: Representative image for FRET between free Citrine and RAMP3-Cerin COS-7 cells: COS-7 cells were transfected with 5µg pcDNA 3.1 Citrine and 15µg pcDNA3.1 cerulean-link-RAMP3 and were imaged using the confocal microscope 48hr post transfection. (A) Expression of RAMP3-cerulean (B) Expression of free Citrine (C) 50 pixel dot ROI around the cell membrane of Citrine only image to measure cell-surface FRET. (D) FRET between citrine and Cer RAMP3. Scale bar 10µm.

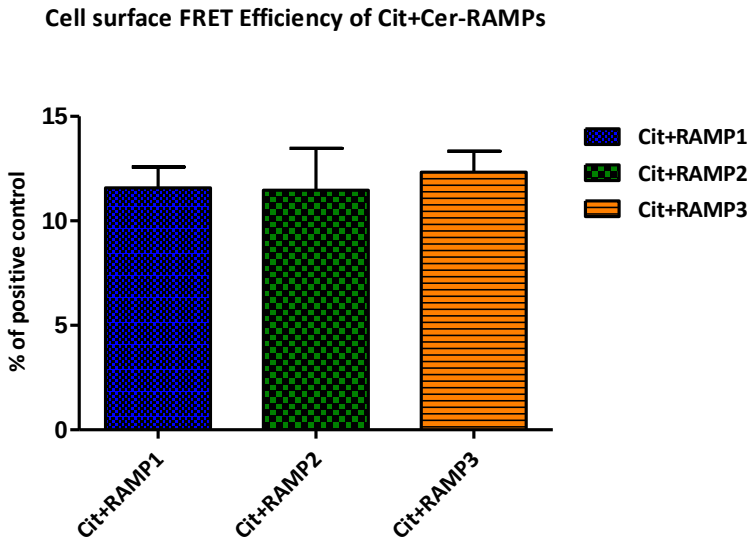

Figure 3.3.4: Graph for FRET negative control

Graph comparing the values of cell-surface NFRET between free citrine and RAMP 1/2/3-cerulean co-transfected in COS-7 cells, as a negative control. These values present background FRET and were used threshold to qualify a FRET interaction as specific for different combinations of GPCR and RAMPs in further experiments.

Cit +RAMPs-Cer	Mean ± SEM of cell-surface NFRET (% of positive control)
Cit + RAMP1-cerulean (n=25)	11.58±1.80
Cit + RAMP2-cerulean (n=24)	11.47±2.92
Cit + RAMP3-cerulean (n=29)	12.30 ±1.60

Table 3.3.1: Cell-surface NFRET values of free citrine co-transfected with RAMPs-cerulean in COS-7 cells, as a negative control.

3.3.2. Receptor positive control for FRET: Interaction of RAMPs with CLR.

In order to determine if the optimization of the FRET technique was efficient, a known RAMP-GPCR interaction was used to calculate the FRET efficiency on cell-surface. CLR was chosen as a positive control [156]. COS-7 cells were co-transfected with CLR-citrine pcDNA 3.1 (3µg) and RAMP-cerulean pcDNA 3.1 (3µg). As shown in the figures 3.3.5, 3.3.6, 3.3.7 specific areas of co-localization of FRET complexes were seen between CLR and all RAMPs ranging from the peri-nuclear region, cytoplasm and the cell membrane. Red arrows on (3.3.5-3.3.7 D) indicate region of co-localization between CLR and RAMPs on cell-surface. Colours from dark to bright indicate low to high levels of co-localization. So, blue areas represent less degree of co-localization; whereas brighter areas from pink to yellow represent higher co-localization.

Using 50-pixel dot ROI on the acceptor image: panel (C) on images 3.3.5-3.3.7; the values for NFRET, fraction of CLR and RAMP in FRET complex on the cell-surface were calculated and are shown in Fig 3.3.8 and Table 3.3.2. Fig 3.3.8 (D) shows that there was no significant difference between the expression levels of individual RAMPs in combination with the CLR on the cell surface of the co-transfected cells. The cell-surface NFRET values for all CLR+RAMP combinations were significantly higher than their corresponding negative controls as determined by 2-way ANOVA, Bonferroni post-test (Fig 3.3.8 A). Cell-surface NFRET efficiency of CLR+RAMP3 complex was statistically significantly higher than CLR+RAMP1, as analysed by Kruskal-Wallis test, Dunn's multiple comparison post-test (Fig 3.3.8 A and Table 3.3.2). The total expression levels of RAMP1, RAMP2 and RAMP3 on cell-surface was ~2 times, ~1.6 times and ~5 times higher than CLR respectively as calculated by the R value. Out of this total expression, the fraction of RAMP1 involved in cell-surface FRET complex was (in %) 10 ± 4.2, RAMP2 14.6 ± 13.8 and RAMP3 9 ± 8.0 (Fig 3.3.8 B and Table 3.3.2). The fraction of CLR present in the FRET complex out of its total expression on cell-surface, was (in %) 50.2 ± 35 (with RAMP1), 46.7 ± 27.4 (with RAMP2) and 46.0 ± 26.8 (with RAMP3) (Fig 3.3.8 C and Table 3.3.2).

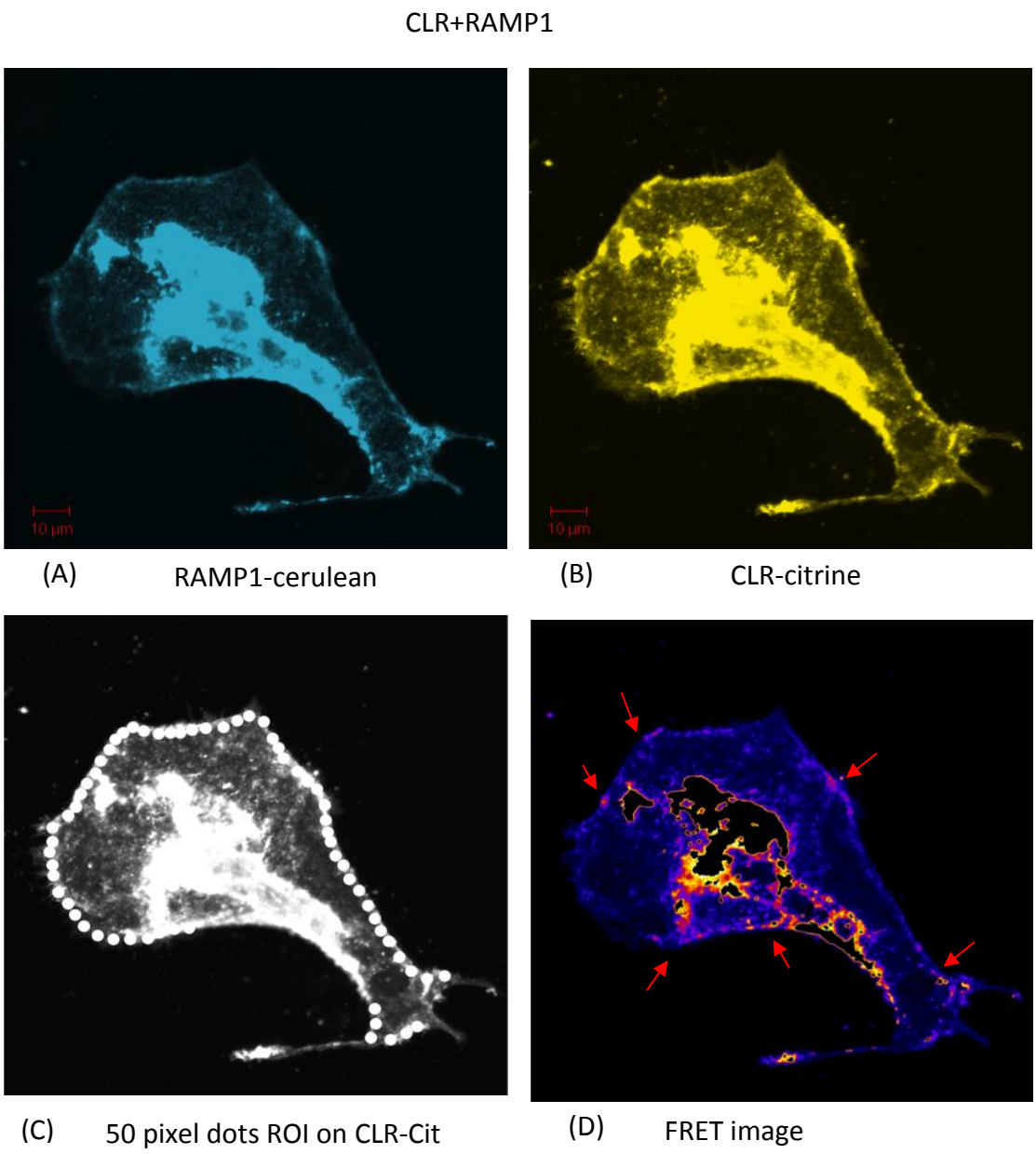

Figure 3.3.5: Representative image for FRET between CLR-citrine and RAMP1-cerulean in COS-7 cells
COS-7 cells were transfected with 3µg pcDNA 3.1 citrine-CLR and 3µg pcDNA3.1 cerulean-link-RAMP1 and were imaged using the confocal microscope 48hr-post transfection. (A) Expression of RAMP1-cerulean (donor) (B) Expression of CLR-citrine (acceptor) (C) 50 pixel dot ROI around the cell membrane of the CLR-citrine image to measure cell-surface FRET. (D) FRET between CLR-citrine and RAMP1-cerulean. Blue areas represent less degree of co-localization; whereas brighter areas from pink to yellow represent higher co-localization. Red arrows indicate areas of co-localization between CLR and RAMP1 on the cell-surface. Scale bar 10µm

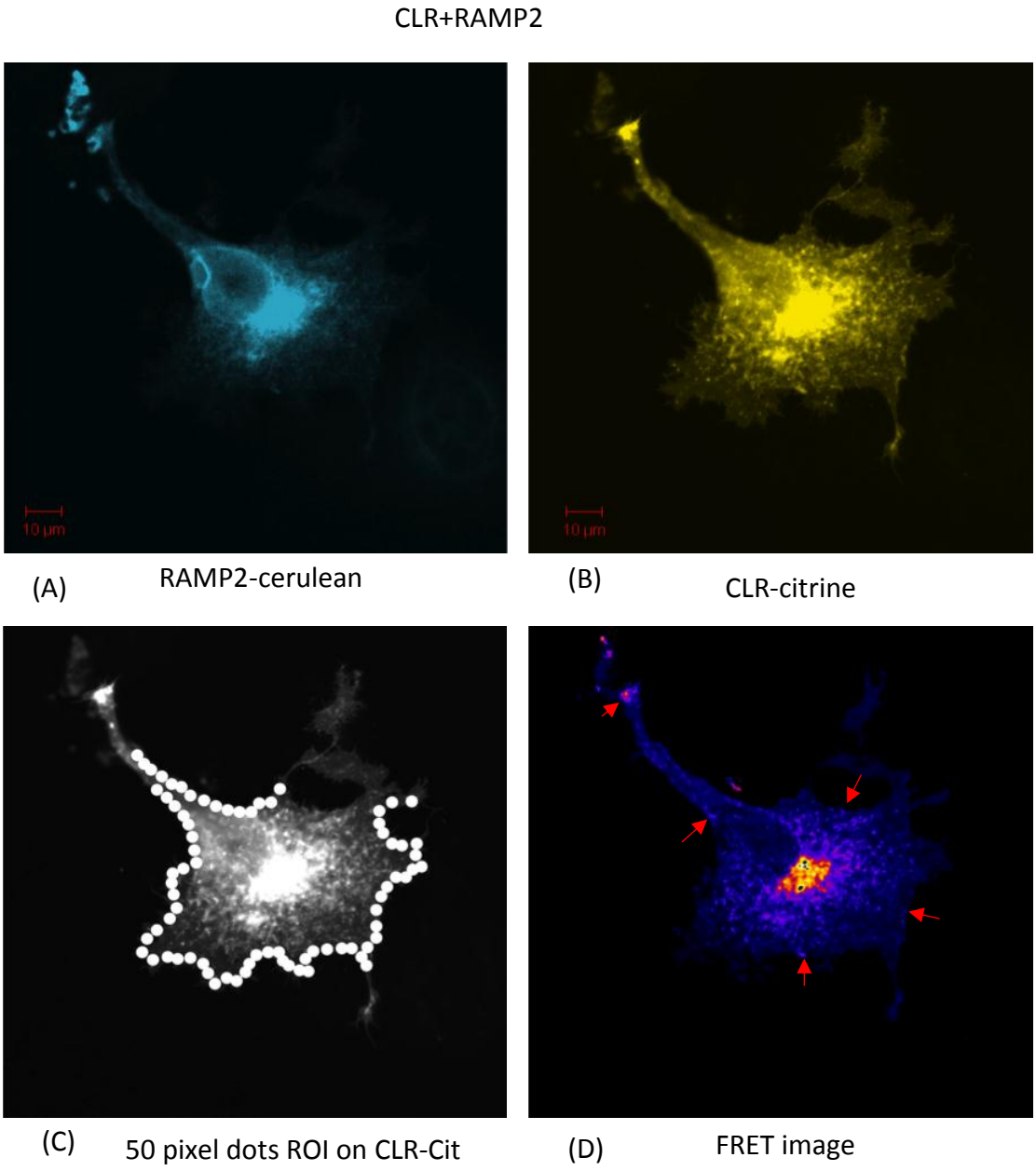

Figure 3.3.6: Representative image for FRET between CLR-citrine and RAMP2-cerulean in COS-7 cells: COS-7 cells were transfected with 3µg pcDNA 3.1 Citrine-CLR and 3µg pcDNA3.1 cerulean-link-RAMP2 and were imaged using the confocal microscope 48hr post transfection. (A) Expression of RAMP2-cerulean (donor) (B) Expression of CLR-citrine (acceptor) (C) 50 pixel dot ROI around the cell membrane of the CLR-citrine image to measure cell-surface FRET. (D) FRET between CLR-citrine and RAMP2-cerulean. Red arrows indicate areas of co-localization between CLR and RAMP2 on the cell-surface. Scale bar 10µm

CLR+RAMP3

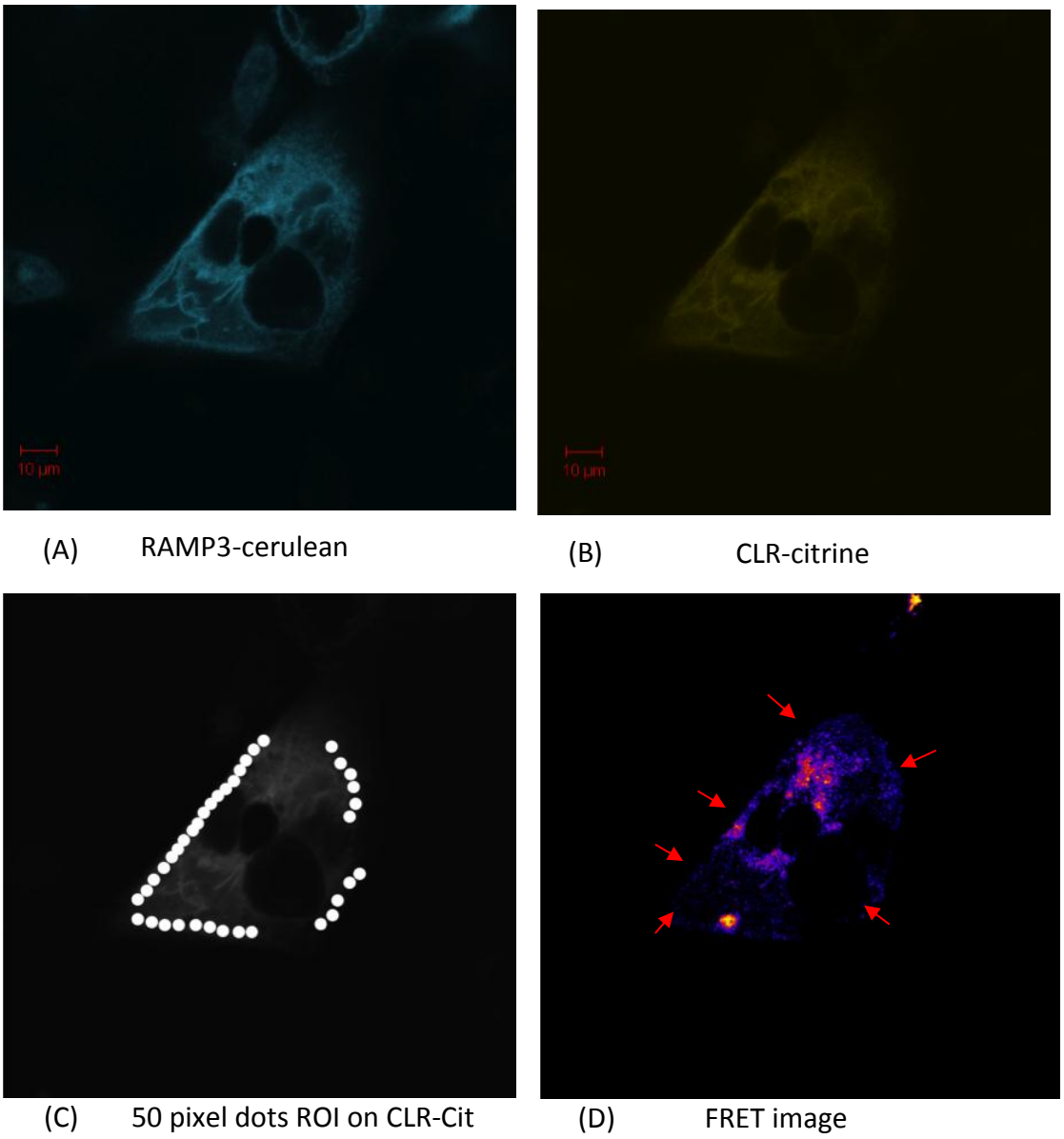

(A) RAMP3-cerulean (B) CLR-citrine

(C) 50 pixel dots ROI on CLR-Cit (D) FRET image

Figure 3.3.7: Representative image for FRET between CLR-citrine and RAMP3-cerulean in COS-7 cells: COS-7 cells were transfected with 3µg pcDNA 3.1 Citrine-CLR and 3µg pcDNA3.1 cerulean-link-RAMP3 and were imaged using the confocal microscope 48hr post transfection. (A) Expression of RAMP3-cerulean (donor) (B) Expression of CLR-citrine (acceptor) (C) 50 pixel dot ROI around the cell membrane of the CLR-citrine image to measure cell-surface FRET. (D) FRET between CLR-citrine and RAMP3-cerulean. Red arrows indicate areas of co-localization between CLR and RAMP3 on the cell-surface. Scale bar 10µm

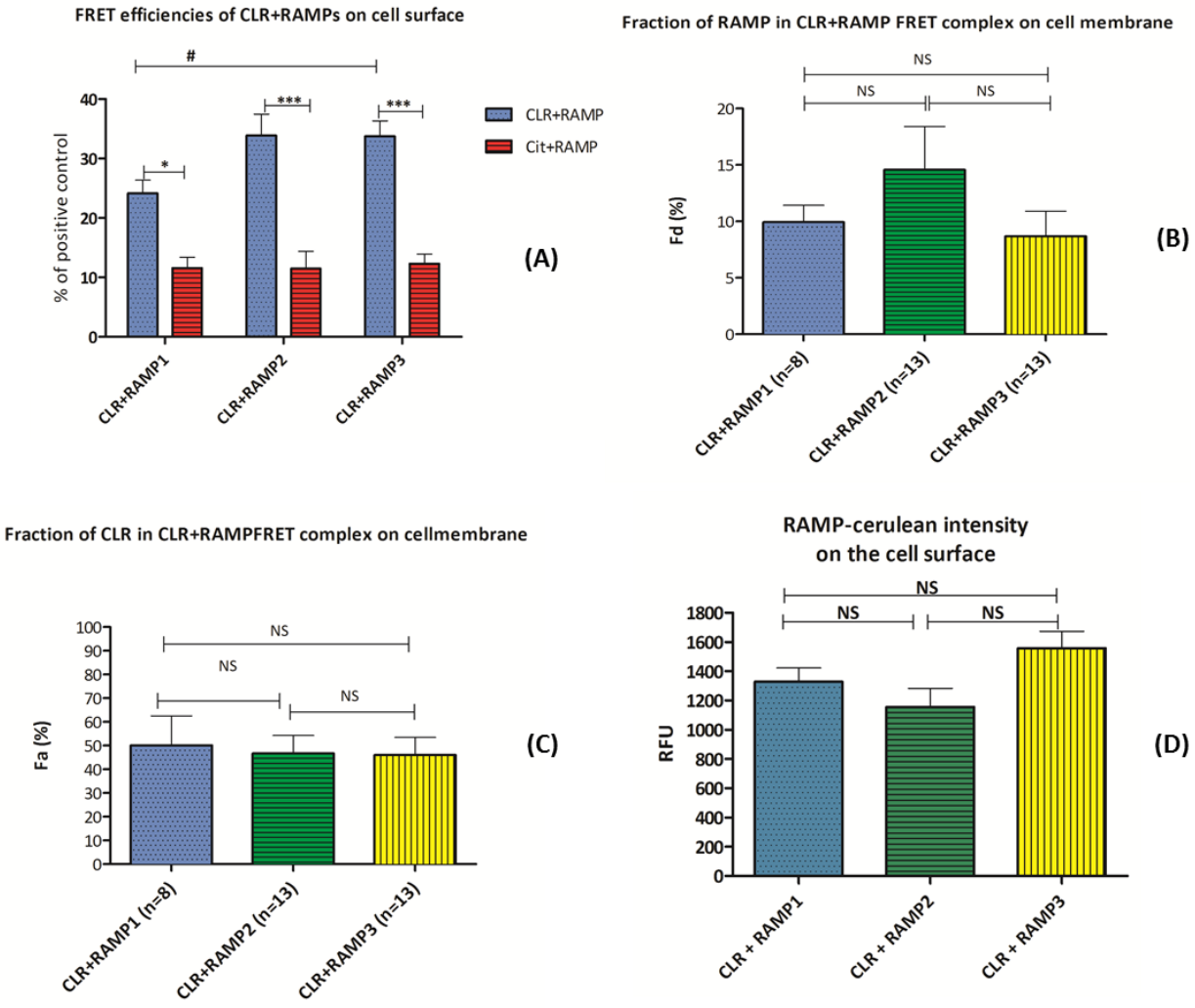

Figure 3.3.8: Cell-surface FRET efficiencies of CLR+RAMPs and fraction of receptor components involved in FRET complex:

(A) Cell-surface FRET efficiencies of individual RAMPs with CLR (blue bars) compared among themselves and also with respective negative control citrine alone+RAMP-cerulean (red bars). *p<0.05 and ***p<0.0001 as determined by 2-way ANOVA, Bonferroni post-test; # p<0.05 Kruskal-Wallis test, Dunn's multiple comparison test. *(B) and (C)* Stoichiometric analysis of fraction of RAMP and CLR present in FRET complex on the cell-surface, respectively. Statistical test used was Kruskal-Wallis test, Dunn's multiple comparison test. *(D)* Fluorescence intensity of the cerulean-tagged RAMPs on the cell surface of CLR + RAMP co-transfected cells (Kruskal-Walis test, Dunn's multiple comparison test). Total cells analysed in 3 separate transfections: CLR+RAMP1 (n=8), CLR+RAMP2 (n=13), CLR+RAMP3 (n=13). Citrine +RAMP1 (n=4), citrine +RAMP2 (n=5), citrine +RAMP3 (n=7). The data was not normally distributed as analysed by D'Agostino & Pearson omnibus normality test.

CLR+RAMP	NFRET % of positive control	Fd(%)	Fa (%)	R
CLR+RAMP1 (n=8)	24.2±2.2	10.0 ±1.5	50.2±12.37	0.5±0.13
CLR+RAMP2 (n=13)	33.9±3.6	14.6±3.8	46.7±7.58	0.6±0.18
CLR+RAMP3 (n=13)	33.8±2.58*	9.0 ± 2.2	46±7.42.8	0.2±0.03

Table 3.3.2: Mean and SEM values of cell membrane FRET efficiency and fraction of receptor components involved in FRET between the CLR and RAMPs:

Significant difference in the NFRET value was observed between CLR+RAMP1 vs CLR+RAMP3 (* = $p<0.05$ Kruskal-Wallis test, Dunn's multiple comparison post-test). The fraction of RAMP and CLR in FRET did not differ significantly between the three complexes as analysed by Kruskal-Wallis test, Dunn's multiple comparison post-test. Combined data of three separate transfections and the values in brackets indicate number of cells analysed.

3.3.3. Measuring interaction between CaSR and RAMPs using FRET-based stoichiometry:

In order to determine if the FRET technique could measure CaSR and RAMP interaction, FRET-based stoichiometric analysis was used on COS-7 cells co-transfected with pcDNA 3.1 CaSR-citrine and pcDNA 3.1 RAMP-cerulean. As shown in the figure 3.3.9 when COS-7 cells were transfected with CaSR alone, majority of the receptor was localized within the peri-nuclear region which indicates failure of trafficking to the cell-surface. However, when RAMP1-cerulean or RAMP3-cerulean (Figure 3.3.10 and 3.3.12) were co-transfected, distinct regions of co-localization of FRET complexes were seen ranging from the peri-nuclear region, cytoplasm and the cell membrane. Red arrows on the FRET figures (panel D; figures 3.3.10-12) indicate cell-surface FRET complexes of CaSR+RAMP1/3. In case of RAMP2-cerulean co-localization with CaSR could be seen in the perinuclear region only with no or little cell-surface co-localization (Figure 3.3.11).

Using 50 pixel-dot ROI on the acceptor image: panel (C) on images 3.3.10.-3.3.12; NFRET values, fraction of CaSR and RAMP in FRET complex were calculated as shown in Figure 3.3.13 and Table 3.3.3. As shown in the figure 3.3.13 (D), the cell surface levels of all RAMPs in combination with CaSR were not different from each other in co-transfected cells. The cell-surface NFRET values for CaSR+RAMP1/3 combinations were significantly higher than their corresponding negative controls ($p<0.0001$, 2-way ANOVA, Bonferroni post-test) (Figure 3.3.13 A) and CaSR+RAMP2 cell-surface FRET complex (Figure 3.3.13 A, Table 3.3.3), ($p<0.0001$, Kruskal-Wallis test, Dunn's multiple comparison post-test). NFRET between CaSR and RAMP2 was similar to the corresponding negative control-RAMP2-cerulean and citrine alone. Also CaSR+RAMP3 cell-surface FRET efficiency was found to be statistically significantly higher by ~1.6 fold compared to CaSR+RAMP1 ($p<0.0001$, Kruskal-Wallis test, Dunn's multiple comparison post-test) (Fig 3.3.13 A, Table 3.3.3).

The total expression levels of RAMP1 and 3 on cell-surface were ~1.6 times higher than CaSR respectively (Table 3.3.3). Out of this, the fraction of RAMP1 (in %) involved in cell-surface FRET complex was 16 ± 1.4 and RAMP3 was 26.0 ± 4.3 (Fig 3.3.13 B and Table 3.3.3). So, the fraction

of RAMP3 was ~1.6 fold higher than RAMP1 in FRET complex with CaSR, which was statistically significant ($p<0.05$, Mann-Whitney two-tailed test).

The fraction of CaSR present in the FRET complex on the cell-surface was 58.4 ± 7.1% (with RAMP1) and 67.00 ± 10.0% (with RAMP3) (Fig 3.2.13 C and Table 3.3.3); out of its total population. There was no statistically significant difference between the fraction of CaSR in RAMP1 and RAMP3 cell-surface FRET complexes.

CaSR alone

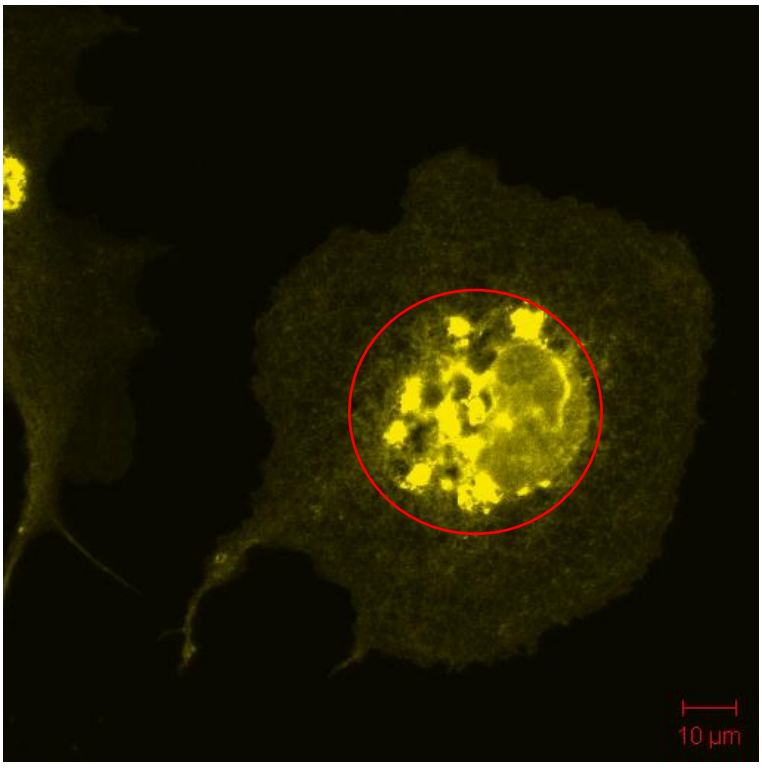

Figure 3.3.9: Representative picture showing expression of CaSR-citrine alone in transfected COS7 cell. Red circle represents the restriction of CaSR within the perinuclear region .

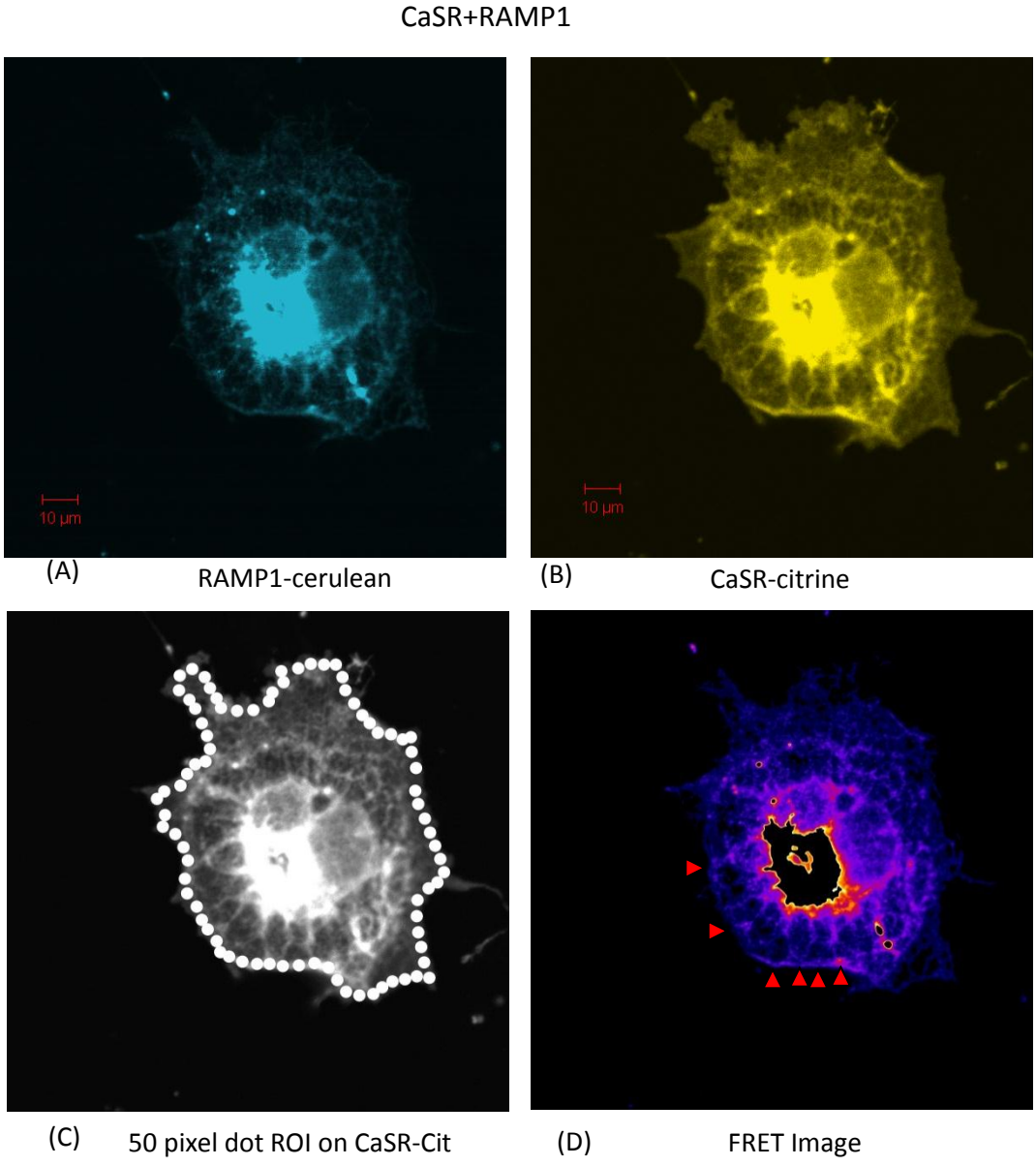

Figure 3.3.10: Representative image for FRET between CaSR-citrine and RAMP1-cerulean in COS-7 cells:

COS-7 cells were transfected with 10µg pcDNA 3.1 Citrine-CaSR and 15µg pcDNA3.1 cerulean-link-RAMP1 and were imaged using the confocal microscope 48hr post transfection. (A) Expression of RAMP1-cerulean (donor) (B) Expression of CaSR-citrine (acceptor) (C) 50 pixel dot ROI around the cell membrane of the CaSR-citrine image to measure cell-surface FRET (D) FRET between CaSR-citrine and RAMP1-cerulean. Blue areas represent less degree of co-localization; whereas brighter areas from pink to yellow represent higher co-localization. Red arrows indicate areas of co-localization between CaSR and RAMP1 on the cell-surface. Scale bar 10µm.

CaSR+RAMP2

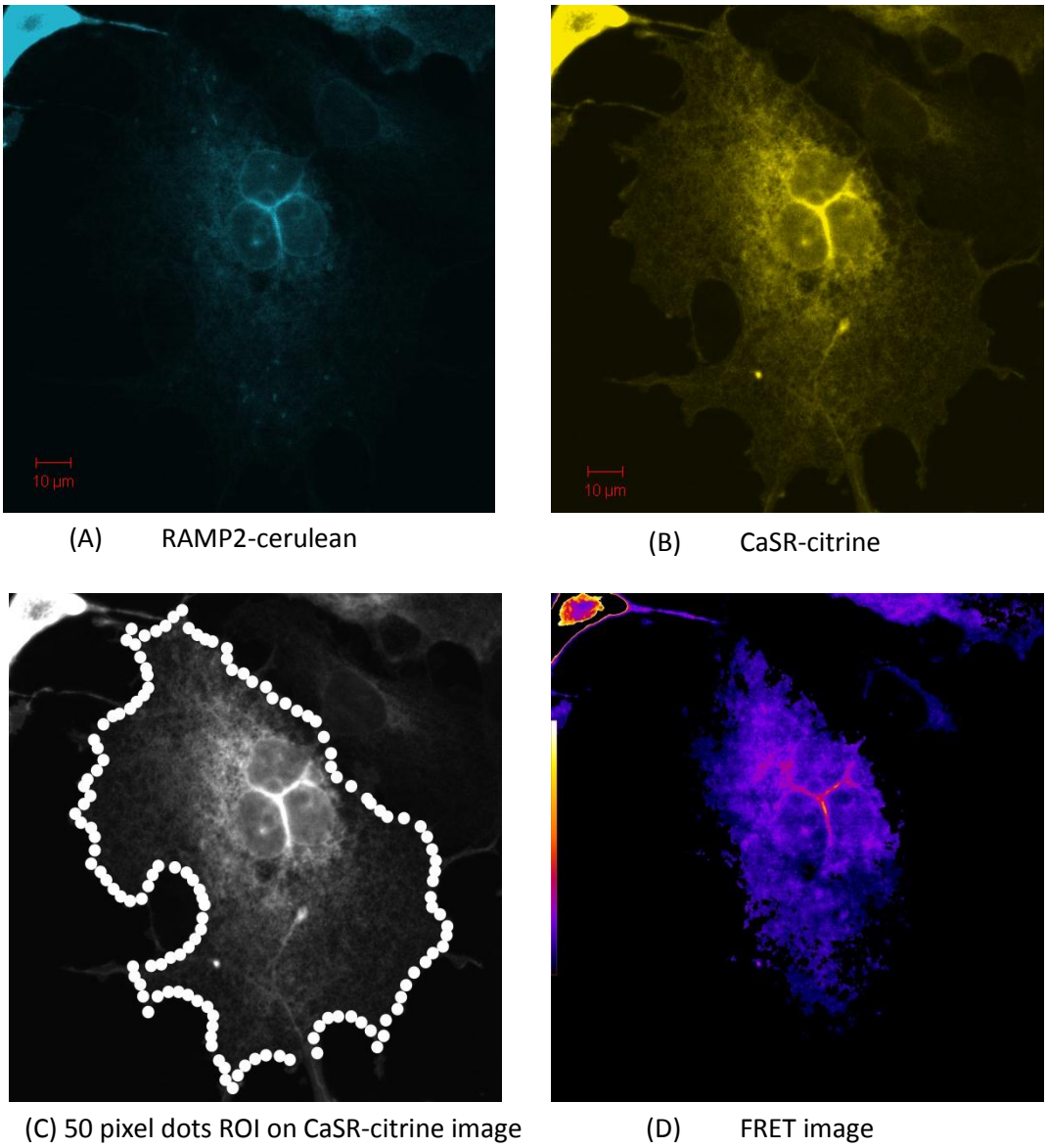

(A) RAMP2-cerulean (B) CaSR-citrine

(C) 50 pixel dots ROI on CaSR-citrine image (D) FRET image

Figure 3.3.11: Representative image for FRET between CaSR-citrine and RAMP2-cerulean in COS-7 cells:

COS-7 cells were transfected with 10µg pcDNA 3.1 citrine-CaSR and 15µg pcDNA3.1 cerulean-link-RAMP2 and were imaged using the confocal microscope 48hr post transfection. (A) Expression of RAMP2-cerulean (donor) (B) Expression of CaSR-citrine (acceptor) (C) 50 pixel dot ROI around the cell membrane of the CaSR-citrine image to measure cell-surface FRET. (D) FRET between CaSR-citrine and RAMP2-cerulean. Scale bar 10µm.

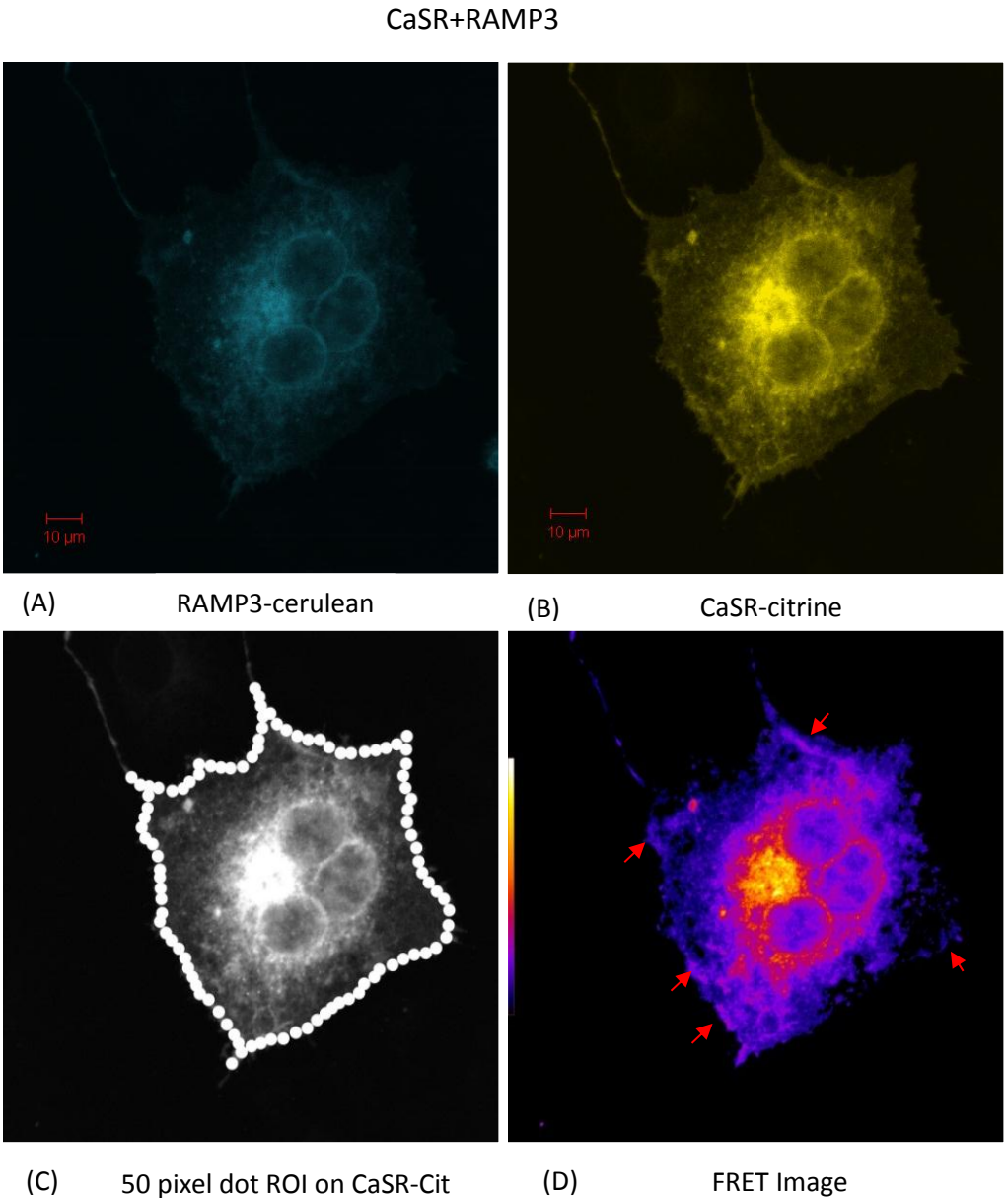

Figure 3.3.12: Representative image for FRET between CaSR-citrine and RAMP3-cerulean in COS-7 cells:

COS-7 cells were transfected with 10µg pcDNA 3.1 Citrine-CaSR and 15µg pcDNA3.1 cerulean-link-RAMP3 and were imaged using the confocal microscope 48hr post transfection. (A) Expression of RAMP3-cerulean (donor) (B) Expression of CaSR-citrine (acceptor) (C) 50 pixel dot ROI around the cell membrane of the CaSR-citrine image to measure cell-surface FRET. (D) FRET between CaSR-citrine and RAMP3-cerulean. . Red arrows indicate areas of co-localization between CaSR and RAMP3 on the cell-surface. Scale bar 10µm.

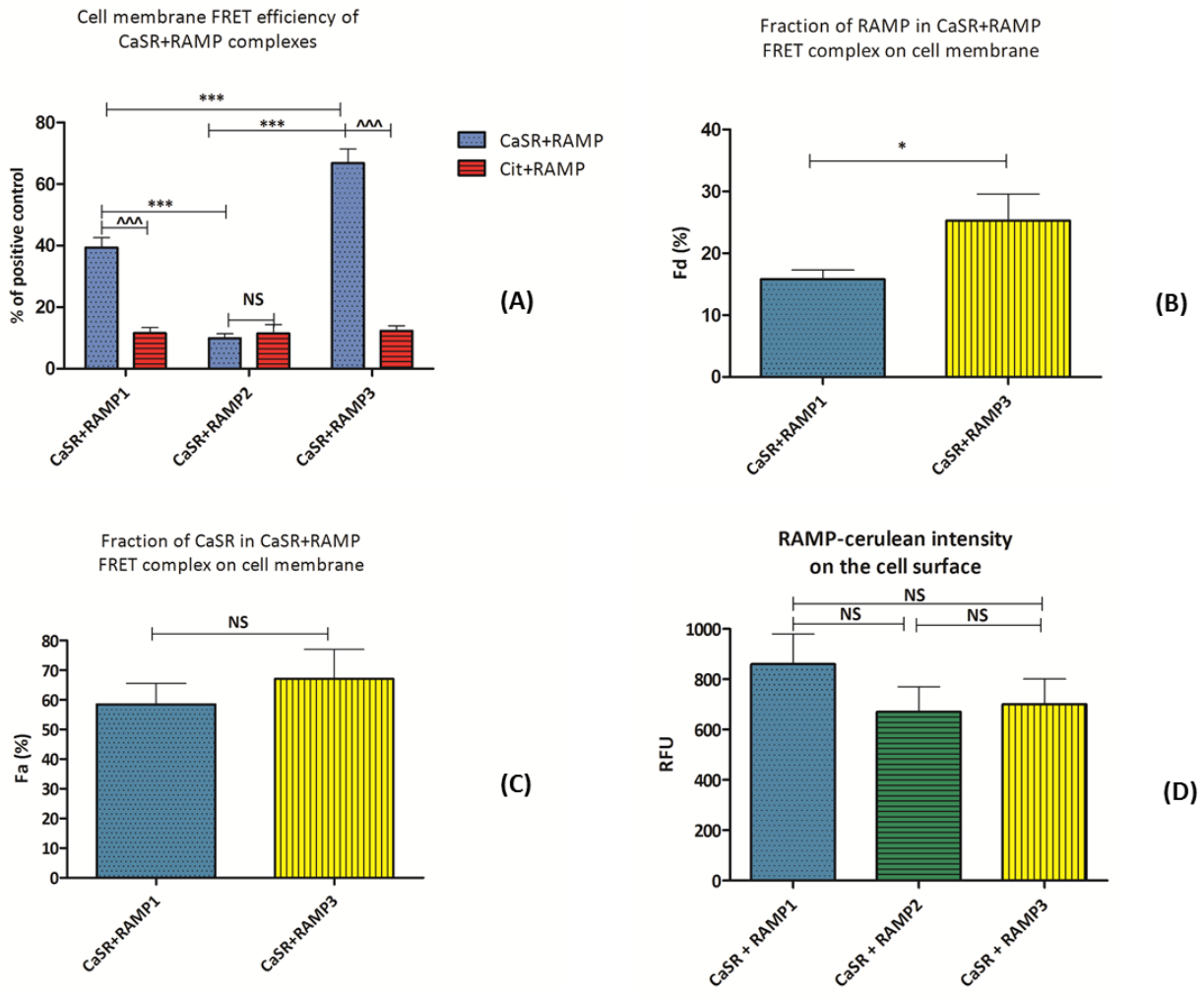

Figure 3.3.13: Cell-surface FRET efficiencies of CaSR+RAMPs and fraction of receptor components involved in FRET complex

(A) Cell-surface FRET efficiencies of individual RAMPs with CaSR (blue bars) compared among themselves and also with respective negative control citrine alone+RAMP (red bars). $^{\wedge\wedge\wedge}$p<0.0001 (2-way ANOVA, Bonferroni post-test) ***p<0.0001 (Kruskal-Wallis test, Dunn's multiple comparison test) *(B) and (C)* Stoichiometirc analysis of fraction of RAMP and CaSR present in FRET complex on the cell-surface, respectively.* p<0.05 Mann Whitney test. *(D)* Fluorescence intensity of the cerulean-tagged RAMPs on the cell surface of CaSR + RAMP co-transfected cells (Kruskal-Walis test, Dunn's multiple comparison test). Total cells analysed in 3 separate transfections for CaSR+RAMP1 (n=13), CaSR+RAMP2 (n=25), and 2 transfections for CaSR+RAMP3 (n=9). Citrine +RAMP1 (n=4), citrine +RAMP2 (n=5), citrine +RAMP3 (n=8).

CaSR+RAMP	NFRET % of positive control	Fa (%)	Fd(%)	R
CaSR+RAMP1 (n=13)	[a]40.0 ± 3.4[*** vs b]	58.4 ± 7.1	16.0 ±1.4	0.6±0.09
CaSR+RAMP2 (n=25)	[b]9.9 ± 1.5	-	-	0.5 ±0.11
CaSR+RAMP3 (n=9)	65.3 ± 4.4 [*** vs a,b]	67.00 ± 10.0	26.0 ± 4.3[#]	0.6±0.2

Table 3.3.3: Mean and SEM values of cell membrane FRET efficiency and fraction of receptor components involved in FRET between the CaSR and RAMPs:
Significant difference in the NFRET value was observed between CaSR+RAMP1 and 3 vs CaSR+RAMP2 ([a]***p<0.0001, Kruskal-Wallis test, Dunn's multiple comparison test) and between CaSR+RAMP1 vs CaSR +RAMP3 ([b]***p<0.0001, Kruskal-Wallis test, Dunn's multiple comparison test). Significant differences were also observed in the fraction of RAMP3 and RAMP1 in cell-surface FRET complex ([#]p<0.05, Mann Whitney test). Combined data of three separate transfections for CaSR+RAMP1 and 2 and two separate transfections for CaSR+RAMP3 and the values in brackets indicate number of cells analysed. The data was not normally distributed as analysed by D'Agostino & Pearson omnibus normality test.

3.3.4. Measuring interaction between GPRC6A and RAMPs using FRET-based stoichiometry:

This part of the work was carried out by Lan Zhu (MSc Molecular medicine student) under my supervision. The possibility of a molecular interaction between GPRC6A and RAMPs was tested using FRET stoichiometry. It was observed that GPRC6A-citrine expression when present on its own was mainly localized within the peri-nuclear region (Figure 3.3.14). Whereas in presence of RAMP1 but not RAMP2 or 3 (Figure 3.3.15; 3.3.16 and 3.3.17 respectively), specific regions of co-localization were observed on the cell-surface (as shown by red arrows in Figure 3.3.15 D). In case of GPRC6A+RAMP2 areas of co-localization were seen in the perinuclear regions which were not very evident with RAMP3 (Figure 3.3.16 D vs 3.3.17 D).

To measure the cell-surface NFRET and the fractions of GPRC6A and RAMP in FRET complex; an ROI was created on the cell-surface of GPRC6A-citrine image using 50 pixel-dots (Figure 3.3.15-3.3.17 panel C). Figure 3.3.18 (D) show that the expression of RAMP1 in GPRC6A+RAMP1 co-transfected cells (blue bar) was higher than GPRC6A+RAMP2 (green bar) co-transfected cells, but similar to GPRC6A + RAMP3 (yellow bar) transfected cells ($p<0.05$, Kruskal-Wallis test, Dunn's multiple comparison post-test). There was no significant difference between the expression of RAMP2 and 3 on the cell surface. Cell-surface NFRET values for GPRC6A with RAMP1 were significantly higher compared to the negative control ($p<0.0001$, 2 way ANOVA, Bonferroni post-test) (Figure 3.3.18 A). On the contrary, no statistical significance was observed for cell-surface NFRET values between GPRC6A+RAMP2 or 3 complexes and their corresponding negative controls (Figure 3.3.18 A). Figure 3.3.18 A and table 3.3.4 show statistically significant increases in cell-surface NFRET between GPRC6A+RAMP1 vs GPRC6A+RAMP2/3 (~3.5 fold vs GPRC6A+RAMP2), (~6 fold vs GPRC6A+RAMP3) ($p<0.0001$, Kruskal Wallis test, Dunn's multiple comparison post-test), thus showing that RAMP1 is an interacting partner responsible for cell-surface trafficking of the GPRC6A.

A deeper insight into the interaction of GPRC6A and RAMPs was provided by FRET based stoichiometric analysis. An excess of total expression of RAMP1 by ~3 times to GPRC6A was measured by absolute concentration ratio R (Table 3.3.4). Out of that 19.72 ± 2.3 % of RAMP1 was present in the FRET complex with the GPRC6A. The total expression of RAMP2 and 3 were

5 times than GPRC6A on the cell-surface where only 3.2± 1.28% and 0.8± 2.3% of RAMP3 and 3 respectively, were measured as present in FRET complex (Figure 3.3.18 B, Table 3.3.4).

The fraction of GPRC6A present in the FRET complex with RAMP1 was 68.4 ± 7.8% out of its total population on the cell-surface; whereas it was 8.56 ± 3.32% and 5% in case of FRET complex with RAMP2 and 3 respectively (Figure 3.3.18 C, Table 3.3.4). So, the fraction of GPRC6A in cell-surface FRET complex with RAMP1 was statistically significantly higher than with RAMP2 (~8 fold higher) and RAMP3 (~14 fold higher). Similarly, the fraction of RAMP1 in cell-surface FRET complex with GPRC6A was statistically significantly higher than RAMP2 with GPRC6A (~6 fold higher) and RAMP3 (~25 fold higher) [(Figure 3.3.18 B, C and Table 3.3.4) ($p<0.0001$, Kruskal Wallis test, Dunn's multiple comparison post-test)].

GPRC6A alone

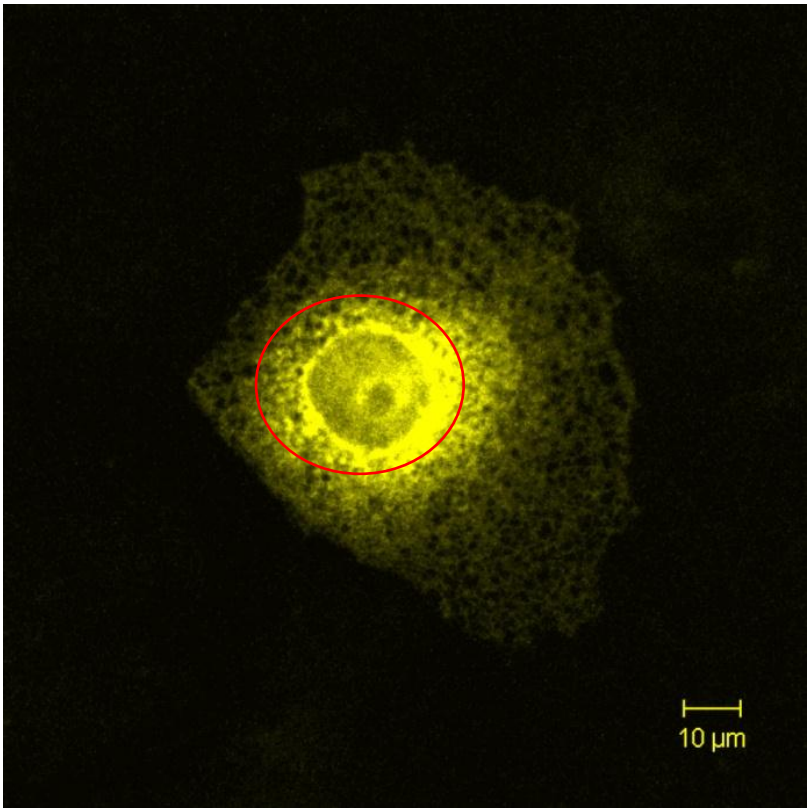

Figure 3.3.14*:* Representative picture showing expression of GPRC6A-citrine alone in COS-7 cell.

GPRC6A+RAMP1

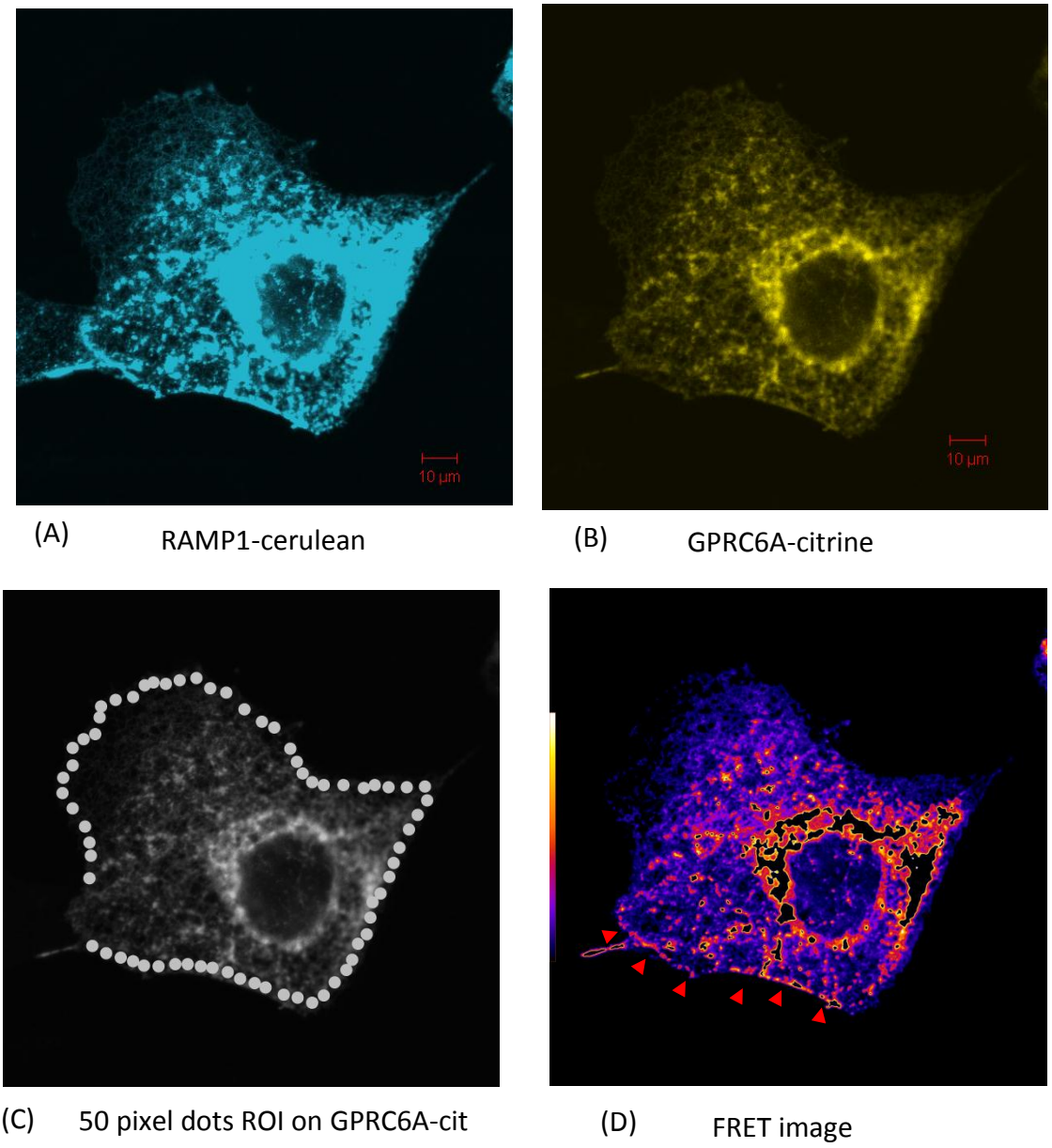

(A) RAMP1-cerulean (B) GPRC6A-citrine

(C) 50 pixel dots ROI on GPRC6A-cit (D) FRET image

Figure 3.3.15: Representative image for FRET between GPRC6A-citrine and RAMP1-cerulean in COS-7 cells:

COS-7 cells were transfected with 10µg pcDNA 3.1 citrine-GPRC6A and 10µg pcDNA3.1 cerulean-link-RAMP1 and were imaged using the confocal microscope 48hr post transfection. (A) Expression of RAMP1-cerulean (donor) (B) Expression of GPRC6A-citrine (acceptor) (C) 50 pixel dot ROI around the cell membrane of the GPRC6A-citrine image to measure cell-surface FRET. (D) FRET between GPRC6A-citrine and RAMP1-cerulean. Blue areas represent less degree of co-localization; whereas brighter areas from pink to yellow represent higher co-localization. Red arrows indicate areas of co-localization between GPRC6A and RAMP1 on the cell-surface. Scale bar 10µm.

GPRC6A+RAMP2

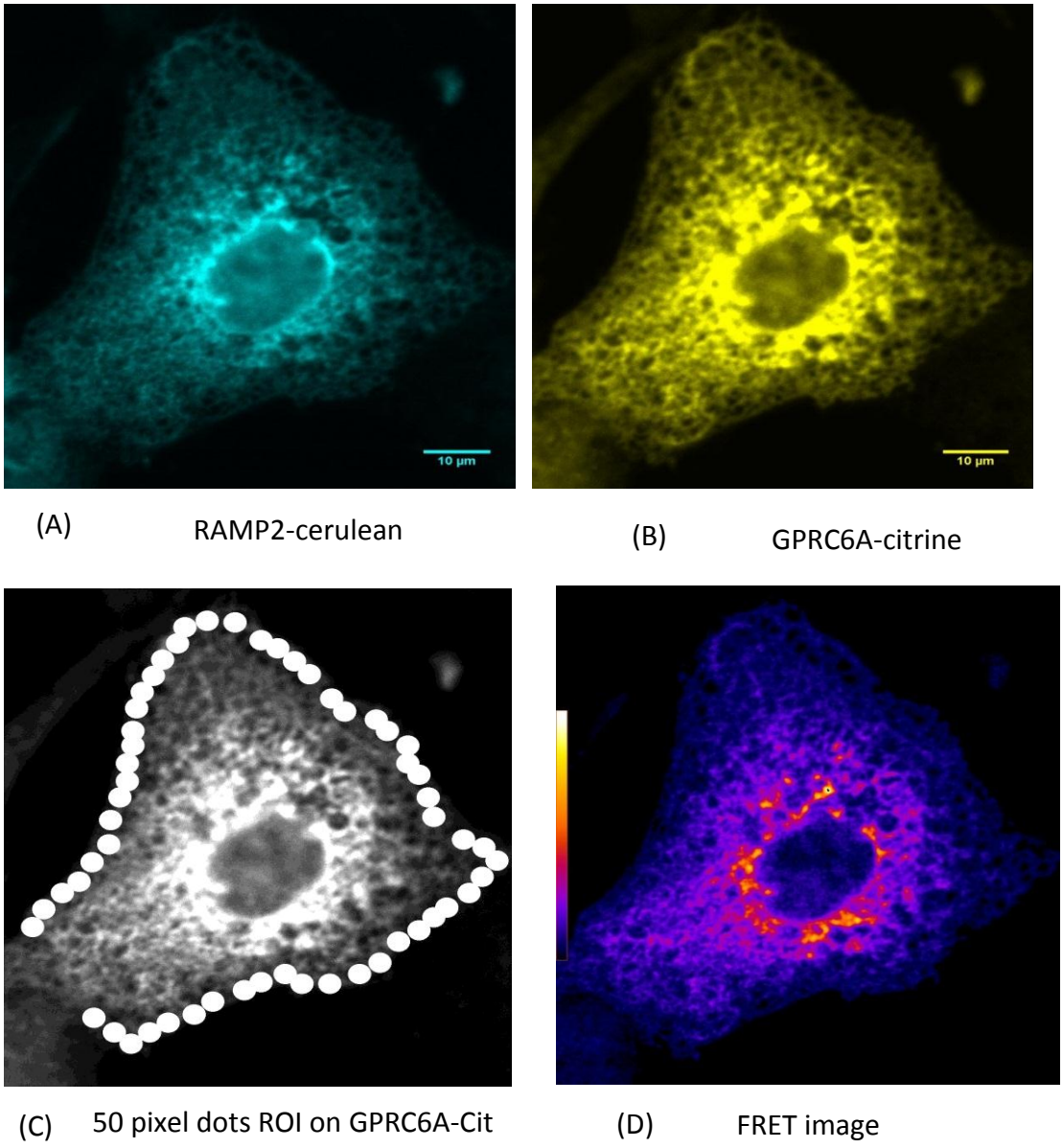

Figure 3.3.16: Representative image for FRET between GPRC6A-citrine and RAMP2-cerulean in COS-7 cells:

COS-7 cells were transfected with 10µg pcDNA 3.1 citrine-GPRC6A and 10µg pcDNA3.1 cerulean-link-RAMP2 and were imaged using the confocal microscope 48hr post transfection. (A) Expression of RAMP2-cerulean (donor) (B) Expression of GPRC6A-citrine (acceptor) (C) 50 pixel dot ROI around the cell membrane of the GPRC6A-citrine image to measure cell-surface FRET. (D) FRET between GPRC6A-citrine and RAMP2-cerulean. Scale bar 10µm.

GPRC6A+RAMP3

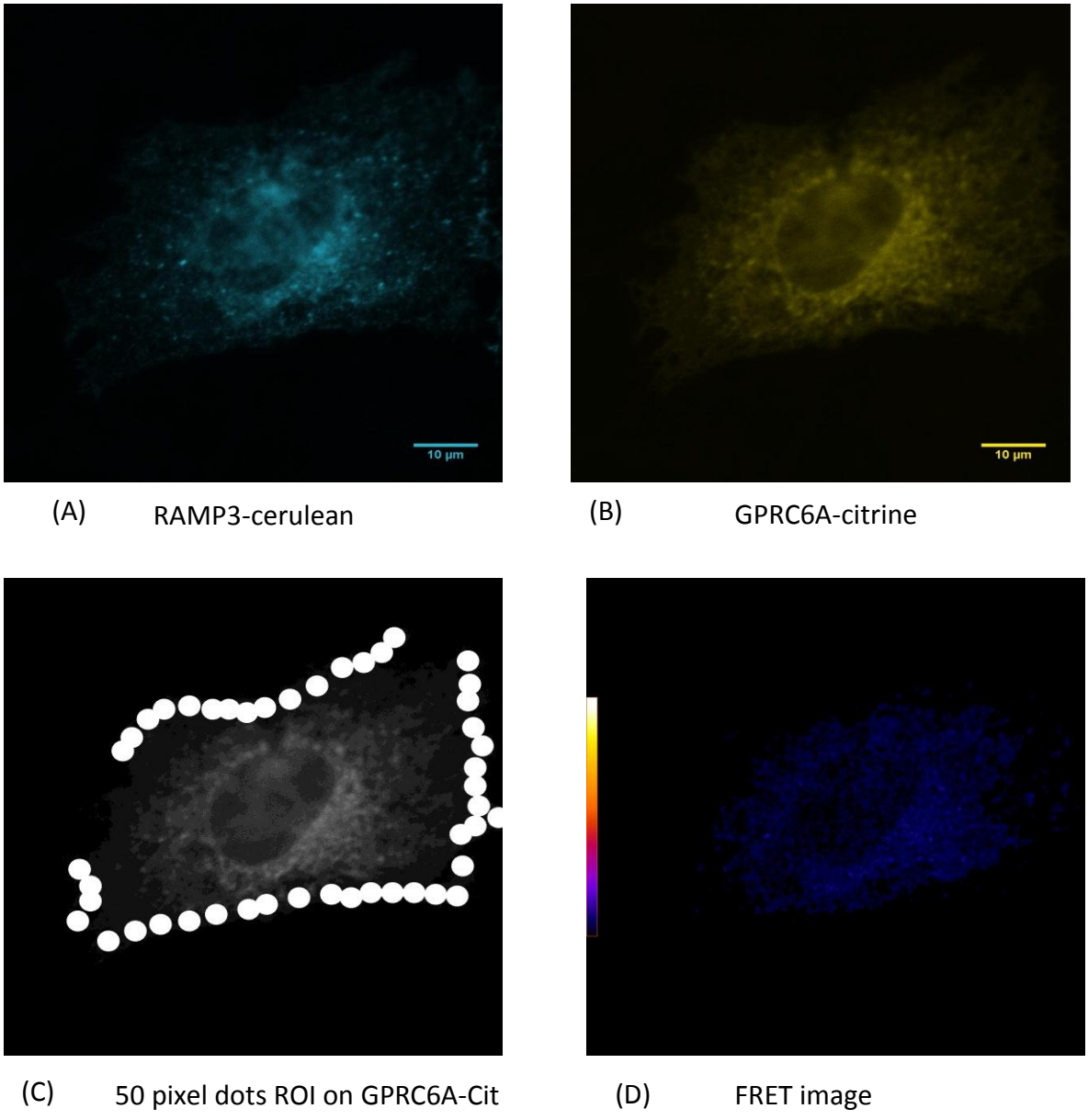

(A) RAMP3-cerulean (B) GPRC6A-citrine

(C) 50 pixel dots ROI on GPRC6A-Cit (D) FRET image

Figure 3.3.17: Representative image for FRET between GPRC6A-citrine and RAMP3-cerulean in COS-7 cells:

COS-7 cells were transfected with 10µg pcDNA 3.1 citrine-GPRC6A and 10µg pcDNA3.1 cerulean-link-RAMP3 and were imaged using the confocal microscope 48hr post transfection. (A) Expression of RAMP3-cerulean (donor) (B) Expression of GPRC6A-citrine (acceptor) (C) 50 pixel dot ROI around the cell membrane of the GPRC6A-citrine image to measure cell-surface FRET. (D) FRET between GPRC6A-citrine and RAMP3-cerulean. Scale bar 10µm

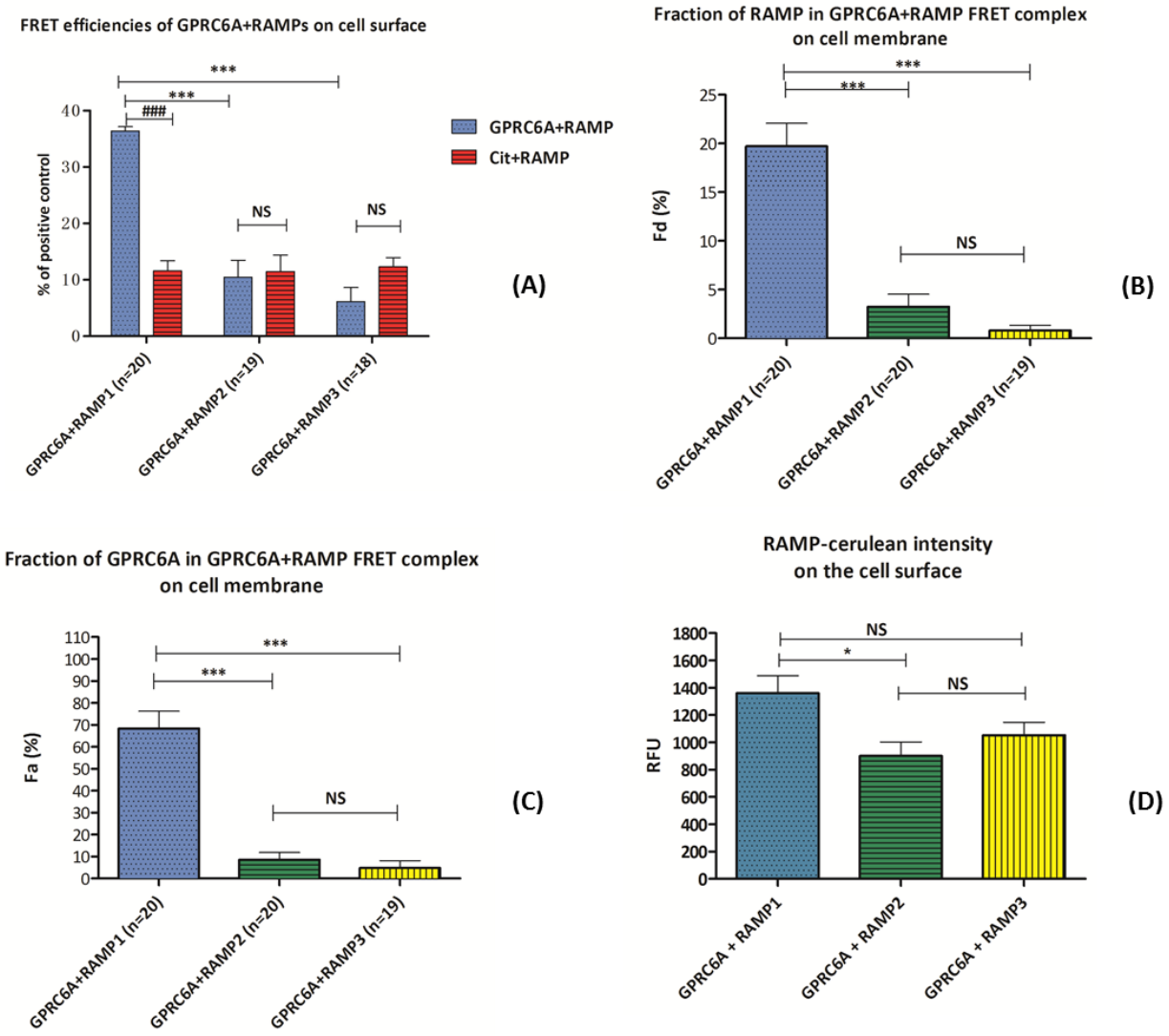

Figure 3.3.18: Cell-surface FRET efficiencies of GPRC6A+RAMPs and fraction of receptor components involved in FRET complex

(A) Cell-surface FRET efficiencies of individual RAMPs with GPRC6A (blue bars) compared among themselves and also with respective negative control citrine alone+RAMP (red bars). $^{###}$ p<0.0001 (2 way ANOVA , Bonferroni post-test), ***p<0.0001 (Kruskal Wallis test, Dunn's multiple comparison post-test) 33*(B) and (C)* Stoichiometric analysis of fraction of RAMP and GPRC6A present in FRET complex on the cell-surface, respectively. *** p<0.0001 (Kruskal Wallis test, Dunn's multiple comparison test). *(D)* Fluorescence intensity of the cerulean-tagged RAMPs on the cell surface of GPRC6A + RAMP transfected cells (* p<0.05 Kruskal-Walis test, Dunn's multiple comparison test). Total cells analysed in 3 separate transfections are shown in brackets. The data was not normally distributed as analysed by D'Agostino & Pearson omnibus normality test.

GPRC6A+RAMP	NFRET % of positive control	Fa (%)	Fd(%)	R
GPRC6A+RAMP1 (n=10)	36.4 ± 2.5**	68.4 ± 7.8***	19.7 ± 2.36***	0.34 ± 0.12
GPRC6A+RAMP2 (n=18)	10.5 ± 3.02	8.56 ± 3.32	3.24 ± 1.28	0.2±0.37
GPRC6A+RAMP3 (n=18)	6.14 ± 2.51	4.828 ± 3.32	0.8 ± 2.3	0.2±0.8

Table 3.3.4: Mean and SEM values of cell membrane FRET efficiency and fraction of receptor components involved in FRET between the GPRC6A and RAMPs:

Significant difference in the NFRET value was observed between GPRC6A+RAMP1 vs CLR+RAMP2 and CLR+RAMP3 The fraction of GPRC6A and RAMP1in FRET complex on the cell membrane is significantly higher than GPRC6A+RAMP2/3 combinations *** $p<0.0001$ (Kruskal Wallis test, Dunn's multiple comparison test. Combined data of three separate transfections and the values in brackets indicate number of cells analysed.

3.4: Discussion

The distribution of expression of RAMPs in the body exceeds the expression of its known partners, which means that there are yet unidentified interacting partners of RAMPs [213]. Most of the interacting GPCR partners of RAMPs belong to the family B [156, 172, 174, 175], until the interaction with CaSR was established by Bouschet *et al* [157]. Based on this it was hypothesised that further insights into this interaction can be gained using FRET-based stoichiometry analysis of the components. Furthermore, this finding leads to another hypothesis that other family C GPCRs may also interact with RAMPs.

Sensitized FRET emission technique was used as it can only occur within a distance of 10nm and is more sensitive than the immunofluorescence approach [222-231]. Accordingly, cerulean and citrine which are enhanced mutants of CFP and YFP respectively [236-238], were chosen as the donor and acceptor fluorophores respectively to measure sensitized emission FRET. This technique also allows the measurements of FRET-based stoichiometry according to the method derived by Hoppe *et al* [224].

Choice of fluorophores, tagging strategy and cell line used:

RAMPs were tagged with the donor cerulean, and the GPCRs were tagged with the acceptor citrine fluorophores. There are certain advantages of using these fluorophores over CFP and YFP. Cerulean is ~2.5 times brighter than CFP, more resistant to photobleaching, has a higher extinction coefficient, improved quantum yield and improved fluorescence lifetime and so it has improved signal to noise ratio [236]. Citrine is one of the longest wavelength mutants of YFP and is more resistant to acid quenching and easily expressible at 37°C [237]. Also, the mutation of alanine to lysine at position 206 of both cerulean and citrine prevents their homo and hetero-dimerization, making them useful for sensitized FRET experiments [236-238]. Using these fluorophores, the receptors and RAMPs were tagged at their C-terminal so that an artificial effect of cell-surface trafficking of the receptor/RAMP caused by signal peptide of the fluorophore tagged to the N-terminal could be avoided. Indeed, it has been shown that N-tagged c-myc RAMP1 could express on the cell-surface in absence of a transfected receptor partner in HEK-293 cells, an effect attributed to signal peptide of c-myc [174]. Primers were designed so that the stop-codon of RAMPs was excluded, in order to avoid cleavage of the

fluorophore. Also, it was important to choose the cells which do not express the receptors and RAMPs endogenously, as it might result in cell-surface trafficking of the transfected receptor due to the expression of endogenous RAMP or vice versa and hence cause inaccurate FRET measurements. Accordingly, COS-7 cells were chosen for this study as they do not express RAMPs (appendix section 7.1, figure 7.1-7.3). We have also shown the absence of CaSR in native COS-7 cells (appendix section 7.4, figure 7.6 and qPCR data on empty COS-7 cells showed absence of any amplified product) Also, COS-7 cells have been widely used to study RAMP-receptor biology due to this feature [156, 157, 174, 175, 198, 211] and have been shown not to express RAMPs.

Negative and positive controls:

A major problem of sensitized FRET is measuring specific FRET from a higher background of fluorescence signal created by over-expressing non-interacting fluorescent labels. So a negative control was used in order to measure basal level of FRET. Citrine alone with RAMP-cerulean constructs were used and FRET measured at cell membrane for each combinations were taken as minimum threshold when measuring GPCR-RAMP interactions (figure 3.3.1-3.3.4).

As a positive control, a fusion protein was created by engineering cerulean protein followed by 18aa linker sequence before the N-terminal domain of citrine, in order to achieve maximum FRET possible. The maximum FRET calculated was ~33%. It has been reported that the large size (~2.4nm in diameter and 4.2nm in length [240]) of the fluorescent proteins limits the useable FRET distance and hence the maximum FRET efficiency that can be measured is around 40% [222, 232].

Advantages of FRET-based stoichiometry:

Methods measuring only FRET efficiency in arbitrary units cannot determine whether a low FRET signal is due to absence of interaction between the components or to local excesses of free donor or acceptor molecules [224]. Using FRET-stoichiometry one can calculate the fraction of acceptor molecules in complex with donor and the fraction of donor molecules in complex by estimating the donor fluorescence lost due to energy transfer [224]. The advantage of using this technique is that it eliminates the need for acceptor photobleaching to determine

total donor concentrations and allows for repeated measurements from the same cell. Also, the R value quantitates relative concentration of total acceptor to the total donor concentrations. This gives an idea about the relative local concentrations of GPCR and RAMPs that do not exhibit FRET. Also, as mentioned before, sensitized FRET emission suffers from drawbacks of cross-talk and bleed-through [9, 10] due to the spectral overlap of the fluorophores. The constants α and β correct for the bleed through of acceptor and donor fluorescence in the FRET channel respectively and an extra constant γ gives the ratio of extinction coefficients for acceptor and donor, excited at the donor's excitation [224]. Also, ξ which is proportionality constant relating the sensitized acceptor emission to the decrease in donor fluorescence due to FRET, allows measurement of donor participation in FRET complexes, and eliminates the need for acceptor photobleaching to determine the fraction of energy lost from the donor [224]. So, in summary FRET stoichiometry has an added advantage as it measures the location and stoichiometry of molecular interactions inside a living cell along with essential corrections.

Ec or FRET efficiency was calculated by sensitized emission using the cerulean-citrine fusion construct as opposed to acceptor photobleaching by Hoppe *et al* [224] as we observed small proportion of photobleaching of donor when acceptor was photobleached using the 514nm laser line, making this technique unusable. Having established the Ec, α, β, γ and ξ (appendix, table 7.1) using the cerulean-citrine fusion construct, an estimate of their stoichiometry revealed that the fraction of citrine in FRET complex determined by whole cell histogram was ~100% whereas ~82% of cerulean was involved in FRET (data not shown in table 8.1). These values of course depend on the arrangement and spatial configuration of both molecules at the time of fixation of cells. It should be noted that the stoichiometry of the positive control is not 1:1 (1:0.82 instead) and so any interpretation for the fraction of donor (RAMP) should be done carefully.

CLR as a GPCR positive control:

CLR which is a known partner of all the RAMPs [156], was used as a GPCR positive control to determine whether the calculated constants and the experimental conditions were efficient enough to detect a FRET interaction at the cell-surface. It can be seen in figure 3.3.5-3.3.7 (D)

that CLR and RAMPs are co-localised together from the cytoplasm to the cell membrane which indicates that they are packaged together in the ER and remain partners throughout the lifecycle of the receptor. Significant increases in FRET efficiencies observed between CLR and all RAMPs compared to the respective negative controls, asserts the fact that specific RAMP-receptor interactions can be measured using this technique along with the quantification of the stoichiometry of the receptors. Interestingly, a significant increase in FRET efficiency was observed in the case of CLR and RAMP3 compared to CLR+RAMP1 (figure 3.3.8 A, table 3.3.2). However, there were no differences in the fraction of RAMP or CLR in the FRET-complex (table 3.3.2), and so the results indicate that RAMP3 with CLR are spatially arranged together in a way that facilitates stronger interaction when compared to RAMP1. Even though the NFRET level of CLR+RAMP2 are similar to CLR+RAMP3, the absence of significant difference with CLR+RAMP1 NFRET could be due to a higher standard error of mean (than CLR+RAMP3) (table 3.3.2). This observation needs to be confirmed by further studies and a strong conclusion cannot be drawn at present.

Interactions with CaSR:

Figure 3.3.9 shows that CaSR when present on its own is mainly localized in the peri-nuclear region which indicates failure of trafficking to the cell-surface. This is in agreement to the observation by Bouschet *et al*, where CaSR could not traffic to the cell-surface in RAMP-negative COS-7 cells [157]. When CaSR was co-expressed with either RAMP1 or 3 in COS-7 cells, distinct regions of co-localization were observed ranging from the perinuclear region to the cytoplasm and cell membrane (Fig 3.3.10 and 3.3.12 D), which indicates that they are packaged together in the ER (perinuclear) and transported to the cell membrane by vesicles (cytoplasm). This pattern of co-localization agrees with the observation made by Bouschet *et al*, where using ER and Golgi apparatus markers revealed that CaSR was co-localized only with calnexin (ER marker) and not giantin (Golgi apparatus marker) in absence of a RAMP, whereas CaSR with RAMP3 was co-localized with both calnexin (ER) and giantin (Golgi apparatus) indicating that RAMP promotes trafficking from ER to the Golgi apparatus [157]. Following this, deglycosylation studies indicated that RAMP3 promoted immature to mature glycosylation of CaSR, which resulted in trafficking of the receptor to the cell-surface [157].

Cell-surface FRET efficiency analysis revealed that RAMP1 and RAMP3 interactions with CaSR were above the background FRET values whereas, NFRET values for CaSR+RAMP2 complex was similar to its corresponding negative control (fig 3.3.13). Hence, CaSR+RAMP2 is not a real interaction and was not included in stoichiometric analysis, which is supported by previous study [157]. Interestingly, RAMP3 showed 1.67 fold higher FRET efficiency than RAMP1 with CaSR on the cell-surface (table 3.3.3), which is a novel observation. The mechanism behind this effect was explained by FRET-stoichiometry analysis. Stoichiometric analysis revealed that the fraction of RAMP3 in FRET complex was ~1.6 fold higher than RAMP1 without any change in the fraction of CaSR involved (Table 3.6). This means that there are more donor molecules in FRET in case of CaSR+RAMP3 complexes compared to CaSR+RAMP1 without any change in the amount of acceptor molecules in FRET. This would result into a higher energy transfer between donor and acceptor fluorophores, leading to an increase in FRET. This observation also indicates that there is no change between efficiency of RAMP1 and 3 to traffic CaSR to cell-surface (reflected by no change in fraction of CaSR in both FRET complexes). Accordingly these results suggest for the first time, that a higher-oligomeric receptor complex in the case of CaSR+RAMP3 traffics to the cell-surface when compared to CaSR+RAMP1 complex. In view of that, since CaSR exists as a dimer in the cell [70, 104, 127] it can be hypothesised ~1.6 times more molecules of RAMP3 exist per dimer of CaSR than RAMP1, resulting into a higher-oligomeric receptor complex. When using over expressing system it should be considered that such results can arise due to unequal expression levels of individual RAMPs, but this can be possibly ruled out in this case as the expression levels of all RAMPs were found to be equal at the cell surface (Figure 3.3.13 D). Also, it should be remembered that the stoichiometry of positive control using this system is not 1:1 (as noted above), and so this result should be confirmed using other independent approaches such as sequential FRET or co-immunoprecipitation.

Interactions with GPRC6A:

It has been reported that c-myc tagged hGPRC6A expresses poorly at the cell-surface in HEK-293 cells, whereas it fails to express on the cell-surface of COS-7 cells [158, 159]. It was observed in our study that GPRC6A was retained inside the cell in the peri-nuclear region when

expressed alone in COS-7 cells (fig 3.3.14). This shows absence of trafficking of the receptor to the cell-surface which is supported by the previous observations [158, 159]. Based on the findings of Boushcet *et al* [157], CaSR could traffic to the cell-surface in HEK-293 cells due to the presence of RAMP1, whereas it failed in the RAMP-negative COS-7 cells. Accordingly it was hypothesised in this study that GPRC6A requires an association with RAMP for efficient delivery to the cell-surface.

Distinct regions of co-localization were observed between GPRC6A and RAMP1 but not RAMP 2 or 3 ranging from the peri-nuclear region to the cell membrane, showing that they associate in the ER and Golgi and are transported together to the cell-surface (fig 3.3.15-3.3.17 panel D). This follows the typical pattern of cell-surface trafficking of GPCRs along with RAMPs as their partner [156, 157]. Hence, it is demonstrated that RAMP1 traffics GPRC6A to the cell-surface in COS-7 cells. This is a novel finding of this study as such an interaction of GPRC6A has not been reported yet. In the case of RAMP2, higher co-localization was observed in the peri-nuclear region than RAMP3 (fig 3.3.16 vs 3.3.17 panel D), which might suggest its interaction with the GPRC6A limited only to that region and its potential role in endo-cellular functions of GPRC6A, like binding testosterone [161, 170, 171]. An effect of over-expression of both the components can be accounted as one of the reasons for this observation. Accordingly, this needs to be tested further as accurate measurements cannot be made due to the over-expression of both the components in the peri-nuclear region. Alternative methods such as co-immunoprecipitation can be used to test this interaction.

Cell-surface stoichiometric analysis further revealed that a higher proportion of the GPRC6A (~69%) out of the total concentration is in FRET complex with RAMP1 (fig 3.3.18, table 3.3.4). A lower value for the fraction of RAMP1 in FRET complex (~20%) should not be confused with a lower number of RAMP1 molecules participating in FRET than GPRC6A, as it is ~18% of ~ 3 times higher total expression than GPRC6A at the cell-surface (as shown by R value of 0.34). It was seen that the cell surface expression levels of RAMP1 with GPRC6A were significantly higher than RAMP2, but not RAMP3 (fig 3.3.18 D). This could be because the expression levels of RAMP1 on the cell surface were enhanced due to its interaction with GPRC6A. However, since

the NFRET values for GPRC6A+RAMP2 and 3 were not significantly higher than their corresponding negative controls, the stoichiometric fractions can be considered as background or baseline values.

It has been mentioned by Hoppe *et al*, that the measured quantities, fraction and efficiency from FRET stoichiometry calculations are transferable from one molecular interaction to another [224]. So, we can compare the stoichiometry data between CaSR+RAMP and GPRC6A+RAMP interactions. It was observed that that the total expression of RAMP1 on the cell-surface, as measured by the R ratio (which includes signal from RAMP1 involved and uninvolved in FRET) was ~3 times higher than GPRC6A (~6 RAMP1 per GPRC6A). This is different from the observations in the case of CaSR, where the total expression of RAMP1 was found to be~1.6 times higher than CaSR (~2 RAMP1 per CaSR). This means that the total RAMP1 on cell-surface in presence of GPRC6A was 1.87 times higher than in the case of CaSR. Out of this higher pool of total RAMP1 on the cell-surface, ~20% was involved in FRET with GPRC6A, whereas ~16% of 1.87 times less total RAMP1 was involved in FRET with CaSR. This can be extrapolated to compare the fractions of RAMP1 involved in FRET complex with both receptors, by normalizing the fraction of RAMP1 involved with GPRC6A by 1.87 times, which would be ~11%. So, the fraction of RAMP1 in FRET complex with CaSR is 1.45 fold more than with GPRC6A, indicating more molecules of RAMP1 interacting per CaSR dimer than with GPRC6A dimer.

Limitations:

One limitation of using this technique is the over-expression of both the fluorophores inside the cell as observed in the all the figures expressing either fluorescent-tagged GPCRs or RAMPs. Hence, FRET occurring inside the cell where the fluorophore intensity is saturated (represented by black areas in FRET images: panel D of 3.3.5-3.3.17) cannot be determined efficiently. Additionally, since the stoichiometry using the positive control was not 1:1 (but 1:0.82 instead), care should be taken while interpreting the fraction of RAMPs in FRET. Also, since the components are being overexpressed, it does not represent conditions in case of a physiological

interaction. Accordingly, the results obtained from this study represent initial information/observations and need to be confirmed by using alternative approaches.

Other approaches tested:

Sensitized FRET was the most robust technique useable in our hands. However, during the process, other techniques were also tested to establish the best technique that could be used. Accordingly, acceptor as well as donor photobleaching techniques were tested. The principle of acceptor photobleaching relies on the fact that when FRET occurs between two proteins, donor fluorescence is quenched as some of donor energy is used to excite acceptor. When acceptor is photobleached, the donor quenching is recovered and consequently its fluorescence increases [222, 231]. The advantage of this method is that the analysis is much simpler compared to other methods and it can be performed on a single sample at specific locus [222, 231]. However, as mentioned before, we found that the donor was also getting photobleached in the process and hence this technique could not be used. Also, it has been shown that due to higher excitation of cerulean at YFP laser wavelength, it is not recommended to be used in acceptor photobleaching technique, as it can lead to false positive results [241].

Donor photobleaching technique [230] was also used, which is based on the fact that FRET if present, has a protective effect on donor bleaching. In this approach, repetitive excitation of the donor fluorophore is followed by synchronous donor/acceptor detection. The rate of decay of donor fluorescence by increase in photobleaching by successive illumination, gives a measure of kinetics for all donor molecules. So a faster decay rate means that the donors is not involved in FRET, whereas a slower decay rate indicates that the donor photobleaching is being protected by FRET and hence the donor is involved in FRET. Also, the simultaneous decrease in acceptor sensitized emission detected, provides a measurement for the donors present only the FRET population [230]. So in theory, when measuring FRET between two molecules (eg RAMP and receptor) two decay rates, one for the donor alone and one for the donor FRET complex should be observed. However, we observed two decay rates for cerulean alone (appendix section 7.2, figure 7.4). This would complicate analysis of experimental FRET decay

curves, because in theory, four decay rates - two for cerulean alone and two for cerulean in FRET should be observed. Although a slower bleaching with the cerulean-citrine fusion was observed (appendix section 7.2, figure 7.4 B), it was not statistically significant and would be far too small to measure in the case of RAMP-receptor experimental data. Bi-exponential decay of cerulean has also been reported in the literature [241]. It was shown that although cerulean was initially reported to decay by mono-exponential kinetics, fitting the cerulean decay to bi-exponential decay model improved the goodness of fit [236]. It has been speculated that like CFP, cerulean also possesses two conformations of chromophore due to interactions with nearby aa, which results into two distinct emitting species [241]. Due to these technical problems both acceptor and donor photobleaching techniques could not be used.

In summary, a deeper insight into the interaction of CaSR and RAMPs was provided by FRET-stoichiometry. It was demonstrated that both RAMP1 and 3 traffic the CaSR to the cell-surface with equal efficiencies; and a higher fraction of RAMP3 than RAMP1 is present in the CaSR receptor complex, suggesting higher stoichiometry of RAMP3 molecules interacting. Also, a novel interaction between GPRC6A and RAMP1 was discovered using this method, where RAMP1 enabled the cell-surface trafficking of the GPRC6A. Of note, since all these studies were done using overexpression system, other independent approaches should be used in both artificial and natively expressing cell systems to confirm these results.

CHAPTER 4: ROLE OF RAMPs IN CaSR SIGNALLING

4.1. Introduction

The classical understanding of GPCR signalling as either an "on" or "off" state, as well as one-ligand-one-receptor model have undergone a paradigm shift. Growing evidence suggests that GPCRs can exist in various conformations which confer subtle signalling and ligand binding properties to the receptor. Apart from their function as chaperone proteins, a direct role of RAMPs in modulating the signalling of GPCRs is also known (described in detail in section 4.1.3). CaSR is a pleiotropic GPCR, activating various signalling pathways via more than one G-protein [128-131]. So far, the only known role of RAMPs in their interaction with CaSR is trafficking of receptor to the cell surface in transfected HEK-293 and COS-7 cells as shown by Bouschet *et al* [157]. Accordingly, we hypothesised that RAMPs play a role in CaSR signalling which could then lead to understanding of new mechanism by which CaSR activates multiple signalling pathways.

4.1.1. GPCR signalling mechanism:

Before reviewing the signalling of the and RAMP-mediated receptor signalling, the basic working model of GPCR signalling should be understood. The mechanism of action of GPCR is explained by the ternary complex model [242], which is simplified in the figure 4.1. In the absence of a bound ligand, the GPCR is said to be in an inactive state (R) (Fig 4.1.1 A). Also, a GPCR can exhibit basal activity in terms of signalling (R*) in the absence of a bound ligand. In this (R*) state, the GPCR can also be pre-coupled to G-protein and so exists in a so-called R*G state. So, in absence of a bound ligand (L), the receptor can exist in three states: L+R+G, L+R*+G, L+R*G. In the R* and R*G states of the receptor, the conformation of the receptor facilitates a higher affinity to bind a ligand than the R state which is a lower affinity state. Accordingly, the order of ligand binding affinity is R*G > R* > R. Accordingly, when the ligand binds to the receptor, conformational change in the structure of the receptor occurs, allowing its interaction with hetero-trimeric G-proteins and hence forming a ligand- receptor-G protein complex (Fig. 4.1.1 B). Normally the G-proteins are in an inactive state composed of a GDP bound α subunit, and a βγ subunit. When the GDP is exchanged by GTP (which is at a higher concentration inside cells), G-proteins are activated. So, as soon as the ligand-receptor-G-protein complex is formed (fig 4.1.1 B), an immediate catalysis of GTP exchange on the α-

subunit of the G-protein takes place which leads to the dissociation of the G-protein into active GTP bound α subunit and βγ subunit (Fig 4.1.1 B). These two sub-units (G_{α}-GTP and βγ) then activate different effector proteins sequentially causing signal transduction (Fig 4.1.1 C). Once the activated G-protein subunits leave the receptor, the activated receptor can bind to more G-proteins, eventually leading to amplification in the number of activated G-protein subunits. The subunits remain activated for as long as the GTP is bound to α sub-unit. Once the GTP is hydrolysed back to GDP (Fig 4.1.1 D), the G-protein re-associates and receptor returns back to the basal state (Fig.4.1.1 E) [242].

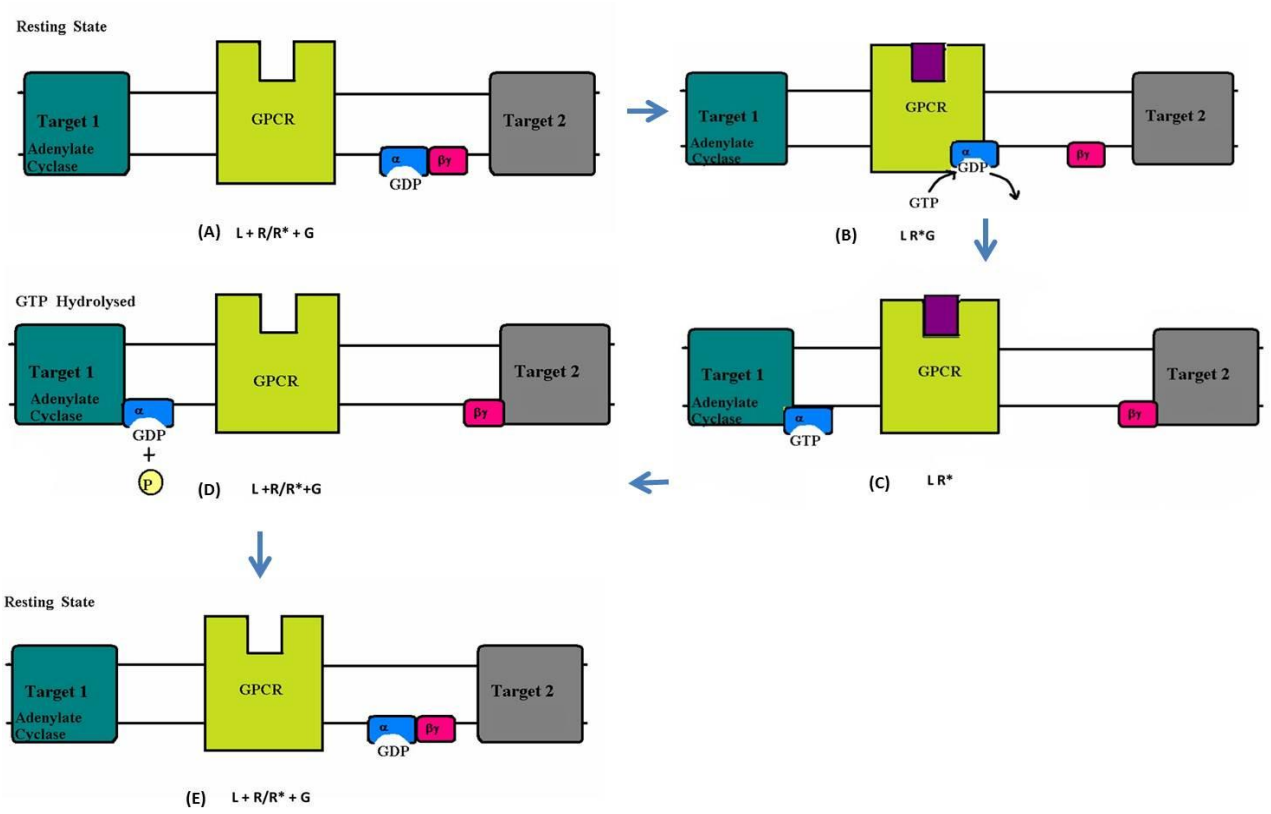

Figure 4.1.1: GPCR signalling mechanism:
GPCR signalling is shown by representation of the ternary complex model. (A) Receptor exists in ligand free state as inactive (R) or basal active (R*) state. (B) Upon ligand binding the GDP is exchanged to GTP which dissociates the G-protein into active α and βγ subunits that activate different effector molecules of signal transduction (C). (D) When GTP is hydrolyzed back to GDP, the receptor returns back to inactive or basal active state (E).

4.1.2: Signalling of the CaSR:

CaSR has been shown to activate various signalling pathways depending on the agonist or the cell type as summarized in the figure 4.1.2.

Promiscuous G-protein coupling:

CaSR couples to more than one G-protein in different cell types [128-131]. The most-characterized mechanism is the $G_{\alpha q}$-mediated PLCβ activation. This causes IP_3 activation which leads to subsequent release of intracellular Ca^{2+} from the internal stores. This PLC-mediated internal Ca^{2+} release by CaSR has been demonstrated in parathyroid cells and transfected HEK-293 cells [132]. The specific activation of $G_{\alpha q}$ has been demonstrated by the use of pertussis toxin in the studies. Pertusis toxin is ineffective in preventing binding of labelled GTP into $G_{\alpha q}$ proteins, which otherwise inhibits this activity by other G-proteins like $G_{\alpha i}$ [128]. Apart from $G_{q/11}$, CaSR can also couple to $G_{\alpha i}$ which inhibits adenylate cyclase activity and thus reduces cAMP production [128]. Interestingly, it has been shown in CaSR transfected-HEK 293 cells, that in addition to the activation of $G_{\alpha i}$, cAMP levels were also affected by a parallel increase in the intracellular Ca^{2+} concentrations ($Ca_{[i]}$) [129]. It was shown that concurrent stimulation of cAMP and Ca^{2+} pathways initially led to increases in the $Ca_{[i]}$ oscillation frequency which eventually fused into a persistent $Ca_{[i]}$ plateau that effectively inhibited cAMP accumulation. So, cAMP machinery could function normally, without any disruptions of its cellular actions in case of transient $Ca_{[i]}$ increase by CaSR agonists; and was inhibited only after a certain length of time of $Ca_{[i]}$ increase [129]. In cells types endogenously expressing the CaSR, activation of $G_{\alpha q}$ and $G_{\alpha i}$ pathways has been demonstrated to be an important mechanism of action of CaSR. Examples of this includes the mouse proximal tubule cells [133], cytotrophoblasts from placenta [134], rat pancreatic cells [135], rat kidney cells [76], intestinal epithelium cells [243], human ovarian surface epithelial cells [244], rat fibroblasts [138].

CaSR also activates $G_{12/13}$ - G-protein sub-types as shown in CaSR-transfected canine kidney cells [130]. This was shown by measuring Rho-mediated PLD activation (a known target of $G_{12/13}$) which was sensitive to the presence of specific inhibitor for $G_{12/13}$ [130]. Interestingly, it was shown that CaSR which couples to $G_{\alpha i}$ in normal breast epithelial cells and inhibits PTHrP

secretion, changes its G-protein preference to $G_{\alpha s}$ in two breast cancer cell lines: Comma-D and MCF-7, and causes PTHrP secretion; an effect linked to hypercalcaemia in malignancies. This shows a role of CaSR in pathogenesis of cancer by causing PTHrP secretion due to changing signalling pathways [131]. The mechanism responsible for this G-protein switching is still unknown.

Phospholipase activation:

It has been shown that following G-protein activation, CaSR activates different phospholipases as the next step in signal transduction cascade. In HEK-293 transfected cells and in primary bovine parathyroid cells, CaSR agonists activated phospholipases C, A_2 and D which form IP_3 and DAG; arachidonic acid; and phosphatidic acid respectively [130, 132]. This shows a co-ordinated, receptor-mediated regulation of multiple signal transduction pathways [119, 120, 245].

PLC activation causes the cleavage of its substrate PIP_2 which then forms IP_3 and DAG. It has been reported that CaSR activating PLC also caused a parallel activation of PI4-kinase which is responsible for replenishment of PIP_2 (substrate for PLC) in a Rho-dependent and $G_{q/11}$ independent pathway, as shown by experiments in transfected HEK-293 cells [245]. The significance of this effect might contribute to the constant supply of PLC-substrate necessary for the signalling of CaSR at basal Ca^{2+} concentration (as a partially active receptor) [245]. It has been shown in transfected HEK 293 cells, that activation of Protein Kinase-C (PKC) causes inhibition of most of the PI-PLC mediated release of $Ca_{[i]}$ stores, following agonist activation [119]. The PKC-dependent phosphorylation of the C-tail of CaSR serves as a negative feedback mechanism, inhibiting constant $Ca_{[i]}$ elevation and alternatively causing oscillations that might protect against cytotoxic effects of otherwise constant elevated $Ca_{[i]}$ [120].

CaSR mediated PLA_2 activation and consequent arachidonic acid (second messenger) activation has been reported in transfected HEK-293 cells. This has been linked to $G_{\alpha q}$ activation, since it was completely abolished by RGS4- a negative regulator of $G_{q/11}$ protein [246]. It has also been reported that PLA_2 mediated arachidonic acid release in cultured parathyroid cells is dependent on PKC activation; as inhibition of PKC reduced arachidonic acid release [132]. CaSR also causes

$G_{12/13}$-mediated activation of PLD [130, 132], which hydrolyses phospholipids to produce the second messenger- phosphatidic acid [132]. This is also shown to be activated in a PKC-dependent mechanism in HEK-293 transfected cells [132]. So, it seems that PKC plays a role in co-ordinating the concert of signal transduction pathways of CaSR as it has a negative feedback effect of PLC and a positive feedback effect on PLA_2 and PLD activation.

Protein kinase activation:

CaSR has been reported to activate various MAPKs that are responsible to trigger several cellular functions. Signal transduction from the activation of GPCR to MAPK is complex; involving interactions between various components of intracellular signalling pool of protein kinases, including cross-talk with tyrosine kinase-dependent signalling pathways [137, 139, 247]. CaSR activates various MAPK to induce mitogenic effects of extracellular Ca^{2+} on cells such as osteoblasts [136], ovarian surface epithelial cells [137], fibroblasts [138].

CaSR activation by Ca^{2+} and calcimimetic NPS R-467 in bovine parathyroid cells and transfected HEK-293 cells has been shown to activate ERK1 (p44) and ERK2 (p42) [141, 142]. In transfected HEK-293 cells this response was partially sensitive to pertusis-toxin treatment as well as PLC inhibition, implicating $G_{\alpha i}$ and $G_{\alpha q}$-dependent pathway [141]. It was also reported that inhibition of MEK - which phosphorylates ERK1/2, attenuated its activation in both transfected HEK-293 cells as well as primary parathyroid cells [141, 142]. ERK1/2 activation has also been observed in cells like fibroblasts [138, 139], osteoblasts [136], ovarian surface epithelial cells [137, 139] and proximal tubule cells [81] linking the mitogenic effects of extracellular Ca^{2+} to CaSR induced MAPK activation.

ERK1/2 activation pathway has been shown to depend on the cell type. In transfected HEK-293 cells, ERK1/2 activation occurs in response to extracellular Ca^{2+} via Ras and PI3-K activation as shown using their specific inhibitors [139]. Interestingly, ERK activation in Rat-1 fibroblast cells was shown to be sensitive to Src-tyrosine kinase inhibitor [138], an effect not observed in transfected HEK-293 cells [139]. This shows that two separate pathways for ERK1/2 activation exist based on cell types. PI3-K mediated ERK1/2 activation has been reported in cells endogenously expressing CaSR like ovarian surface epithelial cells [139] and proximal tubule-

derived opossum kidney cell line [81]. CaSR signal-specific, PI3-K mediated activation of another protein kinase – Akt has been reported in RAW 264.7 murine osteoclast precursor cells [46] and ovarian surface epithelial cells [140].

Other MAPKs such as p38 and JNK are also activated by CaSR [143, 146] as shown by studies involving HEK-293 transfected cells where their activation by increasing Ca^{2+} and neomycin concentrations was inhibited by p38 inhibitor [143]. Similarly, increasing concentrations of CaSR agonists- Ca^{2+}, neomycin, spermine and gadolinium caused p38 and ERK1/2 activation in murine osteoblasts like cells [144], whereas high Ca^{2+}-stimulated PTHrP release from H-500 Leydig cells via p38, ERK1/2, and JNK pathways [145]. JNK was also activated by CaSR in response to Ca^{2+} and gadolinium in canine kidney cells line MDCK [146].

Activation of several MAPKs by CaSR has been speculated to trans-activate tyrosine kinase receptors [137]. It has been shown in PC3 cells that CaSR could trans-activate EGFR signalling pathway to activate ERK1/2 by $G_{q/11}$-Ras-mediated pathway and finally causing secretion of PTHrP [247]. This mechanism is mediated by activation of matrix-metalloproteinase which cleaves the EGF outside the cell into soluble form causing binding to EGFR [247].

So, CaSR activates different MAPKs in various cell types, however the significance for this differential activation of MAPKs has not yet been fully understood in terms of its different biological actions via different ligands. Also, how different signal transduction mechanisms (eg IP_3 and MAPK activation) synchronize inter-dependently or are chosen independently based on agonist/cell type is poorly understood. The figure below summarizes the signalling pathways known to be activated by the CaSR.

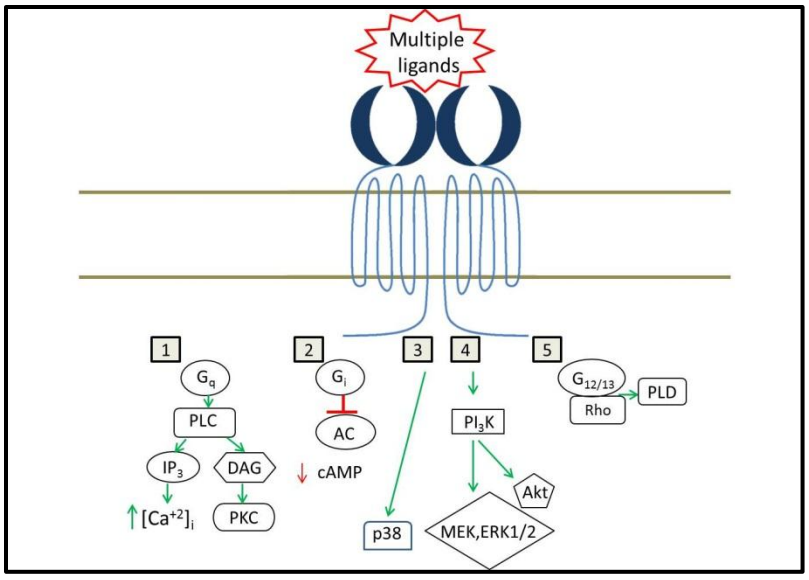

Figure 4.1.2: Overview of the signalling pathways activated by the CaSR. Numbers 1-5 represent different signalling pathways activated by the CaSR.

It can be hypothesised that interaction of CaSR with its interacting partners can be involved in activating multiple signalling pathways. One of the partners of CaSR are RAMPs [157] as discussed in section 1.8.4, chapter 1. RAMPs are known to play role in mediating signalling of certain GPCRs as discussed below.

4.1.3. Role of RAMPs in receptor signalling

Increasing evidence for the role of RAMPs in signalling of family B GPCRs has emerged over the last few years, where RAMPs are either essential or modulate the signalling of the GPCR [33][174]. The C-tail of RAMPs has been shown to play a significant role in signalling of the AMY receptors. It was shown in transfected COS-7 cells that the C-tail truncation mutants of RAMP1, 2 and 3 co-transfected with CTR, decreased the affinity for AMY binding and potency for cAMP activation on the AMYR1 (CTR+RAMP1) and AMYR2 (CTR+RAMP2), but did not for AMYR3 (CTR+RAMP3) [192]. When $G_{\alpha s}$ was overexpressed in these cells, the defect in AMY binding was corrected. This suggests that RAMPs are probably involved in direct G-protein coupling to the AMY receptor [192]. Also, the same study reported that C-tail truncation mutants of RAMPs, did not make any difference in cAMP activation by AM and CGRP [192], indicating the role of C-tail of RAMPs in $G_{\alpha s}$-mediated signalling, exclusively for AMY receptors. A deeper insight into the

role of RAMPs in AMY signalling was given by Morfis *et al*, who observed a marked induction of AMY potency at AMYR1 (CTR+RAMP1) and AMYR3 (CTR+RAMP3) for formation of cAMP and a weaker induction of AMY potency to activate intracellular Ca^{2+} and ERK1/2 signalling; compared to CTR expressed alone in HEK-293 and COS-7 cells [211]. This indicates a clear RAMP-mediated effect in the modulation of signalling of the CTR. The same study also showed that overexpression of G_{α} subunits led to a modulation in ^{125}I-AMY binding. $G_{\alpha s}$ overexpression increased ^{125}I-AMY binding at AMYR2 (CTR+RAMP2), both $G_{\alpha s}$ and $G_{\alpha q}$ increased ^{125}I-AMY binding at AMYR3 (CTR+RAMP3); whereas there was no change for ^{125}I-AMY binding at AM1R (CTR+RAMP1) [211]. This shows that RAMPs probably participate in modulating the direct G-protein coupling efficiencies of AMY receptor [211].

VPAC1 receptor signalling is also modulated by RAMPs. VPAC1 receptor interacts with all RAMPs, but its association with RAMP2 in COS-7 cells caused augmentation in efficacy of PI hydrolysis by VIP with no change in efficacy for cAMP generation, ligand binding affinity and potency; when compared to VPAC1 receptor alone [174]. It was suggested that this effect can be attributed to a change in compartmentalization of the receptor in presence of RAMP2 [174]. However, our group using antibody-capture scintillation proximity assay for measuring specific G-protein activation has shown that there is a decrease in $G_{\alpha i}$ protein activation when VPAC1 receptor is co-transfected with RAMP2, without any change in ligand binding affinity and potency for $G_{\alpha i}$ stimulation [Roberts DJ *et al*, unpublished data].

In addition, we also observed changes at the PTH1R, PTH2R and Glucagon receptor signalling in the presence of RAMPs, where there was an increase in G-protein activation efficacy by the ligands, without any changes in the half maximal effective concentration (Ec_{50}) and ligand binding affinity (K_d) of the ligand. We demonstrate that when compared to PTH1 receptor alone, PTH1R+RAMP2 increased the efficacy of PTH (1-34) to activate $G_{\alpha s}$ (2.3 fold) and $G_{\alpha i}$ (1.6 fold) without any change in potency and ligand binding affinity. Also, the efficacy of PTHrP (1-37) for $G_{\alpha s}$ activation was increased (by 2.5 fold) at PTH1R in complex with RAMP2 [Roberts *et al*, unpublished data]. We also observed that the efficacy of PTH(1-34) at PTH2R+RAMP3 complex to stimulate $G_{\alpha s}$ was higher (by 1.8 fold) than PTH2R alone. Furthermore, RAMP2 co-

expression with glucagon receptor reduced glucagon induced $G_{\alpha i}$ and $G_{\alpha s}$ stimulation (by ~0.3 fold) when compared to the receptor alone [Roberts *et al*, unpublished data]. These observations show for the first time that RAMPs are involved in direct G-protein coupling of the VPAC1, PTH1/2 and Glucagon receptors.

Another intracellular peripheral membrane protein is also involved in RAMP-CLR signalling. The CGRP-receptor component protein (RCP) couples to the AM1R and is involved in generating adrenomedullin-induced cAMP response [212]. It couples AM receptor to the cellular signal transduction pathway. RCP also couples to the CGRP receptor and is also involved in the cAMP stimulation following CGRP-mediated stimulation but does not affect CGRP binding [212].

Similar to the interaction of CaSR with tyrosine kinase pathway as described earlier, cross-talk between AMR/AMYR and IGF-1R has also been reported. It has been shown in rat osteoblasts that the mitogenic actions of amylin, adrenomedullin and IGF-1 are interdependent [248]. It was shown that amylin receptor activation caused $G_{\alpha i}$-mediated ERK1/2 activation; and blocking of IGF-1R and not IGF-1, inhibited the action of amylin. Similarly, adrenomedullin also increased ERK1/2 activation sensitive to IGF-1R blocking [248]. Interestingly, the researchers discussed that they did not observe tyrosine phosphorylation of IGF-1R itself upon treatment with amylin, and so the complete mechanism for this cross-talk is yet to be elucidated. Surprisingly, blocking of amylin and adrenomedullin receptors by antagonists inhibited the mitogenic actions of IGF-1 on IGF-1R, suggesting essentially of a signalling complex consisting amylin/adrenomedullin receptor and IGF-1R where interruption of either, abrogates the actions of their respective ligands [248].

In order to study the role of RAMPs in CaSR signalling, two techniques were used in this project: antibody-capture scintillation proximity assay (SPA) and live cell imaging using Ca^{2+} indicator fluorescent dye. Brief introduction on SPA and Ca^{2+} indicators is given below:

4.1.4. Antibody-capture Scintillation proximity assay (SPA):

This technique was used because, it is able to detect specific-G-protein activation and so multiple G-protein subtype activation by a GPCR can be measured. As discussed earlier (section 4.1.1), a G-protein is activated when GDP is replaced by GTP, the reversal of which, brings it

back to an inactive state. In this assay, $^{[35]}$S-labelled non-hydrolysable GTPγ^{S} (which has γ-thiophosphate bond resistant to hydrolysis by the GTPase), is used to prevent reforming of an activated (and dissociated) hetero-trimeric G-protein into an inactivated state. G-protein specific antibodies towards the α-subunit are used which are subsequently detected by secondary antibody attached to a scintillant bead [249]. The energy transfer between the $^{[35]}$S on the GTPγ^{S} to the scintillant in the bead causes luminescence which can be detected as a specific signal from an activated G-protein. Figure 4.1.3 below shows a schematic of the working of this technique.

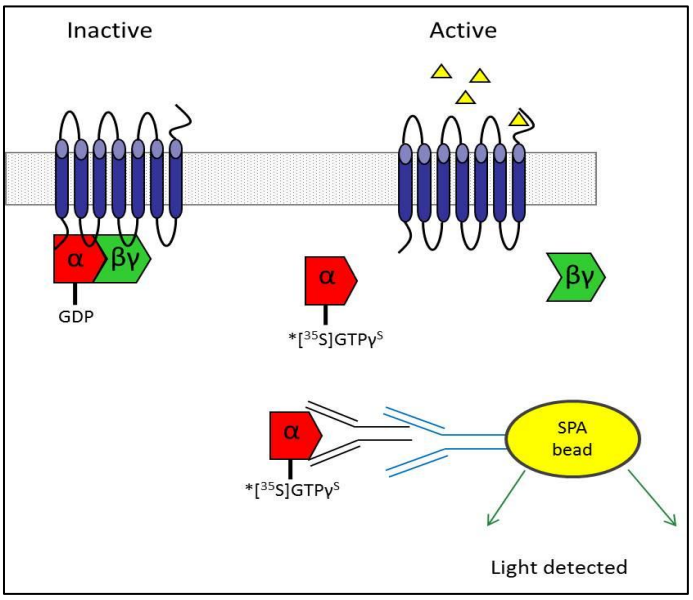

Figure 4.1.3: Schematic of principle for antibody capture SPA.
Upon activation of GPCR, GDP is exchanged with non-hydrolyzable[^{35}S]GTPγ^{s}. A specific G-protein is detected by its antibody which is detected by luminescence resulting from proximity between [^{35}S]GTPγ^{s} and scintillant beads coated with secondary antibodies.

Antibody-capture SPA has been used extensively to measure G-protein activation profiles of different GPCRs [249-254]. This technique was first shown to successfully measure $G_{\alpha q/11}$ activation in muscarinic receptor-transfected in CHO cells [249]. It displayed a higher background-to-signal ratio for $G_{\alpha q/11}$ measurement (as there is a higher concentration of $G_{\alpha i}$ proteins compared to other G-protein subtypes) [249]. This technique was also employed to study the nature of novel compounds against the 5-HT receptor subtypes in transfected HEK-

293 cell membranes and helped in classifying them as partial agonist that specifically activated $G_{\alpha s}$ and corresponding antagonists as the potential candidates for antipsychotics [250]. This technique was also successfully employed to measure $G_{\alpha q/11}$ activation by endogenously expressing 5-HT receptor subtypes in rat frontal cortex membranes [251]. Sensitivity of this technique for $G_{\alpha s}$ was demonstrated by a study measuring D1 receptor-mediated activation of $G_{\alpha s}$ in transfected L-cells [254]; and by another study measuring both $G_{\alpha q/11}$ and $G_{\alpha s}$ to characterise the signalling profiles of full agonist, partial agonist and antagonist in rat striatum and cortex membranes [252]. This shows the ability of the assay to measure differential coupling of receptor subtypes to individual or different G-proteins in native tissues. In conclusion, antibody-capture SPA provides a powerful tool for measuring GPCR coupling to specific G-proteins.

Another technique used in this project was Ca^{2+} imaging technique, which uses Ca^{2+} indicator dyes in order to measure changes in intracellular Ca^{2+} levels upon CaSR activation by a live cell imaging system or a plate reader. This technique is used widely and brief information about the dyes used is given below:

4.1.5. Ca^{2+} indicator dyes:

Chemical Ca^{2+} indicators are widely used to study the change in Ca^{2+} concentrations (second messenger) inside the cells. Fluorescent dyes like Fluo-3, Fluo-4, Ca^{2+} orange, Oregon green, Fura-2 have been developed for cell based applications for Ca^{2+} imaging [255-257]. Most of these dyes are based on Ca^{2+} chelators - EGTA and BAPTA, modified to incorporate fluorescent reporter groups [257]. These chemical dyes have a broad range of Ca^{2+} binding affinities and can be selected based on the experiment of interest. Commercially, these hydrophilic dyes are widely sold conjugated with hydrophobic acetoxymethyl (AM) esters to make them membrane-permeable for passive loading into the cells [258]. DMSO which is used to dissolve the dye protects the hydrolysis of esters in moist conditions preventing the loss of loading of dye into the cells. Once inside, intracellular membrane esterases cleave the AM ester group, thereby concentrating the dye inside the cells and inhibiting their leakage from the cells [259]. Organic

anion-inhibitor like probenecid can be used additionally to prevent the leaking of the dye from the cell [259].

Since the temporal and spatial Ca^{2+} concentrations inside the cells vary greatly, various Ca^{2+} dyes have been synthesized covering a broad spectrum of Ca^{2+} binding affinities [255, 256, 258]. Widely used high affinity Ca^{2+} indicators include single wavelength dyes like Fluo-3 and Fluo4, Ca^{2+} green-1, Fura-2, Indo-1 [259]. Fluo-3 is easily excited using argon laser (488nm) and has fluorescein like spectral properties. Its binding affinity (K_d) is ~390nM, consequently gives less background at resting cell Ca^{2+} levels (~100nM) and gives ~100 times higher fluorescence upon binding to Ca^{2+} [256, 257]. Fluo-4 is an enhanced derivative of Fluo-3 synthesized by substituting two fluorine for the two chlorine substituents in Fluo-3, which results in greater absorbance using argon laser (488nm) and hence has greater fluorescence [252]. So, a lower concentration of dye can yield almost double fluorescence compared to Fluo-3 which is helpful to study small changes in intracellular Ca^{2+} concentrations [252, 257]. Fluo-4 also has a higher rate of cell permeation and a larger dynamic range for Ca^{2+} binding from 100nM to 1µM with a K_d of ~345nM [252]. Another advantage of Fluo-4 over Fluo-3 is its resistance to photobleaching ($t_{1/2}$ 339s vs 143s). Derivatives of Fluo-4 have been synthesized for usage as low affinity Ca^{2+} indicators like Fluo-5F (K_d ~2.3µM), Fluo-5Cl (K_d ~6.2µM), Mag-fluo-4 (K_d~ 22µM), Fluo-5N (K_d ~ 90µM) [256].

In addition to the single wavelengths dyes, ratiometric dyes excited at two-wavelengths are also used. Ratiometric dye Fura-2 is one of the most successful high affinity Ca^{2+} indicators. Peak absorption of the dye shifts from 340nm to 380nm when it binds to Ca^{2+} with the same emission peak at 510nm [258]. The ability to make ratio measurements with fura-2 at low concentrations, allows accurate measurements of the intracellular Ca^{2+} concentrations [258, 259]. Ratio calculations considerably reduces the effects of uneven dye loading, leakage of dye, photobleaching, as well as problems associated with measuring Ca^{2+} in cells of unequal thickness. The K_d of Fura-2 is ~145nM which allows its use to measure very small changes in Ca^{2+} concentrations and has very limited sensitivity to Ca^{2+} concentrations above 1µM [258]. However, the dual excitation of the dye makes it unsuitable for use in live cell imaging.

Derivatives of Fura-2 are used as low affinity Ca^{2+} indicators like Mag-Fura 2 (K_d ~1.9mM), Mag-Fura 5 (K_d ~28µM), Fura-2-FF (K_d ~ 35µM) and so along with Fura-2, these ratiometric dyes have a wide sensitivity range from ~100nM to ~100µM [259].

A major disadvantage of the chemical Ca^{2+} indicator dyes is that their cellular compartmentalization cannot be controlled. For example, a study comparing the properties of various Ca^{2+} indicator dyes reported that Fura-2 loaded HeLa cells showed marked mitochondrial and ER localization, whereas Fluo-3 or Fluo-4 loaded cells showed a uniform cytoplasmic fluorescence [255]. Also, the ratio of compartmentalization of dyes between cytoplasm and specific organelles is sensitive to temperature and time of incubation [255]. Fluorescent dyes also leak out from the cells at different rates when incubated for a longer time [255]. Another drawback of using fluorescent dyes is their susceptibility to photobleaching [255].

4.1.6. Hypotheses and aims:

It was hypothesised that RAMPs are involved in CaSR signalling and alter ligand induced CaSR signalling.

Aims:

The specific aims of this chapter are:

- To differentially measure the G-protein activation profiles of RAMP1 or RAMP3 in complex with CaSR in transfected COS-7 cells using antibody-capture scintillation proximity assay (SPA) technique.
- Study the role of RAMP in CaSR signalling in endogenously expressing thyroid medullary carcinoma cell line (TT) using Ca^{2+} imaging techniques.

4.2. Methods:

Measuring specific G-protein activation using antibody-capture scintillation proximity assay

4.2.1. cDNA constructs used:

pcDNA 3.1 RAMP1, 2 and 3 and pcDNA 3.1 M3 cDNA constructs were purchased from UMR cDNA resource centre. pcDNA 3.1 vector was purchased from Invitrogen corp.

4.2.2. Engineering CaSR gene into pcDNA 3.1 vector:

CaSR was engineered into the pcDNA 3.1 vector from TOPO CaSR vector using the molecular cloning technique described in chapter 3 section 3.2.2 by introducing Hind3 and Xba1 restriction enzyme sites on either ends of the CaSR gene using PCR and ligating it into the pcDNA 3.1 vector between these two sites in the multiple cloning region.

The primers used to engineer Hind3 and Xba1 sites (highlighted) on CaSR are given below:

Gene	Sequence 5' to 3'	Length	Tm (°C)	Annealing Temp (°C)
CaSR	**F(Hind3):**TATCAAGCTTGTCATGGCATTTTATAGCTGCT GCTGGGTCCTC	43	62.41	54.5°C
	R(Xba1): TGAATCTAGATTATGAATTCACTACGTTTTC TGTAACAGTGCTGCC	50	61.07	

Table 4.2.1: Primer sequences for cloning CaSR into pcDNA 3.1 vector.

Sequences of all primers used for the sequencing CaSR in positive clones are given below:

Primer name	Sequence 5' to 3'	Length
CMV primer	CGCAAATGGGCGGTAGGCGTG	21
230-1540	**F:** TGGTAGAGGTGATTCAAAATTC **R:** CTCTCAGAAAGGTGTCCACAGGT	22 23
1160+	TTGGCCTCAAACACCAGGAGGACACGGTT	29
1950+	AACTGGCACCTCTCCCCAGAGGATGGCT	28
2590+	CATTCCAGCCTATGCCAGCACCT	23

Table 4.2.2: Sequences of primers used for sequencing the engineered CaSR in the pcDNA3.1-CaSR positive clones

4.2.3. Transfecting COS-7 cells with GPCR and RAMP constructs:

COS-7 cells were co-transfected using electroporation method described in section 3.2.3 of chapter 3. ~4 million cells per 0.4ml electroporation buffer were transfected with 5µg GPCR construct alone or with 15µg RAMP construct.

4.2.4. Membrane preparation:

Media was removed 48hr post-transfection and cells washed with PBS before removal of the cell layers using 2mm glass beads (Merck Chemicals). The cells were then spun at 300g for 5 minutes and resuspended in 10 ml, ice cold, PBS. On ice, 50 strokes of a 15 ml Dounce homogeniser were used to lyse the cells, after which, the lysate, diluted to 40 ml, was spun at 300g for 10 minutes at 4^{o}C. The supernatant was then spun at 40,000g for 40 minutes at 4^{o}C. The membranes were then resuspended in SPA buffer (100mM NaCl, 50mM HEPES, 5mM $MgCl_2$, adjusted to pH 7.5 with KOH) aliquoted and fast frozen in liquid nitrogen before storage at -80^{o}C. Membranes were thawed on ice fresh before use and not refrozen/reused.

The protein concentration of the membranes was determined using BCA protein assay as described in section 2.11 of chapter 2 using 1mg/ml BSA fraction V in SPA buffer as standard.

4.2.5. Western blotting for detection of G-proteins and CaSR on transfected membranes:

To check for the presence of different G-proteins in membrane preparations, western blotting was used as described in section 2.12 of chapter 2. 10µg of CaSR+RAMP1 COS-7 transfected membranes were resolved on a 10% SDS-PAGE gel. In the case of detecting CaSR in transfected membranes, 40µg of transfected or COS-7 empty membranes were resolved in 8% SDS-PAGE gel according to the previously mentioned protocol (section 2.12, chapter 2) The concentrations of the antibodies used are given in section 2.12 of chapter 2.

4.2.6. Scintillation Proximity Assay (SPA):

SPA using SPA-PVT glass beads:

Scintillation proximity assays were carried out using a modified protocol based on Cussac *et al* [254]. Concentration response curves were constructed by incubating increasing agonist concentrations with receptor transfected cell-membranes and 0.1µM GDP (Sigma Aldrich) in SPA buffer in a total volume of 200µl in white Optiplates (Perkin Elmer). The assay was initiated by addition of 0.5nM [^{35}S] GTPγ^{S} (Perkin Elmer) and incubated for 1 hour at 35^{o}C. The assay was terminated by addition of 20µl 3% Nonidet P40 (Roche) in PBS and incubated at room temperature for 30 minutes on a plate shaker. 10µl of anti-G-protein antibody (G_s sc-383, G_i sc-262, G_q sc-392 Santa Cruz Biotechnology) at a concentration of 0.2µg/µl, was then added, followed by a further 30 minutes at room temperature before addition of 75µl anti-rabbit PVT SPA beads (Perkin Elmer) reconstituted in 25ml PBS. The plate was then sealed, incubated at 4^{o}C for 20 hours, spun at 1300g for 10 minutes at 4^{o}C before reading in a TopCount scintillation counter (Packard). Each well was counted for 2min and average CPM was used.

Agonists used in SPA were:

$CaCl_2$ (Fisher scientific), Gadolinium trichloride (Sigma Aldrich), Neomycin (Bioline), Cinacalcet HCl (Selleck chem).

SPA using Protein-A beads:

In the case of using Protein-A beads, the protocol used was same as above except it was carried out in 1.5ml tubes and 50µl of Protein-A beads (Sigma Aldrich) were added instead of SPA PVT glass beads and incubated for 20hr at 4°C with gentle agitation. This was followed by three washes of 400µl SPA buffer with centrifugation at 10,000g for 5min between each wash. After the last wash, the contents of each tube were resuspended in 300µl of SPA buffer and then pipetted into a 5ml scintillation vial (Fisher scientific) and 1ml of liquid scintillant cocktail (Perkin Elmer) was added. The vials were then counted in LS 6500 multi-purpose scintillation counter (Beckman Coulter). Each vial was counted for 2min and an average CPM was used.

4.2.7. Testing effect of compounds on SPA PVT glass beads:

In order to test the effects of various agonists on SPA beads, the reaction was incubated with the given concentration of agonist and 0.5nM [^{35}S] GTPγ^{S} in a volume of 200µl along with 75µl of anti-rabbit PVT SPA beads, for 20hr at 4^{o}C. The plate was then sealed, incubated at 4^{o}C for 20 hours, spun at 1300g for 10 minutes at 4^{o}C before reading in a TopCount scintillation counter (Packard). Each well was counted for 2min and average CPM was used.

4.2.8. Statistical analysis:

Log (agonist) vs response ordinary fit curves were created using GraphPad Prism version 5.00 for Windows (GraphPad Software, San Diego California USA, www.graphpad.com) to get the top and the bottom of the curves. The bottom of the curve value was subtracted from all the values of the curve and a new Log (agonist) vs response ordinary fit curve was created to calculate the potency (Ec_{50}) values.

Ca^{2+} assay using Live Cell Imaging System:

4.2.9. Seeding cells for imaging:

TT cells were cultured under normal conditions as described in section 2.1 of chapter 2. For the assay, 100,000 TT cells were seeded into each well of a 24-well clear-bottom plate (Costar, Corning). After two days, the cells were used for intracellular Ca^{2+} measurement assay.

4.2.10. Loading cells with Fluo-4 AM dye:

Media was removed and cells were washed twice with PBS and loaded for 45min at 37^{o}C with 500µl of physiological salt solution containing 2mM $CaCl_2$ (recipe in appendix) containing 5µM Fluo-4AM dye (5mM stock in DMSO) and 2.5mM water soluble probenecid. Dye was then removed and cells were washed three times with physiological salt solution and further incubated with 500µl of physiological salt solution containing 2mM $CaCl_2$ for 45 min at 37^{o}C. During this incubation, the cells were treated with antibodies or compounds according to the requirement of the experiment. After 45min, the buffer was replaced with 360µl of

physiological salt solution containing 1.5mM $CaCl_2$ and the plate was taken to the live cell imaging system.

4.2.11. Imaging cells:

HCX PL FLUOTAR 10.0x0.30 dry objective on an Inverted wide field fluorescence microscope Leica AF6000 Time Lapse was used to image cells. The cells were imaged at 37^{o}C in single channel fluorescence image using the L5 filter, with exposure of 1sec, at gain and intensity of 5. Images were taken at 12bit resolution at every 1.2sec with first 35 frames recorded as baseline after which 40µl of 10X solution of agonist was added carefully using a P200 pipette (Gilson) and images were recorded for further 3min.

The compounds used in different experiments were:

Cinacalcet HCl, Neomycin, RAMP1 mouse polyclonal antibody (ab 67151, product discontinued, Abcam), Mouse control IgG (Vector labs), RAMP1 goat polyclonal antibody (sc-8850, Santacruz biotech), Goat control IgG (Vector labs), Ionomycin (Sigma Aldrich), NPS 2390 (Sigma Aldrich), DMSO (Sigma Aldrich) and physiological salt solution (recipe in appendix).

4.2.12. Knock-down of RAMP1 mRNA expression in TT cells using siRNA:

In order to knock-down RAMP1 mRNA expression, TT cells were transfected with RAMP1 siRNA or scrambled (sc) siRNA using electroporation, with a slight change in protocol from described in section 3.2.3 of chapter 3. ~1.5 million TT cells were transfected with 1.5µg of RAMP1 or sc siRNA in 0.4ml final volume at 960µF and 0.22kV. After electroporation, TT cells were cultured in 24-well clear bottom plates in normal F-12K medium for 72hr, before using them for further experiments.

4.2.13. Validating knockdown of RAMP1 mRNA expression:

RNA extraction and cDNA synthesis:

After 48hr from transfection, RNA was extracted using Trizol reagent as described in section 2.4 of chapter 2. RNA pellet was resuspended in 12µl of Nuclease-free water. cDNA was synthesized from equal amounts of RNA for RAMP1 and siRNA transfected samples as described earlier in section 2.6 of chapter 2.

Real-time PCR to measure gene expression of CaSR and RAMPs in siRNA transfected TT cells:

RAMP1 mRNA expression along with the expression of CaSR and RAMP2 and 3 was measured using Taqman probes in real-time PCR as described in section 2.9 of chapter 2.

4.2.14. Data analysis for live cell imaging:

Images from each well were exported in .tiff format and were analysed using ImageJ software. Series of images for a well were opened in ImageJ and converted into a stack. Next, ROIs were selected for a number of cells as well as for the background. Fluorescence intensity for each cell was measured and the background intensity value was subtracted from all the values using Microsoft Excel. A time-dependent response curve was plotted using GraphPad Prism version 5.00 for Windows (GraphPad Software, San Diego California USA, www.graphpad.com) and peak value of response for each cell was calculated using AUC function. The peak value of response for each cell was then calculated as percentage change from baseline fluorescence and expressed in the graph as percentage above baseline. For calculating dose-response curves, these values were plotted against their respective doses and log agonist vs response curve was fitted using Graphpad prism 5 to obtain the Ec_{50} values. Normalcy test was done on each set of data using D'Agostino & Pearson omnibus normality test using Graphpad prism 5 software.

4.3: Results:

Part 1- Antibody-capture scintillation proximity assay

4.3.1. M3 as a positive control for $G_{\alpha q}$ protein activation using SPA PVT beads in antibody-capture SPA.

Activation of $G_{\alpha q}$ protein is the most characterized signalling pathway of CaSR as described in section 4.1.2. To test if the conditions of SPA were optimized to measure $G_{\alpha q}$ activation, Muscarinic receptor type 3 (M3) which is a known $G_{\alpha q}$ protein-coupled receptor [249, 260, 261], was used as a positive control for the SPA. COS-7 cells were transfected with 5µg of M3 receptor. 15µg of M3 COS-7 membranes were incubated with increasing doses of acetylcholine chloride ranging from 100pM to 1mM in presence of [^{35}S]GTPγ^{S} . A dose-responsive activation of $G_{\alpha q}$ protein was observed as shown in Fig 4.3.1 and the potency (Ec_{50}) calculated was 176 ± 4.27 nM (n=3). The Y-axis on the graph shows counts per-minute (CPM) normalized to the baseline value of the graph. Thus, it was confirmed that $G_{\alpha q}$ protein activation could be detected using antibody-capture SPA in transfected COS-7 cell membranes.

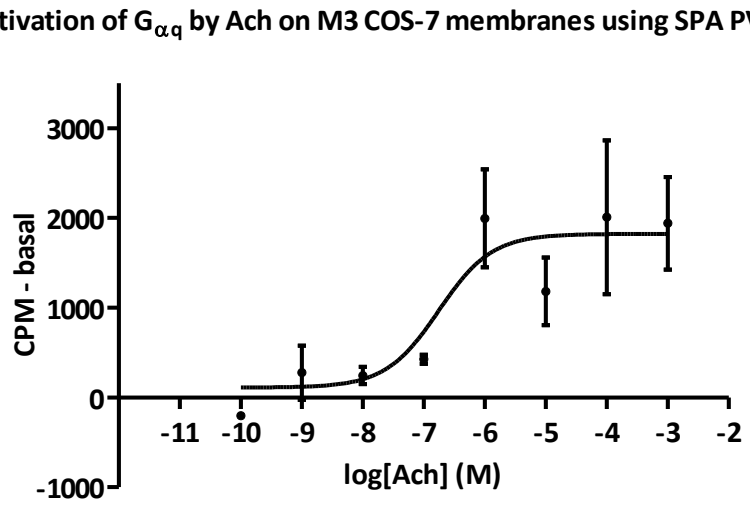

Best-fit values	
Bottom	110.2
Top	1823
LogEC50	-6.754
EC50	1.763e-007

Std. Error	
Bottom	356.8
Top	267.4
LogEC50	0.6315

Figure 4.3.1 Activation of $G_{\alpha q}$ by Acetylcholine chloride on M3 receptor transfected COS-7 membranes using SPA PVT beads:

COS-7 cells were transfected with M3 receptor and the effect of acetylcholine chloride on the activation of $G_{\alpha q}$ was checked using antibody-capture SPA. 100pM to 1mM of acetylcholine chloride was incubated with 15µg of M3 transfected COS-7 membranes in separate wells to measure the $G_{\alpha q}$ activation at each dose. The CPM values shown are normalized to the bottom of the curve. Log agonist vs dose response curve was plotted which is shown above and the Ec50 value obtained was 176 ± 4.27 nM. This is a combined curve of three separate experiments performed in duplicates using the same batch of transfected membranes.

4.3.2. Effect of compounds on SPA PVT beads:

Initial testing using $CaCl_2$ indicated a possible non-specific effect of the ligand on the SPA-PVT beads. So in order to confirm that, increasing doses of $CaCl_2$ ranging from 100nM to 100mM were incubated with 500pM of $^{35}SGTP\gamma^S$ and 75µl of SPA PVT beads in the SPA buffer for 20 hr at 4°C. It was observed that doses higher than 1mM of $CaCl_2$ artificially increased the signal (fig 4.3.2 A), which resulted into false positive results in previous experiments, rendering those doses unusable.

Similarly, the effect of gadolinium chloride on SPA PVT beads was tested by incubating a high dose of 200µM Gadolinium chloride and 10mM $CaCl_2$ for comparison with 500pM of $[^{35}S]GTP\gamma^S$ and 75µl of SPA PVT beads for 20hr at 4°C. A slight increase from basal signal was observed in case of 200µM Gadolinium chloride (Fig 4.3.2 B), suggesting that this compound had less non-specific effects on the SPA PVT beads as 10mM $CaCl_2$.

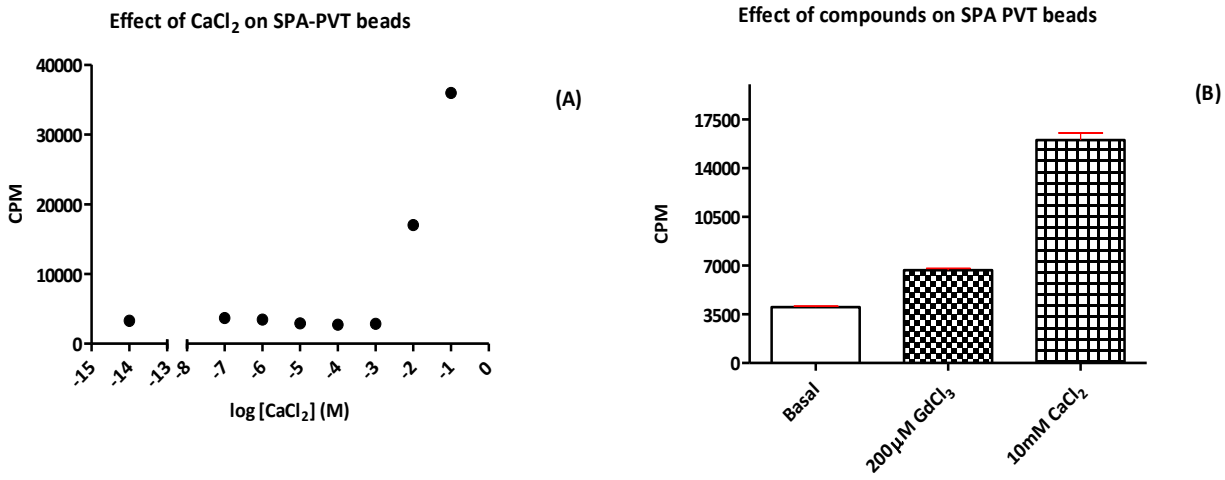

Figure 4.3.2 Effect of increasing concentrations of $CaCl_2$ on SPA-PVT beads:
Given doses of ligands were incubated with 500pM of $[^{35}S]GTP\gamma^S$ for 1 hr without any membranes. (A) It was observed that there was an increase in CPM after 1mM $CaCl_2$ indicating non-specific effect of the compound on SPA beads. (B) It was observed that CPM for 10mM $CaCl_2$ was the highest over basal compared to the 200µM $GdCl_3$ (A) n=1. (B) n=2

4.3.3: Use of Protein-A beads instead of SPA PVT beads and M3 as a receptor positive control for $G_{\alpha q}$ protein activation:

Due to the non-specific effects of $CaCl_2$ on the SPA-PVT beads, Protein-A beads were used instead. In the experiment, 15µg of M3 COS-7 membranes were incubated with increasing doses of acetylcholine chloride ranging from 100pM to 1mM in presence of $[^{35}S]GTP\gamma^{S}$. A dose responsive activation of $G_{\alpha q}$ protein was observed as shown in Fig 4.3.3 and the Ec_{50} value obtained was 147.7 ± 1.57 nM (n=3). The Y-axis on the graph shows CPM normalized to the baseline value of the graph. Thus, it was confirmed that $G_{\alpha q}$ protein activation could be detected using Protein-A beads in SPA.

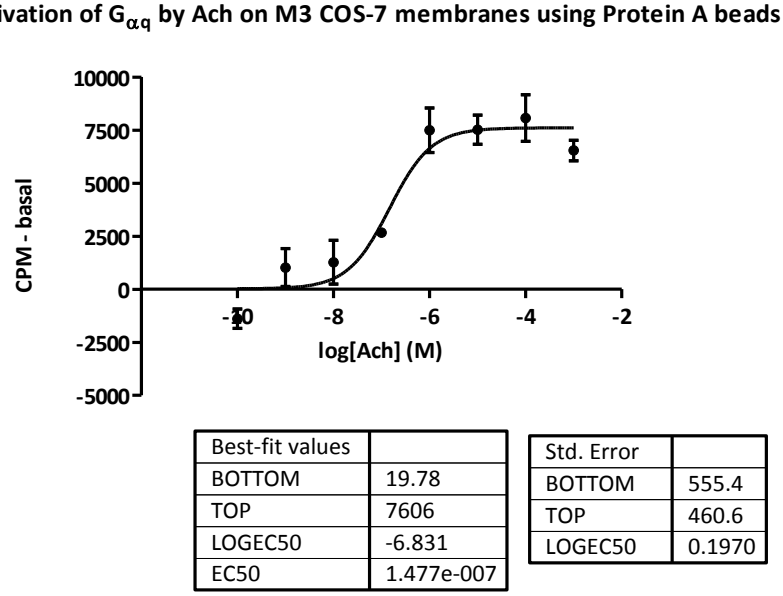

Best-fit values	
BOTTOM	19.78
TOP	7606
LOGEC50	-6.831
EC50	1.477e-007

Std. Error	
BOTTOM	555.4
TOP	460.6
LOGEC50	0.1970

Figure 4.3.3: Activation of Gαq by Acetylcholine chloride on M3 receptor transfected COS-7 membranes using Protein-A beads:

COS-7 cells were transfected with M3 receptor and the effect of acetylcholine chloride on the activation of $G_{\alpha q}$ was checked using Protein-A beads. Acetylcholine chloride was incubated from 100pM to 1mM doses with 15µg of M3 transfected COS-7 membranes in separate wells to measure the $G_{\alpha q}$ activation at each dose. The CPM values shown are normalized to the bottom of the curve. Ec_{50} value obtained was 147.7 ± 1.57 nM. This is a combined curve from three separate experiments performed in duplicates using the same batch of transfected membranes.

4.3.4: Use of Protein-A beads to measure $G_{\alpha q}$ activation by increasing doses of $CaCl_2$ on empty COS-7 and CaSR+RAMP1 membranes measured using Protein-A beads in SPA:

Protein-A beads were used instead of SPA PVT beads in order to use higher doses of $CaCl_2$ in SPA. First the negative control COS-7 membranes were incubated with 10nM to 10mM of $CaCl_2$ in order to measure $G_{\alpha q}$ activation (Fig 4.3.4 A). Log agonist vs response curves were plotted as shown in the Fig 4.3.4 A. The negative control COS-7 empty membranes exhibited $G_{\alpha q}$ activation responses with Ec_{50} values of 0.5 ± 0.18 mM. The maximal stimulation (efficacy) for COS-7 was 2315 ± 301 cpm (n=3). Expression of CaSR in CaSR+RAMP1/3 membranes was checked using western blotting as shown in appendix section 7.4, figure 7.6. CaSR+RAMP1 membranes were also run in parallel to COS-7 membranes (figure 4.3.4 B) to see a change in response, it was observed that the Ec_{50} obtained was 41 ± 4 µM and the efficacy was 3290 ± 418 cpm (n=2). However, as the negative control also showed a similar response; no comparisons were made with CaSR+RAMP1 membranes.

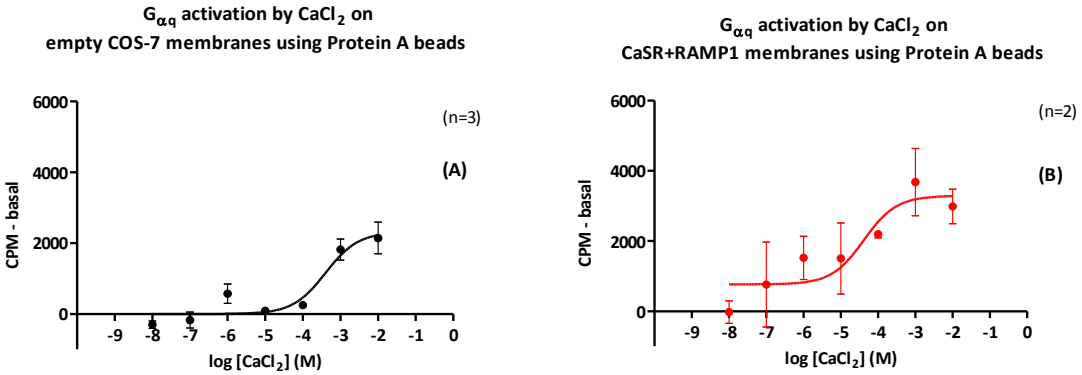

Best-fit values	
Bottom	-1.390
Top	2315
LogEC50	-3.396
EC50	0.0004019

Best-fit values	
Bottom	764.4
Top	3290
LogEC50	-4.381
EC50	4.161e-005

Figure 4.3.4: Effect of $CaCl_2$ doses on $G_{\alpha q}$ activation on empty COS-7 and CaSR+RAMP1 membranes measured using Protein-A beads in SPA:

15µg of empty COS-7 (A) or CaSR+RAMP1 transfected membranes (B) were incubated with 10nM to 10mM of $CaCl_2$ in separate wells and SPA was performed using 50µl of Protein-A beads instead of SPA PVT beads, followed by addition of scintillation liquid before counting on top count plate reader. The graphs show combined data from three (A) and two (B) individual experiments performed in duplicates.

4.3.5: Use of $GdCl_3$ with SPA PVT beads to measure $G_{\alpha q}$ activation in empty COS-7 and CaSR+R1/3 membranes:

$GdCl_3$ was used instead of $CaCl_2$ as an agonist, as $CaCl_2$ but not $GdCl_3$ showed non-specific effects on the SPA PVT beads as shown earlier. Accordingly, 20µg of empty COS-7 membranes (figure 4.3.5 A), CaSR+RAMP1 membranes (figure 4.3.5 B) and CaSR+RAMP3 membranes (figure 4.3.5 C) were incubated with 0.1nM to 1mM $GdCl_3$. However, $G_{\alpha q}$ activation was observed in the negative control COS-7 membranes with an Ec_{50} of 0.1mM. The Ec_{50} for the CaSR+RAMP1 (B) and CaSR+RAMP3 (C) membranes were 0.12mM and 0.25mM respectively. Again, the comparisons cannot be made due the non-specific effect of $GdCl_3$ on the negative control membranes.

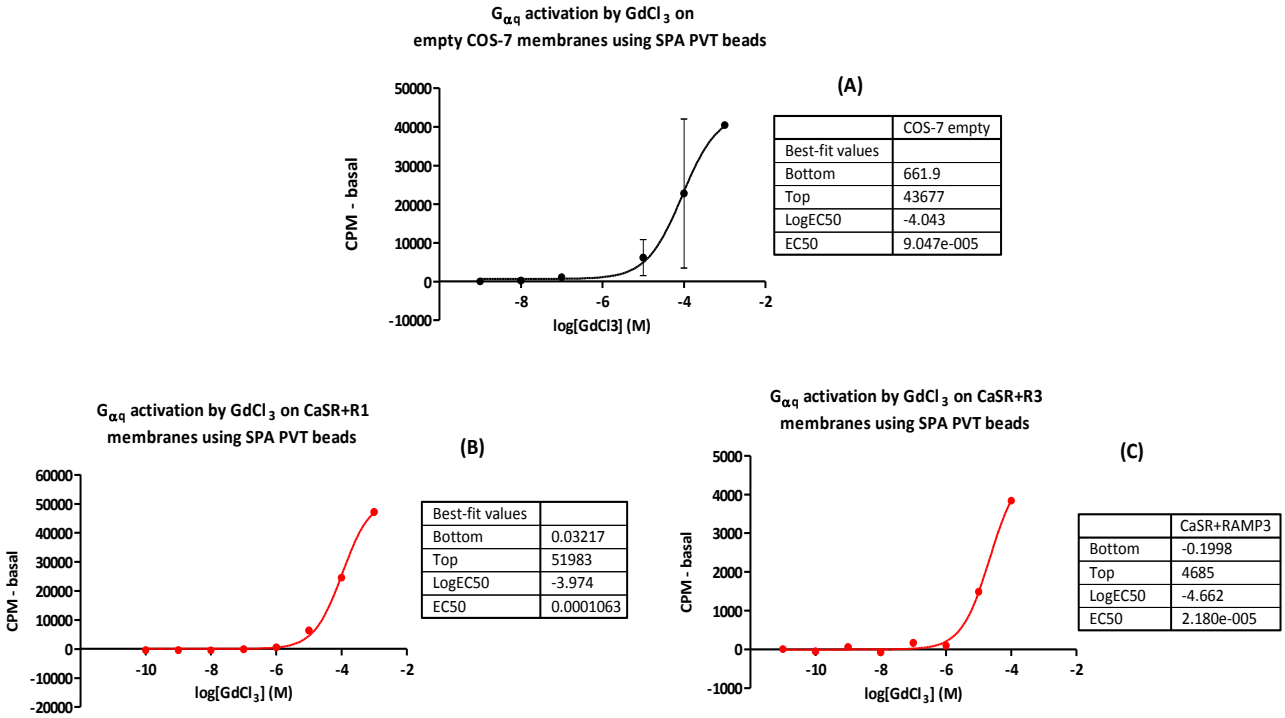

Figure 4.3.5: $G_{\alpha q}$ activation by increasing doses of $GdCl_3$ in empty COS-7 and CaSR+RAMP1/3 membranes measured using SPA PVT beads:

20µg of empty COS-7 (A) CaSR+RAMP1 (B) or CaSR+RAMP3 (C) membranes were incubated with 0.1nM to 1mM $GdCl_3$ and $G_{\alpha q}$ responses were measured using SPA PVT beads. The Ec_{50} are shown in the table below each graphs. (A) n=2 (B) and (C) n=1.

4.3.6.: Using Protein-A beads to measure $G_{\alpha q}$ responses to increasing $GdCl_3$ doses on empty COS-7 and CaSR+RAMP1/3 membranes*:*

Protein-A beads were used instead of SPA PVT beads to measure $G_{\alpha q}$ activation by $GdCl_3$. So, 20µg of empty COS-7 membranes (Fig 4.3.6 A, CaSR+RAMP1 (4.3.6 B), or CaSR+RAMP3 (figure 4.3.6 C) were incubated with 0.1nM to 0.1mM of $GdCl_3$ and $G_{\alpha q}$ responses were measured by pulling out $G_{\alpha q}$ antibodies using Protein-A beads. A dose dependent $G_{\alpha q}$ activation in response to $GdCl_3$ was observed for both- negative control empty COS-7 membranes as well as CaSR+RAMP1 membranes (figure 4.3.6 A and B) with Ec_{50} of 1.2µM and 0.31 µM respectively. The curve for CaSR+RAMP3 was not converged as the top plateau was not obtained (figure 4.3.6 C).

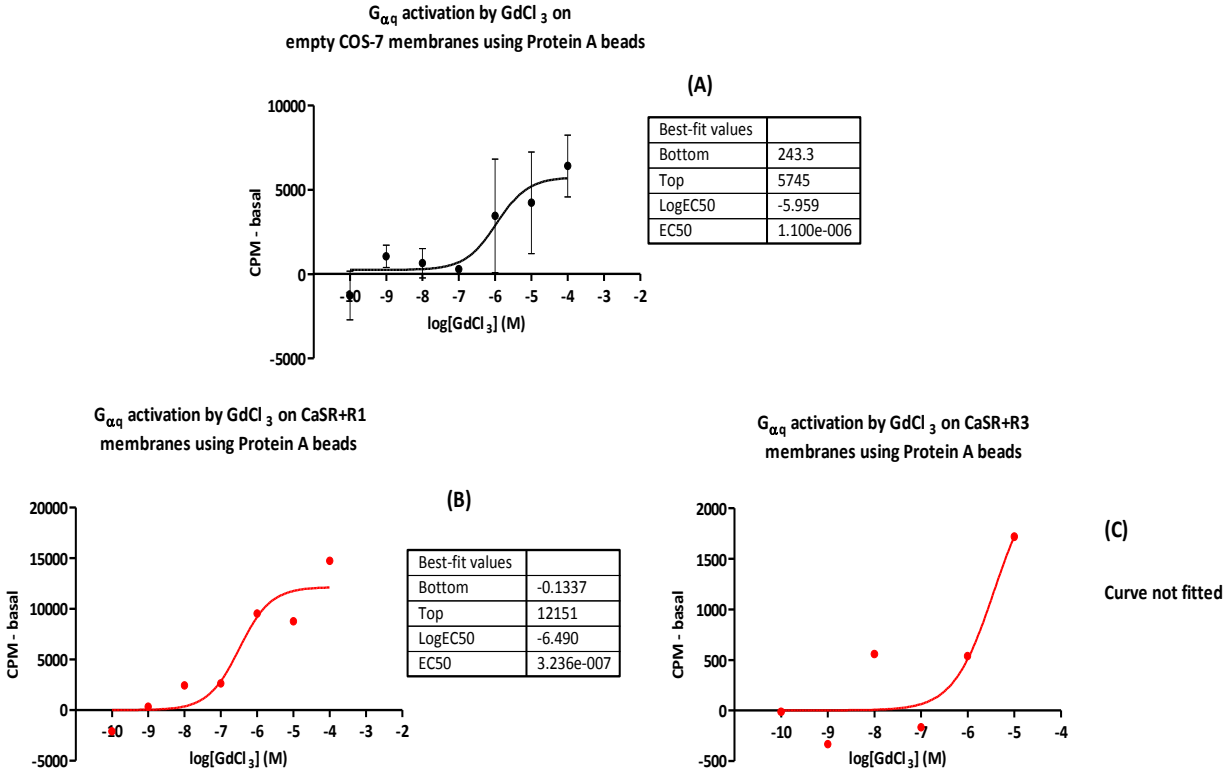

Figure 4.3.6: $G_{\alpha q}$ responses to increasing $GdCl_3$ doses on empty COS-7 and CaSR+RAMP1/3 membranes measured using Protein-A beads in SPA:

Empty COS-7 (A), CaSR+RAMP1 (B) CaSR+RAMP3 (C) membranes were incubated with 0.1nM to 0.1mM of $GdCl_3$ and $G_{\alpha q}$ responses were measured. The Ec_{50} are given in the table below the graphs. (A) n=3 (B) and (C) n=1, all performed in duplicates.

4.3.7: Using allosteric modulator Cinacalcet HCl to measure activation of $G_{\alpha q}$ proteins in CaSR+R1/3 and COS-7 empty membranes using SPA PVT beads:

Due to the non-specific effects of the orthosteric ligands- $CaCl_2$ and $GdCl_3$; Cinacalcet hydrochloride, an allosteric activator of CaSR was used in presence of 0.5mM $CaCl_2$ to measure G-protein activation in SPA. Accordingly, 20µg of COS-7 empty or CaSR+RAMP1/3 membranes were incubated with a high dose of 10µM Cinacalcet HCl in presence of 0.5mM $CaCl_2$ to measure change in $G_{\alpha q}$ activation levels in different membranes using SPA PVT beads. As shown in figure 4.3.7, there was no activation of $G_{\alpha q}$ protein over basal in any combinations including the negative control. Also, the basal activity of $G_{\alpha q}$ was higher in CaSR+RAMP1 membranes than empty COS-7 membranes and highest in CaSR+RAMP3 membranes.

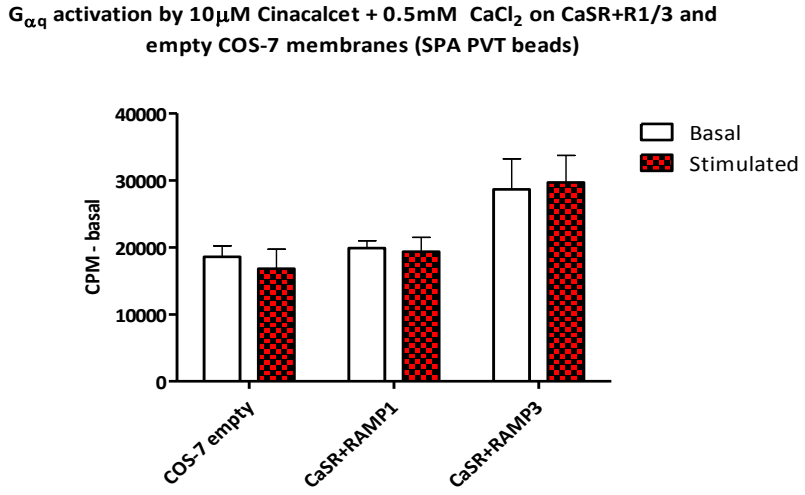

Figure 4.3.7: $G_{\alpha q}$ activation by 10µM Cinacalcet hydrochloride in presence of 0.5mM $CaCl_2$ measured using SPA PVT beads:

COS-7 empty or CaSR+RAMP1/3 membranes (20µg) were incubated 10µM of Cinacalcet HCl to measure $G_{\alpha q}$ activation differences. No activation of $G_{\alpha q}$ was observed in any membrane sets. n=3 performed in duplicates.

4.3.8: Effects of different cell backgrounds on the effect of 10µM Cinacalcet HCl on $G_{\alpha q}$ activation measured using SPA PVT beads:

In order to determine whether using a different cell type would affect the response of $G_{\alpha q}$ activation; CaSR-transfected HEK-293 and TT cell membranes were used in SPA. As a negative control, empty HEK-293 membranes were used. It was observed that there was stimulation over basal in both HEK-293 empty and CaSR-transfected HEK-293 membranes and that the stimulation of $G_{\alpha q}$ was not different between either (figure 4.3.8 A). In the case of TT membranes which natively express CaSR and RAMP1, there was no stimulation of $G_{\alpha q}$ over basal (figure 4.3.8 B).

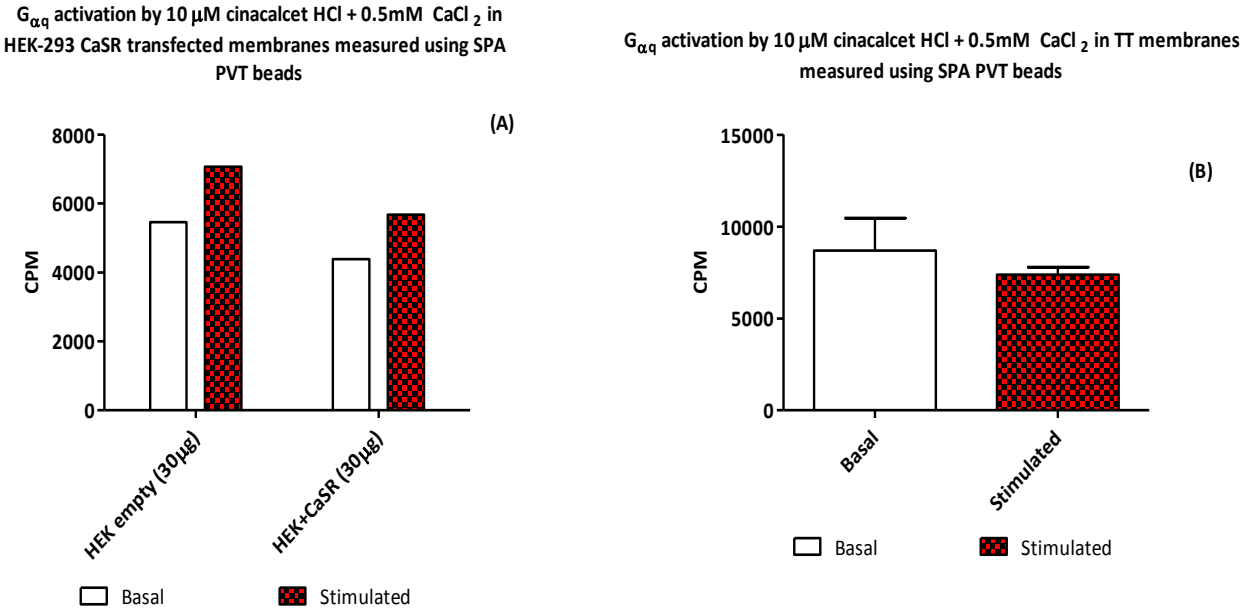

Figure 4.3.8: Activation of $G_{\alpha q}$ proteins in transfected HEK-293 and TT membranes by 10µM Cinacalcet HCl measured using SPA-PVT beads*:*

30µg of HEK-293 non-transfected, CaSR-transfected or 40µg of TT cell membranes were incubated with 10µM Cinacalcet HCl in presence of 0.5mM $CaCl_2$ and $G_{\alpha q}$ activation was measured using SPA PVT. The graph shows $G_{\alpha q}$ activation as CPM for non-stimulated basal (white) and 10µM Cinacalcet HCl stimulated (red) membranes. (A) n=1 and (B) n=3.

Part 2 : Live cell imaging

4.3.9: Testing for functionality of CaSR expressed in TT cells:

Due to the technical problems associated with the SPA, live cell Ca^{2+} imaging was used to measure the signalling of the CaSR. TT cells were used for this which endogenously expressed CaSR RAMP1 and 2 but not 3 (please see appendix section 7.6, figure 7.8 for this result and its discussion). The activity of CaSR expressed on TT cells was studied using specific ligands of the CaSR like Cinacalcet HCl and Neomycin. Intracellular Ca^{2+} increase resulting due to activation of the CaSR was measured using a live cell imaging system. A typical trace obtained is shown in Figure 4.3.9 A where, following the baseline, an increase in fluorescence due to rise in intracellular Ca^{2+} concentration by 1µM Cinacalcet HCl is observed; followed by a sharp increase in intracellular Ca^{2+} concentration due the positive control 10µM ionomycin. Ionomycin was used as a positive control to check the viability of the cells, in the case of absence of a response (especially for the concentrations forming the bottom of the curve). Representative images of cells at different time points are shown in pictures above the graph.

Figure 4.3.9 B shows response of the CaSR to increasing doses of Cinacalcet HCl from 10pM to 100µM in presence of 1.5mM $CaCl_2$ in buffer. A dose dependent increase in intracellular Ca^{2+} was observed and Ec_{50} calculated was 503 ± 1.29 nM. Neomycin was also used as a specific agonist of CaSR; and Figure 4.3.10 shows a dose dependent increase in intracellular Ca^{2+} by increasing doses of Neomycin from 5nM to 2mM. The Ec_{50} calculated was 91 ± 1.45 µM.

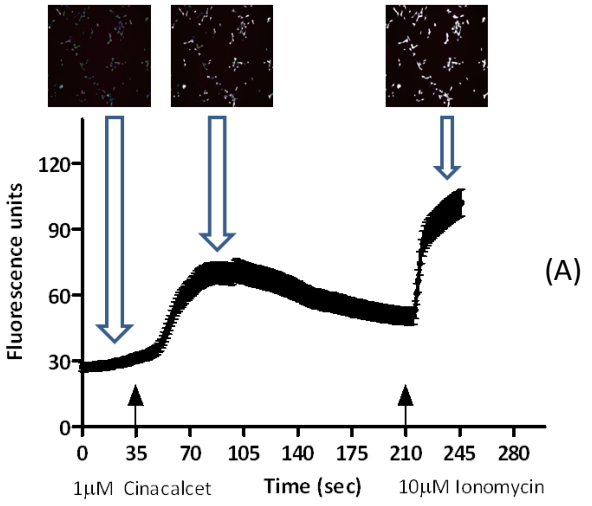

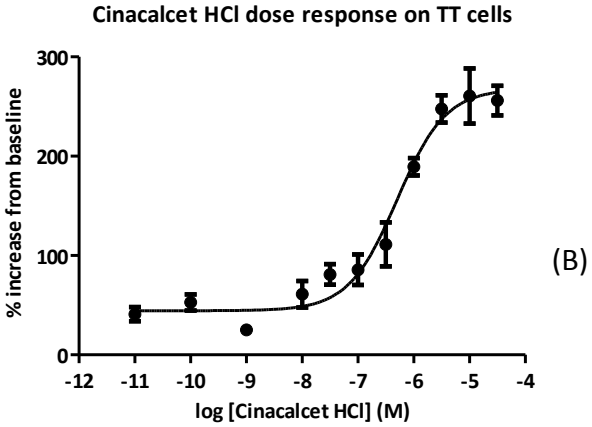

Best-fit values	
Bottom	44.40
Top	267.9
LogEC50	-6.298
EC50	5.032e-007

Std. Error	
Bottom	7.256
Top	9.591
LogEC50	0.1102

Figure 4.3.9: Intracellular Ca^{2+} activation in TT cells by Cinacalcet HCl measured using Fluo-4 AM dye and live cell imaging system*:*

(A) A representative response to 1µM Cinacalet HCl in presence of 1.5mM $CaCl_2$ followed by response to 10µM ionomycin. Representative images at different time points in the response curve are shown in inset. (B) Increase in intracellular Ca^{2+} in TT cells by increasing doses of Cinacalcet HCl from 10pM to 100µM in presence of 1.5mM $CaCl_2$ with an Ec_{50} of 503 ± 1.29 nM. The data is combined from two-three independent experiments with at least 20 cells or more analysed per dose.

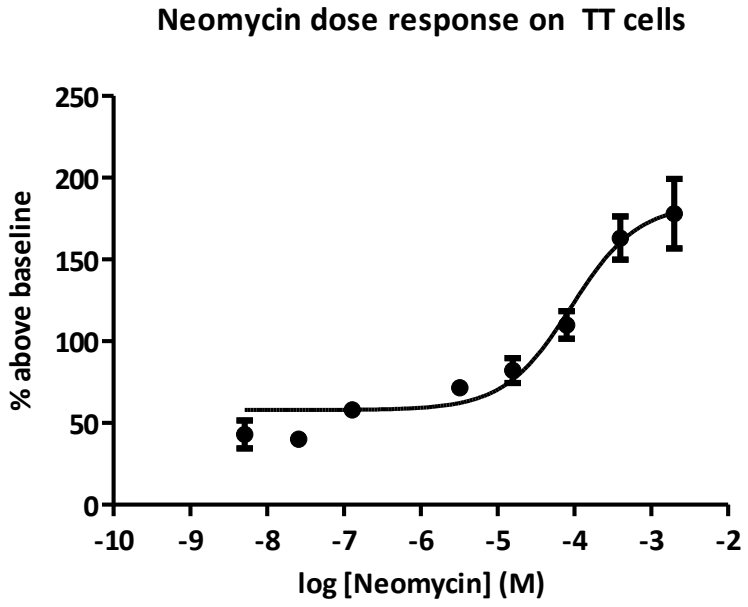

Best-fit values	
Bottom	57.95
Top	184.0
LogEC50	-4.041
EC50	9.100e-005

Std. Error	
Bottom	4.713
Top	10.44
LogEC50	0.1620

Figure 4.3.10: Intracellular Ca^{2+} activation in TT cells by Neomycin measured using Fluo 4 AM dye and live cell imaging system:

Increase in intracellular Ca^{2+} in TT cells by increasing doses of Neomycin from 5nM to 2mM. log agonist vs response curve was plotted using Graphpad prism 5 and the Ec_{50} calculated was 91 ± 1.45 µM. The data is combined from two independent experiments with at least 20 cells or more analysed per dose.

4.3.10: Determining the effect of RAMP1 siRNA-mediated knock-down on CaSR signalling in TT cells:

In order to study the effect of RAMP1 mRNA knock-down on the CaSR signalling in TT cells, siRNA approach was used and its effect on the functional response of TT cells to Cinacalcet HCl was measured using live cell imaging. Figure 4.3.11 shows the mRNA expression levels of RAMP1 and 2 and CaSR in TT cells 72hr-post transfection with 1.5µg RAMP1 or scrambled or random siRNA (negative control). Expression of RAMP3 was not detected. The mRNA expression levels of the genes were normalized to Actβ and expressed as % relative to Actβ. At 72hr after transfection, mRNA expression of RAMP1 was decreased by 80% in RAMP1 siRNA-transfected cells compared to scrambled siRNA transfected cells, which was statistically significant (Figure 4.3.11) ($p<0.05$, two-tailed Mann-Whitney test). There was no effect of RAMP1 or scrambled siRNA transfection on the mRNA expression levels of other genes as shown in Figure 4.3.11.

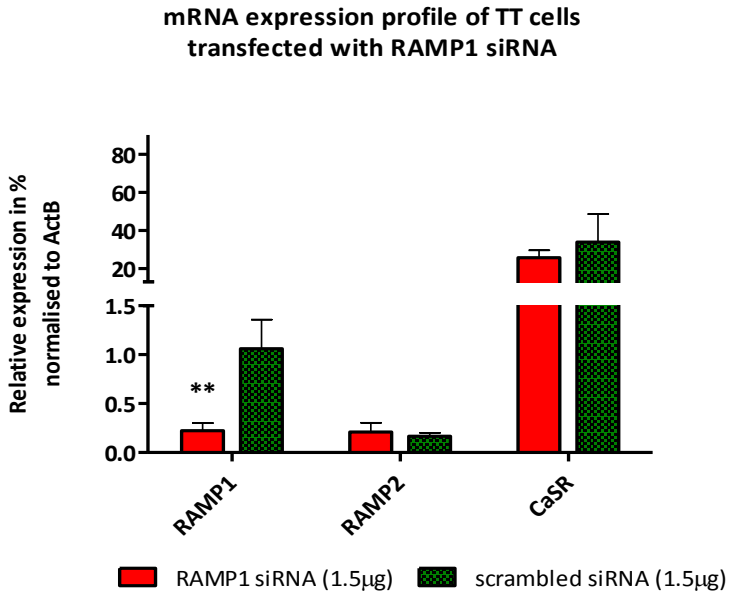

Figure 4.3.11: mRNA expression levels of RAMPs and CaSR in TT cells 48hr post transfection with RAMP1 siRNA:

TT cells were transfected with RAMP1 or scrambled siRNA (1.5µg per 1.5 million cells) using electroporation. 72hr post-transfection samples were collected to check the effect of RAMP1 siRNA on the mRNA levels of RAMP1 using real-time PCR. The mRNA expression levels of the genes of interest were normalized to Actβ and are presented as fold change relative to Actβ in %. The data is combined from five independent experiments. $p<0.05$ as analysed by two-tailed Mann-Whitney test.

Next, it was tested whether RAMP1 mRNA knock-down corresponded to a change in the functional of CaSR. For this CaSR was stimulated using 100µM Neomycin and 1µM Cinacalcet HCl and its signalling was tested by measuring increase in $Ca_{[i]}$ using live cell imaging system. Accordingly, 1.5µg RAMP1 or scrambled sequence siRNA was transfected in TT cells and 72hr-post transfection, cells were loaded with Fluo-4AM dye to measure intracellular Ca^{2+} increase. As shown in figure 4.3.12 (A), there was ~50% decrease in the intracellular Ca^{2+} release in RAMP1 siRNA-transfected cells (red bar) compared to the negative control- scrambled sequence siRNA-transfected cells (green bar). This was statistically significant with $p<0.0001$ as analysed by Kruskal-Wallis test, Dunn's multiple comparison post-test as data was not normally distributed according to D'Agostino & Pearson omnibus normality test. Also, there was no difference between the signalling of the scrambled siRNA transfected cells and the normal untransfected TT cells (white bar), thus excluding any non-specific effects due to the transfection procedure. Data is represented as % increase from basal fluorescence of the cells.

As shown in figure 4.3.12 (B), 1µM Cinacalcet HCl response was attenuated by 42% in RAMP1 siRNA-transfected cells compared to the negative control. This decrease was also statistically significant with $p<0.0001$ as analysed by Kruskal-Wallis test, Dunn's multiple comparison post-test, as data was not normally distributed according to D'Agostino & Pearson omnibus normality test. Again there was no difference between the signalling of the negative control and the normal non-transfected TT cells (white bar).

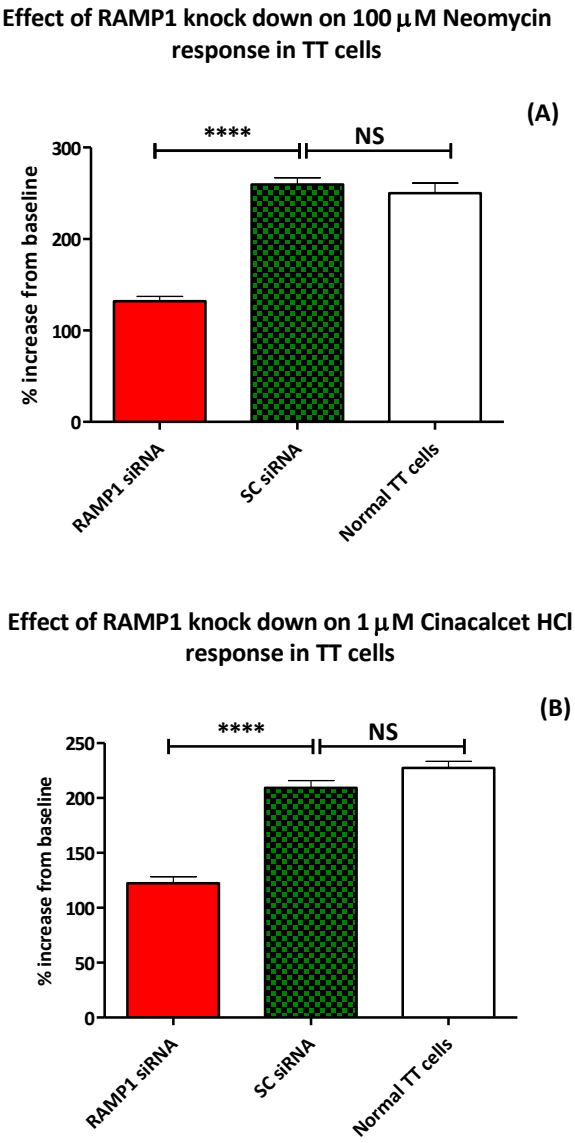

Figure 4.3.12: Effect of RAMP1 knock down on 100µM neomycin and 1µM Cinacaclet HCl signalling on TT cells:

TT cells were transfected with 1.5µg RAMP1 or SC siRNA. 72hr post-transfection the cells were loaded with Fluo-4AM and treated with (A) 100µM Neomycin (B) 1µM Cinacalcet HCl which showed ~50% and ~42% decrease respectively in $Ca_{[i]}$ increase in RAMP1 siRNA transfected cells compared to siRNA to scrambled sequence. Red bar represents cells transfected with RAMP1 siRNA, green -scrambled siRNA (negative control) and white- normal untransfected TT cells. The data is combined from three independent experiments for (A) and two independent experiments for (B) and the total number of cells were (A) 354 each (RAMP1 and SC siRNA transfected) and 120 normal TT cells (B) 241 (RAMP1 siRNA transfected); 231 (SC siRNA transfected) and 154 normal TT cells.

4.3.11: Studying the role of RAMP1 in CaSR signalling in TT cells using RAMP1 antibodies:

In order to test whether RAMP1 is involved in the signalling of CaSR in TT cells, the effect of RAMP1 blocking antibody on CaSR signalling was tested using live cell Ca^{2+} imaging. Different RAMP1 antibodies were tested for their effect on CaSR signalling. Figure 4.3.13 shows the effect of using RAMP1 polyclonal antibodies (poly Ab) raised in mouse (Ms) on 10µM Cinacalcet HCl signalling in TT cells. The data shows the peak of response represented as % increase of fluorescence from baseline fluorescence. White bar shows the response of 10µM Cinacaclet HCl which was 245% above basal. Blue bars show the effect of Mouse control IgG and the red bars show the effect of 5µg and 10µg of RAMP1 Ms poly Abs. Statistical comparisons were made for the RAMP1 antibodies against their respective doses of Control IgG. It was observed that 5µg and 10µg RAMP1 Ms poly Ab caused 57.5% and 76.2% decrease in 10µM Cinacalcet signalling compared to their respective Control IgG doses ($p<0.0001$ as analysed by Kruskal-Wallis test, Dunn's multiple comparison post-test). So, a further significant attenuation by 19% was observed for 10µg RAMP1 Ab compared to 5µg dose ($p<0.0001$, as analysed by two-tailed Mann-Whitney test).

RAMP1 poly Ab raised in goat (Gt) showed a dose-dependent attenuation of 1µM Cinacalcet signalling as shown in Figure 4.3.14. 5µg and 10µg of RAMP1 Gt poly Ab attenuated 1µM Cinacalcet signal by 35% and 57% respectively compared to their respective control IgG Ab. This decrease was statistically significant with $p<0.0001$, as analysed by Kruskal-Wallis test and Dunn's multiple comparison post-test. Also the difference between the effect of 5µg and 10µg RAMP1 Ab (21%) was statistically significant ($p<0.001$, as analysed by two-tailed Mann-Whitney test).

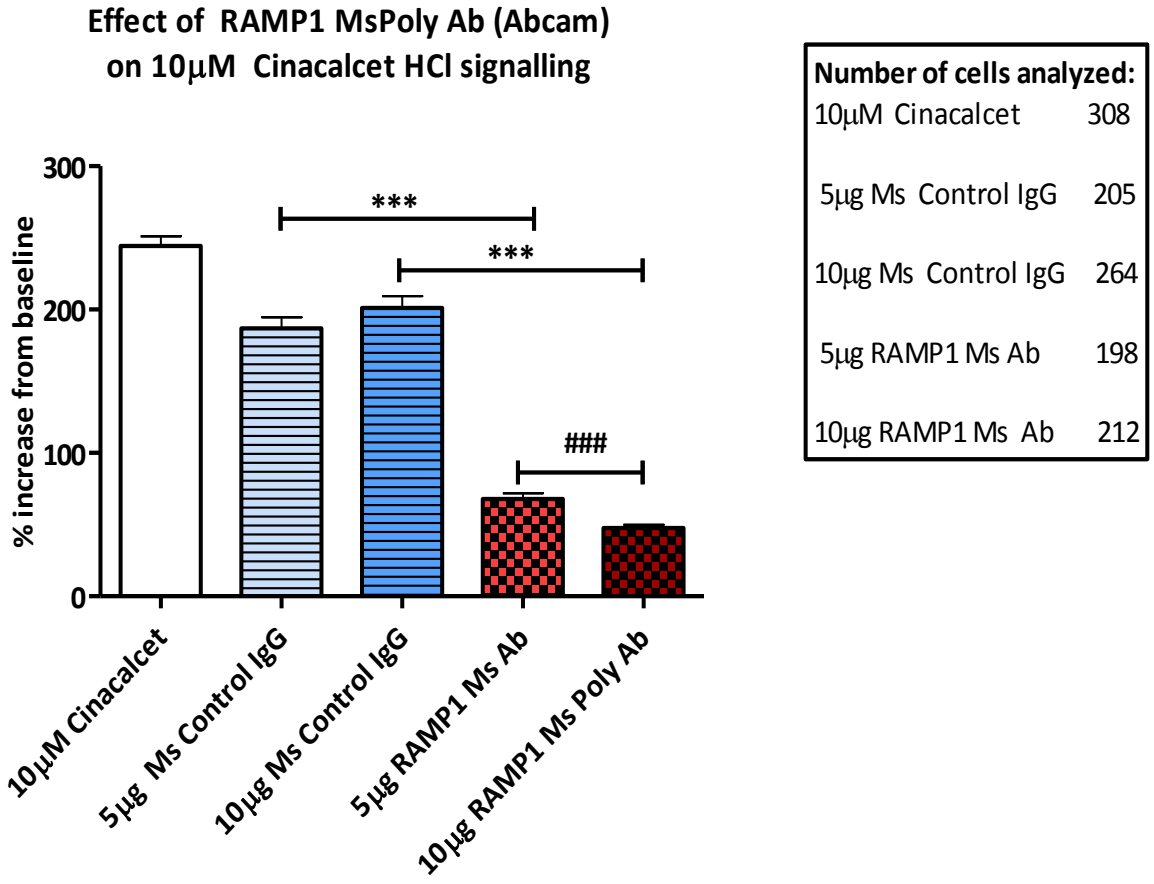

Figure 4.3.13: Effect of mouse polyclonal RAMP1 antibodies on signalling of 10μM Cinacalcet HCl in TT cells:

TT cells were incubated with the given concentrations of antibodies for 45 min at 37^{o}C after Fluo 4 AM loading and the effect of 10μM Cinacalcet HCl in presence of 1.5mM $CaCl_2$ on intracellular Ca^{2+} activation was measured using live cell imaging system. The attenuation effect by 5μg and 10μg of RAMP1 mouse polyclonal (Abcam) on the intracellular Ca^{2+} activation by 10μM Cinacalcet HCl are shown in the graph. The data is from single experiment and the numbers of cells analysed per set are shown in the legend on the graph. *** $p<0.0001$ analysed using Kruskal-Wallis test and Dunn's multiple comparison post-test as the data was not normally distributed according to D'Agostino & Pearson omnibus normality test. ### $p<0.0001$ two-tailed Mann-Whitney test.

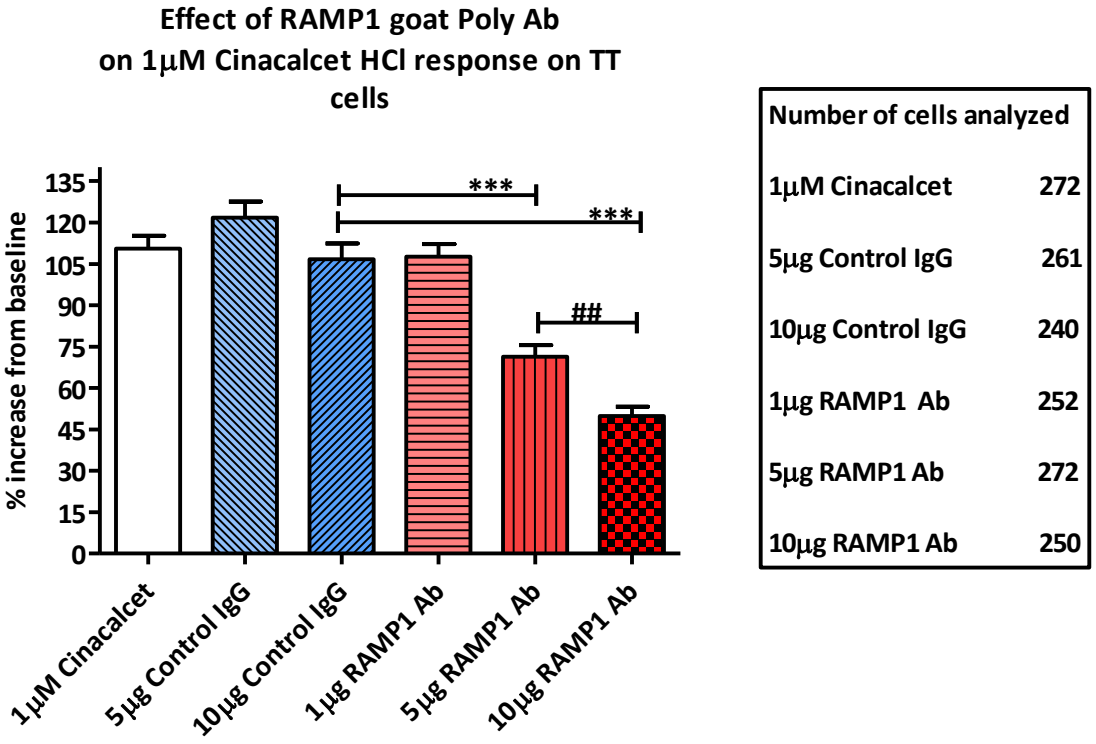

Figure 4.3.14: Attenuation of 1μM Cinacalcet response on TT cells by RAMP1 polyclonal Ab raised in goat:

TT cells were treated with the given concentrations of RAMP1 goat Poly Ab (SantaCruz) or Control IgG for 45 min at 37^{o}C after loading Fluo4 AM. A RAMP1 antibody dose dependant decrease in intracellular Ca^{2+} activation due to 1μM Cinacalcet HCl in presence of 1.5mM $CaCl_2$ was observed (red bars). There was no attenuation of 1μM Cinacalcet response by control IgG (blue bars). The data is combined from 5 independent experiments and the total number of cells analysed is shown. The data is not normally distributed according to D'Agostino & Pearson omnibus normality test. *** $p<0.0001$ determined by Kruskal-Wallis test, Dunn's multiple comparison post-test, ## $p<0.001$ two-tailed Mann-Whitney test.

4.3.12: Comparing the efficacy of RAMP1 goat Poly Ab to NPS 2390 in attenuating responses to 1µM Cinacalcet HCl, 100µM Neomycin and 5mM $CaCl_2$ in TT cells:

The effect of 10µg RAMP1 goat poly Ab on attenuation of CaSR signalling was compared with different concentrations of CaSR antagonist NPS 2390. The final bath concentration of the RAMP1 goat poly Ab in a single well was calculated to be 133.3nM using the typical molecular weight of IgG as 150kDa. Three CaSR agonists: Cinacalcet, Neomycin and Ca^{2+} were used to compare the effects of RAMP1 Ab and NPS 2390 on CaSR signalling in TT cells.

Although there was a slight attenuation of 1µM Cinacalcet response by 1µM (~16%), 5µM (~16%) and 10µM NPS 2390 (~21%), it was not statistically significant (Figure 4.3.15). Whereas 50µM NPS 2390 caused 68.5% decrease which was statistically significant ($p<0.0001$, analysed by Kruskal-Wallis test and Dunn's multiple comparison post-test) (Figure 4.3.15). RAMP1 goat Poly Ab (133.3nM) caused a statistically significant attenuation of 1µM Cinacalcet HCl response by 46% ($p<0.0001$, analysed by Kruskal-Wallis test and Dunn's multiple comparison post-test). So in comparison, 133.3nM RAMP1 Ab was 30% more effective in attenuating 1µM Cinacalcet response than 10µM NPS 2390 ($p<0.001$, two-tailed Mann-Whitney test); whereas there was no statistically significant difference between the effects of RAMP1 Ab and 50µM NPS 2390 (two-tailed Mann-Whitney test).

In the case of 100µM Neomycin, there was a dose-dependent decrease in 100µM Neomycin response by 10µM (44%) and 50µM (65.34%) NPS 2390 ($p<0.0001$, analysed by Kruskal-Wallis test, Dunn's multiple comparison post-test). It was observed that 133.3nM RAMP1 poly Ab attenuated 100µM Neomycin response by ~48% compared to Control IgG ($p<0.0001$, Kruskal-wallis test, Dunn's multiple comparison post-test). There was no statistically significant difference between the effects 10µM/50µM NPS 2390 and 133.3nM RAMP1 Poly Ab (two tailed Mann-Whitney test) (Figure 4.2.16).

There was no attenuation of 5mM $CaCl_2$ response by 133.3nM RAMP1 Poly Ab or 10µM NPS 2390; whereas 50µM NPS 2390 attenuated the response by 42% ($p<0.0001$, Kruskal-Wallis test, Dunn's multiple comparison post-test) (Figure 4.3.17).

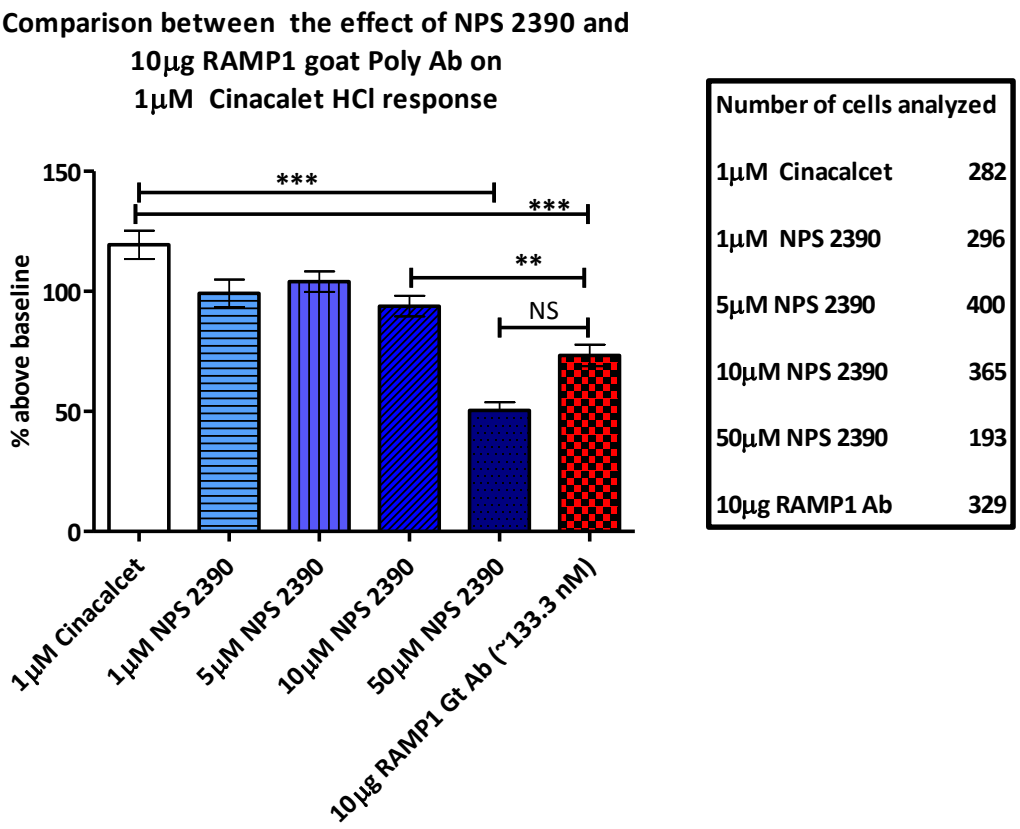

Figure 4.3.15: Comparison between NPS 2390 and RAMP1 goat antibody efficacy in attenuating 1µM cinacalcet response in TT cells:

TT cells were pre-treated with 1, 5, 10 or 50µM of NPS 2390 or 10µg RAMP1 goat polyclonal antibody from SantaCruz for 45 min at 37°C, before measuring 1µM cinacalcet HCl response in presence of 1.5mM $CaCl_2$. The concentration of RAMP1 Ab was calculated to be 133.3nM based on typical weight of IgG as 150 kDa. ** $p<0.001$ and *** $p< 0.0001$ as determined by Kruskal-Wallis test using Dunn's multiple comparison post-test. The data was not normally distributed according to D'Agostino & Pearson omnibus normality test. The data represented is combined from three independent experiments and total number of cells analysed are shown in the box.

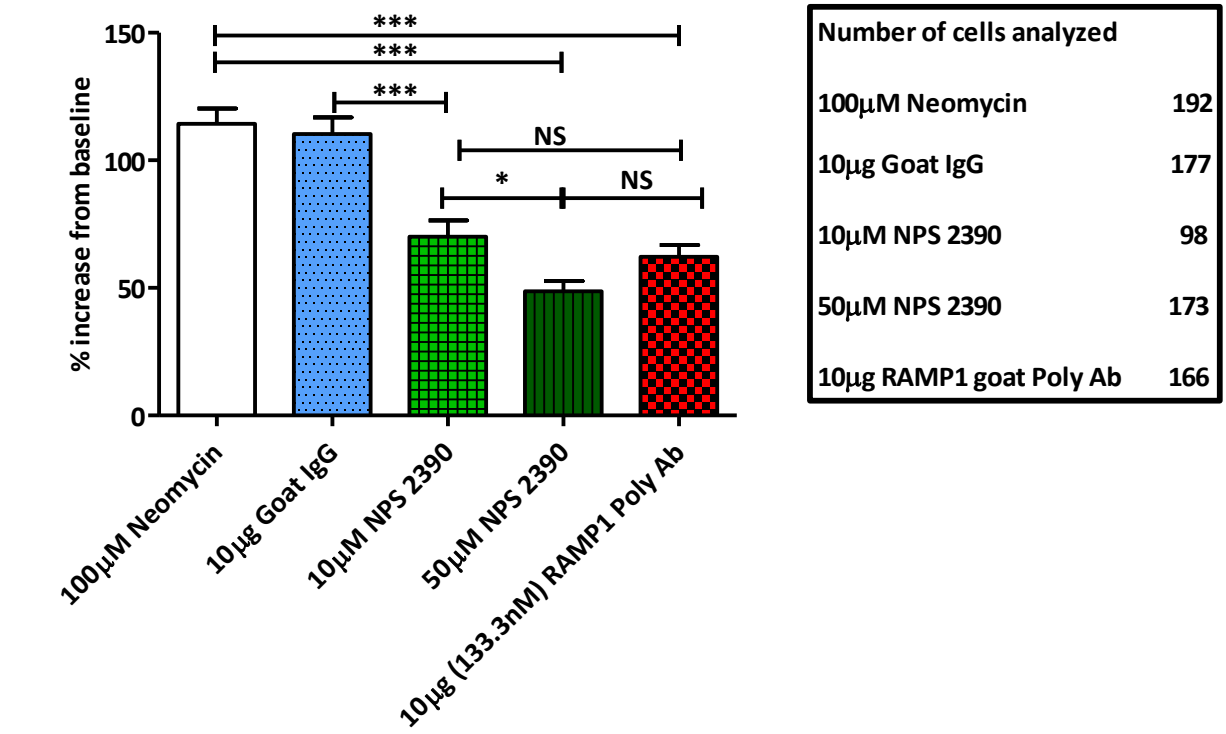

Figure 4.3.16: Comparison between NPS 2390 and RAMP1 goat antibody efficacy in attenuating 100µM Neomycin response in TT cells:

TT cells were pre-treated with either 10µg of RAMP1 goat Poly Ab or 10 or 50µM of NPS 2390 for 45 min at 37°C, before measuring intracellular Ca^{2+} activation by 100µM Neomycin. * $p<0.05$ and *** $p< 0.0001$ as determined by Kruskal-Wallis test using Dunn's multiple comparison post-test. The data was not normally distributed according to D'Agostino & Pearson omnibus normality test. The data represented is combined from three independent experiments and total number of cells analysed are shown in the box.

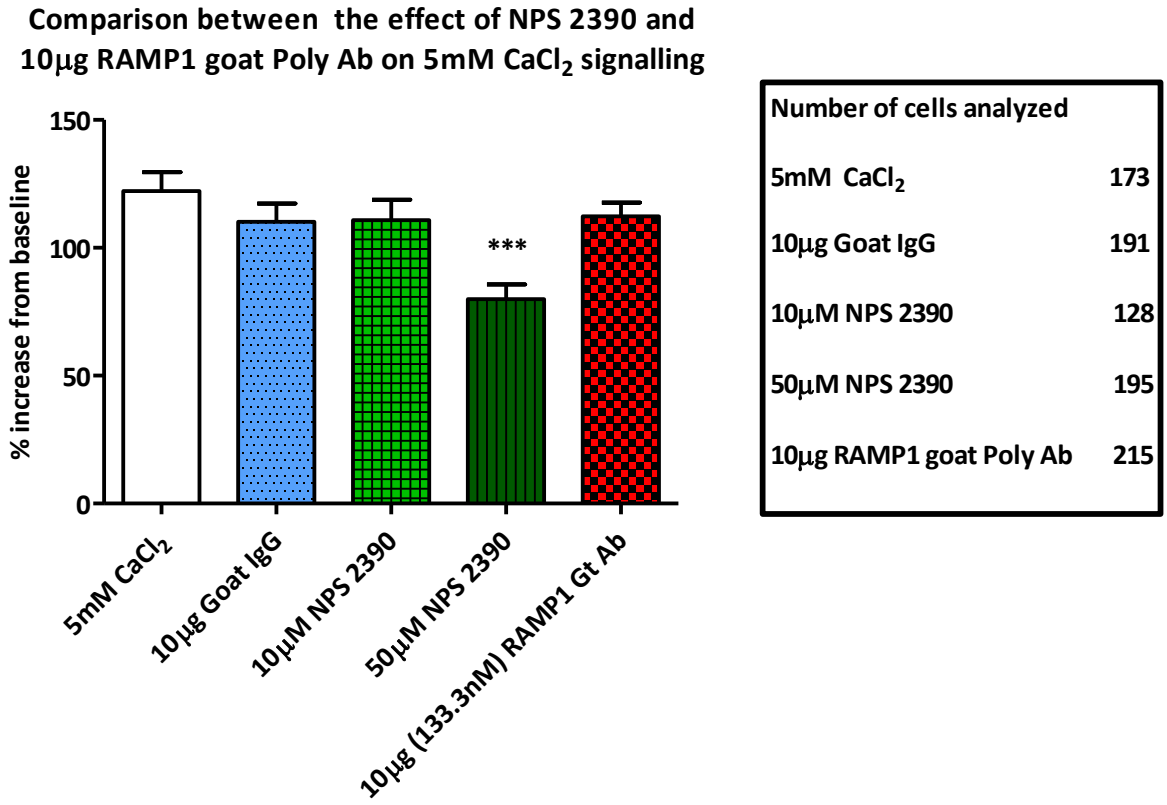

Figure 4.3.17: Comparison between NPS 2390 and RAMP1 goat antibody efficacy in attenuating 5mM $CaCl_2$ response in TT cells:

TT cells were pre-treated with either 10µg of RAMP1 goat Poly Ab or 10 or 50µM of NPS 2390 for 45 min at 37°C, before measuring intracellular Ca^{2+} activation by 5mM $CaCl_2$. *** $p < 0.0001$ as determined by Kruskal-Wallis test using Dunn's multiple comparison post-test. The data was not normally distributed according to D'Agostino & Pearson omnibus normality test. The data represented is combined from three independent experiments and total number of cells analysed are shown in the box.

4.4. Discussion.

It was hypothesised that RAMPs play a role in CaSR signalling. CaSR is a pleiotropic GPCR which activates various signalling pathways via different G-proteins as discussed in detail in section 4.1.2 in introduction to this chapter. Also, increasing evidence is suggesting a direct role of RAMPs in GPCR signalling (section 4.1.3, introduction to this chapter). So, direct and differential roles of RAMP1 and 3 on CaSR signalling were tested using antibody-capture SPA (section 4.1.4, introduction to this chapter) in transfected COS-7 cell membranes.

Measuring differential signalling by CaSR+RAMP1/3 complexes using antibody-capture SPA:

Since G-protein activation is the top in the hierarchy of GPCR signalling, it would be important to differentially determine the G-protein activation profile of CaSR with each- RAMP1 and 3. For this, the use of antibody-capture SPA was proposed, as this technique can detect specific G-protein activation and the need for immunoprecipitation steps involved in [^{35}S]GTPγ^{S} binding assay is eliminated [249]. pcDNA3.1 CaSR and pcDNA 3.1 RAMP constructs were used to transfect COS-7 cells. pcDNA3.1 CaSR construct was engineered and sequencing of the cloned construct from bps 300-3220 out of 3300bps in total, was performed to ensure the absence of any mutations that may have risen during the cloning procedure (data not shown). The RAMP cDNA used were also present in pcDNA3.1, so that using the same vectors for both CaSR and RAMPs would ensure similar expression levels due to the activity of the same promoter.

Since $G_{\alpha q}$ activation is the most common signalling pathway of the CaSR [119, 132, 141, 245, 246], SPA was used to measure $G_{\alpha q}$ protein levels in CaSR+RAMP1/3 membrane preparations. The adequate optimization of the assay to detect $G_{\alpha q}$ was tested by using M3 receptor as a positive control (figure 4.3.1 and 4.3.3), since it is known to activate the $G_{\alpha q}$ protein [249, 260, 261]. The results confirmed that the conditions for the experiment were optimized and that in our hands, $G_{\alpha q/11}$ activation could be detected by SPA.

Next the presence of G-proteins in COS-7 membrane preparations was tested using western blotting (Appendix section 7.3, figure 7.5) using the same antibodies used in the SPA. This would test the specificity of the antibodies and consequently ensure that the signal observed in

SPA, corresponded to the respective, specific G-protein activation. Comparing our results (appendix section 7.3, figure 7.5) with the information in the literature and [250, 251] and the results obtained for antibody testing by the manufacturers -Santacruz biotechnology Ltd, it was observed that the bands at ~42-45KDa correspond to specific G-protein of interest (appendix section 7.3, figure 7.5) whereas bands at ~22KDa correspond to non-specific binding of antibodies. However, the ability to detect dose-dependent $G_{\alpha q}$ activation by acetylcholine on M3 receptor (figure 4.3.1 and 4.3.3) shows that the antibody could specifically capture $G_{\alpha q}$ protein. In addition this, these anti-G-protein antibodies are well-characterized and have been used successfully in antibody-capture SPA by others as shown in the literature: anti-$G_{\alpha s}$ [250, 253, 254], $G_{\alpha i}$ [249], $G_{\alpha q}$ [249-251, 253]; where it was also shown that anti-$G_{\alpha s}$ and $G_{\alpha q}$ antibodies are not cross-reactive to each other [250, 251].

The expression of CaSR was checked in the transfected CaSR+RAMP1 and CaSR+RAMP3 membrane preparations; with COS-7 empty membranes as the negative control using western blotting (Appendix section 7.4, figure 7.6). This shows that the co-transfection efficiency was appropriate and that CaSR was trafficked to the cell-surface by RAMP1 or 3.

Use of Ca^{2+} and Gd^{3+} in the SPA and technical problems associated:

Since Ca^{2+} is the natural agonist of the CaSR, $CaCl_2$ was used in SPA on CaSR+RAMP1/3 transfected COS-7 membranes to measure differences in $G_{\alpha q/11}$ activation. However, it was discovered that doses higher than 1mM exhibited non-specific effect by increasing the signal artificially, even in absence of any cell-membranes in the assay (figure 4.3.2 A). Since, the Ec_{50} of Ca^{2+} is ~3mM [10][28][68], this non-specific effect prevented the use of $CaCl_2$ in further experiments. There are no studies in the literature using this technique on CaSR or using Ca^{2+} in the assay. It should be tested if this can be attributed to the effect of Ca^{2+} or Cl^- on the scintillant present in the beads.

Accordingly, the protocol was modified to using Protein-A beads (as there is no scintillant in the beads) instead of SPA PVT beads. Protein-A beads immunoprecipitated the specific G-protein antibody and following the washes, radioactivity corresponding to the activated $G_{\alpha q}$ was measured. This modified protocol was tested for its ability to detect $G_{\alpha q}$ protein activation using

the same batch of M3 receptor transfected COS-7 membranes (Figure 4.3.3). However, on using this modified protocol to measure $G_{\alpha q}$ activation by $CaCl_2$, it was observed that the negative control empty COS-7 membranes, which do not express CaSR (appendix section 7.4, figure 8.6), showed $G_{\alpha q}$ activation in response to higher doses of $CaCl_2$ (figure 4.3.4 A). Even though a left-ward shift to the curve (figure 4.3.4 B) was observed using CaSR+RAMP1 membranes, this result cannot be accepted for further interpretation due to the non-specific effects observed with the empty COS-7 membranes. Similar results were observed when Gadolinium (figures 4.3.5, 4.3.6) and neomycin (data not shown) were used as an agonist. This shows that probably the higher doses of these ligands cause non-specific activation of G-proteins. Such an effect was also hypothesised but not tested by Mamillapalli *et al* in their $[^{35}S]GTP\gamma^{S}$ binding assays using immunoprecipitation method on breast cancer cell line membranes [131]. Alternatively, increase of $G_{\alpha q}$ in negative control membranes might also suggest an alternative cation-sensing receptor in COS-7 cells which is not recognized using human CaSR Taqman® probes and CaSR Ab. GPRC6A mRNA expression was found to be absent in these cells (data not shown) which excludes its likelihood as an alternative cation-sensing receptor present in these cells.

Using allosteric activator Cinacalcet HCl:

Due to the technical problems associated with higher doses of the orthosteric agonists, an allosteric activator of the CaSR called Cinacalcet HCl [86] was used instead, as it requires much lower extracellular Ca^{2+} concentration (0.5mM) for its function. So, CaSR activation can be achieved with a low $CaCl_2$ concentration in the assay, which does not have any non-specific effect on the SPA PVT beads (figure 4.3.2). Also, any non-specific activation of $G_{\alpha q}$ in COS-7 empty membranes even at a very high dose of 10µM Cinacalcet HCl (figure 4.3.7) (reported Ec_{50} is 51nM [86]) was not observed. This confirms that the non-specific effect on G-protein activation was limited to the orthosteric agonists. However, using Cinacaclet HCl, stimulation of $G_{\alpha q}$ could not be detected in either of CaSR+RAMP1/3 membranes (figure 4.3.7). This could either be due to the assay sensitivity towards the concentrations of the $G_{\alpha q}$ protein activated, or a low receptor number being expressed on the cell surface; or both. An activation of other G-proteins was also tested and preliminary experiments using co-transfected COS-7 and TT cell-membranes failed to detect any activation of $G_{\alpha s}$ and $G_{\alpha i}$ by Cinacalcet HCl (data not shown). So,

the possibility of activation of an alternative G-protein pathway could not be detected as well. This shows that the failure to detect the activation of $G_{\alpha q}$ was most likely due to the technical problems mentioned above.

During my MSc project in the past, which involved the use of SPA on the adrenomedullin receptors, it was observed that this technique is very sensitive to the receptor number present in the transfected membranes. Initial testing of this protocol showed that $G_{\alpha s}$ activation by adrenomedullin was not recorded on CLR+RAMP3 membranes at receptor expression levels of 3.1pM/mg of protein. But at high receptor expression levels of 11pM/mg of protein, dose-dependent $G_{\alpha s}$ activation was observed (data not shown). It can be hypothesised that optimal receptor number necessary for G-protein detection by SPA in the batches of CaSR and RAMP co-transfected membranes was not achieved.

It was postulated that the cell-background could be associated with the failure to detect specific G-protein activation in SPA. Differences in cell background have been shown to affect receptor phenotypes involving RAMPs. It was observed by Tilakaratne *et al,* that RAMP2 induced a weak AMY receptor phenotype in transfected COS-7 cells, whereas a relatively stronger AMY receptor phenotype in transfected CHO cells; thus reflecting changes in G-protein coupling efficiencies between different cell types [262]. To test if a similar phenomenon existed with CaSR and RAMPs co-expression levels, CaSR-transfected HEK-293 cells were used, although they were initially not selected for use due to endogenous expression of RAMP1 [157], which would make the comparison with CaSR+RAMP3 difficult. Also, TT cells which endogenously express both CaSR and RAMP1 but not RAMP3, were chosen. However, there was no specific increase in $G_{\alpha q}$ activation in either of the cell-types (figure 4.3.8 A & B). As mentioned earlier, this could be due to low CaSR receptor number in these cells, especially in TT cells, relative to transfected cells, as the expression is endogenous. Consequently, the amount of $G_{\alpha q}$ protein activated by the activation of lower CaSR numbers could not be detected by the assay.

Transfection efficiency and consequently receptor number can be improved by using alternate protein expression methods like MembranePro^{TM} functional protein expression system from Life Science technologies, which co-transfects virus like particles along with the receptor of

interest inside the cells. Here, viral core proteins gag are transfected in the cells which bud from the cell under lipid rafts in the plasma membrane, capturing and displaying raft contents (receptors) in their native form as particles and secreting into culture medium, which can be easily collected. Alternatively, CHO cells could be used for this technique as they have been successfully used to study RAMP biology [175, 262], to test whether better co-transfection efficiency can be achieved. An alternative technique can be used incorporating antibodies against the active GTP-bound G-proteins (NewEast biosciences) [263] that are immobilized to fluorescent beads with distinct emission profiles and hence enabling multiple G-protein activation measurement from a single reaction.

So to conclude, it is not recommended to use high concentrations of $CaCl_2$, $GdCl_3$ or Neomycin in antibody-capture SPA, as they have non-specific activation of $G_{\alpha q}$ protein in the assay. Another hypothesis suggests the presence of an alternative cation-sensing receptor in COS-7 cells which could not be probed for using CaSR primers. No measurable $G_{\alpha q}$ activation by the allosteric modulator Cinacalcet HCl was achieved in transfected or natively expressing CaSR membranes. This problem was probably due to the receptor number in the membranes which do not cause sufficient $G_{\alpha q}$ activation within the sensitive-limit of the assay.

Studying the role of RAMP1 in CaSR signalling in endogenous expression system using Ca^{2+} imaging techniques:

Due to the inability to detect direct G-protein activation, intracellular Ca^{2+} release upon CaSR activation was studied as an alternative. Intracellular Ca^{2+} increase upon activation of the CaSR is a well-characterized pathway, where, IP3 activation which is shown to be mediated by $G_{\alpha q}$ (as shown by the inability of the pertusis-toxin to inhibit the response, a characteristic feature of $G_{\alpha q}$) causes release of Ca^{2+} from the internal stores [52, 71, 81, 82, 86, 94, 145, 157, 264]. Measurement of intracellular Ca^{2+} levels has widely been done using Ca^{2+} indicator fluorescent dyes in live imaging system or plate reader [52, 71, 81, 82, 86, 94, 145, 157, 264].

For this approach TT cells which express CaSR, RAMP1 and 2 but not 3 endogenously (result and its discussion in appendix section 7.6, figure 7.8); as well as stably co-transfected COS-7 cells

were used. COS-7 cells were stably transfected with different combinations of CaSR+RAMP1/2/3 whose mRNA expression levels are shown in appendix section 7.5, figure 7.7.

Measuring intracellular Ca^{2+} release:

Measuring intracellular Ca^{2+} release using live cell imaging system allows the real-time visualization of the cell signalling and also checks for sufficient dye loading, cell viability and morphology. Fluo-4AM dye was used for all the experiments and the recipe for physiological salt solution used in this study, has been successfully used before [264]. The concentration of $CaCl_2$ was 1.5mM, which is less than Ec_{50} of Ca^{2+} for CaSR (3mM). Initially, plate reader with a dispensing system was used because compared to the live cell imaging system, it is relatively high-throughput, automated and the fluorescence from an entire well can be measured. Hence, it would give an average response of the entire cell population in the well (especially useful for transfected cells). However, technical problems associated with the machine prevented from getting useful and robust results and hence are not included in the thesis. Alternatively, live cell imaging using a fluorescent microscope was used.

Initial experimentation using live cell imaging system revealed that COS-7 cells stably transfected with CaSR+RAMP1/3 did not react to doses of Cinacalcet lower than 100µM (reported Ec_{50} ~51nM in transfected HEK-293 cells [86]), indicating an absence of specific dose dependent functional response (data not shown). It is noteworthy that the cells were always kept under selection antibiotic G418; and so it was hypothesised that cells machinery might be stressed to produce more antibiotic-resistant protein, compromising on the production of other proteins like CaSR and RAMPs. Also, it is noteworthy to mention that G418 belongs to the same family of antibiotics as the CaSR agonists- neomycin and gentamycin; and has a similar structure to gentamycin. 500µM gentamycin has shown to elicit responses in opossum kidney cells [81]. So, it can be hypothesised that the failure of cells to respond to Cinacalcet activation could be due to desensitization of CaSR under constant exposure to high doses of G418 in the medium (1.44mM or 721µM). Although other studies have used G418 for selection of HEK-293 or other cells stably transfected with CaSR, the doses used to maintain the cell lines were lower- 433µM [138, 265]; 300µM (upto 3 days prior to experiment) [266]. Some studies which used G418 for

selection of stable cells do not mention if they decreased the antibiotic concentration after initial round of selection or exclude it completely from the culture medium, days/hours before the experiment. Lowering the doses in the experiments and completely removing the antibiotic 24hr before experimentation did not produce any changes in the results.

Due to the above stated problems associated with stable COS-7 cells, TT cells were used for further experiments as they express the CaSR as well as RAMP1 and 2, but not 3 endogenously (appendix, section 7.6) and hence could provide insight into their interaction at endogenous expression levels in contrast to much higher expression levels in transfected cells.

Figures 4.3.9 and 4.3.10 show the presence of a functional CaSR expressed on TT cells and thus demonstrate that the technique used was sensitive to measuring changes in intracellular Ca^{2+} concentrations caused by increasing doses of Cinacalcet and Neomycin. The Ec_{50} recorded (500 ± 1.29 nM and 91 ± 1.45 µM respectively) are different from those reported in the literature for intracellular Ca^{2+} activation. In HEK-293 cells transfected with CaSR, an Ec_{50} of ~51nM was reported for Cinacalcet [86], whereas an Ec_{50} of ~41µM was recorded for neomycin [82]. The difference in cell-type and presumably higher receptor expression due to transfection could be one of the reasons for the differences in the potencies recorded. Another reason could be related to the fact that in both the studies a different dye-Fura-2AM (ratiometric dye) was used and the fluorescence was measured using different instruments (fluorescent plate reader [86] and an inverted fluorescence microscope [82] of a different make from the one used in this study). There are no studies yet showing a dose-response curve in TT cells for the same agonists, using intracellular Ca^{2+} release as a measure; so it is not possible to make exact comparisons. However, it was established in this study that the TT cells express a functional CaSR.

The effect of RAMP1 mRNA knock-down on CaSR signalling in TT cells:

It has been already shown by Bouschet *et al* using co-immunoprecipitation and immunofluorescence techniques [157]; and by the FRET results in this study that CaSR interacts with RAMP1 and 3 in over-expressing cells, an effect responsible for its cell-surface trafficking. However, there is no evidence showing this interaction in an endogenously expressing cell type.

Since TT cells express RAMP1 as the only RAMP partner of the CaSR; it was hypothesised that they interact in these cells and RAMP1 causes cell-surface trafficking of the receptor. Accordingly, RAMP1 mRNA expression was obstructed by siRNA to test for its effects on CaSR signalling. The sequences for siRNAs used have been published before by Bouschet *et al* [157]. The target specificity for RAMP1 siRNA, and an absence of homology with any known gene for the negative control siRNA were confirmed using BLAST search. mRNA knock-down ability of both the siRNAs used in this study have been successfully demonstrated and published by Bouschet *et al* [157] and were confirmed in this study as well (figure 4.3.11). Indeed as hypothesised, it was observed that in TT cells transiently transfected with RAMP1 siRNA, there was statistically significant reductions of CaSR signalling by Cinacalcet and Neomycin (figure 4.3.12 A & B respectively); compared to negative control siRNA transfected cells. The most likely explanation for these results is that the siRNA specifically inhibited the expression of RAMP1 (figure 4.3.11), due to which there were lesser numbers of interacting RAMP1 partners with CaSR, which subsequently resulted into relatively less CaSR+RAMP1 complex on the cell-surface. This was checked by measuring the response of the cells to CaSR specific agonists (figure 4.3.12). So, it is demonstrated for the first time that inhibition of RAMP1 expression leads to a decrease in CaSR signalling in TT cells, which probably indicates that they interact in TT cells and RAMP1 can be responsible for CaSR cell-surface trafficking.

In order to test this explanation, immuno-staining should be performed for CaSR on RAMP1 knocked-down TT cells to check for the localization of the receptor in the cell. If there is more CaSR trapped inside the cell (in the perinuclear region) as observed by Bouschet *et al* in transfected HEK-293 cells [157], then the explanation would hold true. Alternatively, co-immunoprecipitation studies should be performed using CaSR or RAMP1 antibody to pull-out the receptor complex, and then probing for the other component on a western blot. This should confirm that CaSR interacts specifically with RAMP1 in endogenously expressing TT cells. Attempts to co-immunoprecipitate CaSR and RAMP1 using TT cells during this study failed to generate robust results. Even the CaSR-transfected HEK-293 as a positive control [157] (since HEK-293 cells express RAMP1), failed to show positive results. Since, the results produced were not robust enough and also lacked the inclusion of a control IgG as a negative control; they are

not included in the thesis. Further optimization of the conditions is required to achieve good quality results.

Effect of RAMP1 blocking antibody on CaSR signalling:

Since TT cells only express RAMP1 and not 3, they are a good model to study the role of RAMP1 in CaSR signalling (appendix, section 7.6). Also, this study suggested an interaction between CaSR interacts with RAMP1 in TT cells, with an implication of RAMP1 being responsible for cell-surface trafficking of CaSR. So, it was hypothesised that blocking RAMP1 using specific antibody would modify signalling of CaSR; which will be measured by intracellular Ca^{2+} increases. Different RAMP1 polyclonal antibodies were tested for their effects on CaSR signalling. Of these, RAMP1 polyclonal Ab raised in mouse from Abcam caused the maximum attenuation followed by RAMP1 Ab raised goat from Santacruz biotech (figures 4.3.13 and 4.3.14 respectively). It was observed that although the RAMP1 Ab raised in rabbit caused significant attenuation of Cinacalcet response, the corresponding rabbit control IgG was non-specific and also caused attenuation similar to RAMP1 Ab (data not shown). So they were discontinued for use from future experiments. Control IgGs for the other two antibodies (mouse and goat) did not have an effect on CaSR signalling; indicating the absence of non-specific effects. Although the RAMP1 mouse Ab caused statistically significant attenuation of Cinacalcet response (figure 4.3.13); the experiment could not be repeated because the company discontinued the production of that antibody.

Accordingly, RAMP1 goat polyclonal Ab from Santacruz biotech was used for further experiments. The specificity of the Ab for RAMP1 was checked by western blotting for the protein using TT cell samples and performing immuno-cytochemistry on TT cells (appendix section 7.6, figure 7.8 C and G); which showed that the antibody could recognize both the linearized form (shown by western blotting) and natural conformation (shown by immuno-staining) of RAMP1. Subsequent treatment of TT cells, with RAMP1 Ab showed repeatable, dose-dependent and statistically significant attenuation of 1µM Cinacalcet response (figure 4.3.14). Thus, it is demonstrated for the first time that blocking RAMP1 attenuates CaSR

signalling in endogenously expressing cells indicating a possible role of RAMP1 in CaSR signalling.

A causative mechanism behind the observed effect could be a conformational change of the CaSR induced by the antibody. This could subsequently affect ligand binding or coupling to the G-proteins, which would result in attenuated signal transduction. There is no information so far about the involvement of RAMP1 in forming a part of ligand binding epitope with CaSR; contrary to the case with CLR where it is involved in the same [200] (section 1.13.2, chapter 1). However based on the current information, the binding sites for Ca^{2+} [108] (ECD), neomycin (ECD) [107] and the calcimimetic Cinacalcet (TM domain) [113, 116] have all been mapped on the CaSR itself (as discussed in detail in section 1.5 of chapter 1). So based on this information it seems improbable that the RAMP1 antibody binding inhibits the ligand binding directly by blocking the epitope, a part of which could be present on the RAMP1 itself. So, a change in conformation of the CaSR compromising the G-protein coupling could be proposed as the mechanism of action of RAMP1 Ab.

This hypothesis can primarily be tested by observing the change in FRET efficiency of CaSR+RAMP1 complex on the cell surface after treatment with RAMP1 antibody. If a change in FRET efficiency between CaSR and RAMP1 is observed, then it indicates a change in conformation of the receptor complex, which changed the distance and hence the efficiency of energy transfer between CaSR and RAMP1. Similar approaches have demonstrated the effects of antagonists and agonists on melatonin receptor; and monoclonal antibody on CCR5 receptor using Bioluminescence energy transfer (BRET) [267, 268].

The effect of RAMP1 antibody on CaSR signalling can be further confirmed by heterologous competition experiments in TT cells using increasing doses of RAMP1 Ab against a single dose of Cinacalcet; as well as dose-response curve shift assays studying the effect of a single dose of RAMP1 Ab on a dose-response of Cinacalcet. The effect of RAMP1 antibody on the binding kinetics of Cinacalcet can be tested using radioligand binding assay incorporating $GTP\gamma^{S}$ and compared to the effect of CaSR antagonist on Cinacalcet binding. These experiments would give further information on the action of the antibody by providing the binding affinity and

effectiveness in inhibiting CaSR signalling (Ic_{50}) of the antibody. It would be interesting to observe any change in binding affinities in presence/absence of $GTP\gamma^S$ (which should bring all the receptors to the basal state – R), as it would indicate conformational bias of the antibody (R*/R*G vs R; antagonists are not biased towards conformation of a receptor) and consequently give an estimate of the number of receptors actually affected by antibody binding.

The functional changes in the downstream of signalling caused by RAMP1 Ab can be studied by measuring the change in calcitonin secretion in the medium. As CaSR activation stimulates calcitonin secretion from TT cells [5], attenuation of its signalling by RAMP1 Ab would cause a decrease in calcitonin secretion. So, this would further confirm the effect observed by RAMP1 Ab on CaSR signalling.

Although there are no studies showing the effects of RAMP1 blocking antibody on the signalling of any of its GPCR partners, CGRP antagonist BIBN4096BS, which binds to the pocket formed by both CLR and RAMP1 residues, has been developed as an anti-migraine drug [200]. This competes for ligand (CGRP) binding and consequently reduces the signalling of CGRP [269, 270]. So, targeting RAMP1 has been shown to be successful for inhibition of receptor's activity, supporting the results in this study. CaSR antagonists are available that bind to their sites in the TM domain and inhibit the signalling of the receptor [94-96]. Consequently, the efficiencies of CaSR antagonist NPS 2390 and RAMP1 antibody in attenuating CaSR signalling were compared.

Comparison between the effects of RAMP1 antibody and NPS 2390 on CaSR signalling:

NPS 2390 is an inhibitor of CaSR [94] and other family C GPCRs like mGluR1 and mGluR5 [94, 271]. It has been shown to inhibit effects of CaSR in various cell types such as human adipocytes (20µM)[272]; mouse mesenglial cells (5µM, 10µM) [273]; rat liver cell line (10µM) [274]; osteosarcoma cells (1mM, 10mM) [275]. So, in order to compare the ability of RAMP1 Ab to a known CaSR antagonist in attenuating CaSR signalling, NPS 2390 was used. It was observed that 133nM RAMP1 antibody was more efficient than 10µM NPS 2390 and equally efficient as 50µM NPS 2390 in attenuating 1µM Cinacalcet response (Figure 4.3.15). It has been shown that calcimimetics and calcilytics bind to the same regions of the TM domain of CaSR at exclusive yet

some overlapping sites [115, 117]. So, it is possible that for NPS 2390 and Cinacalcet a competition for the same binding residues or pocket exists, requiring higher dose (50µM) of NPS 2390 to cause an immediate decrease in response to Cinacalcet. Another possibility is that Cinacalcet has a higher binding affinity than NPS 2390 for CaSR. On the other hand, RAMP1 Ab used was a polyclonal Ab which can bind to different binding sites on the ECD of RAMP1 and hence does not compete with NPS 2390; and may even have higher affinity for binding.

Interestingly, differential effects were observed for the attenuation of Ca^{2+} and neomycin signalling by RAMP1 Ab vs NPS 2390. It was observed that 100µM neomycin response was statistically significantly attenuated by RAMP1 Ab (46%), 10µM NPS 2390 (44%) and 50µM NPS 2390 (65%) (figure 4.3.16). On the other hand, 133.3nM RAMP1 Ab and 10µM NPS 2390 did not cause any attenuation of 5mM $CaCl_2$ signalling, whereas 50µM NPS 2390 caused ~42% decrease (figure 4.3.17). These different effects observed, might suggest a possible change in conformation of CaSR caused by RAMP1 Ab binding that inhibits efficient binding of neomycin, but not Ca^{2+}; probably because Ca^{2+} has multiple binding sites on the CaSR ECD [108]. The effects of decreasing the dose of Ca^{2+} or increasing the dose of RAMP1 Ab remain to be tested.

It is also interesting to note that NPS 2390 showed differential effects on neomycin and Cinacalcet (10µM caused attenuation of neomycin signalling but not Cinacalcet: figures 4.3.15 and 4.3.16); whereas RAMP1 Ab caused equal attenuation for both agonists (~46% Cinacalcet and ~48% Neomycin). As already mentioned before, there might be competition for binding or differences in binding affinities (not reported yet) between Cinacalcet and NPS 2390 on the TM domain of the CaSR. Whereas, since neomycin binds to the N-terminal region of CaSR, it probably doesn't compete with NPS 2390 and so 10µM NPS 2390 could cause significant attenuation of neomycin. On the other hand, RAMP1 Ab which is polyclonal, can bind to different sites and too not on the CaSR; hence precluding any competition for binding with the agonists. Taken together, the attenuation of CaSR response to specific agonists Cinacalcet and neomycin by RAMP1 Ab shows that RAMP1 plays a role in signalling of CaSR in TT cells and could probably be more effective than NPS 2390.

In order to test whether a combined treatment consisting of RAMP1 Ab and NPS 2390 together would produce a greater inhibitory effect than either of the treatments alone; TT cells were pre-treated with 10µg RAMP1 Gt poly Ab together with 10µM NPS 2390 (appendix section 7.7, figure 7.9). Although it appeared that the combined treatment had a greater inhibitory effect on 100µM neomycin signalling, it was discovered to be caused by non-specific effect of DMSO (solvent for NPS 2390). Accordingly, when the RAMP1 antibody was incubated with 0.1 or 0.5% DMSO (corresponding to the v/v addition of NPS 2390 stock into buffer to prepare desired concentration) as a vehicle control, similar attenuation of 100µM neomycin signalling was observed. It has been reported that DMSO at concentrations between 0.1-5% can cause protein denaturation, aggregation, or degradation; thus changing the properties of protein in the solution [276]. DMSO can also change apparent binding properties of the protein [276]. The effect of DMSO on the binding affinity for antibody was demonstrated using column chromatography experiments, where buffers with low DMSO content (2%) resulted in irreversible binding of the antibody; whereas buffers with high DMSO content (30%) destroyed the antibody interaction [277]. These evidences support our observation of a non-specific effect of DMSO by modulating RAMP1 Ab activity. As a result of this, successful combinatorial treatments with RAMP1 Ab were not possible using NPS 2390 dissolved in DMSO.

Since there were technical issues regarding the use of DMSO, ethanol or cyclodextrin could be used as a solvent for dissolving the compound. Also in future, specific CaSR antagonists, like SB-423557 [96], compound 7h and 11m, JTT-305 [97, 98] could be used instead for both comparative and combined effect in attenuating CaSR signalling with RAMP1 Ab. This would be interesting to study and might provide a new insight into development of calcilytics.

Limitations:

In this study the activity of RAMP1 antibodies were compared to a small molecule antagonist in inhibiting the activity of the CaSR. However, it should be noted that there are two epitope-binding sites per antibody compared to one for a small molecule. So, the comparison may not be equal. Also, since polyclonal antibodies raised against RAMP1 were used, there was a mixed population of antibodies having varying pharmacological profiles and binding sites. Antibodies

have been used in GPCR studies [268, 278], but usually monoclonal Abs are preferred as they have a known binding site; and being clonal, have same binding characteristics such as affinity and avidity. On the other hand, the binding affinity and avidity of the RAMP1 polyclonal antibodies was not characterised and hence their pharmacological profile is unknown. Due to these reasons care should be taken in interpreting the data for comparing RAMP1 polyclonal antibody activity to the inhibitory action of NPS 2390, as it is not an equal comparison. However, they do support and strengthen the observation that RAMP1 plays an inhibitory role in CaSR signalling. In future, monoclonal antibodies or single chain variable fragments against RAMP1 should be used. In addition to this, a final concentration of 1µM Cinacalcet used in the experiments is a higher dose of the compound. So, there is a possibility that it could lead to non-specific effects, which were not addressed in this study. However, in a study by Davey *et al* [279], 1µM Cinacalcet in presence of increasing concentration of extracellular Ca^{2+} (0-3mM) was successfully used to study CaSR signalling. Nevertheless, in future, lower doses should be used and as suggested earlier the effect of RAMP1 Ab on Cinacalcet dose-response should be tested in this context.

Conclusions:

The study reports a novel discovery using an endogenous expression system of TT cells, which showed that inhibiting RAMP1 expression using siRNA reduced CaSR signalling, indicating an interaction between the two that is responsible for the cell-surface expression of the CaSR. Moreover, it was demonstrated that blocking RAMP1 by Ab caused attenuation of Cinacalcet and Neomycin-mediated signalling of the CaSR. These results provide the first evidence for a potential role of RAMPs in CaSR signalling. It was also observed that the RAMP1 Ab attenuated Cinacalcet and neomycin-mediated signalling at a lower dose, when compared to NPS 2390. This might suggest that RAMP1 Ab could be more efficacious than NPS 2390 in inhibiting CaSR signalling, although care should be taken while interpreting this data (as discussed above). It was also demonstrated that antibody-capture SPA could not be used to measure specific G-protein activation of CaSR+RAMP1/3 combinations, due to unwanted non-specific effects of Ca^{2+}, gadolinium and neomycin on G-protein activation and consequently the technique probably needs further optimization in the sense of higher receptor expression levels.

CHAPTER 5: GENE EXPRESSION ANALYSIS OF CaSR AND RAMPs UPON INTERVENTION BY THE AGENTS OF Ca^{2+} HOMEOSTASIS.

5.1. Introduction:

CaSR is an essential cell surface receptor involved in Ca^{2+} homeostasis, where it plays important roles of sensing minute changes in extracellular Ca^{2+} concentrations to regulate PTH secretion as well as sensing Ca^{2+} in bone microenvironment to modulate the activity of bone cells. Accordingly, its abnormal expression is related to the pathophysiological conditions of Ca^{2+} homeostasis, as discussed in detail below. Since, RAMPs 1 and 3 are required for cell-surface trafficking of the CaSR [157] (and section 3.3.3, chapter 3), it is important to study whether RAMP expression is modulated by agents of Ca^{2+} homeostasis, as this could affect the cell-surface expression and hence population of the CaSR. This could provide more information on the nature of the physiological interaction of CaSR and RAMPs as well as indicate a role of RAMPs in Ca^{2+} homeostasis.

The following sections give a brief background on regulation of CaSR and RAMP expression in physiology, based on existing information from the literature:

5.1.1: Regulation of CaSR expression:

CaSR gene is located on chromosome 3 (3q21-q24) in humans [280]. It contains seven exons [281]-six of which encode the ECD and its upstream untranslated regions, while a single exon codes for the TMDs and C-tail [55, 281]. Studies have demonstrated that regulation of CaSR expression occurs under a variety of circumstances, although the mechanisms responsible are not well understood.

In primary parathyroid cell culture from bovine parathyroid gland, reduced sensitivity to extracellular Ca^{2+} with progression of days in culture was observed [282, 283]. This reduced sensitivity has been associated with a marked and rapid decrease in CaSR expression. It has been reported that CaSR mRNA and protein expression decreased by 70% within 4hr and 85% within 24hr in parathyroid cell suspensions; and by 75% within 24hr in monolayer cultures, which was not recoverable at later time points [283]. The decrease in CaSR expression was also not sensitive to changes in media serum, Ca^{2+} and 1,25-dihydroxyvitamin D_3 concentration [283]. However, it is interesting to note that, bovine parathyroid cells when grown in collagen coalesce into an organoid ("pseudogland") with stable Ca^{2+} responsiveness, where the initial

drop in expression of CaSR after 24hr is recovered significantly compared to no recovery in monolayer cultures as mentioned above; thus illustrating the importance of 3D cellular architecture in parathyroid gland function [284].

Ca^{2+} is the key component in mediating the function of CaSR for regulating PTH secretion and enabling divalent ion excretion. Therefore, extracellular Ca^{2+} has been widely hypothesised to be potentially an important regulator of CaSR gene expression in physiology. However, studies have failed to demonstrate an effect of extracellular Ca^{2+} on CaSR mRNA expression in the rat parathyroid cells and osteoblasts *in vitro* [285] and parathyroid and kidney CaSR mRNA expression *in vivo* [286, 287]. In view of that, it has been hypothesised that, since CaSR acts as a sensitive calciostat in these tissues, a change in CaSR synthesis corresponding to changes in extracellular Ca^{2+} could have unwanted effects on Ca^{2+} homeostasis [288].

Another important component of Ca^{2+} homeostasis is the active form of vitamin D_3- calcitriol. Interaction between 1,25-dihydroxyvitaminD_3 and CaSR expression has been well demonstrated by different studies. Primary rat parathyroid cell *in vitro* cultures and *in vivo* mRNA expression studies in rat thyroid and kidney, have reported an increase in CaSR mRNA expression by ~2 fold upon treatment with 1,25-dihydroxyvitamin D_3 [285, 286]. Also, in the medullary thyroid cell line TT and the kidney proximal tubule cells (HKC), CaSR gene transcription increased ~2-fold at 8 and 12 h after 1,25-dihydroxyvitamin D_3 treatment [288]. The same study further identified the presence of functional 1,25-dihydroxyvitamin D_3 response elements in both promoters -P1 and P2 of the human CaSR gene, thus uncovering the mechanism behind the observed effect [288]. The relevance of this effect was speculated on a physiological level by the authors at different sites of Ca^{2+} homeostasis. Accordingly, an increase in CaSR expression in parathyroid and kidneys by 1,25-dihydroxyvitamin D_3 could increase the sensitivity of the organ to detect extracellular Ca^{2+} and to reduce PTH secretion and facilitate divalent ion excretion respectively [288]. This would work as an auto regulatory feed-back loop as an initial increase in the systemic PTH levels due to release from parathyroid, would facilitate vitamin D_3 maturation in the kidneys, which would consequently inhibit PTH secretion.

There is also evidence in the literature showing that in chronic kidney disease patients suffering from secondary hyperparathyroidism, decreased CaSR expression is associated with an increase in the set-point for Ca^{2+} sensing and consequently increased PTH secretion [289, 290]. In these patients hyperplasticity of parathyroid gland is observed and the resulting proliferation of parathyroid cells is associated with decreasing CaSR expression [289]. A study using calcimimetic NPS R-568 (which increases the sensitivity of CaSR to Ca^{2+}), successfully reversed the reduced parathyroid CaSR expression without any changes in vitamin D levels and decreased parathyroid cell proliferation in experimental rat models of chronic kidney disease suffering from hyperparathyroidism at 8 weeks from nephrectomy [291]. This confirms the above stated observations of association of reduced CaSR expression to this pathology.

Regulation of CaSR expression is also observed during foetal development. Significant developmental increases in CaSR expression in kidney [292] and brain [293] of the rat have been observed. It has been reported that in rats, the perinatal expression of CaSR was very low; whereas it increased immediately postnatally during the first week and stayed constant after postnatal day 14 through to adulthood [292]. This regulation is thought to be related to changes in renal handling of divalent ions and water from perinatal to post-natal conditions [292]. On the other hand, in the rat brain, CaSR was expressed at low levels until 5 days postnatally, then increasing markedly at 10^{th} day until 30 days, when it gradually decreased by 3-fold to reach the adult level of expression [293].

Hypocalcaemia related with the increased proinflammatory cytokine levels in critically ill patients has been associated with altered CaSR expression [294, 295]. It was shown *in vivo* in the rat parathyroid, thyroid and kidney; and *in vitro* in TT and kidney proximal tubule (HKC) cells, that the CaSR mRNA and protein expression increased after injection of interleukin-1β. This was associated with decreased circulating parathyroid hormone, Ca^{2+}, and 1,25-dihydroxyvitamin D_3 levels. The mechanism behind this effect was uncovered by the discovery of functional elements in CaSR promoter that mediate its upregulation [294].

So taken together, altered CaSR expression has been associated to different conditions such as harmful pathological effects and even organ development.

5.1.2: RAMP gene regulation:

In humans, the gene for RAMP1 is present on chromosome 2 (2q36-q37.1), RAMP2 on chromosome 17 (17q12-q21.1) and RAMP3 on chromosome 7 (7p13-p12) [296]. RAMPs are essential for the CGRP, AM, and AMY receptor functioning, and so it is implicative that changes in RAMP expression due to pathological conditions would influence the expression of these receptors and consequently the sensitivity of cells and tissues to CGRP, AM, and AMY; in addition to any drugs that may be targeted to a specific RAMP/receptor complex.

Studies using disease models have demonstrated that pathologies related to the hormones of calcitonin peptide family are associated with regulation of RAMP expression. Since AM and CGRP are vasodilators, cardiac pathology has been shown to alter RAMP expression, consequently altering the functioning/signalling of these hormones. In a rat model of chronic cardiac failure induced by aortic stenosis, it was observed that RAMP1 and 3 mRNA and protein expression levels were upregulated after 6 months of surgery, whereas RAMP2 expression was unchanged [297]. This upregulation is speculated to support the protective role of CGRP and AM during heart failure. In addition to myocardial infarction, RAMP regulation is also modified in the cases of hypertension. In rat malignant models of hypertension induced using hypertensive aldosterone precursor (deoxycorticosterone acetate) loading, as well as salt loading, it was observed that after 3 weeks of loading, RAMP2, RAMP3 and CLR mRNA expression levels were upregulated in the left-ventricle, with increased AM levels in circulation [298]. Similar results were observed in a spontaneously hypertensive rat model in a different study where they also observed increased RAMP1 expression levels in heart in addition to the components of AM receptors [299]. So, the AM and CGRP functioning in these cardiovascular pathologies has been related to altered RAMP expression.

RAMP expression is also modulated in kidneys, which is not only a site of action of adrenomedullin, but also a major site of Ca^{2+} homeostasis. However, studies have only demonstrated the change in expression of RAMPs in terms of the actions of adrenomedullin or CGRP. The models of hypertension induced using aldosterone precursor (deoxycorticosterone acetate) loading, as well as salt loading; demonstrated increased RAMP1, 2 and 3 expression in kidneys along with increased AM levels; indicating a role of AM in maintaining water/ion

balance and counteracting hypertension via its hypotensive, natriuretic and diuretic functions [300, 301]. RAMP1 and 3 mRNA expression was also upregulated in rat kidneys with obstructive nephropathy (kidney failure [183]. Since AM has protective role in kidney it has been hypothesised that upregulation of RAMPs may favour this protective effect against fibrotic changes or proliferative effect during obstructive nephropathy [183]. There are no studies till date studying RAMP expression regulation by any agents involved in Ca^{2+} homeostasis in the kidneys.

There is further evidence of RAMP expression regulation at sites of action of calcitonin family of peptides such as lungs. In lungs, AM is responsible for pulmonary circulation mainly through AM1 receptor [214]. However, in case of lung sepsis induced by LPS in mouse, RAMP2 and CLR mRNA expression was down-regulated, whereas RAMP3 mRNA expression was upregulated. Accordingly, it is revealed that the distributions of receptor or binding sites of AM are changed in sepsis, and it is suggested that AM plays distinct roles in the clinical course of this syndrome [214]. This also points to a pathological role of RAMP3 mediated receptor signalling. As in case of hypoxic rat lungs, RAMP1 and RAMP3 mRNA were upregulated without any change in RAMP2 and CLR expression, again indicating a change in AM receptor distribution [302].

Regulation of RAMP expression by other steroids (in addition to aldosterone as mentioned above) is also studied in context to the role of adrenomedullin and CGRP in conditions like pregnancy [303, 304]. RAMPs are regulated by oestrogen and progesterone, where oestrogen downregulates the expression of RAMPs in rat uterus, whereas progesterone upregulates their expression [303, 304]. It has been demonstrated using mouse uterine cDNA that oestrogen responsive element (ERE) motif is found in the 1^{st} intron of RAMP3 gene where the activated oestrogen receptor binds and regulates the transcription of these genes [305]. Since estradiol is increased at time of labour, it is speculated that it probably counters vasoldilatory effects of CGRP and AM in order to prevent blood loss during delivery [303, 304]. Glucocorticoids like dexamethasone which is used as an anti-inflammatory or immunosuppressant agent also affects RAMP expression. It is reported that dexamethasone treatment on mouse primary osteoblasts down-regulated the expression of CLR and increased the expression of RAMP1 and

RAMP2 both at mRNA and protein levels [306]. Since it is known that AM stimulates osteoblastic proliferation and promotes bone growth both *in vitro* and *in vivo* [307], dexamethasone might prevent its effect by altering AM receptor level.

Although caution must be applied when extrapolating to protein expression using mRNA expression levels alone as shown by a lot of studies mentioned above, the data definitely demonstrates regulation of RAMP expression physiologically in context to the functions of the calcitonin family of peptides. However, there are no studies so far demonstrating the changes in RAMP expression by agents of Ca^{2+} homeostasis.

5.1.3: Hypothesis and aims:

It was hypothesised that RAMP mRNA is differentially regulated in human medullary thyroid carcinoma and human osteosarcoma cell line by agents involved in Ca^{2+} homeostasis.

The specific aims were:

- To measure the effect of extracellular Ca^{2+} and 1,25-dihyroxyvitamin D_3 on the expression levels of CaSR and RAMPs in the TT cell line (medullary thyroid carcinoma cell line).
- To measure the changes in the expression levels of CaSR and RAMPs in MG63, SAOS-2 and TE85 osteosarcoma cell lines upon treatment with extracellular Ca^{2+}.
- To measure the effect of differentiation of osteosarcoma cell lines into mature osteoblasts on the expression levels of CaSR and RAMPs.

5.2. Materials and Methods

5.2.1. Culture of TT and osteosarcoma cell lines:

TT, MG63, SAOS-2 and TE85 cell lines were cultured under normal conditions as described in section 2.1 and 2.2 of chapter 2.

5.2.2. Treatment of TT cells:

TT, MG63, SAOS-2 and TE85 cells were cultured under normal conditions and grown until 60-70% confluency in T-25cm^2 flasks (Nunclon, Thermo scientific). TT cells were then treated with different compounds (10mM $CaCl_2$ (pH 7.4) or 1µM 1,25-dihydroxyvitamin D_3 (Sigma Aldrich)) dissolved in F-12K complete medium. Osteosarcoma cells were treated with 30mM $CaCl_2$ (pH 7.4) dissolved in complete DMEM medium. In the untreated controls flasks, fresh medium was replaced instead. The treated and untreated cells were harvested in Trizol reagent using a cell scraper, following two washes with sterile-PBS at each time point:

For TT- 0hr, 5min, 15min, 30min, 1hr, 2hr, 5hr, 24hr and 48hr and

For osteosarcoma cells- 0hr, 1hr, 2hr, 5hr, 12hr, 24hr and 48hr

The harvested samples were stored in a sterile 1.5ml tube and snap frozen using liquid nitrogen and kept at -80°C until use.

5.2.3. Differentiation of osteosarcoma cell lines into mature osteoblasts:

Osteosarcoma cell lines were cultured under normal conditions in 6cm^2 peri-dishes (Iwaki) until the dishes reach confluency as described in section 2.1 of chapter 2, following which they were treated with differentiation medium (recipe in appendix) for 21 days. Fresh differentiation medium was replaced twice-a-week. Treated and untreated cells were harvested in Trizol reagent using a cell scraper at each time point (0hr, day 5, day 10, day 15, day 21) in a sterile 1.5ml tube and snap frozen using liquid nitrogen.

5.2.4. Gene expression analysis:

In order to study the change in gene expression of CaSR and RAMPs in TT and osteosarcoma cells by various interventions, real time PCR was used. RNA was extracted from TT cells using Trizol reagent as described in section 2.4 of chapter 2 and cDNA was synthesized using 2µg of RNA using high capacity RNA-to-cDNA kit as described in section 2.6 of chapter 2.

Real time PCR was performed using Taqman® probes to measure CaSR and RAMPs mRNA expression using ΔC_t analysis as described in section 2.9 of chapter 2. According to the ABi manual, a Ct value of more than 35 could be inaccurate and so the limit for analysis for this study was restricted to the Ct value of 34.

Validation experiments for real-time PCR:

For validation experiments checking the efficiency of the PCR reaction, pcDNA 3.1 RAMP/CaSR vectors were used containing cDNA of the gene. 6 dilutions were prepared with 10-fold difference in concentrations and were run in the PCR reaction as described in section 2.9 of chapter 2. The C_t values were plotted on a graph using GraphPad Prism version 5.00 for Windows (GraphPad Software, San Diego California USA, www.graphpad.com) and regression analysis was performed to obtain the R^2 value and the value of the slope.

In order to validate the relative expression analysis, the equal amplifying efficiencies of the primers for the genes of interest and house-keeping gene were tested as shown in [308]. For this, cDNA sample of TT cells was used. Dilutions of the cDNA were prepared as -[(µg of input RNA): 1, 0.5, 0.2, 0.1 0.05, 0.02, 0.01.] and the reaction was carried out as mentioned in section 2.9 of chapter 2 for 40 cycles. The ΔC_t value was calculated (Ct_{gene}-$Ct_{\beta\text{-actin}}$) and plotted on a graph using GraphPad Prism version 5.00 for Windows (GraphPad Software, San Diego California USA, www.graphpad.com) against its respective cDNA dilution and linear regression analysis was performed to obtain the value of the slope.

5.3. Results

5.3.1. . Validation of efficiency of CaSR, RAMP1, 2 and 3 TaqMan® probes in PCR reaction and their usage for relative quantification method:

To check the efficiency of the TaqMan® probes to amplify their respective targets in the PCR reaction, pcDNA 3.1 vectors containing the gene of interest were used as a positive control. Accordingly, serial dilutions of pcDNA 3.1 CaSR and pcDNA 3.1 RAMP vectors were prepared and real time PCR was performed. Figure 5.3.1 shows graph plotted for Ct values against cDNA concentrations and the goodness of fit was analysed by linear regression analysis calculating the R^2 values of 0.99 for CaSR (Figure 5.3.1 A), 0.98 for RAMP1 (Figure 5.3.1 B), 0.98 for RAMP2 (Figure 5.3.1 C) and 0.95 for RAMP3 (Figure 5.3.1 D). The slopes of the standard curves were approximately -2.7, -3.0, -3.3 and -3.5 for CaSR, RAMP1, RAMP2 and RAMP3 respectively.

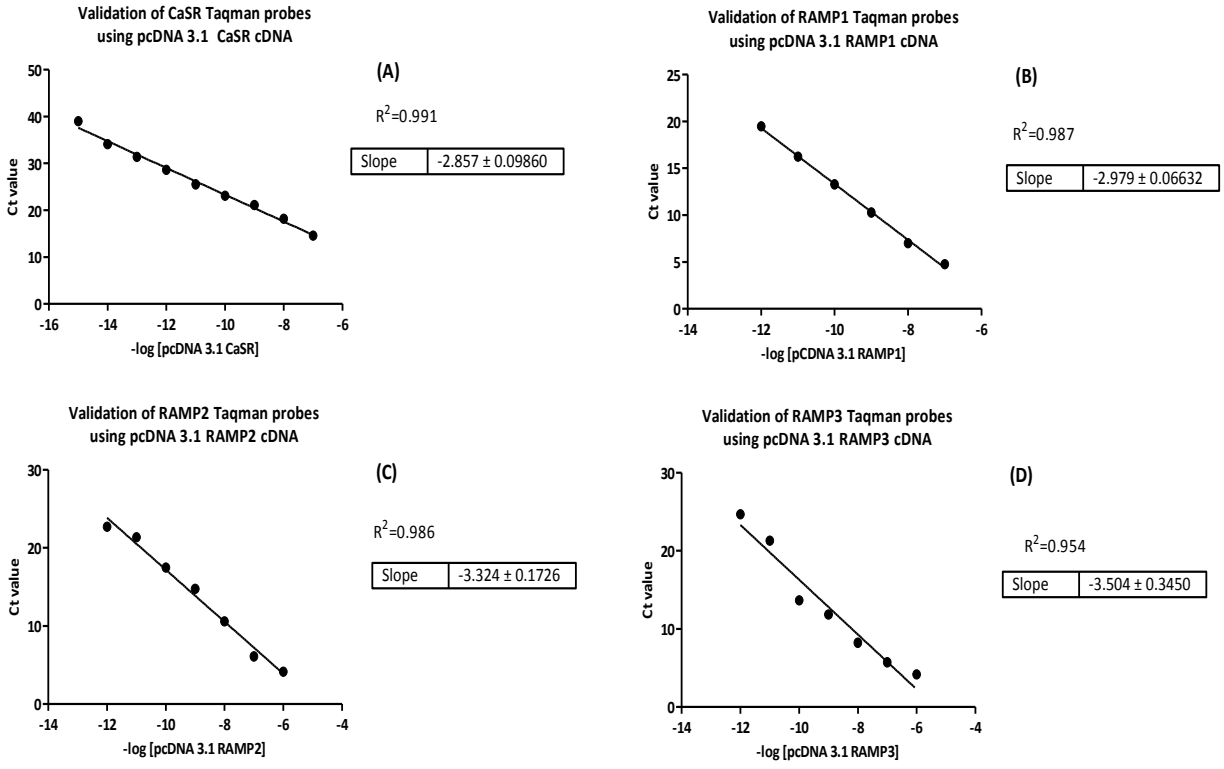

Figure 5.3.1: Validation of TaqMan® probes using serial dilutions of pcDNA 3.1 CaSR and pcDNA 3.1 RAMP vectors:

Serial dilutions from 1fg to 1µg of TOPO CaSR and 1pg to 1µg for pcDNA 3.1 RAMP vector DNA were prepared and real-time PCR was performed. The graphs show linear regression analysis for pcDNA 3.1 CaSR (A), pcDNA 3.1 RAMP1 (B), pcDNA 3.1 RAMP2 (C) and pcDNA 3.1 RAMP3 (D).

For all experiments, Actβ and HPRT1 were used as house-keeping genes. The expression of Actβ was less variable by different treatments in experiments compared to HPRT1 (Appendix section 7.8, figure 7.10) and so was used as an endogenous control gene to normalize the expression of genes of interest. To validate the use of TaqMan® probes for relative quantification method, the efficiencies of all TaqMan® probes were tested using a serial dilution of TT cell cDNA. Figure 5.3.2 shows graphs with the ΔC_t values normalized to Actβ on the Y-axis, plotted against the cDNA dilutions on the X-axis. The value of the slope for CaSR TaqMan® probe was ~0.03 (Figure 5.3.2 A), RAMP1 TaqMan® probe was ~0.078 (Figure 5.3.2 B) and RAMP2 was ~0.072 (Figure 5.3.2 C); all of which are within the acceptable limit of <0.1 as mentioned in the user's manual of ABI. RAMP3 was not detected at any concentrations within 40 cycles.

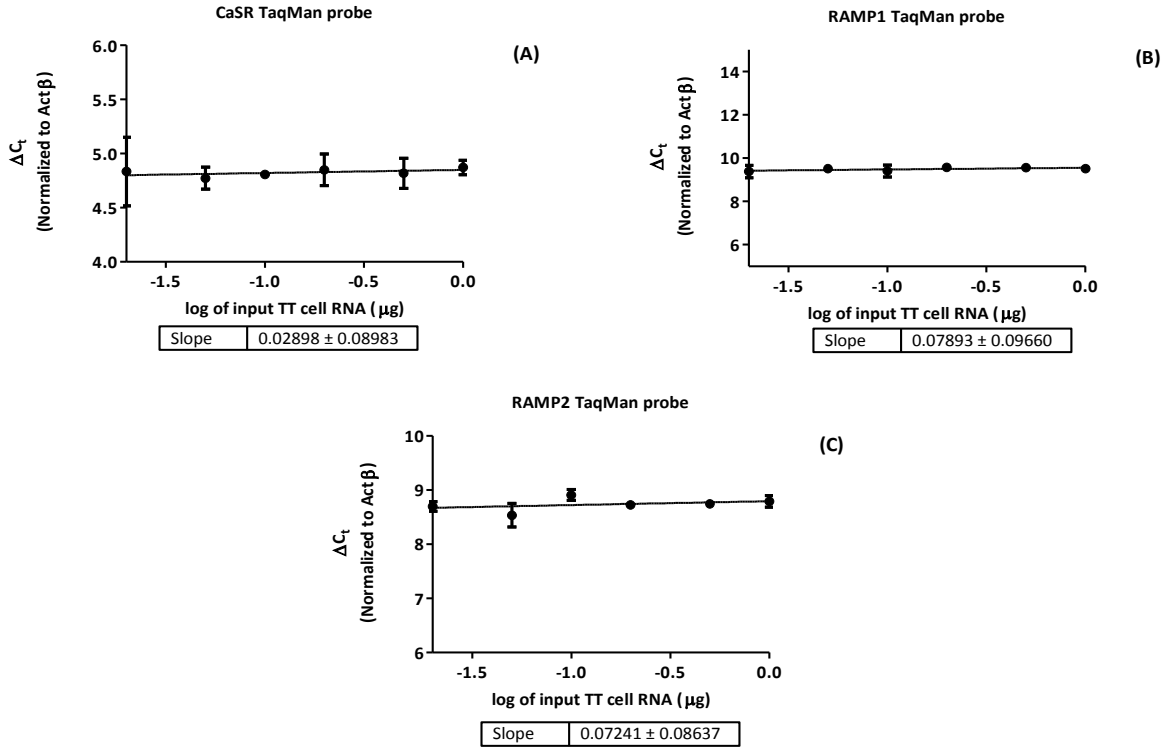

Figure 5.3.2: Validation of the TaqMan® probes for the usage of relative quantification method
TT cell cDNA was prepared using 1µg of total RNA and then serially diluted to achieve the concentrations (µg)- 0.5, 0.2, 0.1, 0.05 0.02, 0.01. ΔC_t for each gene was calculated by normalizing against Actβ for respective concentration of cDNA. The slopes for (A) CaSR (B) RAMP1 and (C) RAMP2 are shown.

5.3.2. Measuring the effect of 10mM $CaCl_2$ on mRNA expression levels of CaSR and RAMPs in TT cells at different time points using real-time PCR:

Different interventions were used to study the change in CaSR and RAMP mRNA expression in TT cells. The first intervention used was 10mM $CaCl_2$ and a time-course study was done to measure the consequent changes in mRNA expression levels of CaSR and RAMP by TaqMan® probes using real time PCR. In figure 5.3.3 mRNA expression levels of CaSR (A), RAMP1 (B) and RAMP2 (C) are shown in control (white bars) and treated samples (blue bars) at different time points as fold change to the expression of Actβ as the mRNA expression of each gene was normalized to the expression of Actβ. There was no statistical significant change of CaSR (figure 5.3.3 A), RAMP1 (figure 5.3.3 B) and RAMP2 (figure 5.3.3 C) in TT cells treated with 10mM $CaCl_2$ compared to untreated cells as analysed using 2-way ANOVA and Bonferroni post-test. The expression of RAMP3 mRNA could not be determined by the given TaqMan® probes in these cells and within 40 cycles in either group (control or treatment).

The average ± SD C_t values for CaSR were 23.90 ± 1.05 (control) and 23.9 ± 1.21 (treated), for RAMP1 were 26.59 ± 1.08 (control) and 26.63 ± 0.87 (treated) and for RAMP2 were 27.48 ± 1.19 (control) and 27.46 ± 1.41 (treated). So, amongst the measured genes in TT cells; the average normalized expression (to Actβ) was highest for CaSR, followed by RAMP1 (~8.5 fold lower than CaSR) and then RAMP2 (~14 fold lower than CaSR and ~ 1.7 fold less than RAMP1) (as measured at 0min time point).

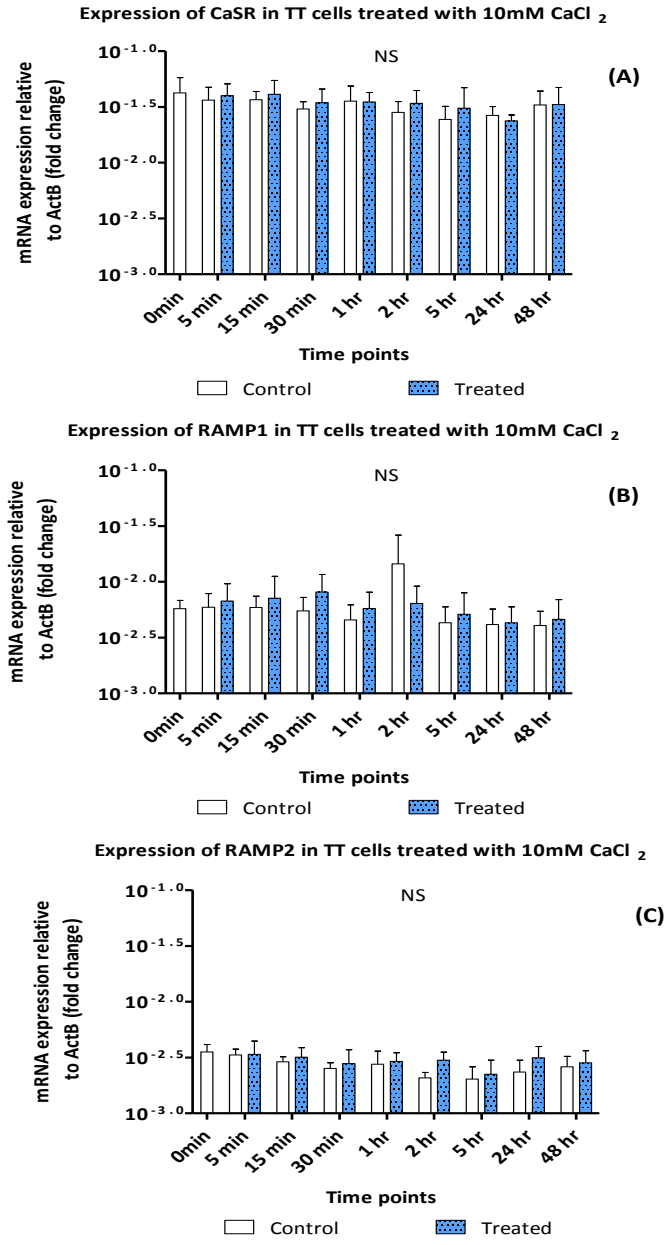

Figure 5.3.3: mRNA expression profile of CaSR and RAMPs in TT cells treated with 10mM $CaCl_2$ at different time points measured using real time PCR:

TT cells were cultured normally to 60-70% confluency and then treated with 10mM $CaCl_2$ for the given time points. mRNA expression levels were determined using real-time PCR using TaqMan® probes. The graph shows expression levels of CaSR (A), RAMP1 (B) and RAMP2 (C) at different time points for untreated (white bars) and treated (blue bars) samples; relative to expression of Actβ. The graph shows combined data from three independent experiments. Statistical test performed was 2-way ANOVA, Bonferroni post-test. NS = differences are not statistically significant.

5.3.3. Measuring the effect of 1μM 1,25-dihydroxyvitamin D3 on mRNA expression levels of CaSR and RAMPs in TT cells at different time points using real time PCR:

Treating TT cells with 1μM 1,25-dihydroxyvitamin D_3 (blue bars, figure 5.3.4) did not cause a statistically significant change in the expression of CaSR, RAMP1 or RAMP2 compared to untreated control (white bars, figure 5.3.4) as detected using TaqMan® probes in real time PCR, shown in Figure 5.3.4 A,B and C respectively and as analysed using 2-way ANOVA and Bonferroni post-test. The mRNA expression of each gene was normalized to the expression of Actβ and is shown in the graph as fold change to the expression of Actβ. Expression of RAMP3 was not detected using the given TaqMan® probes within 40 cycles; even upon treatment.

The average ± SD Ct values were 23.21 ± 0.96 (control) and 23.37 ± 0.95 (treated) for CaSR, 26.61 ± 0.90 (control) and 26.54 ± 0.94 (treated) for RAMP1 and 27.24 ± 0.46 (control) and 27.37 ± 0.49 (treated) for RAMP2. Accordingly, the average normalized expression levels of the genes in descending order were same as mentioned in section 5.3.2.

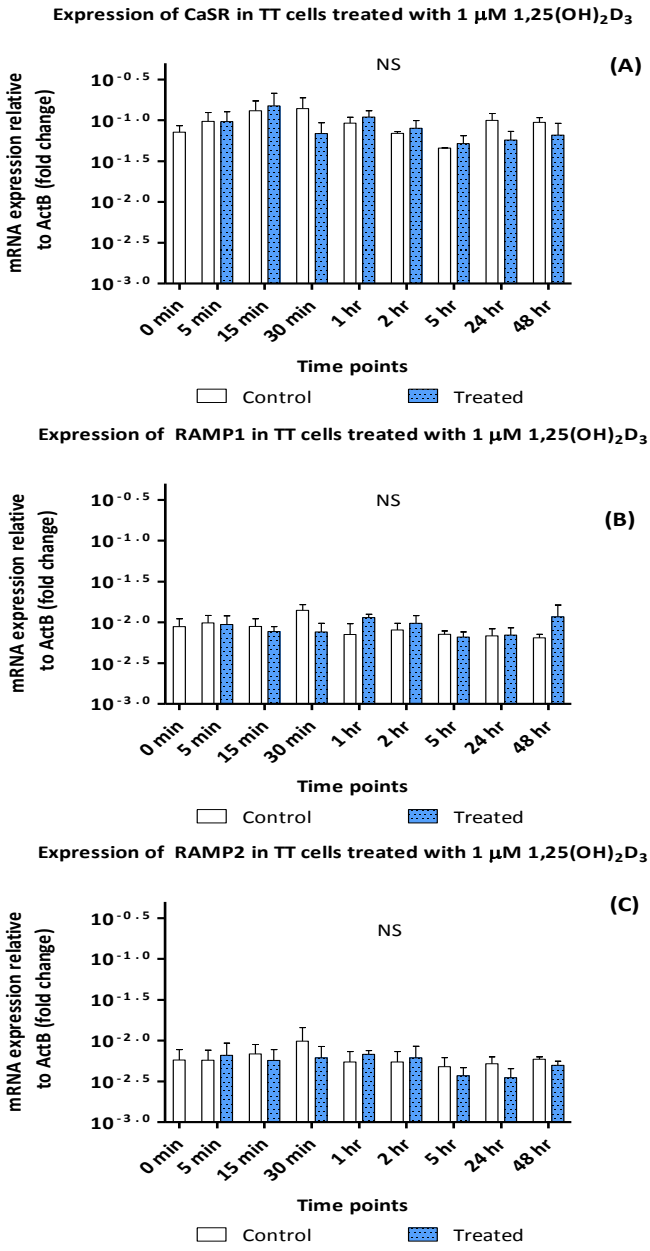

Figure 5.3.4: mRNA expression profile of CaSR and RAMPs in TT cells treated with 1µM 1,25-dihydroxyvitamin D_3 at different time points measured using real time PCR

TT cells were cultured normally to 60-70% confluency and then treated with 1µM 1,25-dihyrodxyvitamin D_3 for the given time points. mRNA expression levels were determined using real-time PCR using TaqMan® probes. The graph shows expression levels of CaSR (A), RAMP1 (B) and RAMP2 (C) at different time points for untreated (white bars) and treated (blue bars) samples, relative to expression at Actβ. The graph shows combined data from three independent experiments. Statistical test performed was 2-way ANOVA, Bonferroni post-test. NS = differences are statistically non-significant.

5.3.4. Measuring the changes in gene expression of CaSR and RAMPs by 30mM $CaCl_2$ in MG63, SAOS-2 and TE85 osteosarcoma cell lines using real time PCR:

To study the effect of high concentrations of extracellular Ca^{2+} on the gene expression of CaSR and RAMPs, three osteosarcoma cell lines were used: MG63, SAOS-2 and TE85.

MG63 cells were treated with 30mM $CaCl_2$ for different time lengths up to 48hr. The mRNA expression levels for RAMP1 and 2 are shown in figure 5.3.5 A and B respectively; quantified using TaqMan® probes in real time PCR for control (white bars) and treated (blue bars) samples. The levels of mRNA expression of these genes were normalized to the expression of Actβ and are expressed on the graph as fold change to the expression of Actβ. The mRNA expression of RAMP1 and 2 were not altered statistically significantly by 30mM $CaCl_2$ treatment at any given time point when compared to untreated samples (2-way ANOVA, Bonferroni post-test). Although the expression of RAMP1 at 1hr in treated group (blue bar, figure 5.3.5 A) was ~3.2 fold higher than in untreated group, the difference was not statistically significant as analysed by 2-way ANOVA and Bonferroni post-test. mRNA expression levels of CaSR and RAMP3 were not detected using the given TaqMan® probes, within 40 cycles.

The average ± SD Ct values were 27.31 ± 0.8 (control) and 27.51 ± 0.73 (treated) for RAMP1, 31.9 ± 0.85 (control) and 32.4 ± 0.99 (treated) for RAMP2. Accordingly, the average expression of RAMP1 was ~16 fold higher than RAMP2 after normalization with Actβ (as measured at 0hr time point).

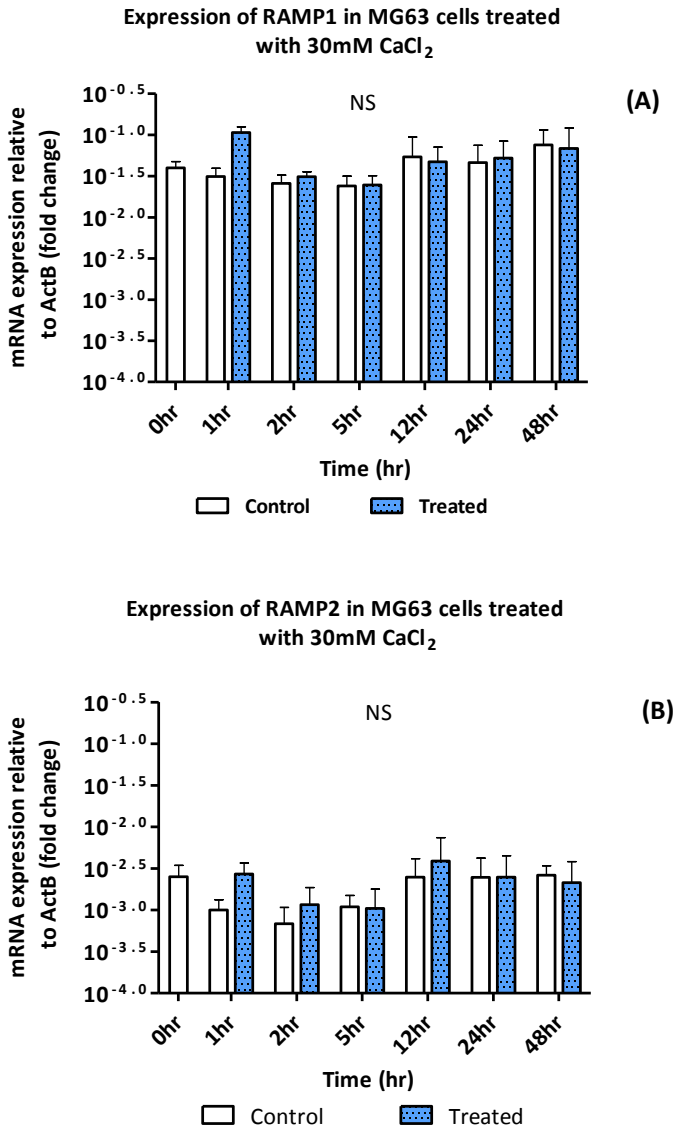

Figure 5.3.5: mRNA expression profile of RAMP1 and 2 in MG63 cells treated with 30mM $CaCl_2$ at different time points measured using real time PCR:

MG63 cells were cultured normally to 60-70% confluency and then treated with 30mM $CaCl_2$ for the given time points. mRNA expression levels were determined using TaqMan® probes in real time PCR. The graph shows expression levels of RAMP1 (A) and RAMP2 (B) at different time points relative to expression at Actβ. The graph shows combined data from three independent experiments. Statistical used 2-way ANOVA, Bonferroni post-test. NS = differences are not statistically significant.

The second osteosarcoma cell line - SAOS-2 was also treated with 30mM $CaCl_2$ for up to 48hr and the mRNA expression levels of CaSR and RAMPs were measured using TaqMan® probes in real time PCR. The mRNA expression levels for RAMP1 and 2 are shown in Figure 5.3.6 A and B respectively and there were no statistically significant differences in their expression levels after treatment with 30mM $CaCl_2$ (blue bars) at any time point compared to untreated samples (white bars) as analysed by 2-way ANOVA and Bonferroni post-test. mRNA expression levels of CaSR and RAMP3 were not detected using the given TaqMan® probes within 40 cycles. The expression levels of RAMP2 were decreased in both control and treatment groups after 1hr, however this effect was not statistically significant as measured by Bonferroni post-test. The average normalized expression of RAMP1 was ~2.5 fold higher than RAMP2 in SAOS-2 cells (as measured at 0hr time point).

The average ± SD Ct values were 32.56 ± 1.77 (control) and 32.43 ± 1.94 (treated) for RAMP1, 33.16 ± 1.64 (control) and 33.43 ± 1.49 (treated) for RAMP2.

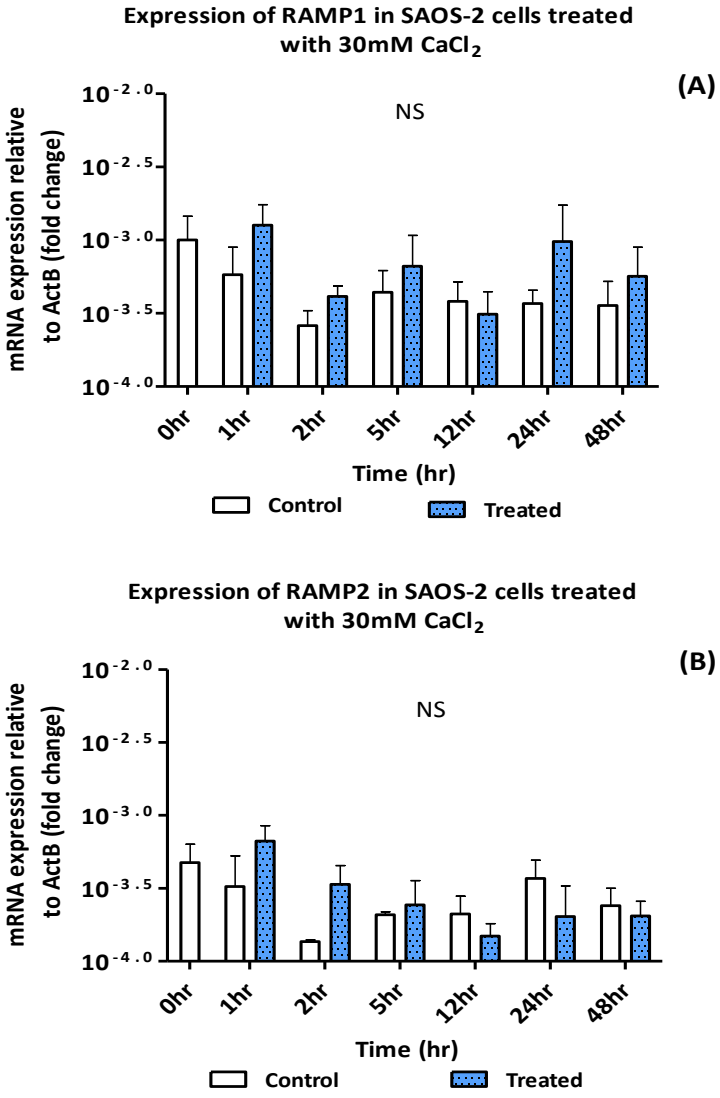

Figure 5.3.6: mRNA expression profile of RAMP1 and 2 in SAOS-2 cells treated with 30mM $CaCl_2$ at different time points measured using real time PCR:

SAOS-2 cells were cultured normally till 60-70% confluency and then treated with 30mM $CaCl_2$ for the given time points. mRNA expression levels were determined using TaqMan® probes in real time PCR. The graph shows expression levels of RAMP1 (A) and RAMP2 (B) at different time points relative to expression at Actβ. The graph shows combined data from three independent experiments. Statistical test performed: 2-way ANOVA, Bonferroni post-test. NS = differences are not statistically significant.

The third cell osteosarcoma cell line- TE85 were also treated with 30mM $CaCl_2$ for up to 48hr to measure any change in mRNA expression levels of CaSR and RAMPs using TaqMan® probes in real time PCR. The mRNA expression levels for RAMP1 and 2 are shown in Figure 5.3.7 A and B respectively and there was no statistically significant change in their expression after treatment with 30mM $CaCl_2$ (blue bars) at any time point compared to control samples (white bars) as measured using 2-way ANOVA and Bonferroni post-test. mRNA expression levels of CaSR and RAMP3 were not detected using the given TaqMan® probes within 40 cycles.

The average ± SD Ct values were 28.35 ± 0.99 (control) and 28.32 ± 1.09 (treated) for RAMP1, 30.80 ± 0.91 (control) and 31.04 ± 1.14 (treated) for RAMP2. The average normalized expression of RAMP1 was ~3.8 fold higher than RAMP2 (as measured at 0hr time point).

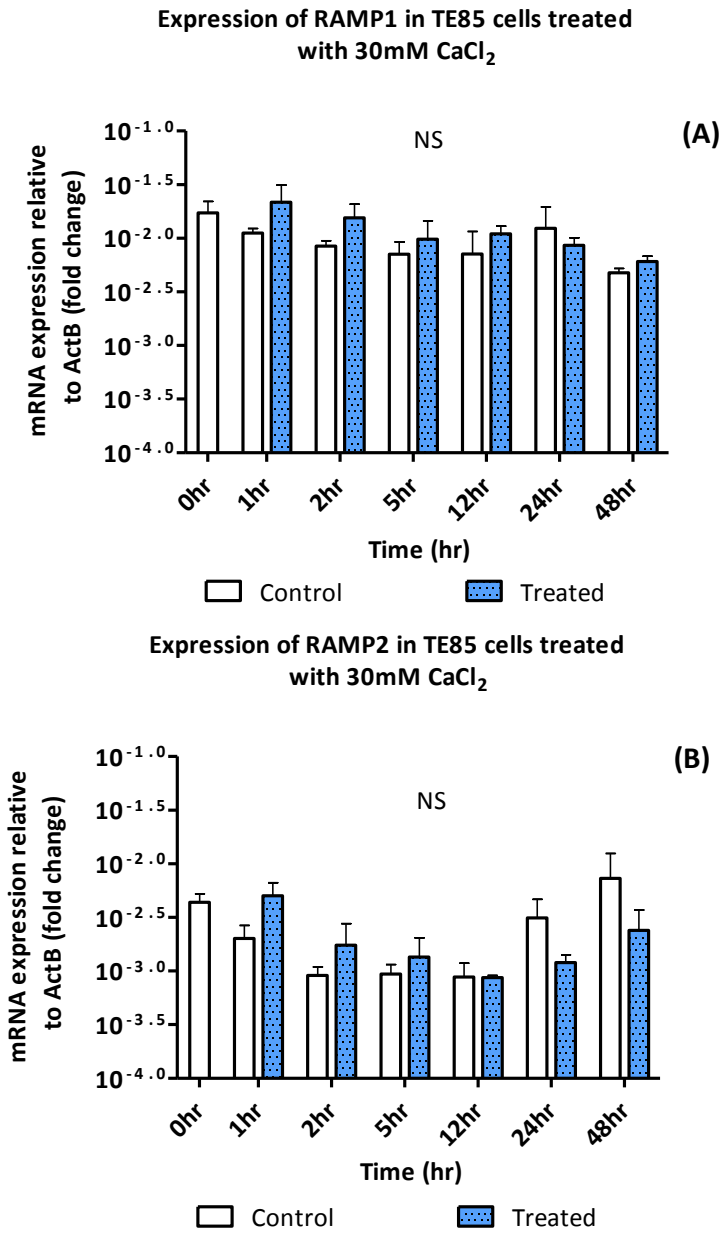

Figure 5.3.7: mRNA expression profile of RAMP1 and 2 in TE85 cells treated with 30mM $CaCl_2$ at different time points measured using real time PCR:

TE85 cells were cultured normally till 60-70% confluency and then treated with 30mM $CaCl_2$ for the given time points. mRNA expression levels were determined using TaqMan® probes in real time PCR. The graph shows expression levels of RAMP1 (A) and RAMP2 (B) at different time points relative to expression at Actβ. The graph shows combined data from three independent experiments. Statistical test performed was 2-way ANOVA, Bonferroni post-test. NS = differences are statistically non-significant.

5.3.5. Measuring the changes in mRNA expression levels of CaSR and RAMPs during the differentiation of MG63, SAOS-2 and TE85 cell lines measured using real time PCR:

The immature osteoblasts like osteosarcoma cell lines - MG63, SAOS-2 and TE85 were treated with osteoblast differentiation medium and the changes in gene expression of CaSR and RAMPs was measured at different time points of maturation until 21 days. mRNA expression of CaSR and RAMPs was checked using TaqMan® probes in real time PCR at Days 5, 10, 15 and 21. Figures 5.3.8, 5.3.9 and 5.3.10 illustrate the expression of RAMP1 (A) and RAMP2 (B) at different time points in MG63, SAOS-2 and TE85 cells respectively treated with differentiation (blue bars) or normal DMEM (white bars) medium. The expressions of genes of interest were normalized to Actβ and are expressed as fold change to its expression on the graphs. The expression of CaSR and RAMP3 were not detected in any cell line using the given TaqMan® probes within 40 cycles; even after treatment with differentiation medium for 21 days.

There was no statistically significant change in the expression of RAMP1 or 2 in any cell line treated with the differentiation medium (blue bars) compared to the untreated controls (white bars) as analysed by 2-way ANOVA, Bonferroni post-test.

However, as seen in figure 5.3.9 A, there was an increase in expression of RAMP1 in SAOS-2 cells in both control and treated groups from day 5 onwards. Also, there was an increase in RAMP1 expression in treated samples compared to control samples during the same time range. However, these effects were not statistically significant as determined by Bonferroni post-test.

The average ± SD Ct values were:

MG63 cells: 24.10 ± 1.05 (control) and 23.84 ± 0.79 (treated) for RAMP1 and 30.26 ± 0.87 (control) and 29.72 ± 0.77 (treated) for RAMP2.

SAOS-2 cells: 31.24 ± 1.27 (control) and 29.87 ± 1.60 (treated) for RAMP1 and 32.07 ± 0.91 (control) and 32.13 ± 1.6 (treated) for RAMP2.

TE85 cells: 26.68 ± 0.87 (control) and 26.09 ± 0.98 (treated) for RAMP1 and 28.63 ± 0.51 (control) and 28.41 ± 0.54 (treated) for RAMP 2.

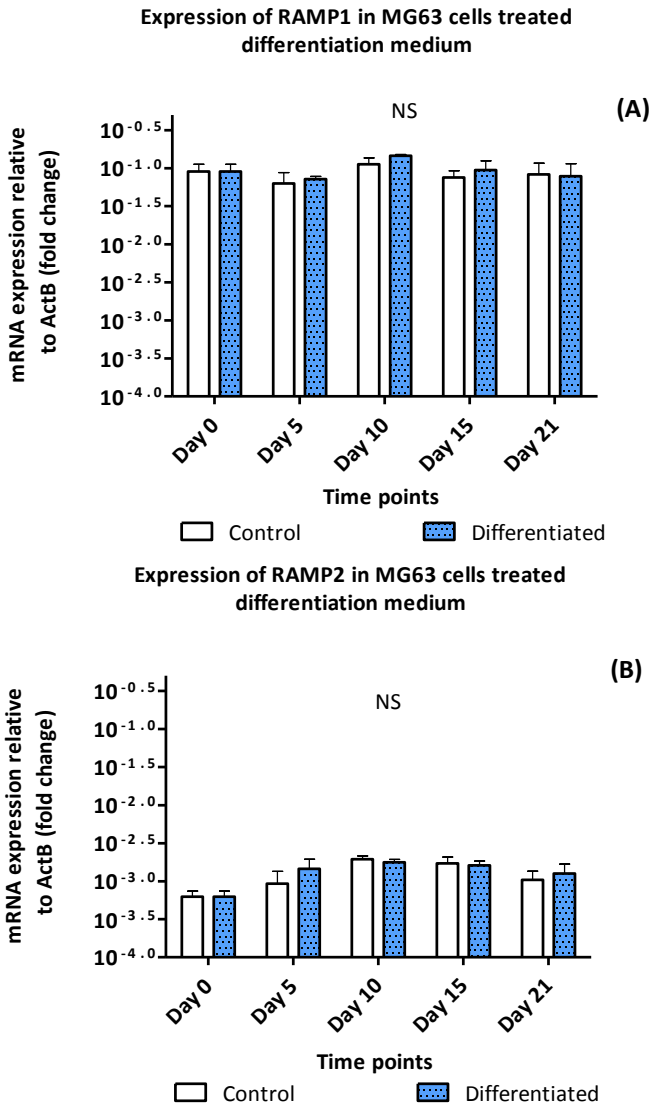

Figure 5.3.8: Change in mRNA expression of RAMP 1 and 2 during differentiation of MG63 cells:
MG63 cells were grown till 100% confluency under normal conditions and then treated with differentiation medium for 21 days. mRNA expression levels of CaSR and RAMPs was measured at different time points as shown in the graph using TaqMan® probes in qPCR. The graphs show the mRNA expression of RAMP 1 (A) and RAMP 2 (B) in cells treated with differentiation medium (blue) and normal DMEM (white) at different time points, relative to the respective expression levels of Actβ. The data shown is combined from three separate experiments. Statistical test used: 2-way ANOVA, Bonferroni post-test. NS = differences are not statistically significant.

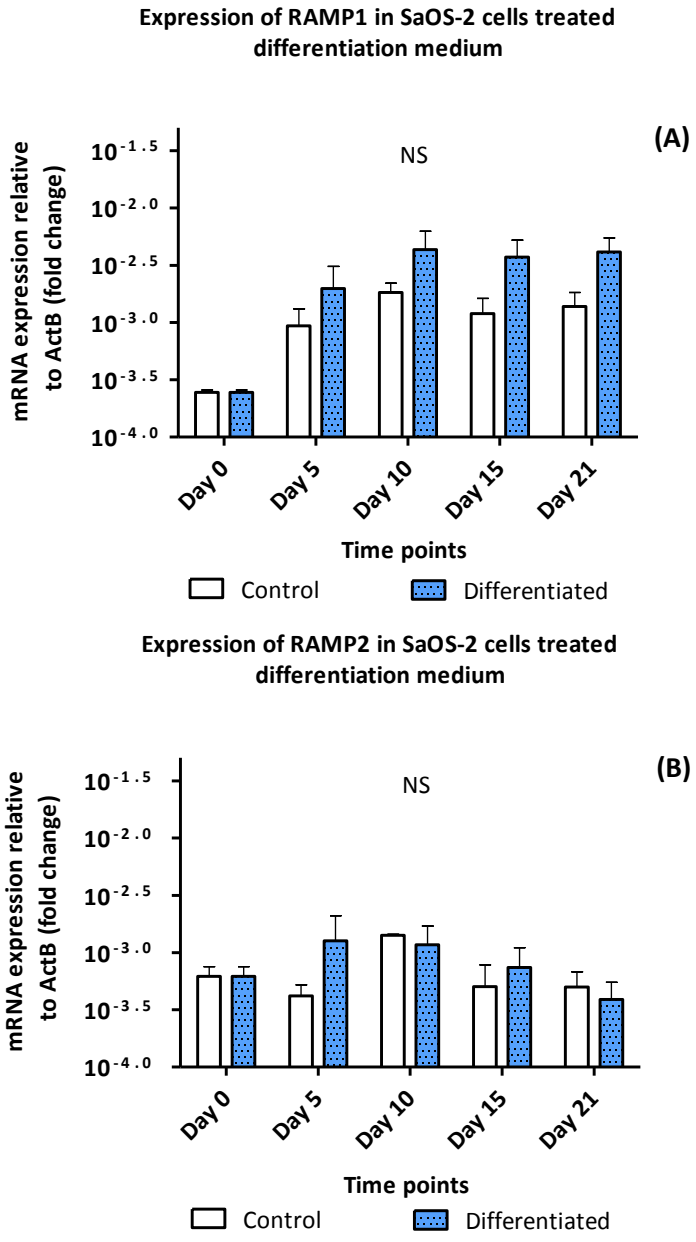

Figure 5.3.9: Change in mRNA expression of RAMP 1 and 2 during differentiation of SAOS-2 cells:
SAOS-2 cells were grown till 100% confluency under normal conditions and then treated with differentiation medium for 21 days. mRNA expression levels of CaSR and RAMPs was measured at different time points as shown in the graph using TaqMan® probes in qPCR. The graphs show the mRNA expression of RAMP 1 (A) and RAMP 2 (B) in cells treated with differentiation medium (blue) and normal DMEM (white) at different time points, relative to the respective expression levels of Actβ. The data shown is combined from three separate experiments. Statistical test used: 2-way ANOVA, Bonferroni post-test. NS = differences are not statistically significant.

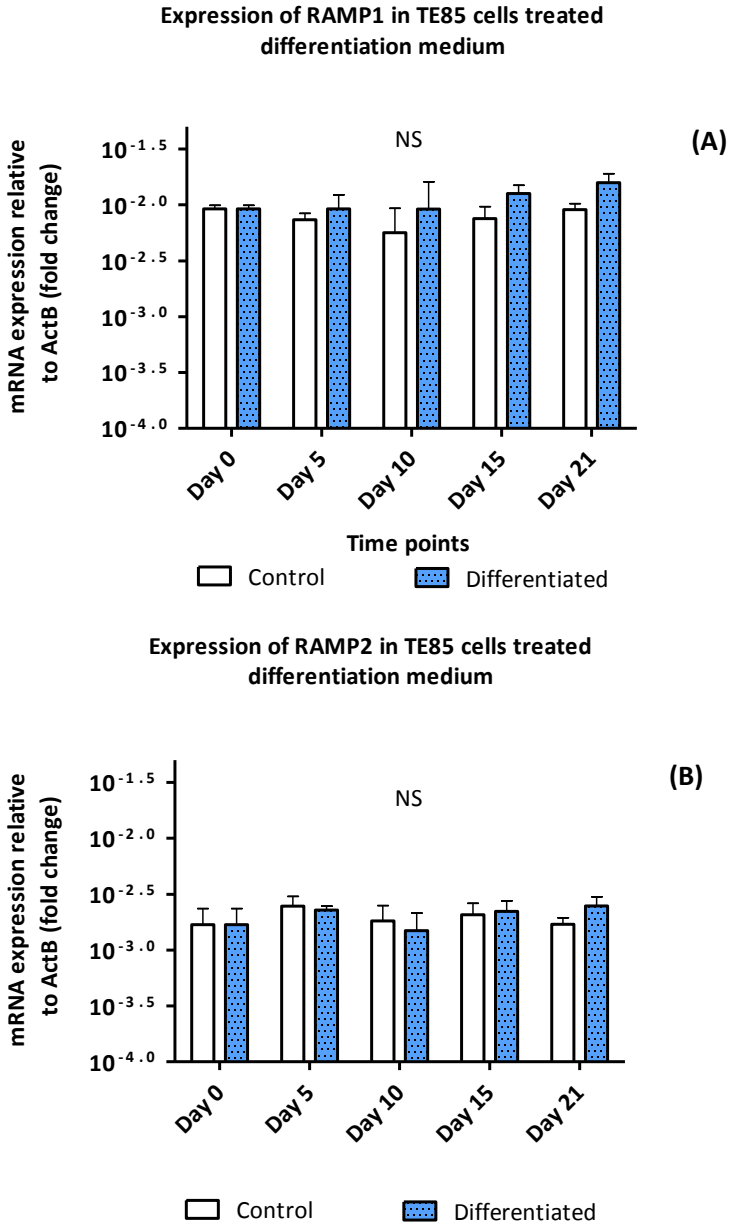

Figure 5.3.10: Change in mRNA expression of RAMP 1 and 2 during differentiation of TE85 cells:
TE85 cells were grown till 100% confluency under normal conditions and then treated with differentiation medium till 21 days. mRNA expression levels of CaSR and RAMPs was measured at different time points as shown in the graph using TaqMan® probes in qPCR. The graphs show the mRNA expression of RAMP1 (A) and RAMP2 (B) in cells treated with differentiation medium (blue) and normal DMEM (white) at different time points, relative to the respective expression levels of Actβ. The data shown is combined from two separate experiments. Statistical test used: 2-way ANOVA, Bonferroni post- test. NS = differences are not statistically significant.

5.4. Discussion

It is known that the expression of CaSR and RAMPs is regulated under various physiological circumstances as described in detail in section 5.1 of this chapter. So, it was hypothesised that the agents involved in Ca^{2+} homeostasis will alter the expression levels of CaSR and RAMPs 1-3 in cells natively expressing these proteins. There is no information regarding the regulation of RAMPs by such components, and the results could point towards a role of RAMPs in CaSR-mediated Ca^{2+} homeostasis. Accordingly, TT cells and osteoblast-like osteosarcoma cell lines were chosen for the interventional experiments.

Cell lines used:

It was proposed to measure the changes in expression of CaSR and RAMPs by agents of Ca^{2+} homeostasis and so it was important to select the cells which represented the tissues involved in Ca^{2+} homeostasis. TT cells were chosen as they are differentiated medullary thyroid carcinoma cells from human [5]. They express CaSR which mediates the calcitonin secretion when activated by 3mM extracellular Ca^{2+} [5]. Accordingly, they represent medullary thyroid, which is a major site for CaSR-mediated Ca^{2+} homeostasis because it secretes the hypocalcaemic hormone calcitonin in response to increasing levels of Ca^{2+}. TT cells have been used previously as a model of thyroid C-cells to study the regulation of CaSR expression by 1,25-dihydroxyvitaminD_3 [288] and have been accepted as an appropriate model for functional studies.

Another site for Ca^{2+} homeostasis is bone. MG63, SAOS-2 and TE85 are human osteosarcoma cell lines derived from human malignant bone tumours; and evidence from the literature show that they possess the characteristics of osteoblasts. A study measuring mRNA expression levels of a total of 58 cytokines, growth factors, and their corresponding receptors and bone matrix proteins showed that the similarity in expression profiles between MG63, SAOS-2, TE85 cells and human primary osteoblast cells were highly comparable [309]. Also, 1,25-dihydroxyvitaminD_3 increased alkaline phosphatase levels in SAOS-2 and TE85 cells which

is a typical characteristic of osteoblasts [310]. In addition to this, the advantages of using these cell lines were their easier availability, relative ease of culture, quicker and longer growth in cultures and provision of extensive cellular material.

Use of real-time PCR:

Quantitative real-time PCR technique was used in order to accurately measure any changes in mRNA expression levels by various interventions of the genes of interest. Real-time PCR allows the detection of products during the early phases of the reaction as opposed to semi-quantitative PCR where quantitation is based on the band intensity of the end product on an agarose gel. Accordingly, real-time PCR detects the accumulation of amplicon during the reaction and the data is then measured at the exponential phase of the PCR reaction. The TaqMan® probes used were inventoried by Applied Biosystems and designed such that they span exon-exon junctions for the particular gene of interest (this prevents the amplification of genomic DNA). Also, the detection is fluorescence based due to the presence of reporter dye at the 5' end, and a low-energy molecule- 'quencher' at the 3' end of the probe; and hence works on the principle of FRET (when the probe is cleaved by the 5' exonuclease activity of the polymerase enzyme, it produces reporter dye signal which is quenched in absence of polymerase activity). Due to this property, accurate data corresponding to the cycle number of a gene at which the specific fluorescence corresponding to its amplification above the background fluorescence in the reaction (C_t value) is used for quantification.

In order to check if the inventoried TaqMan® probes worked efficiently in our hands, pcDNA 3.1 CaSR or RAMP1-3 cDNA doses were prepared to check for the linearity of target amplification by the probes (Figure 5.3.1). According to the guidelines provided by Applied Biosystems a standard curve slope of -3.3 indicates a PCR reaction with 100% efficiency. The results show that reaction efficiencies for all the TaqMan® probes were very high and could be used to accurately detect changes in gene expression. Next, the variability in expression of the endogenous controls (Actβ and HPRT1) was checked in all the cell lines used (Appendix figure 7.10), where it was found that Actβ expression was less variable than HPRT1, upon treatment and between different experiments. Accordingly, the expression of test genes was normalized

by the expression of Actβ for relative quantification in all experiments. For a valid relative quantification calculation, the efficiency of the target amplification and the efficiency of the reference amplification must be approximately equal [308]. So, the amplification reaction efficiencies of the TaqMan® probes were checked by comparing ΔC_t values (normalized to Actβ) against serial dilutions of TT cell cDNA (figure 5.3.2) and it was found that according to the accepted standard [308], the values of the slope of the line was <0.1 for CaSR, RAMP1 and RAMP2; indicating that the TaqMan® probes and the reaction conditions were appropriate for performing relative quantification calculations.

Measuring changes in the expression levels of CaSR and RAMP mRNA in TT cells by various interventions:

The expression of CaSR was confirmed at both mRNA and protein levels (as shown in figure 7.8 in section 7.6 of appendix), along with the expression of RAMP1 and RAMP2 genes. We hypothesised to study the effect of Ca^{2+} and Ca^{2+}-regulators on the expression levels of CaSR and RAMPs in TT cells. TT cells were cultured in F-12K medium containing 0.9mM $CaCl_2$ which is below the Ec_{50} of CaSR (~3mM). Earlier time points were included in this study to check for an immediate change in expression levels; and 24 and 48hr time-points were included to check for chronic changes in expression levels. A high dose of 10mM $CaCl_2$, ~3 times higher than Ec_{50} was used to induce an effect on the expression levels of the genes for up to 48hr. This dose was selected because it is higher than Ec_{50} and could exhibit a stronger effect, or in other words it could be more efficacious. No statistical significant changes in expression of CaSR and RAMPs were observed (Fig 5.3.3) upon treatment. This might suggest that changes in CaSR expression are robustly maintained against changing extracellular Ca^{2+} levels because of its essential role of secreting calcitonin; and any changes in its expression levels might produce undesirable effects in Ca^{2+} homeostasis.

No measurable effect of 1μM 1,25-dihyroxyvitamin D_3 was observed on the expression levels of CaSR and RAMP1-3 at any time points (Figure 5.3.4). In contrast to these results, 1,25-dihydroxyvitamin D_3 has been shown to upregulate CaSR mRNA by ~2.3 fold *in vivo* in thyroid

gland (dose of 250pmol/100g body weight) and *in vitro* in TT cells (10nM) [288] using ribonuclease protection assay. However, they observed statistically significant upregulation of CaSR mRNA at 8hr and 12hr post-treatment, followed by a decrease to basal levels of expression by 24hr in case of *in vivo* experiments; and upregulation at 8hr *in vitro* in TT cells [288]. They only used the 8hr time point for *in vitro* experiments using TT cells and the effect on CaSR mRNA expression at time points earlier or later were not studied. However, in this study, it is possible to have missed the time-frame where a possible effect could have been observed.

TT cells modulate calcitonin secretion levels upon treatment with 10mM $CaCl_2$ and 1,25-dihyrdoxyvitamin D_3 [5, 311]. Accordingly, the calcitonin secretion in the medium by TT cells upon treatment with these compounds could have been measured to confirm their definite effect on these cells at the given conditions. In both the interventions, the expression of RAMP3 was undetectable, which is discussed later in the chapter.

Measuring changes in the mRNA expression levels of CaSR and RAMPs mRNA in osteosarcoma cell lines by 30mM $CaCl_2$ treatment:

In osteosarcoma cells- MG63, SAOS-2 and TE85 CaSR transcripts were not detected within 40 cycles using the given TaqMan® probes. High extracellular Ca^{2+} via CaSR, has been shown to exhibit mitogenic actions on mouse-derived primary osteoblast and enhance their differentiation [41]. Osteoclastic bone resorption can generate very high levels of Ca^{2+} within a range of 8-40 mM [312] and so it has been suggested that in the bone microenvironment where bone resorption occurs, osteoblasts sense high Ca^{2+} generated within the immediate microenvironment of resorbing osteoclasts within the same range [41]. Accordingly, it was hypothesised, that high extracellular Ca^{2+} (30mM) in media will induce expression of CaSR in osteosarcoma cell lines. The dose was chosen based on the above stated information and secondly because it is a ~10 fold higher dose than Ec_{50} of Ca^{2+} for CaSR (~3mM) and should represent the top-plateau of a dose-response curve. However, no CaSR mRNA expression could be detected within 48hr of treatment in either of the osteosarcoma cell lines, indicating a failure of ligand (Ca^{2+}) induced expression. The changes in RAMP1 and 2 mRNA expression levels upon treatment were not statistically significant; whereas RAMP3 mRNA expression was

not detected (figure 5.3.5, 5.3.6 and 5.3.7). This shows that RAMP expression is not affected by increasing extracellular Ca^{2+} concentrations, probably because maintaining robust RAMP expression might be important for functioning of other GPCR partners of RAMPs.

There has been a debate in the literature regarding the presence of CaSR expression in the clonal osteoblast-like osteosarcoma cell lines. There are studies showing the expression of CaSR mRNA and protein (similar to parathyroid transcript) in MG63, SAOS-2, UMR-106 and MC3T3 cells [313-315]. However, differences in band-size for CaSR protein were observed between CaSR and MC3T3 compared to CaSR-transfected HEK-293 cells in one study [315]; whereas very low expression of CaSR with a presence of multiple bands at lower size (incorrect sizes) than expected (representing degradation product according to the authors) were observed in MG63 and SAOS-2 protein samples (pre-adsorption of CaSR antisera abolished all bands) [313, 314]. The mRNA transcript reported using RT-PCR in MG63 cells by Yamaguchi *et al*, shared sequence identity to known parathyroid derived CaSR transcript [313]. Using the same CaSR antisera as [313, 314] but different primers for PCR, a different group failed to detect CaSR mRNA and protein expression in MG63 and SAOS-2 cell lines, compared to the positive controls - CaSR-transfected HEK-293 cells, mouse kidney cells and human parathyroid cells [316]. However, the authors could detect specific CaSR bands in their positive controls only, upon using a different and more specific CaSR antibody; in contrast to the CaSR antisera. They observed multiple cross-reacting bands in both their positive controls and negative control- HEK-293 non-transfected cells, using the CaSR antisera used in [313, 314]. The authors [316] confidently suggested that none of the non-specific bands observed congruent to [313, 314] represent either the dimeric or differentially glycosylated forms of CaSR, according to the suggestions made in [313, 314]. They reasoned that pre-adsorption to a blocking peptide does not necessarily suggest the specificity of the antibody; as hybridization to a cross-reacting (non-specific) protein would also be eliminated by such pre-adsorption. There was another study by the same group as [316]; showing the absence of CaSR expression in MC3T3 cells which showed normal maturation and display of osteoblast like characteristics [317].

Our results using the same TaqMan ® probes show successful detection of CaSR mRNA in TT cells. This shows that the absence of CaSR in these osteosarcoma cell lines is not due to a technical error. Accordingly, it can also be speculated that CaSR expression in our osteosarcoma cell lines was beyond the detection limit of the assay. As shown in figure 5.3.1 (A), the C_t value of 34.1 was obtained for TOPO CaSR cDNA concentration of 1fg. Accordingly it can be speculated that the MG63, SAOS-2 or TE85 cDNA concentration of CaSR in the reaction was at least less than 1fg, as a C_t value 34 was not accepted for analysis (however, the output at the end of the reaction showed 'undetermined' and gave no C_t value). Even doubling the amount of cDNA in the reaction failed to detect any expression of CaSR in these samples. Interestingly, it has been shown using cultured primary mouse calvarial osteoblasts from *Casr*$^{-/-}$, that CaSR agonists like Ca^{2+}, Gd^{3+} and Al^{3+} could induce similar responses in these cells compared to wild type [318]. This suggests a novel cation-sensing mechanism in osteoblasts. Accordingly functional response such as increase in intracellular Ca^{2+} by CaSR specific agonists should be tested in these cells, in order to study if an alternative cation-sensing mechanism exists.

Measuring changes in mRNA expression of CaSR and RAMPs upon differentiation of osteosarcoma cell lines:

MG63, SAOS-2 and TE85 cell lines are immature osteoblast-like cells, derived from human osteosarcoma [309, 319]. It was hypothesised that inducing differentiation in these cells to force them into a more mature osteoblast phenotype, might change expression profiles of CaSR and RAMPs. The differentiation medium recipe has been used in previous studies [320, 321]. There was still no expression of CaSR and RAMP3 upon differentiation of osteosarcoma cell lines. This shows that even differentiated osteosarcoma cells are not a good model to study CaSR biology. The expression levels of RAMP1 and 2 did not show a statistically significant change in expression during differentiation (figure 5.3.8, 5.3.9 and 5.3.10). However, the expression levels of RAMP1 mRNA when compared to day 0, increased in both control and treatment groups from day 5 up to day 21 in SAOS-2 cells, with an apparent increase in the treatment group compared the control at each time point. However, this change between the control and treatment groups at individual time points was not significant statistically, meaning that differentiation does not have an effect at all values of time. Evidence from the literature

show a presence of CaSR and RAMPs in cultured primary osteoblasts [41, 42, 307, 322] and so they should be used for future experiments to study the hypothesis of change in expression patterns of CaSR and RAMPs by different interventions.

As mentioned earlier, there are speculations of a novel cation-sensing mechanism in osteoblasts derived from *Casr*$^{-/-}$ mice [318]. Similarly, it can be hypothesised that MG63, SAOS-2 and TE85 cells might have an alternative Ca^{2+}/cation-sensing mechanism such as presence of GPRC6A which is an alternative cation-sensing receptor [165].

Undetermined RAMP3 mRNA expression in all the cell lines used:

In none of the cell lines studied, was the expression of RAMP3 mRNA detected within 40 cycles using the given TaqMan® probes. There is currently no evidence using TaqMan® probes or any other techniques, showing the presence of RAMP3 in any of these cell lines studied. According to the Applied Biosystem's manual, a C_t value of more than 35 could be inaccurate and so the limit for analysis for this study was restricted to the C_t value of 34. However, for all the samples, RAMP3 Ct value was undetermined, i.e. not assigned a C_t number. This indicates that either RAMP3 is completely absent or expressed at extremely low levels at outside the detection limits of the reaction using this assay at given conditions. Figure 5.3.1 D using pcDNA3.1 RAMP3 cDNA provides the evidence that the TaqMan® probes could definitely detect RAMP3. Also two other evidences- detection of RAMP3 expression in COS-7 CaSR+RAMP3 transfected cells (appendix section 7.5, figure 7.7) and C_t value of 32 obtained for 0.5ng lung cDNA sample from Ambion (data not shown) using same conditions; confirm that RAMP3 expression could be detected by the given Taqman® probe.

Also, using the information from figure 5.3.1 D, the lowest concentration of pcDNA3.1 RAMP3 used was 12pg corresponding to the C_t value of 25. Now, if we extrapolate this, C_t value of 34.9 may correspond to ~ 1fg (10^{-15} g), (as 3.3 cycles = 10 fold difference in expression level, according to the Applied Biosystem's manual). Given that the efficiency of the TaqMan® probe will not be 100%, it can still be roughly speculated that the concentrations of RAMP3 transcripts in the samples in the reaction were probably less than ~$10^{-14.5}$ to 10^{-15} g. The efficiency of the

reverse-transcription reaction, oligo- dT primers in the cDNA synthesis kit and the presence of any secondary structures of mRNA that can inhibit efficient cDNA conversion remain unknown; which could lead to loss of already extremely low levels of mRNA transcripts.

An additional control can be included in the reaction to check for any inhibitors present that can lead to a loss in mRNA transcripts from extraction to the PCR stages. This information would be useful especially, when considering that the copies of gene of interest (RAMP3 in all cell lines or CaSR in osteosarcoma cells) are very low, and that they are diluted during the processing of the sample at several stages: extraction of RNA, preparing cDNA (only an aliquote of RNA used), preparing qPCR reaction (only an aliquote of the total cDNA used per reaction in a well). Accordingly, a known quantity of exogenous, unrelated RNA can be spiked into the cell sample before the RNA extraction process. The qPCR reaction performed for the gene of the exogenous RNA using the cDNA sample processed is then compared to the qPCR results from cDNA synthesized directly from exogenous RNA sample (without going-through extraction procedure). This would measure for the loss of transcripts caused by the processing or presence of inhibitors of reaction.

Differential RAMP expression between the osteosarcoma cell lines:

Within the three osteosarcoma cell lines, the normal (untreated) expression levels of RAMP1 and 2 were found to be different (figure 5.3.5, 5.3.6 and 5.3.7). The expression of RAMP1 was highest in MG63 cells (4% of Actβ expression), followed by TE85 cells (1.7% of Actβ expression) and lowest in SAOS-2 cells (0.1% of Actβ expression). In case of RAMP2, TE85 expressed its highest levels (0.4% of Actβ), followed by MG63 (0.2% of Actβ) and the lowest expression was observed in SAOS-2 cells (0.04% of Actβ). The significance of this observation is not known yet, but might suggest a role of individual RAMP-specific receptor partners in these cells. It is also noteworthy that the expression levels of RAMP1 were higher than RAMP2 in TT, MG63, SAOS-2 and TE85 cell lines; suggesting a higher presence of RAMP1 GPCR partners in these cells. Presence of a RAMP1 has been reported in MG63 cells by studies showing presence of distinct

CGRP receptor phenotype in these cells [323]. Whereas, TT cells express CTR [324], which is a partner for both RAMP1 and 2 to form amylin receptors.

In summary, it was found that there was no change in mRNA expression levels of CaSR, RAMP1 and 2 with 10mM $CaCl_2$ or 1µM calcitriol treatment in TT cells at any of the time points studied, which probably leads to the hypothesis that major changes in gene expression levels of CaSR or RAMPS can lead to unwanted changes in Ca^{2+} homeostasis. However, this remains to be tested and also the corresponding protein levels remain to be detected. CaSR mRNA expression was undetected in MG63, SAOS-2 and TE85 osteosarcoma cell lines and treatment with 30mM $CaCl_2$ or differentiation into mature osteoblasts did not induce detectable levels of CaSR mRNA expression. Also, the expression of RAMP1 and 2 was not altered by interventions in these cells. Expression of RAMP3 was undetected in all the cell lines. The results also show that osteosarcoma cell lines are not a good model to study CaSR biology.

CHAPTER 6: GENERAL DISCUSSION

CaSR is a pleiotropic GPCR that plays an important role in Ca^{2+} homeostasis. It was discovered that an association with RAMPs is essential for its cell-surface trafficking in transfected cells [157]. This was the first reported interaction of RAMPs with a family C GPCR. The mechanisms behind the characteristics of CaSR such as binding multiple ligands, and activation of multiple signalling pathways are not fully understood. RAMPs are promiscuous proteins that engender different receptor phenotypes, ligand binding affinities, and signalling patterns to family B GPCRs [156, 172, 174, 175]. Based on this information, it was hypothesised that RAMPs contribute to more than just the cell surface trafficking of the CaSR. Accordingly, this project was based to characterize this interaction further, and was divided into three parts relating to different aspects of the interaction:

- To get a deeper insight into the molecular interaction between CaSR and RAMPs
- To identify a possible role of RAMPs in signalling of CaSR
- To measure the regulation of expression of RAMPs along with CaSR by agents involved in Ca^{2+} homeostasis; which can point towards a possible role of RAMPs in Ca^{2+} homeostasis.

Additionally, it was hypothesised that RAMPs interact with GPRC6A, a family C GPCR closely related to the CaSR [158]. This is because like CaSR [157], it fails to traffic to the cell surface in certain transfected cell-types [158, 159]. So, it was hypothesised that RAMPs function as chaperones for GPRC6A and enable its cell-surface expression.

Hetero-oligomerization of CaSR with RAMPs:

The molecular interaction of CaSR and RAMPs was studied in detail using FRET-based stoichiometry. Firstly the interaction of CaSR with RAMP1 or 3 was examined for efficiency of cell-surface trafficking using sensitized FRET emission (section 3.3.3, chapter 3). Using FRET stoichiometry it was observed that equal fractions of CaSR were present on the cell surface in the FRET complex with either RAMP1 or 3. This indicates that both RAMP1 and 3 had equal efficiencies in trafficking the receptor to the cell surface. However, it was found that the fraction of RAMP3 was ~1.6 fold higher than RAMP1 (Table 3.3.3, chapter 3) in the CaSR-FRET

complex. Now, it is already known from the literature that CaSR exists as a dimer on the cell surface [105, 325]. So, the FRET stoichiometry data suggests that for every dimer of CaSR there is ~1.6 times more RAMP3 than RAMP1 (figure 6.1) in respective complexes. Also, it should be noted that this defines a single unit of the CaSR-complex, and so it is still unknown as to how many of such units can heteromerize to form a larger oligomeric complex on the cell surface. In summary, results from FRET stoichiometry suggest the presence of a higher oligomeric receptor complex in the case of CaSR and RAMP interaction, where more molecules of RAMP3 than RAMP1 can be associated with a dimer of CaSR.

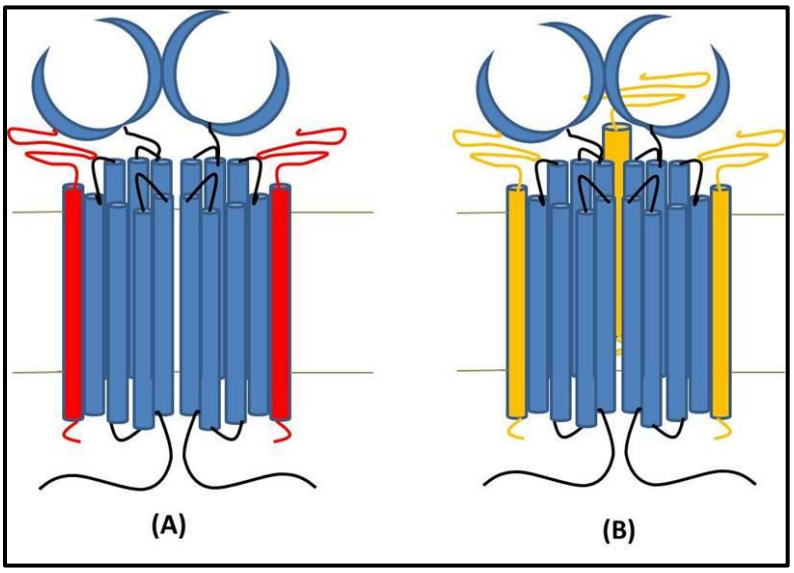

Figure 6.1: Possible stoichiometry of CaSR and RAMP complexes:
(A) CaSR homodimer (blue) with RAMP1 (red) in complex probably has a lower RAMP:CaSR molecules number than with (B) in complex with RAMP3 (orange). The numbers represented here are only to aid understanding and do not represent the actual number of molecules of either RAMP present in complex with CaSR.

FRET based approaches have been successfully utilized to determine the stoichiometry of GPCRs involved in homo or hetero-oligomerization [240, 326-328]. These approaches are based on sequential FRET using three different fluorophores, where the signal resulting from successful FRET between the first two components of the complex, results into FRET with the third component. This approach has been used successfully in detecting hetero-oligomerization between homodimer of CLR and monomer of RAMP1, where FRET occurring between two CLRs

tagged with two different fluorophores, transfers the energy to cause excitation of another fluorophore tagged to the third interacting protein (RAMP) [328]. So a similar approach can be used to identify the exact stoichiometry of RAMP molecules associating with CaSR homodimer.

In addition to the FRET results which are obtained using an artificial expression system, RAMP1 knock-down in TT cells showed significant attenuation of CaSR signalling, which most likely means that they interact in these cells, and that RAMP1 is probably involved in cell-surface trafficking of the CaSR (section 4.3.10, chapter 4). Accordingly, this points towards a possible interaction of CaSR with RAMPs in a physiological setting, although its stoichiometry is not yet determined.

In addition to the interaction studies, this study has also discovered that RAMP1 plays a role in the signalling of the CaSR (chapter 4, section 4.3.11). Based on information from the literature on the effects of hetero and oligomerization of GPCRs [329-331], the findings from the FRET stoichiometry (hetero-oligomerization) and signalling studies (role of RAMP1 in CaSR signalling), lead to new hypotheses as briefly noted below.

It can be hypothesised that the promiscuity of the CaSR to bind different ligands [10, 29, 52, 69-74, 76, 81, 82, 86, 87, 94] can be influenced by its differential interaction with either RAMP1 or 3. This is supported by the fact that RAMPs can alter the ligand binding specificity for the CLR and CTR and consequently forming distinct receptor phenotypes [156, 172]. Secondly, CaSR has been shown to exhibit ligand-dependent functional selectivity, by preferentially activating either $G_{i/o}$ or ERK pathways when binding specific orthosteric agonists in transfected HEK-293 cells [332] (expressing RAMP1 [157]). The authors suggested that this could occur because different agonists cause different yet specific conformational changes in the receptor structure which lead to the activation of a specific signalling pathway [332]. However, in addition to this it will be interesting to test whether there is a direct involvement of RAMP to this effect at any level from ligand binding to coupling G proteins. (as RAMP1 affects CaSR signalling-chapter 4, section 4.3.11). We have shown (in a different study) using the antibody-capture SPA technique, that the presence of a RAMP can modulate the specific G-protein signalling pattern of the family B GPCRs like the PTH1R, VPAC1R and Glucagon receptors (figure 6.2) (Roberts *et*

al, unpublished data). We demonstrated that although these receptors are capable of trafficking to the cell-surface and signalling on their own, presence of RAMP2 with PTH1R and VPAC1R, and RAMP3 with glucagon receptor; increased the efficacy of G-protein responses without any changes in ligand binding affinities and potencies. This data thus conclusively shows that RAMPs are involved in direct G-protein coupling of the VPAC1, PTH1/2 and glucagon receptors (Roberts *et al*, unpublished data), and so it will be interesting to test whether a similar effect is observed with a different GPCR partner of RAMPs such as the CaSR.

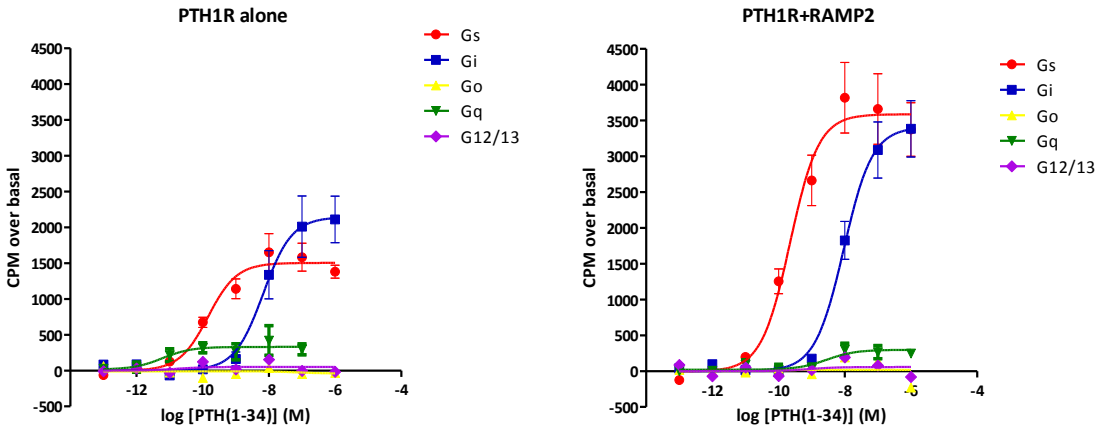

Figure 6.2: RAMPs modulate specific G-protein signalling profile of the PTH1R:
It is seen that in presence of RAMP2, there is an increase in efficacy of $G_{\alpha s}$ (140%) and $G_{\alpha i}$ (60%) activation by PTH (1-34) on the PTH1R. Roberts et al, unpublished data.

In addition to the implications on signalling, the interaction of CaSR with RAMPs can also have an effect on the internalization and recycling of the receptor post-stimulation. RAMP3, which is an interacting partner of CaSR (section 3.3.3, chapter 3) contains a PDZ-binding motif that interacts with NSF or NHERF-1 to affect internalization and recycling of the CLR [209, 210]. Accordingly, it can be hypothesised that similar consequences may lead to differences in regulation of the CaSR following agonist stimulation.

Although the observations of receptor interactions and signalling from this project were based on *in vitro* studies, they can be expanded onto a physiological level in future, an idea which was also proposed by Bouschet *et al* [157]. Accordingly, apart from confirming the interaction of

CaSR and RAMPs in physiology, it will be interesting to test whether the variation in the physiological expression of RAMPs [156, 182, 183, 214, 215] can alter their availability and consequently cell surface trafficking and signalling of the CaSR. This will help in determining whether RAMPs play a role in Ca^{2+} homeostasis. Although further studies need to be done to confirm the role of RAMP1 in CaSR signalling, it will be very interesting to study whether RAMP1 can be used as a target to develop calcilytics - which have a potential to treat disorders like osteoporosis. The precedent for RAMP as drug targets has already been provided by studies for conditions such as migraine (involving CGRP receptor) [333], and cancer (anti-RAMP3 antibodies significantly reduce tumour burden in mice, Richards GO unpublished data).

Future work:

Further work elucidating the residues of the CaSR and RAMPs responsible for the interaction will be important. This information will help in providing key structural information of this receptor complex. FRET-based approaches have been used by other researchers in this regard. An approach measuring bioluminescence resonance energy transfer (BRET) signal between different TM domain mutants of the secretin receptor and RAMP3 has helped to identify TM6 and TM7 responsible for the interaction [175]. A similar approach using sensitized emission FRET can be used to identify whether the TM domain of CaSR is involved in the interaction with the RAMPs. ECD mutants of CaSR cannot be used since the ECD is responsible for the formation of dimer (obligatory for its function), and so RAMP ECD chimeras can be created instead by swapping RAMP1 or RAMP3 ECD with RAMP2 ECD; since RAMP2 does not interact with CaSR. Once the domains responsible are identified, the effect of point mutations of certain residues on change in cell surface FRET can be tested to identify the exact residues responsible for complex formation. It is also essential to study the role of RAMP3 in CaSR signalling. Further characterization of the signalling pathway in presence of either RAMP1 or RAMP3 should be done at both G-protein and downstream levels. To differentiate the signalling at the G-protein level, techniques incorporating antibodies against the active GTP-bound G-proteins (NewEast biosciences) [263] can be used. These antibodies can be immobilized to fluorescent beads with distinct emission profiles and subsequently enabling multiple G-protein activation measurement from a single reaction. Alternatively, high-throughput label-free technique using

cellular dielectric spectroscopy technology [334] could be used in future. This technique identifies the specific G-protein activation based on the impedance measurements of the applied electric current as it flows through a cell monolayer. Next, the difference in activation of downstream effectors by the CaSR-complex in presence of either RAMP (1 or 3) should be deciphered by measuring intracellular Ca^{2+} activation, cAMP activation and ERK phosphorylation in presence of inhibitors of signalling molecules like U73122 (PLCβ inhibitor), Wortmannin (PIP2 inhibitor), thapsigargin (inhibitor of ER Ca^{2+} pumps), PTX (inhibitor of Gi protein), PMA (PKC inhibitor) and ERK 1/2 inhibitor.

First evidence for association of RAMP with GPRC6A:

This study also identified a novel interaction of RAMP with another family C GPCR using FRET. GPRC6A is a recently identified member of family C GPCRs and shares maximum homology with CaSR (34% aa sequence identity) [158]. Studies using c-myc tagged hGPRC6A have reported poor or no cell surface expression of GPRC6A based on cell types [158, 159]. This situation is similar to that observed for CaSR, where no cell surface expression was observed in COS-7 cells by us (chapter 3, figure 3.3.14) and Bouschet *et al* [157]. Having already established the interaction of RAMPs with CaSR using FRET technique (section 3.3.3, chapter 3), it was hypothesised that RAMPs may also facilitate the cell surface expression of GPRC6A. It was observed conclusively that RAMP1 but not 2 and 3 could traffic GPRC6A to the cell surface in COS-7 cells using this technique (chapter 3, section 3.3.4). It is known that RAMP1 cannot reach the cell surface on its own [156, 193]. This evidence supports the observation that FRET measured is because of the specific interaction with GPRC6A, and is not an artefact of RAMP1 trafficking to the cell surface independently. There is an ER retention motif on the C-tail of GPRC6A, and attempts of co-expressing $GABAB_2$ or T1R3 receptors have proved to be futile to facilitate the cell surface expression of GPRC6A [159]. The presence of an ER retention motif on the CaSR also prevents the dimer from escaping the ER [93]. It is known in the case of CaSR that the core-glycosylated form of the receptor which is trapped inside the ER interacts with RAMP1, which then causes its exit to the Golgi apparatus where it is terminally glycosylated and is finally transported to the cell-surface in the form of a receptor complex [157]. Similarly, it can be hypothesised that the interaction with RAMP1 facilitates the exit of the GPRC6A from the ER to

the Golgi, where it is terminally glycosylated and then delivered to the cell-surface as observed by FRET (chapter 3, section 3.3.4), possibly in the form of a mature glycosylated receptor complex.

Interestingly, it was observed that the FRET efficiency between GPRC6A and RAMP1; and CaSR and RAMP1 was not significantly different, however the fraction of RAMP1 involved in FRET complex with CaSR was ~1.45 fold higher than with GPRC6A (table 3.3.3 vs table 3.3.4, chapter 3). This comparison probably suggests a lower number of RAMP1 molecules in the FRET complex with GPRC6A than with the CaSR. This means that less molecules of RAMP1 are required for cell-surface trafficking of GPRC6A than for the CaSR.

An observation from this study indicating an interaction of CaSR with RAMP1 in an endogenous expression system (section 4.3.10, chapter 4), certainly encourages a similar possibility in the case of GPRC6A and RAMP1 interaction. It is known that GPRC6A binds various ligands such as L-aa [159, 160], divalent ions and calcimimetic [165], osteocalcin (in presence of Ca^{2+}) [165, 168] and testosterone [170]. The alignment of CaSR with GPRC6A has shown that the Ca^{2+} and calcimimetic binding sites of CaSR are conserved in GPRC6A [165]. Since, RAMP1 is characteristically involved in the ligand binding of other GPCRs (CGRP receptor-CLR+RAMP1) [200], it should be tested whether it aids ligand binding selectivity of GPRC6A. Additionally, as discovered in this project in case of the CaSR, it will be important to test whether RAMP1 is involved in the signalling of GPRC6A. Of note, two different GPRC6A knock-out mice models-global exon-2 (coding ECD) and exon-6 (coding TMD and C-tail) null mice have provided interesting evidence on the functions of these segments of the receptor. *Gprc6a*$^{-/-}$ mice lacking exon-2 (ECD) exhibited osteopenia, hepatic steatosis (fatty liver), hyperglycaemia, glucose intolerance and insulin resistance as well as increased renal Ca^{2+} and phosphorous excretion [161, 166]. In contrast, *Gprc6a*$^{-/-}$ mice lacking exon 6 (TMD and C-tail), exhibited no difference in phenotype from wild-type [167]. Accordingly, it can be hypothesised that the ECD of GPRC6A is essential for ligand-sensing for metabolic signals, where the presence of the TMD and C-tail is not essential. One hypothesis that can be proposed is that GPRC6A interacts with an accessory protein like RAMP1, which can play a role in its signalling. Also, the effects of various RAMP1

mutants on the effect of GPRC6A trafficking and signalling should be studied in order to establish which residues are responsible for the interaction and also establish a role of RAMP1 in the signalling of the GPRC6A. This approach has already been used successfully with the CLR [201].

Conclusions:

In conclusion, a deeper insight into the interaction of CaSR and RAMPs has been provided by this study which points towards the presence of a higher oligomeric receptor-complex with more than one RAMP3 molecule participating in the interaction. Furthermore, the results indicate for the first time that RAMP1 possibly traffics the CaSR to the cell-surface at endogenous expression levels demonstrating a physiological interaction. Another novel finding from this study is that RAMP1 plays a role in CaSR signalling in TT cells. Further confirmation of this effect might lead to evidences regarding role of RAMPs contributing towards the pleiotropic nature of ligand binding and signalling of the CaSR and its subsequent functioning in Ca^{2+} homeostasis. Consequently, RAMP1 may be proven as an important target for development of calcilytics and drugs targeting both CaSR and RAMP1 might prove to be more efficacious than current strategies.

Furthermore, a novel interaction between GPRC6A and RAMP1 has been discovered using FRET technique. This discovery opens areas of further research regarding the role of RAMPs in GPRC6A function of processing a variety of nutritional and hormonal anabolic signals and co-ordinating the functions of multiple organs in response to changes of the signals.

CHAPTER 7: APPENDIX

Part-1: Appendix for materials and methods:

DNA loading buffer:
23.54mM xylene or 3.73mM bromophenol blue
1.16M sucrose

TaqMan® gene specific inventoried assay accession numbers

Gene	Assay accession number
Human RAMP1	Hs00195288_m1
Human RAMP2	Hs00359352_m1
Human RAMP3	Hs00234665_m1
Human CaSR	Hs01047795_m1
Human β-actin	Hs99999903_m1
Human HPRT1	Hs01003267_m1

5X Tris-borate EDTA (TBE) recipe:
0.45M Tris-Borate
0.01 M EDTA; pH 8.3

Cell lysis buffer:
150mM NaCl
10mM Tris Cl
2mM EDTA
100mM Iodoacetamide
1% Triton X-100
1% NP-40 (Roche),
1X Protease inhibitor cocktail
pH 7.4 at 25^{o}C.

Recipe for 10ml 8% SDS-PAGE separating gel:

Component	Volume added for 10ml gel
Distilled H_20	4.6ml
Tris Cl (pH 8.8)	2.5ml
SDS 10% (w/v)	100µl
A/bis A (30%:0.8%)	2.67ml
APS (10%) (made fresh)	100µl
TEMED	10µl

Recipe for 10ml 10% SDS-PAGE separating gel:

Component	**Volume added for 10ml gel**
Distilled H_20	4.0ml
Tris Cl (pH 8.8)	2.5ml
SDS 10% (w/v)	100µl
A/bis A (30%:0.8%)	3.33ml
APS (10%) (made fresh)	100µl
TEMED	10µl

Recipe for 10ml 12% SDS-PAGE separating gel:

Component	Volume added for 10ml gel
Distilled H_20	3.3ml
Tris Cl (pH 8.8)	2.5ml
SDS 10% (w/v)	100µl
A/bis A (30%:0.8%)	4.0ml
APS (10%) (made fresh)	100µl
TEMED	10µl

Recipe for 10ml 5% SDS-PAGE stacking gel:

Component	Volume added for 10ml gel
Distilled H_20	5.67ml
Tris Cl (pH 6.8)	2.5ml
SDS 10% (w/v)	100µl
A/bis A (30%:0.8%)	1.67ml
APS (10%)	50µl
TEMED	20µl

Running buffer recipe:
0.2M Glycine,
26mM Tris base,
4% SDS

6X Laemmli buffer recipe:
375mM Tris HCl
9% SDS
50% glycerol
0.03% bromophenol blue
600mM DTT
pH 6.8 at 25^{o}C.

Transfer buffer recipe:
25mM Tris base
200mM glycine
20% (v/v) methanol

Tris-buffered saline (TBS):
0.136M NaCl
2.68mM KCl
24.7mM Tris base
pH 7.4 using HCl at 25^{o}C.

NEbuffer 2 composition:
50mM NaCl
10mM Tris HCl
10mM $MgCl_2$

1mM DTT
pH 7.9 at 25^{o}C

Antarctic phosphatase buffer composition:
50mM Bis-Tris-propane HCl
1mM $MgCl_2$
0.1mM $ZnCl_2$
pH 6.0 at 25^{o}C

T4 DNA ligase reaction buffer:
50mM Tris-HCl,
10mM $MgCl_2$
1mM ATP
10mM DTT
pH 7.5 at 25^{o}C

Electroporation buffer recipe:
20mM HEPES
135mM KCl
2mM $MgCl_2$
0.5% Ficoll 400 (Sigma Aldrich)
2mM ATP (added before use)
5mM glutathione (added before use)
pH 7.6 using KOH at 25^{o}C.

Mowiol recipe
2.4g Mowiol (Sigma Aldrich), 6ml glycerol and 6ml water were mixed for 2hr and then 12ml of 200mM Tris-HCl, pH 8.5 was added with a further incubation for 5-6hr at 50^{o}C. The solution was then centrifuged at 2000g for 10min at room temperature and then aliquoted in 1.5ml tubes and stored at -20^{o}C.

Physiological Salt Solution recipe:
100mM NaCl
5.4mM KCl
1.2mM $MgSO_4$
1.5mM / 2mM $CaCl_2$

5.5mM Glucose
6mM $NaHCO_3$
1.2mM Na_2HPO_4
20mM HEPES
pH 7.4 at 25^{o}C.

1x NEBuffer Ssp1:
50mM NaCl
100mM Tris-HCl
10mM $MgCl_2$
0.025% Triton X-100
pH 7.5 at 25^{o}C.

Differentiation medium recipe:
Complete DMEM containing:
10nM Dexamethasone (Sigma Aldrich)
2mM β-glycerolphosphate (Sigma-Aldrich)
50µg/ml L-ascorbic acid (Sigma Aldrich)

Sodium Citrate buffer recipe:
135mM KCl
15mM Sodium citrate dehydrate
pH 7.5 at 25^{o}C

Part:2. Appendix for results:

7.1 Determining the expression of RAMPs in COS-7 cell line:

To check for presence of RAMPs in COS-7 cells, RT-PCR was performed as described in section 2.7, chapter 2. pcDNA 3.1 RAMP vectors were used as positive controls and HPRT1 was used as an endogenous control. Figure 7.1-7.3 show the absence of RAMP1, 2 and 3 respectively in COS-7 samples (Lane 2,3). Lane 1 in figure 7.1 and 7.2 show the correct sized amplicon for the pcDNA3.1 RAMP 1 and 2 positive control cDNA samples. However, pcDNA 3.1 RAMP3 (Lane1, figure 7.3) did not give correct sized product. This was because the reverse primer was complimentary to the region of exon 3 which was not present in the RAMP3 sequence of pcDNA 3.1 RAMP3. Database search revealed that the corresponding sequence was 3'UTR and so was not present in the pcDNA3.1 RAMP3 vector. However, the absence of RAMP3 along with other RAMPs in COS-7 cells was confirmed using real-time PCR where its expression remained undetermined; whereas a Ct value of 32 was obtained for 0.5ng of human lung cDNA sample.

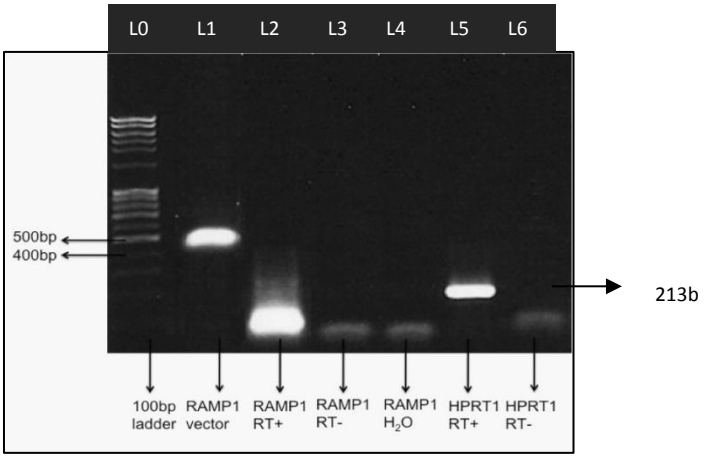

Figure 7.1: Expression of RAMP1 in COS-7 cell determined by RT-PCR:

COS-7 cDNA and pcDNA3.1 RAMP1 vector DNA were amplified using RAMP1 primers for 35 cycles in thermocycler and the products were separated on 1% agarose gel containing and visualized under UV light. (L0) 100bp DNA ladder Amplified products by lane (L1) pcDNA3.1 RAMP1 vector (L2) COS-7 RT+ (L3) COS-7 RT- (L4) H_2O control (L5) HPRT1 RT+ (L6) HPRT1 RT-. The expected product size for RAMP1 is 445bp and HPRT1 is 213bp.

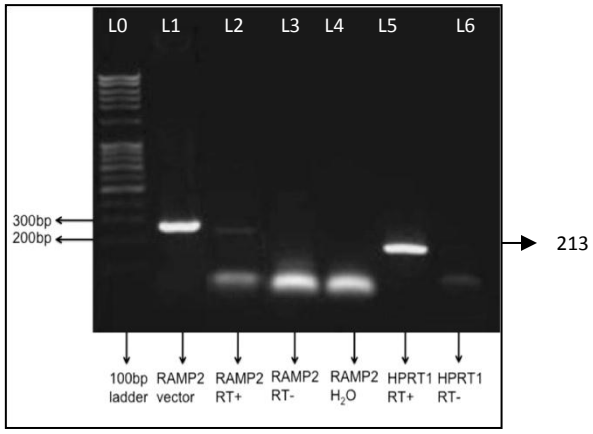

Figure 7.2: Expression of RAMP2 in COS-7 cell determined by RT-PCR

COS-7 cDNA and pcDNA3.1 RAMP2 vector DNA were amplified using RAMP2 primers for 35 cycles in thermocycler and the products were separated on 1% agarose gel containing and visualized under UV light. (L0) 100bp DNA ladder Amplified products by lane (L1) pcDNA3.1 RAMP2 vector (L2) COS-7 RT+ (L3) COS-7 RT- (L4) H_2O control (L5) HPRT1 RT+ (L6) HPRT1 RT-. The expected product size for RAMP2 is 282bp and HPRT1 is 213bp.

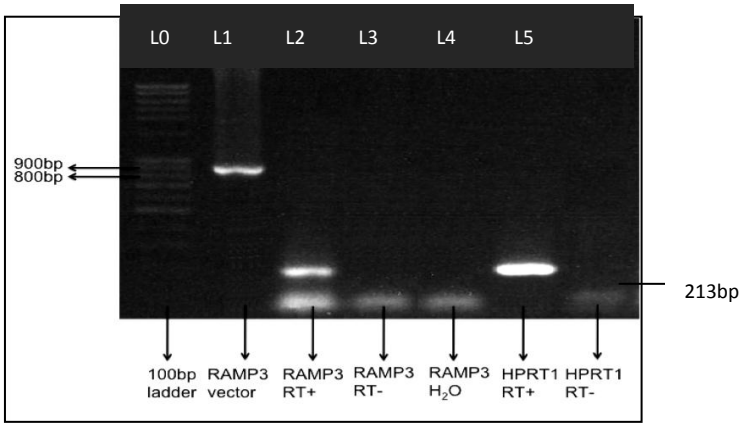

Figure 7.3:: Expression of RAMP3 in COS-7 cell determined by RT-PCR.
COS-7 cDNA and pcDNA3.1 RAMP3 vector DNA were amplified using RAMP3 primers for 35 cycles in thermocycler and the products were separated on 1% agarose gel containing ethidium bromide and visualized under UV light. (L0) 100bp DNA ladder Amplified products by lane (L1) pcDNA3.1 RAMP3 vector (L2) COS-7 RT+ (L3) COS-7 RT- (L4) H_2O control (L5) HPRT1 RT+ (L6) HPRT1 RT-. The expected product size for RAMP3 is 693bp and HPRT1 is 213bp.

7.2. Donor bleaching technique:

Donor bleaching technique was used in order to establish FRET methodology according to [230]. Cerulean pcDNA3.1 and Cerulean-citrine fusion pcDNA3.1 were transfected in COS-7 cells and their bleaching kinetics is shown in figure 7.4 (A) and (B) respectively. It can be seen that cerulean exhibited bi-exponential decay. Kfast and K slow (sec^{-1}) for cerulean alone were 0.9 and 0.0088 and for cerulean in cerulean-citrine fusion were 1.96 and 0.0188 respectively. There was no statistical difference between the decay rates between (A) and (B) as shown by graph in (C) as analysed by unpaired t-test.

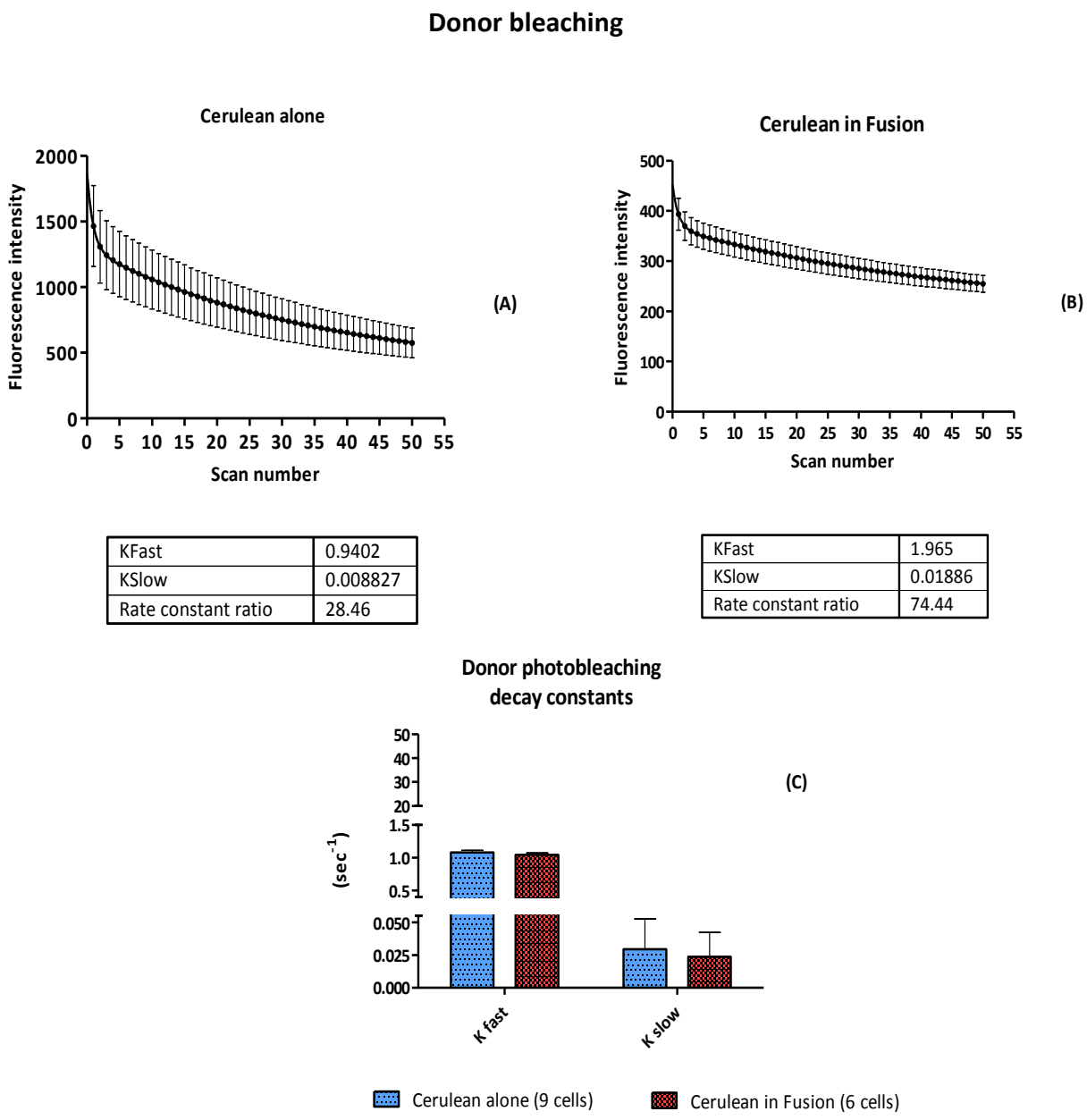

Figure 7.4: Donor bleaching technique:

Cerulean alone or Cerulean-citrine fusion construct were excited sequentially 50 times at donor wavelength and images were collected. Whole cell intensity was calculated (A) bleaching curve of cerulean alone (B) bleaching curve for cerulean in Cerulean-citrine fusion (C) comparison between decay constants between (A) and (B). number of cells analysed for cer alone were 9 and for cerulean-citrine fusion were 6.

Values of FRET stoichiometric constants:

Constant	Mean /± SD	Number of ROIs	Number of cells analysed
β	0.31	-	8-10
α	0.126	-	8-10
γ	0.30 ± 0.02	41	9
ξ	0.20 ± 0.03	27	6
E_c	32.80 ± 2.9	27	6

Table 7.1: Calculated mean/ ± SD values of FRET stoichiometric constants:
β and α were calculated by Bleed through calc plugin in ImageJ using Cer only and citrine only transfected COS-7 cell images. γ, ξ and E_c were calculated using the equations given in the section 3.2.6 and 3.2.7 of methods using the donor, acceptor and the FRET intensities measured by drawing ROIs on the positive control citrine-cerulean fusion images. The table shows the mean ± SD values of the constants calculated and the number of ROIs and cells used in analysis

7.3. Detecting the presence of G_α proteins in COS7 transfected membranes:

To detect the presence of specific subtypes of G_α proteins in COS-7 transfected membranes preparations, CaSR+RAMP1 membranes were subjected to western blotting as described in section 2.12, chapter 2 using the same antibodies used in the SPA for G_α proteins. Bands were observed for $G_{\alpha s}$ at ~22 KDa, ~25 KDa, ~30-40 KDa, and 2 bands between 40-50KDa (Figure 7.5, Lane 1). For $G_{\alpha i}$ (Figure 7.5, lane 2) bands were observed at ~22 KDa, ~40KDa and ~45 KDa and for $G_{\alpha q}$ bands were observed at ~22 KDa and ~42 KDa.

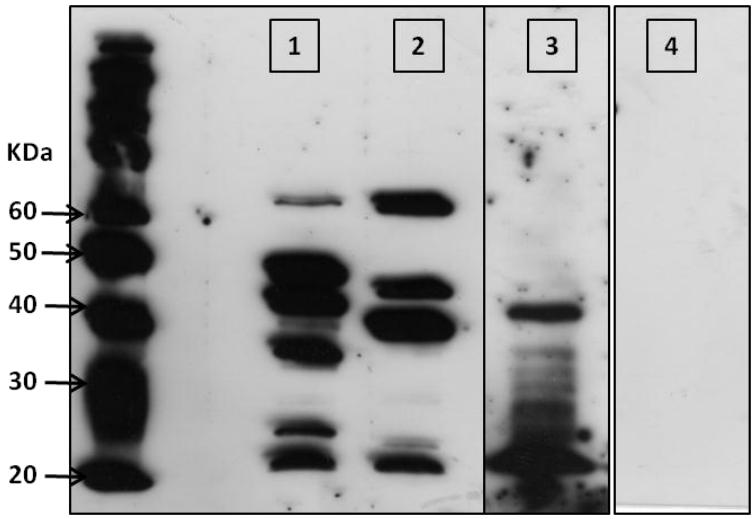

Figure 7.5: Presence of G_{α}-proteins in membrane preparations

CaSR+RAMP1 COS7 membrane preparation were immunoblotted to check the presence of G proteins. 10µg/well CaSR+RAMP1 COS7 membranes were separated on a -10**%** gel by SDS-PAGE and transferred on a PVDF membrane. Specific G-proteins were detected using specific antibodies and were revealed using an HRP conjugated secondary antibody on a hyperfilm. Lane 1, $G_{\alpha s}$, Lane 2 $G_{\alpha i}$, Lane 3 shows $G_{\alpha q}$. Lane 4 shows background by the secondary antibody alone.

7.4. Expression of CaSR in CaSR+RAMP1/3 membranes:

To check for the expression of CaSR in CaSR+RAMP1/3 membranes, 80µg of protein sample was separated on 8% SDS-PAGE gel and probed for the presence of CaSR. Empty COS-7 membranes were used as a negative control. Figure 7.6 shows specific band for CaSR in CasR+RAMP1 and 3 membranes (Lanes 2 and 3 respectively) which is not present in empty COS-7 membranes (Lane 1).

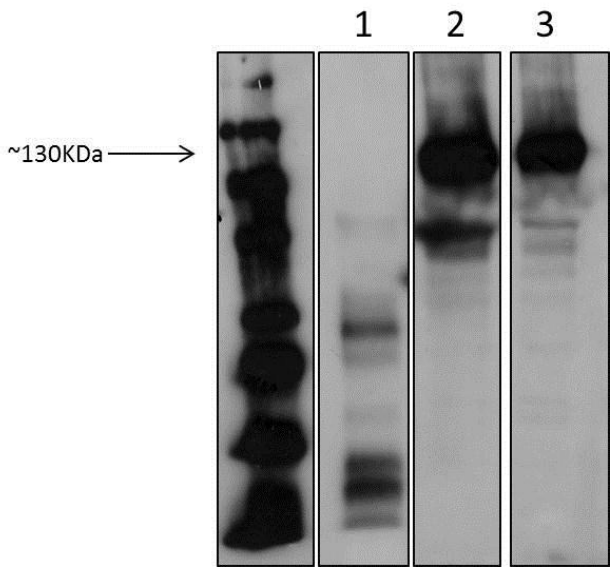

Figure 7.6: Presence of CaSR in membrane preparations

Empty COS-7 (lane 1), CaSR+RAMP1 and 3 (lane 2 and 3 respectively) membranes were immunoblotted to check the presence of CaSR. 80µg/well membranes were separated on 8**%** gel by SDS-PAGE and transferred on a PVDF membrane. CaSR protein was detected using monoclonal antibodies against CaSR and was revealed using an HRP conjugated secondary antibody on a hyperfilm.

7.5. Validation of COS-7 stable cell lines for mRNA expression of receptor components:

In order to study the role of RAMPs in CaSR signalling, COS-7 cells were stably transfected with CaSR, RAMP1, 2, and 3. mRNA expression of the transfected receptor components were measured by real time PCR using Taqman® probes**.** Expression of CaSR and RAMPs was normalized to ActB which was used as a house keeping gene and are shown on Y axis as fold change in %. The average Ct values for each gene in all the stable COS-7 cells are shown in the table (figure 7.7). CaSR mRNA expression was not detectable in COS-7 empty cells.

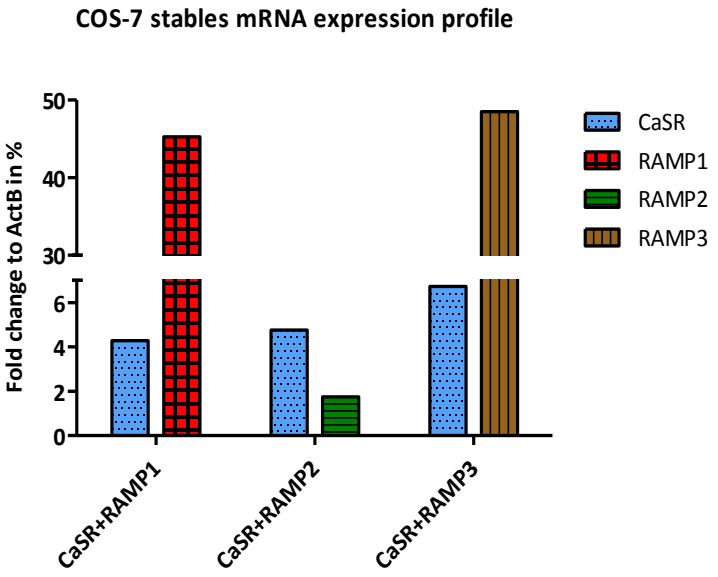

Avg Ct values

	CaSR	RAMP1	RAMP2	RAMP3	ActB
CaSR+R1	21.6	18.2	undetermined	undetermined	23.7
CaSR+R2	21.55	undetermined	23	undetermined	23.8
CaSR+R3	21.05	undetermined	undetermined	18.2	23.8

Figure 7.7: Validation of COS-7 stable cell lines for mRNA expression of receptor components

Real time PCR data showing expression of mRNA of the receptor components as fold change to expression ActB which was used to normalize the differences in cDNA loading. The table shows the average Ct values of different genes expressed in CaSR+RAMPs COS-7 stable cell lines. n=1 performed in duplicates.

7.6. Expression of CaSR and RAMPs in TT cells:

mRNA expression:

Expression of CaSR and RAMPs in TT cells was determined using real time PCR and western blotting as described in sections 2.9 and 2.12, chapter 2. Figure 7.8 (A) shows the mRNA expression profile of TT cells determined using Taqman probes in real time PCR. The Ct values observed were 21.5 (CaSR), 26.1 (RAMP1) and 27.1 (RAMP2) and the expression of RAMP3 was not determined. The graph shows the expression of CaSR, RAMP1 and 2 relative to the expression of HPRT1, normalized to Actb.

Protein expression:

CaSR: (Figure 7.8 B) Lane 1 shows specific bands at ~60KDa ~135-140KDa, ~160-170KDa, above 200KDa and fainter bands at ~70 and ~80 KDa for CaSR. There was no background by the secondary antibody alone as shown in Lane 2. CaSR can exist in immature form glycosylated with carbohydrates with high mannose content (130-140kDa immune-reactive band) present intracellularly, as well as in mature form glycosylated with complex carbohydrates (150-160kDa immune-reactive band) located on the cell surface [70, 104]. Accordingly, the band at ~140KDa represents core glycosylated form whereas the 150-160kDa bands correspond to the mature glycosylated form of the CaSR. In HEK-293 CaSR transfected cells, non-reducing SDS-PAGE showed dimeric CaSR at a size greater than 200kDa, a proportion of which got converted into a 160kDa band under reducing conditions. Also, higher oligomeric forms at 280kDa were also observed using cell surface crosslinking [125]. This explains that the higher band at >200kDa observed in figure 7.8 B corresponds to the oligomeric form of the receptor.

RAMP1: (Figure 7.8 C). Bright bands were observed at ~14kDa and ~19KDa both of which have been reported as monomeric bands in the literature [180, 335, 336]. Bands were also seen at ~40 and ~50KDa which have also been reported in literature likely to represent multimeric form [156, 193, 335] as RAMP1 is present in multimeric form inside the cell [156, 193].

RAMP2: (Figure 7.8 D) Multiple bands were observed for RAMP2 with brighter bands at ~22KDa, ~40 and ~65KDa and fainter bands at ~10KDa, ~30KDa, ~50, ~60 and ~70KDa (Figure 7.8 D). Bands at ~22 kDa have been reported for monomers which are possibly glycosylated

[211]. Bands at ~35kDa, ~42kDa, ~50kDa, ~73kDa, have been reported [211, 337, 338]. Based on the reported observations and their inferences by other researchers, it can be suggested that these bands represent unglycosylated/glycosylated dimeric form (35-50kDa) and GPCR complexed forms (~73kDa) [337].

However, it has also been shown that commercially available RAMP antibodies raised against same epitope as the antibodies used in this study but in rabbit instead, are not very specific to RAMPs exclusively and they can detect non-specific targets at ~40kDa, ~50ka and ~35kDa [336]. So, it cannot be disregarded that the bands observed at higher molecular weight could be non-specific targets. However, a study using antibody adsorption method has shown that bands at ~35kDa, ~50kDa and ~73KDa for RAMP2 were specific for RAMP2 [337]. Since, a control peptide to pre-adsorb antibody was not used, a definitive answer for the higher molecular weight bands cannot be given.

RAMP3: (Figure 7.8 E,F) Multiple bands are observed for RAMP3. Brighter bands were seen at ~40, ~42, ~50 and ~60 KDa and three faint bands between 20 and 30 KDa, a faint bands at ~30 and ~35 KDa (Figure 7.8 E). As a positive control for RAMP3, rat brain sample was used (Figure 7.8 F) which shows specific bands at ~18KDa, ~28KDa ad ~33 KDa respectively. Since RAMP3 mRNA was not detected using real-time PCR, the presence of multiple bands on western blot is both surprising and inconclusive. As described earlier in detail in chapter 5, the observation that RAMP3 mRNA was undetectable is convincing, as regression analysis using pcDNA3.1 RAMP3 cDNA construct has shown a linear relationship with a R^2 value of 0.95 (figure 5.3.1, chapter 5). Also transfected COS-7 cells stably expressing CaSR and RAMP3 also show a Ct value of 18.2 for RAMP3, which was not observed for COS-7 non-transfected cells (appendix, figure 7.7). So, rat brain sample was used as a positive control for RAMP3, since it is shown to express RAMP3 at both mRNA and protein levels [337]. Band observed at ~18kDa represents RAMP3 monomer [337], whereas ~28KDa band has been reported to represent fully glycosylated RAMP3 [181] and ~33KDa could represent a RAMP3 dimer (figure 7.8 F). Taken together it suggests that bands observed for RAMP3 are non-specific.

In order to check whether the RAMP1 Ab could bind to RAMP1 in its native conformation in contrast to linearized protein in western blots, immuno-cytochemistry was performed on the TT cells as described in section 2.13, chapter 2. Figure 7.8 (G) shows the staining for RAMP1 in non-permeabilized (top panel) and permeabilized (bottom panel) TT cells. The pattern of staining on the cell membrane can be seen in the non-permeabilized cells, whereas in permeabilized cells, the staining intensity is stronger and staining for RAMP1 protein is seen in the cytoplasm as well. Negligible background staining was observed with control IgG, as a negative control. This result shows that RAMP1 antibody gave specific binding pattern in TT cells, corresponding to RAMP1 expression.

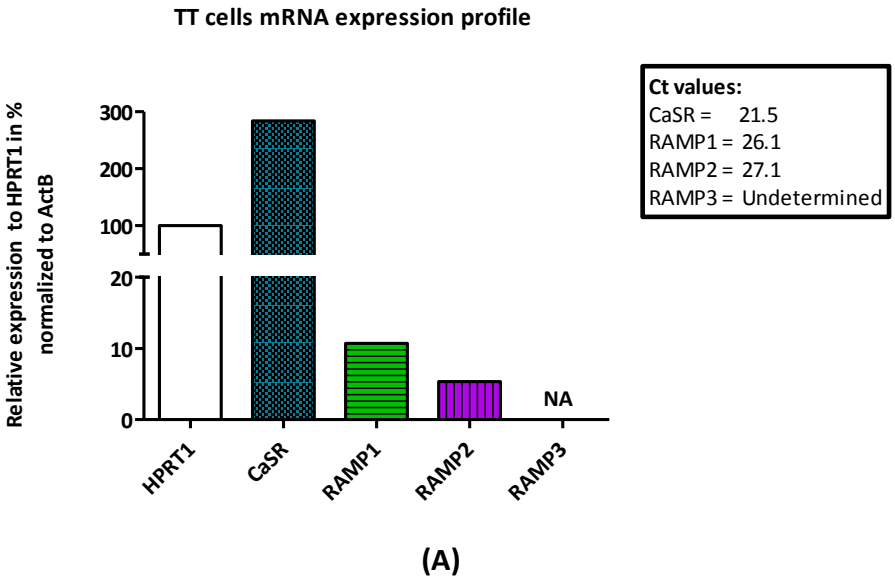

Figure 7.8: Expression of CaSR and RAMPs in TT cells:
(A) mRNA expression of CaSR and RAMPs in TT cells was determined using Taqman probes in real-time PCR. The expression of the genes was normalized to ActB and the expression of CaSR, RAMP1 and 2 is shown as relative to the expression of HPRT1 using the ΔΔCt method. The Ct values are shown in the box. Expression of RAMP3 was undetermined.

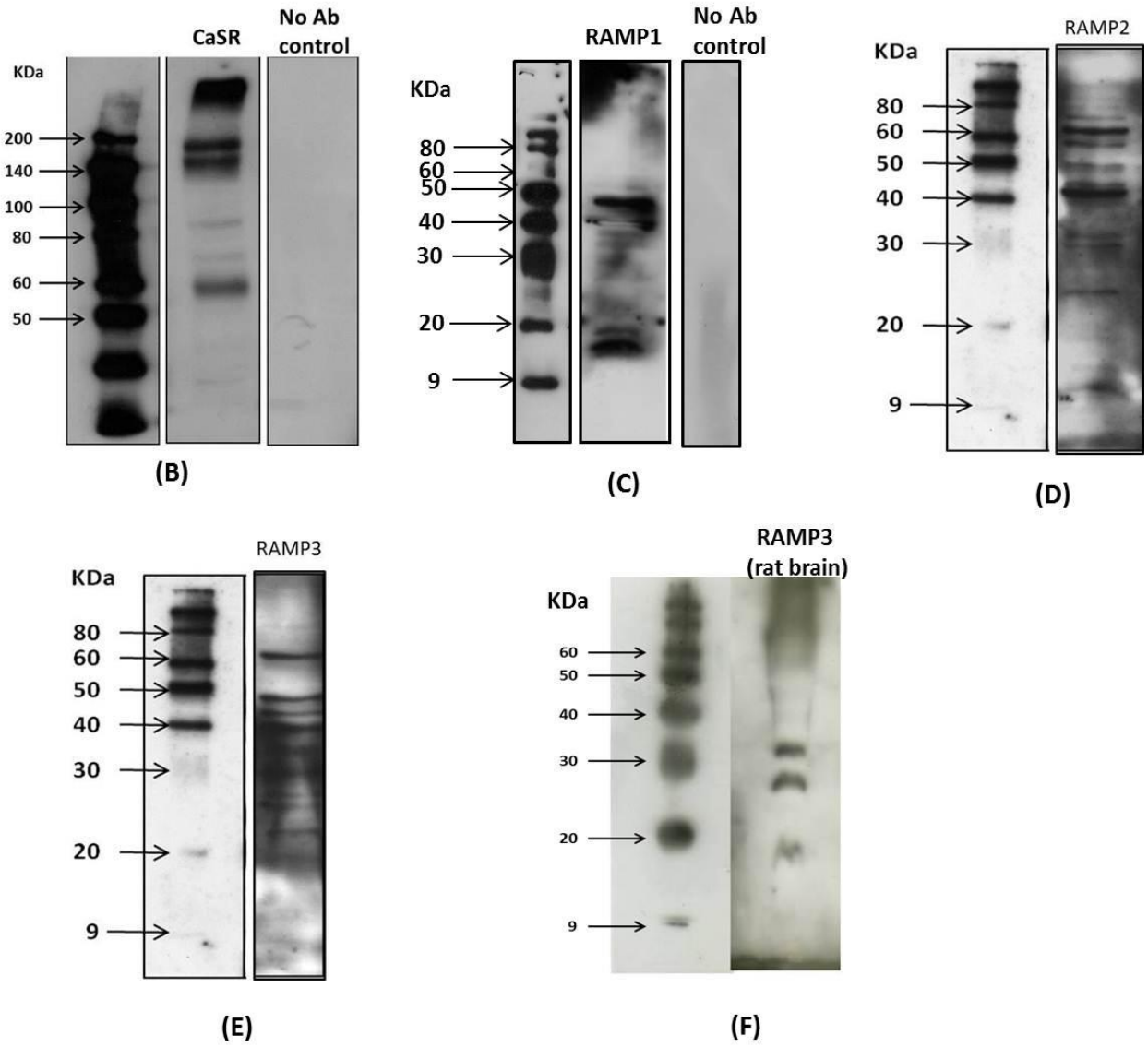

Figure 7.8: Expression of CaSR and RAMPs in TT cells:

Representative western blots for the expression of CaSR (B), RAMP1 (C), RAMP2 (D) and RAMP3 (E) proteins in TT cells and (F) shows the expression of RAMP3 in rat brain as a positive control. 8% polyacrylamide gel for (B) and 12% for (C), (D), (E) and (F) were used to separate 30µg of TT protein by SDS-PAGE and then transferred to PVDF and probed for CaSR and RAMPs using specific antibodies as described in detail in section 2.12 of chapter 2.

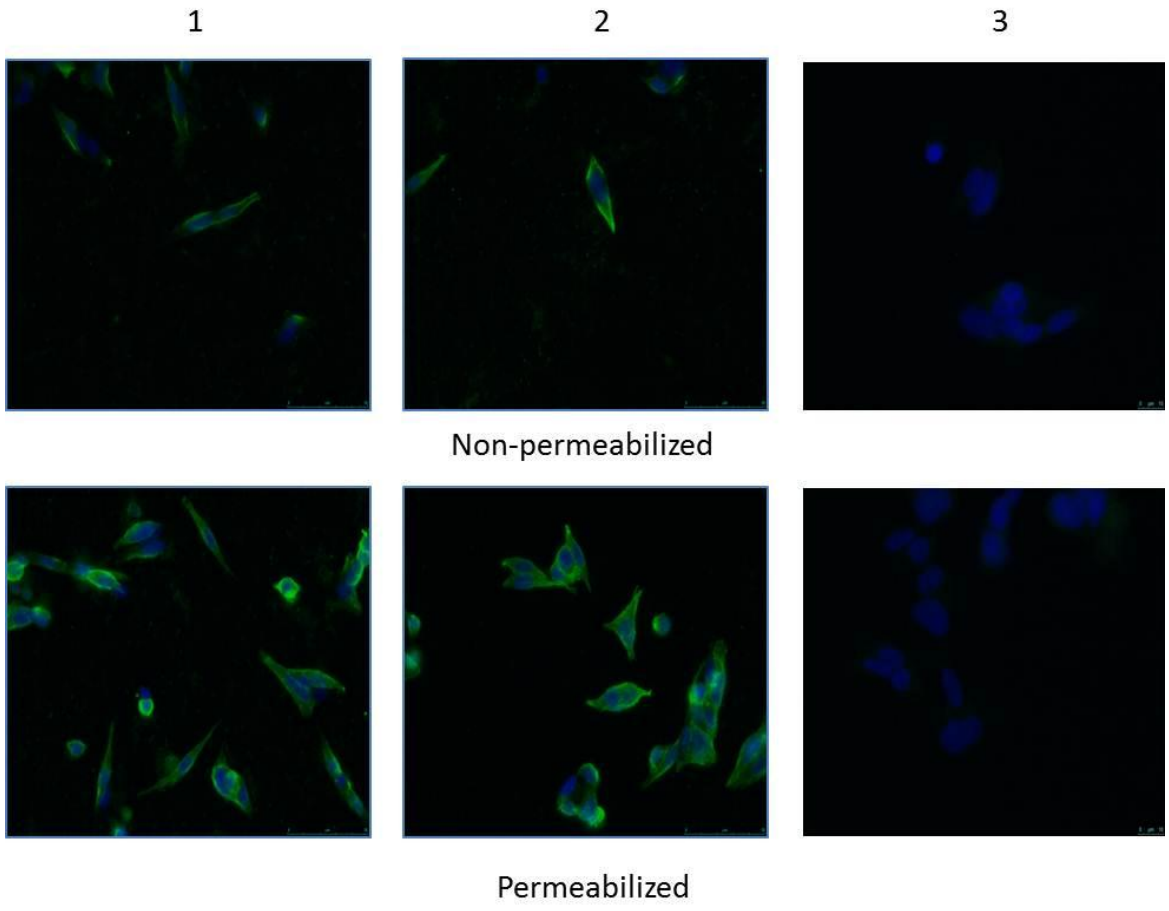

(G)

Figure 7.8: Expression of CaSR and RAMPs in TT cells:
(G) Two representative images (1) and (2) for expression of RAMP1 in non-permeabilized (top panel) and permeabilized (bottom panel) TT cells, shown using immunocytochemistry. Column 3 in both panels show background staining by control IgG. In all the images, the nuclei are counter-stained in blue.

7.7. Effect of DMSO on RAMP1 Ab in experiments to study the effects of combined treatment of RAMP1 Ab and NPS 2390 on CaSR signalling:

In order to test whether combined treatment with 10µg RAMP1 Gt poly Ab and CaSR antagonist NPS 2390 would create a greater effect than the individual treatments, Fluo-4 loaded cells were treated with either 10µg RAMP1 Gt poly Ab/ goat IgG, 10µM or 50 µM of NPS 2390 or both 10µg RAMP1 Gt poly Ab and 10µM NPS 2390 for 45min at 37°C. The effect of CaSR agonist 100µM Neomycin was tested on these cells using live cell imaging system. As shown in figure

7.9 (A) it seemed that the combinatorial treatment was more effective than either 10 or 50µM NPS 2390 or 10µg RAMP1 Gt poly Ab.

However, when the effect of DMSO, which was the solvent for NPS 2390 was tested (vehicle control), shown in figure 7.9 B, similar effect as (A) was seen. This shows that the results observed for combined treatment was due to the non-specific effect of DMSO; giving false positive result. The concentrations of DMSO used: 0.1% and 0.5% corresponded to the v/v addition of NPS 2390 stock into buffer to prepare the desired concentrations used in the experiment.

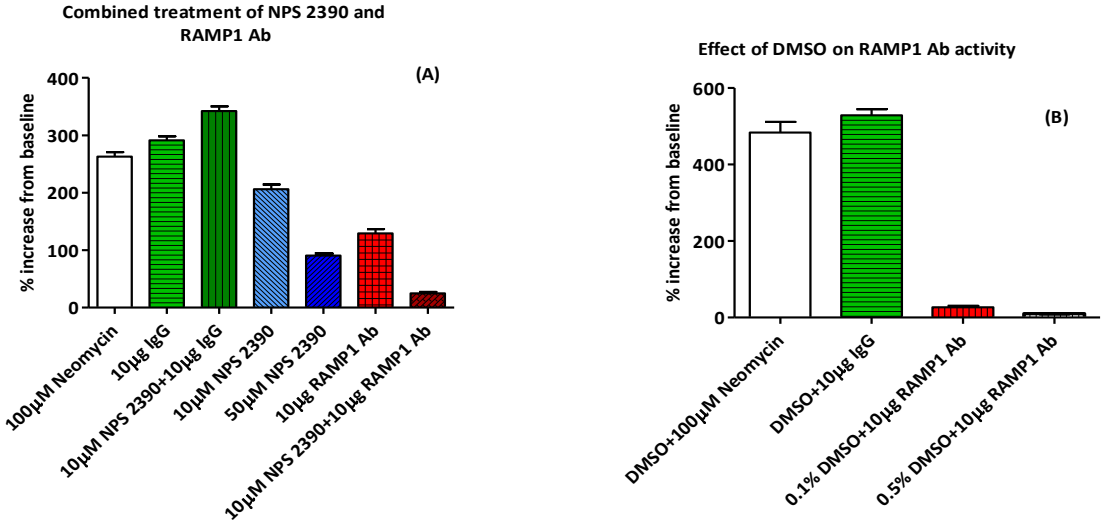

Figure 7.9: Effect of DMSO on RAMP1 Ab in combined treatment of NPS 2390 and RAMP1 Ab

TT cells were pre-treated with either 10µg of RAMP1 goat Poly Ab, 10µM or 50µM NPS 2390 alone or in combination with 10µg RAMP1 Ab or control IgG (A) or 0.1% or 0.5% DMSO with 10µg RAMP1 Ab or control IgG for 45 min at 37°C, before measuring intracellular Ca^{2+} activation by 100µM neomycin. Representative graph for three experiments performed separately.

7.8. Expression of house-keeping genes in cell lines

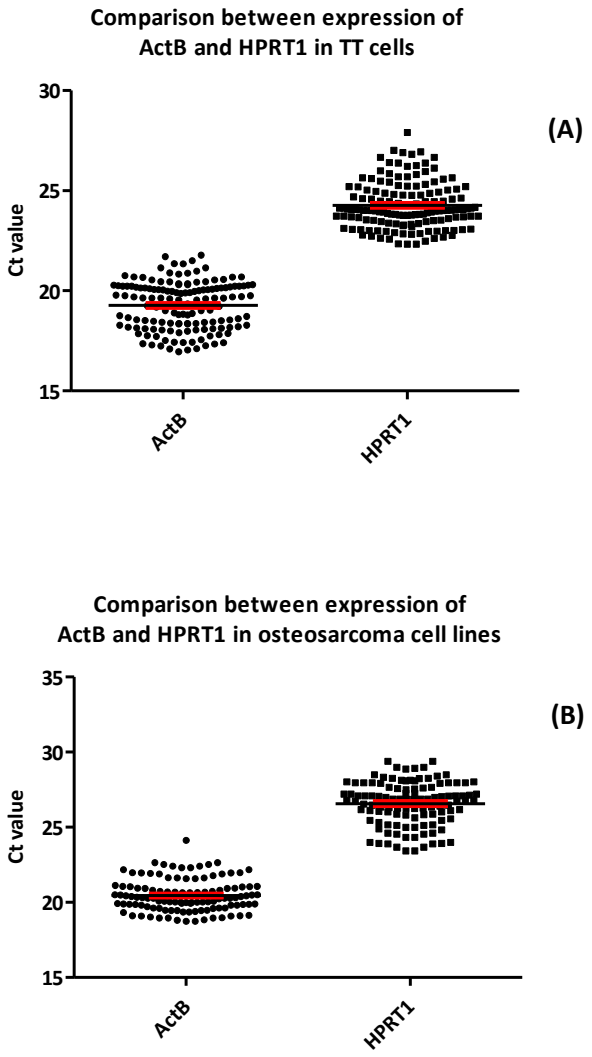

Figure 7.10: Expression levels of ActB and HPRT1 in TT cells and osteosarcoma cell lines:
mRNA expression of ActB and HPRT1 house-keeping genes were analysed in TT cells and osteosarcoma cell lines- MG63, SAOS-2 and TE85 to check the variation in their expression levels using TaqMan® probes in real time PCR. (A) Pooled Ct values for ActB and HPRT1 from all the experiments on TT cells and it appears that ActB is less variable than HPRT1. (B) Pooled Ct values for ActB and HPRT1 from all the experiments on MG63, SAOS-2 and TE85 cells and ActB was found to be less variable in expression than HPRT1.

Bibliography:

1. Pietrobon, D., F. Di Virgilio, and T. Pozzan, *Structural and functional aspects of Ca^{2+} homeostasis in eukaryotic cells.* Eur J Biochem, 1990. **193**(3): p. 599-622.
2. Brown, E.M., *Extracellular Ca^{2+} sensing, regulation of parathyroid cell function, and role of Ca^{2+} and other ions as extracellular (first) messengers.* Physiol Rev, 1991. **71**(2): p. 371-411.
3. Nemeth, E.F. and A. Scarpa, *Cytosolic Ca^{2+} and the regulation of secretion in parathyroid cells.* FEBS Lett, 1986. **203**(1): p. 15-9.
4. Copp, D.H., et al., *Evidence for calcitonin--a new hormone from the parathyroid that lowers blood Ca^{2+}.* Endocrinology, 1962. **70**: p. 638-49.
5. Freichel, M., et al., *Expression of a Ca^{2+}-sensing receptor in a human medullary thyroid carcinoma cell line and its contribution to calcitonin secretion.* Endocrinology, 1996. **137**(9): p. 3842-8.
6. Hughes, M.R., et al., *Regulation of serum 1alpha,25-dihydroxyvitamin D3 by Ca^{2+} and phosphate in the rat.* Science, 1975. **190**(4214): p. 578-80.
7. Xue, Y., et al., *Genetic models show that parathyroid hormone and 1,25-dihydroxyvitamin D3 play distinct and synergistic roles in postnatal mineral ion homeostasis and skeletal development.* Hum Mol Genet, 2005. **14**(11): p. 1515-28.
8. Bouhtiauy, I., D. Lajeunesse, and M.G. Brunette, *Effect of vitamin D depletion on Ca^{2+} transport by the luminal and basolateral membranes of the proximal and distal nephrons.* Endocrinology, 1993. **132**(1): p. 115-20.
9. Silver, J., et al., *Regulation by vitamin D metabolites of parathyroid hormone gene transcription in vivo in the rat.* J Clin Invest, 1986. **78**(5): p. 1296-301.
10. Brown, E.M., et al., *Cloning and characterization of an extracellular $Ca(^{2+})$-sensing receptor from bovine parathyroid.* Nature, 1993. **366**(6455): p. 575-80.
11. Jacoby, E., et al., *The 7 TM DOMAING-protein-coupled receptor target family.* ChemMedChem, 2006. **1**(8): p. 761-82.
12. Palczewski, K., et al., *Crystal structure of rhodopsin: A G protein-coupled receptor.* Science, 2000. **289**(5480): p. 739-45.
13. Rasmussen, S.G., et al., *Crystal structure of the beta2 adrenergic receptor-Gs protein complex.* Nature, 2011. **477**(7366): p. 549-55.
14. Rosenbaum, D.M., et al., *Structure and function of an irreversible agonist-beta(2) adrenoceptor complex.* Nature, 2011. **469**(7329): p. 236-40.
15. Rasmussen, S.G., et al., *Crystal structure of the human beta2 adrenergic G-protein-coupled receptor.* Nature, 2007. **450**(7168): p. 383-7.
16. Granier, S., et al., *Structure of the delta-opioid receptor bound to naltrindole.* Nature, 2012. **485**(7398): p. 400-4.
17. Manglik, A., et al., *Crystal structure of the micro-opioid receptor bound to a morphinan antagonist.* Nature, 2012. **485**(7398): p. 321-6.
18. Kruse, A.C., et al., *Structure and dynamics of the M3 muscarinic acetylcholine receptor.* Nature, 2012. **482**(7386): p. 552-6.
19. Thompson, A.A., et al., *Structure of the nociceptin/orphanin FQ receptor in complex with a peptide mimetic.* Nature, 2012. **485**(7398): p. 395-9.
20. Dror, R.O., et al., *Activation mechanism of the beta2-adrenergic receptor.* Proc Natl Acad Sci U S A, 2011. **108**(46): p. 18684-9.
21. Rasmussen, S.G., et al., *Structure of a nanobody-stabilized active state of the beta(2) adrenoceptor.* Nature, 2011. **469**(7329): p. 175-80.

22. Lebon, G., et al., *Agonist-bound adenosine A2A receptor structures reveal common features of GPCR activation.* Nature, 2011. **474**(7352): p. 521-5.
23. Cabrera-Vera, T.M., et al., *Insights into G protein structure, function, and regulation.* Endocr Rev, 2003. **24**(6): p. 765-81.
24. Lefkowitz, R.J. and S.K. Shenoy, *Transduction of receptor signals by beta-arrestins.* Science, 2005. **308**(5721): p. 512-7.
25. Bockaert, J. and J.P. Pin, *Molecular tinkering of G protein-coupled receptors: an evolutionary success.* EMBO J, 1999. **18**(7): p. 1723-9.
26. Fredriksson, R., et al., *The G-protein-coupled receptors in the human genome form five main families. Phylogenetic analysis, paralogon groups, and fingerprints.* Mol Pharmacol, 2003. **63**(6): p. 1256-72.
27. Harmar, A.J., et al., *IUPHAR-DB: the IUPHAR database of G protein-coupled receptors and ion channels.* Nucleic Acids Res, 2009. **37**(Database issue): p. D680-5.
28. Garrett, J.E., et al., *Molecular cloning and functional expression of human parathyroid Ca^{2+} receptor cDNAs.* J Biol Chem, 1995. **270**(21): p. 12919-25.
29. Nemeth, E.F., et al., *Calcimimetics with potent and selective activity on the parathyroid Ca^{2+} receptor.* Proc Natl Acad Sci U S A, 1998. **95**(7): p. 4040-5.
30. Toribio, R.E., et al., *Parathyroid hormone (PTH) secretion, PTH mRNA and Ca^{2+}-sensing receptor mRNA expression in equine parathyroid cells, and effects of interleukin (IL)-1, IL-6, and tumor necrosis factor-alpha on equine parathyroid cell function.* J Mol Endocrinol, 2003. **31**(3): p. 609-20.
31. Roussanne, M.C., et al., *Human parathyroid cell proliferation in response to Ca^{2+}, NPS R-467, calcitriol and phosphate.* Eur J Clin Invest, 2001. **31**(7): p. 610-6.
32. Kantham, L., et al., *The Ca^{2+}-sensing receptor (CaSR) defends against hypercalcemia independently of its regulation of parathyroid hormone secretion.* Am J Physiol Endocrinol Metab, 2009. **297**(4): p. E915-23.
33. Garrett, J.E., et al., *Calcitonin-secreting cells of the thyroid express an extracellular Ca^{2+} receptor gene.* Endocrinology, 1995. **136**(11): p. 5202-11.
34. Fudge, N.J. and C.S. Kovacs, *Physiological studies in heterozygous Ca^{2+} sensing receptor (CaSR) gene-ablated mice confirm that the CaSR regulates calcitonin release in vivo.* BMC Physiol, 2004. **4**: p. 5.
35. Kos, C.H., et al., *The Ca^{2+}-sensing receptor is required for normal Ca^{2+} homeostasis independent of parathyroid hormone.* J Clin Invest, 2003. **111**(7): p. 1021-8.
36. Riccardi, D., et al., *Localization of the extracellular Ca^{2+}/polyvalent cation-sensing protein in rat kidney.* Am J Physiol, 1998. **274**(3 Pt 2): p. F611-22.
37. Ba, J., D. Brown, and P.A. Friedman, *Ca^{2+}-sensing receptor regulation of PTH-inhibitable proximal tubule phosphate transport.* Am J Physiol Renal Physiol, 2003. **285**(6): p. F1233-43.
38. Wang, W.H., M. Lu, and S.C. Hebert, *Cytochrome P-450 metabolites mediate extracellular Ca($^{2+}$)-induced inhibition of apical K+ channels in the TAL.* Am J Physiol, 1996. **271**(1 Pt 1): p. C103-11.
39. Bland, R., et al., *Constitutive expression of 25-hydroxyvitamin D3-1alpha-hydroxylase in a transformed human proximal tubule cell line: evidence for direct regulation of vitamin D metabolism by Ca^{2+}.* Endocrinology, 1999. **140**(5): p. 2027-34.
40. Egbuna, O., et al., *The full-length Ca^{2+}-sensing receptor dampens the calcemic response to 1alpha,25(OH)2 vitamin D3 in vivo independently of parathyroid hormone.* Am J Physiol Renal Physiol, 2009. **297**(3): p. F720-8.
41. Chattopadhyay, N., et al., *Mitogenic action of Ca^{2+}-sensing receptor on rat calvarial osteoblasts.* Endocrinology, 2004. **145**(7): p. 3451-62.

42. Dvorak, M.M., et al., *Physiological changes in extracellular Ca^{2+} concentration directly control osteoblast function in the absence of calciotropic hormones.* Proc Natl Acad Sci U S A, 2004. **101**(14): p. 5140-5.
43. Chang, W., et al., *The extracellular Ca^{2+}-sensing receptor (CaSR) is a critical modulator of skeletal development.* Sci Signal, 2008. **1**(35): p. ra1.
44. Kameda, T., et al., *Ca^{2+}-sensing receptor in mature osteoclasts, which are bone resorbing cells.* Biochem Biophys Res Commun, 1998. **245**(2): p. 419-22.
45. Mentaverri, R., et al., *The Ca^{2+} sensing receptor is directly involved in both osteoclast differentiation and apoptosis.* FASEB J, 2006. **20**(14): p. 2562-4.
46. Boudot, C., et al., *Implication of the Ca^{2+} sensing receptor and the Phosphoinositide 3-kinase/Akt pathway in the extracellular Ca^{2+}-mediated migration of RAW 264.7 osteoclast precursor cells.* Bone, 2010. **46**(5): p. 1416-23.
47. Dvorak-Ewell, M.M., et al., *Osteoblast extracellular $Ca(^{2+})$ -sensing receptor regulates bone development, mineralization, and turnover.* J Bone Miner Res, 2011. **26**(12): p. 2935-47.
48. Marie, P.J., *The Ca^{2+}-sensing receptor in bone cells: a potential therapeutic target in osteoporosis.* Bone, 2010. **46**(3): p. 571-6.
49. Buchan, A.M., et al., *Mechanism of action of the Ca^{2+}-sensing receptor in human antral gastrin cells.* Gastroenterology, 2001. **120**(5): p. 1128-39.
50. Chattopadhyay, N., et al., *Identification and localization of extracellular $Ca(^{2+})$-sensing receptor in rat intestine.* Am J Physiol, 1998. **274**(1 Pt 1): p. G122-30.
51. Cheng, S.X., et al., *Expression of Ca^{2+}-sensing receptor in rat colonic epithelium: evidence for modulation of fluid secretion.* Am J Physiol Gastrointest Liver Physiol, 2002. **283**(1): p. G240-50.
52. Conigrave, A.D., S.J. Quinn, and E.M. Brown, *L-amino acid sensing by the extracellular Ca^{2+}-sensing receptor.* Proc Natl Acad Sci U S A, 2000. **97**(9): p. 4814-9.
53. Wang, Y., et al., *Amino acids stimulate cholecystokinin release through the Ca^{2+}-sensing receptor.* Am J Physiol Gastrointest Liver Physiol, 2011. **300**(4): p. G528-37.
54. Geibel, J.P. and S.C. Hebert, *The functions and roles of the extracellular Ca^{2+}-sensing receptor along the gastrointestinal tract.* Annu Rev Physiol, 2009. **71**: p. 205-17.
55. Pollak, M.R., et al., *Mutations in the human $Ca(^{2+})$-sensing receptor gene cause familial hypocalciuric hypercalcemia and neonatal severe hyperparathyroidism.* Cell, 1993. **75**(7): p. 1297-303.
56. Law, W.M., Jr. and H. Heath, 3rd, *Familial benign hypercalcemia (hypocalciuric hypercalcemia). Clinical and pathogenetic studies in 21 families.* Ann Intern Med, 1985. **102**(4): p. 511-9.
57. Kifor, O., et al., *A syndrome of hypocalciuric hypercalcemia caused by autoantibodies directed at the Ca^{2+}-sensing receptor.* J Clin Endocrinol Metab, 2003. **88**(1): p. 60-72.
58. Pallais, J.C., et al., *Acquired hypocalciuric hypercalcemia due to autoantibodies against the Ca^{2+}-sensing receptor.* N Engl J Med, 2004. **351**(4): p. 362-9.
59. Cole, D., et al., *Primary neonatal hyperparathyroidism: a devastating neurodevelopmental disorder if left untreated.* J Craniofac Genet Dev Biol, 1990. **10**(2): p. 205-14.
60. Eftekhari, F. and D.K. Yousefzadeh, *Primary infantile hyperparathyroidism: clinical, laboratory, and radiographic features in 21 cases.* Skeletal Radiol, 1982. **8**(3): p. 201-8.
61. Khosla, S., et al., *Ca^{2+} infusion suggests a "set-point" abnormality of parathyroid gland function in familial benign hypercalcemia and more complex disturbances in primary hyperparathyroidism.* J Clin Endocrinol Metab, 1993. **76**(3): p. 715-20.
62. Pearce, S.H., et al., *A familial syndrome of hypocalcemia with hypercalciuria due to mutations in the Ca^{2+}-sensing receptor.* N Engl J Med, 1996. **335**(15): p. 1115-22.
63. Ho, C., et al., *A mouse model of human familial hypocalciuric hypercalcemia and neonatal severe hyperparathyroidism.* Nat Genet, 1995. **11**(4): p. 389-94.

64. Tu, Q., et al., *Rescue of the skeletal phenotype in CasR-deficient mice by transfer onto the Gcm2 null background.* J Clin Invest, 2003. **111**(7): p. 1029-37.
65. Oda, Y., et al., *The Ca^{2+} sensing receptor and its alternatively spliced form in murine epidermal differentiation.* J Biol Chem, 2000. **275**(2): p. 1183-90.
66. Rodriguez, L., et al., *Expression and functional assessment of an alternatively spliced extracellular Ca^{2+}-sensing receptor in growth plate chondrocytes.* Endocrinology, 2005. **146**(12): p. 5294-303.
67. Finney, B., et al., *An exon 5-less splice variant of the extracellular Ca^{2+}-sensing receptor rescues absence of the full-length receptor in the developing mouse lung.* Exp Lung Res, 2011. **37**(5): p. 269-78.
68. Hu, J., et al., *A region in the seven-transmembrane domain of the human Ca^{2+} receptor critical for response to Ca^{2+}.* J Biol Chem, 2005. **280**(6): p. 5113-20.
69. Gama, L. and G.E. Breitwieser, *A carboxyl-terminal domain controls the cooperativity for extracellular Ca^{2+} activation of the human Ca^{2+} sensing receptor. A study with receptor-green fluorescent protein fusions.* J Biol Chem, 1998. **273**(45): p. 29712-8.
70. Bai, M., et al., *Expression and characterization of inactivating and activating mutations in the human Ca^{2+}o-sensing receptor.* J Biol Chem, 1996. **271**(32): p. 19537-45.
71. Quinn, S.J., et al., *The Ca^{2+}-sensing receptor: a target for polyamines.* Am J Physiol, 1997. **273**(4 Pt 1): p. C1315-23.
72. Ruat, M., et al., *Cloned and expressed rat Ca^{2+}-sensing receptor.* J Biol Chem, 1996. **271**(11): p. 5972-5.
73. Chang, W., et al., *Coupling of Ca^{2+} receptors to inositol phosphate and cyclic AMP generation in mammalian cells and Xenopus laevis oocytes and immunodetection of receptor protein by region-specific antipeptide antisera.* J Bone Miner Res, 1998. **13**(4): p. 570-80.
74. Handlogten, M.E., et al., *Extracellular Ca($^{2+}$)-sensing receptor is a promiscuous divalent cation sensor that responds to lead.* Am J Physiol Renal Physiol, 2000. **279**(6): p. F1083-91.
75. Timonov, E.V. and L.N. Silakova, *[Feeding behavior of Trichinella as a leading factor of adaptation to the body of the mammals].* Parazitologiia, 1976. **10**(6): p. 506-13.
76. Riccardi, D., et al., *Cloning and functional expression of a rat kidney extracellular Ca^{2+}/polyvalent cation-sensing receptor.* Proc Natl Acad Sci U S A, 1995. **92**(1): p. 131-5.
77. Faurskov, B. and H.F. Bjerregaard, *Evidence for cadmium mobilization of intracellular Ca^{2+} through a divalent cation receptor in renal distal epithelial A6 cells.* Pflugers Arch, 2002. **445**(1): p. 40-50.
78. Spurney, R.F., et al., *Aluminum is a weak agonist for the Ca^{2+}-sensing receptor.* Kidney Int, 1999. **55**(5): p. 1750-8.
79. Chattopadhyay, N., et al., *The Ca^{2+}-sensing receptor (CaR) is involved in strontium ranelate-induced osteoblast proliferation.* Biochem Pharmacol, 2007. **74**(3): p. 438-47.
80. Hurtel-Lemaire, A.S., et al., *The Ca^{2+}-sensing receptor is involved in strontium ranelate-induced osteoclast apoptosis. New insights into the associated signaling pathways.* J Biol Chem, 2009. **284**(1): p. 575-84.
81. Ward, D.T., S.J. McLarnon, and D. Riccardi, *Aminoglycosides increase intracellular Ca^{2+} levels and ERK activity in proximal tubular OK cells expressing the extracellular Ca^{2+}-sensing receptor.* J Am Soc Nephrol, 2002. **13**(6): p. 1481-9.
82. McLarnon, S., et al., *Aminoglycoside antibiotics induce pH-sensitive activation of the Ca^{2+}-sensing receptor.* Biochem Biophys Res Commun, 2002. **297**(1): p. 71-7.
83. Ye, C., et al., *Amyloid-beta proteins activate Ca($^{2+}$)-permeable channels through Ca^{2+}-sensing receptors.* J Neurosci Res, 1997. **47**(5): p. 547-54.

84. Antonsen, J.E., D.J. Sherrard, and D.L. Andress, *A calcimimetic agent acutely suppresses parathyroid hormone levels in patients with chronic renal failure. Rapid communication.* Kidney Int, 1998. **53**(1): p. 223-7.
85. Goodman, W.G., et al., *A calcimimetic agent lowers plasma parathyroid hormone levels in patients with secondary hyperparathyroidism.* Kidney Int, 2000. **58**(1): p. 436-45.
86. Nemeth, E.F., et al., *Pharmacodynamics of the type II calcimimetic compound cinacalcet HCl.* J Pharmacol Exp Ther, 2004. **308**(2): p. 627-35.
87. Kumar, G.N., et al., *Metabolism and disposition of calcimimetic agent cinacalcet HCl in humans and animal models.* Drug Metab Dispos, 2004. **32**(12): p. 1491-500.
88. Block, G.A., et al., *Cinacalcet for secondary hyperparathyroidism in patients receiving hemodialysis.* N Engl J Med, 2004. **350**(15): p. 1516-25.
89. Fukagawa, M., et al., *Cinacalcet (KRN1493) effectively decreases the serum intact PTH level with favorable control of the serum phosphorus and Ca^{2+} levels in Japanese dialysis patients.* Nephrol Dial Transplant, 2008. **23**(1): p. 328-35.
90. Fishbane, S., et al., *Cinacalcet HCl and concurrent low-dose vitamin D improves treatment of secondary hyperparathyroidism in dialysis patients compared with vitamin D alone: the ACHIEVE study results.* Clin J Am Soc Nephrol, 2008. **3**(6): p. 1718-25.
91. Komaba, H., et al., *Cinacalcet effectively reduces parathyroid hormone secretion and gland volume regardless of pretreatment gland size in patients with secondary hyperparathyroidism.* Clin J Am Soc Nephrol, 2010. **5**(12): p. 2305-14.
92. Huang, Y. and G.E. Breitwieser, *Rescue of Ca^{2+}-sensing receptor mutants by allosteric modulators reveals a conformational checkpoint in receptor biogenesis.* J Biol Chem, 2007. **282**(13): p. 9517-25.
93. Cavanaugh, A., et al., *Ca^{2+}-sensing receptor biosynthesis includes a cotranslational conformational checkpoint and endoplasmic reticulum retention.* J Biol Chem, 2010. **285**(26): p. 19854-64.
94. Nemeth, E.F., et al., *Calcilytic compounds: potent and selective Ca^{2+} receptor antagonists that stimulate secretion of parathyroid hormone.* J Pharmacol Exp Ther, 2001. **299**(1): p. 323-31.
95. Gowen, M., et al., *Antagonizing the parathyroid Ca^{2+} receptor stimulates parathyroid hormone secretion and bone formation in osteopenic rats.* J Clin Invest, 2000. **105**(11): p. 1595-604.
96. Kumar, S., et al., *An orally active Ca^{2+}-sensing receptor antagonist that transiently increases plasma concentrations of PTH and stimulates bone formation.* Bone, 2010. **46**(2): p. 534-42.
97. Widler, L., et al., *1-Alkyl-4-phenyl-6-alkoxy-1H-quinazolin-2-ones: a novel series of potent Ca^{2+}-sensing receptor antagonists.* J Med Chem, 2010. **53**(5): p. 2250-63.
98. Kimura, S., et al., *JTT-305, an orally active Ca^{2+}-sensing receptor antagonist, stimulates transient parathyroid hormone release and bone formation in ovariectomized rats.* Eur J Pharmacol, 2011. **668**(1-2): p. 331-6.
99. O'Hara, P.J., et al., *The ligand-binding domain in metabotropic glutamate receptors is related to bacterial periplasmic binding proteins.* Neuron, 1993. **11**(1): p. 41-52.
100. Kunishima, N., et al., *Structural basis of glutamate recognition by a dimeric metabotropic glutamate receptor.* Nature, 2000. **407**(6807): p. 971-7.
101. Muto, T., et al., *Structures of the extracellular regions of the group II/III metabotropic glutamate receptors.* Proc Natl Acad Sci U S A, 2007. **104**(10): p. 3759-64.
102. Hu, J., O. Hauache, and A.M. Spiegel, *Human Ca^{2+} receptor cysteine-rich domain. Analysis of function of mutant and chimeric receptors.* J Biol Chem, 2000. **275**(21): p. 16382-9.
103. Goldsmith, P.K., et al., *Expression, purification, and biochemical characterization of the amino-terminal extracellular domain of the human Ca^{2+} receptor.* J Biol Chem, 1999. **274**(16): p. 11303-9.

104. Fan, G., et al., *N-linked glycosylation of the human Ca^{2+} receptor is essential for its expression at the cell surface.* Endocrinology, 1997. **138**(5): p. 1916-22.
105. Ray, K., et al., *Identification of the sites of N-linked glycosylation on the human Ca^{2+} receptor and assessment of their role in cell surface expression and signal transduction.* J Biol Chem, 1998. **273**(51): p. 34558-67.
106. Brauner-Osborne, H., et al., *The agonist-binding domain of the Ca^{2+}-sensing receptor is located at the amino-terminal domain.* J Biol Chem, 1999. **274**(26): p. 18382-6.
107. Hammerland, L.G., et al., *Domains determining ligand specificity for Ca^{2+} receptors.* Mol Pharmacol, 1999. **55**(4): p. 642-8.
108. Huang, Y., et al., *Multiple $Ca(^{2+})$-binding sites in the extracellular domain of the $Ca(^{2+})$-sensing receptor corresponding to cooperative $Ca(^{2+})$ response.* Biochemistry, 2009. **48**(2): p. 388-98.
109. Ray, K., et al., *Identification of the cysteine residues in the amino-terminal extracellular domain of the human $Ca(^{2+})$ receptor critical for dimerization. Implications for function of monomeric $Ca(^{2+})$ receptor.* J Biol Chem, 1999. **274**(39): p. 27642-50.
110. Hu, J., et al., *The Venus's-flytrap and cysteine-rich domains of the human Ca^{2+} receptor are not linked by disulfide bonds.* J Biol Chem, 2001. **276**(10): p. 6901-4.
111. Ray, K., et al., *The carboxyl terminus of the human Ca^{2+} receptor. Requirements for cell-surface expression and signal transduction.* J Biol Chem, 1997. **272**(50): p. 31355-61.
112. Hu, J., et al., *Identification of acidic residues in the extracellular loops of the seven-transmembrane domain of the human Ca^{2+} receptor critical for response to Ca^{2+} and a positive allosteric modulator.* J Biol Chem, 2002. **277**(48): p. 46622-31.
113. Ray, K. and J. Northup, *Evidence for distinct cation and calcimimetic compound (NPS 568) recognition domains in the transmembrane regions of the human Ca^{2+} receptor.* J Biol Chem, 2002. **277**(21): p. 18908-13.
114. Chang, W., et al., *Amino acids in the second and third intracellular loops of the parathyroid Ca^{2+}-sensing receptor mediate efficient coupling to phospholipase C.* J Biol Chem, 2000. **275**(26): p. 19955-63.
115. Miedlich, S.U., et al., *Homology modeling of the transmembrane domain of the human Ca^{2+} sensing receptor and localization of an allosteric binding site.* J Biol Chem, 2004. **279**(8): p. 7254-63.
116. Bu, L., et al., *Improved model building and assessment of the Ca^{2+}-sensing receptor transmembrane domain.* Proteins, 2008. **71**(1): p. 215-26.
117. Petrel, C., et al., *Positive and negative allosteric modulators of the Ca^{2+}-sensing receptor interact within overlapping but not identical binding sites in the transmembrane domain.* J Biol Chem, 2004. **279**(18): p. 18990-7.
118. Khan, M.A. and A.D. Conigrave, *Mechanisms of multimodal sensing by extracellular $Ca(^{2+})$-sensing receptors: a domain-based survey of requirements for binding and signalling.* Br J Pharmacol, 2010. **159**(5): p. 1039-50.
119. Bai, M., et al., *Protein kinase C phosphorylation of threonine at position 888 in Ca^{2+}o-sensing receptor (CaR) inhibits coupling to Ca^{2+} store release.* J Biol Chem, 1998. **273**(33): p. 21267-75.
120. Young, S.H., S.V. Wu, and E. Rozengurt, *Ca^{2+}-stimulated Ca^{2+} oscillations produced by the Ca^{2+}-sensing receptor require negative feedback by protein kinase C.* J Biol Chem, 2002. **277**(49): p. 46871-6.
121. Pi, M., et al., *Beta-arrestin- and G protein receptor kinase-mediated Ca^{2+}-sensing receptor desensitization.* Mol Endocrinol, 2005. **19**(4): p. 1078-87.
122. Lorenz, S., et al., *Functional desensitization of the extracellular Ca^{2+}-sensing receptor is regulated via distinct mechanisms: role of G protein-coupled receptor kinases, protein kinase C and beta-arrestins.* Endocrinology, 2007. **148**(5): p. 2398-404.

123. Romano, C., W.L. Yang, and K.L. O'Malley, *Metabotropic glutamate receptor 5 is a disulfide-linked dimer.* J Biol Chem, 1996. **271**(45): p. 28612-6.
124. Kaupmann, K., et al., *GABA(B)-receptor subtypes assemble into functional heteromeric complexes.* Nature, 1998. **396**(6712): p. 683-7.
125. Bai, M., S. Trivedi, and E.M. Brown, *Dimerization of the extracellular Ca^{2+}-sensing receptor (CaR) on the cell surface of CaR-transfected HEK293 cells.* J Biol Chem, 1998. **273**(36): p. 23605-10.
126. Zhang, Z., et al., *The extracellular Ca^{2+}-sensing receptor dimerizes through multiple types of intermolecular interactions.* J Biol Chem, 2001. **276**(7): p. 5316-22.
127. Bai, M., et al., *Intermolecular interactions between dimeric Ca^{2+}-sensing receptor monomers are important for its normal function.* Proc Natl Acad Sci U S A, 1999. **96**(6): p. 2834-9.
128. Arthur, J.M., et al., *Specific coupling of a cation-sensing receptor to G protein alpha-subunits in MDCK cells.* Am J Physiol, 1997. **273**(1 Pt 2): p. F129-35.
129. Gerbino, A., et al., *Termination of cAMP signals by Ca^{2+} and G(alpha)i via extracellular Ca^{2+} sensors: a link to intracellular Ca^{2+} oscillations.* J Cell Biol, 2005. **171**(2): p. 303-12.
130. Huang, C., et al., *The Ca^{2+}-sensing receptor couples to Galpha12/13 to activate phospholipase D in Madin-Darby canine kidney cells.* Am J Physiol Cell Physiol, 2004. **286**(1): p. C22-30.
131. Mamillapalli, R., et al., *Switching of G-protein usage by the Ca^{2+}-sensing receptor reverses its effect on parathyroid hormone-related protein secretion in normal versus malignant breast cells.* J Biol Chem, 2008. **283**(36): p. 24435-47.
132. Kifor, O., et al., *The Ca^{2+}-sensing receptor (CaR) activates phospholipases C, A2, and D in bovine parathyroid and CaR-transfected, human embryonic kidney (HEK293) cells.* J Bone Miner Res, 1997. **12**(5): p. 715-25.
133. Bapty, B.W., et al., *Extracellular Mg2(+)- and Ca2(+)-sensing in mouse distal convoluted tubule cells.* Kidney Int, 1998. **53**(3): p. 583-92.
134. Bradbury, R.A., et al., *Expression of the parathyroid Ca($^{2+}$)-sensing receptor in cytotrophoblasts from human term placenta.* J Endocrinol, 1998. **156**(3): p. 425-30.
135. Bruce, J.I., et al., *Molecular and functional identification of a Ca^{2+} (polyvalent cation)-sensing receptor in rat pancreas.* J Biol Chem, 1999. **274**(29): p. 20561-8.
136. Huang, Z., S.L. Cheng, and E. Slatopolsky, *Sustained activation of the extracellular signal-regulated kinase pathway is required for extracellular Ca^{2+} stimulation of human osteoblast proliferation.* J Biol Chem, 2001. **276**(24): p. 21351-8.
137. Hobson, S.A., et al., *Signal transduction mechanisms linking increased extracellular Ca^{2+} to proliferation in ovarian surface epithelial cells.* Exp Cell Res, 2000. **258**(1): p. 1-11.
138. McNeil, S.E., et al., *Functional Ca^{2+}-sensing receptors in rat fibroblasts are required for activation of SRC kinase and mitogen-activated protein kinase in response to extracellular Ca^{2+}.* J Biol Chem, 1998. **273**(2): p. 1114-20.
139. Hobson, S.A., et al., *Activation of the MAP kinase cascade by exogenous Ca^{2+}-sensing receptor.* Mol Cell Endocrinol, 2003. **200**(1-2): p. 189-98.
140. Bilderback, T.R., et al., *Phosphatidylinositol 3-kinase-dependent, MEK- independent proliferation in response to CaR activation.* Am J Physiol Cell Physiol, 2002. **283**(1): p. C282-8.
141. Kifor, O., et al., *Regulation of MAP kinase by Ca^{2+}-sensing receptor in bovine parathyroid and CaR-transfected HEK293 cells.* Am J Physiol Renal Physiol, 2001. **280**(2): p. F291-302.
142. Corbetta, S., et al., *Mitogen-activated protein kinase cascade in human normal and tumoral parathyroid cells.* J Clin Endocrinol Metab, 2002. **87**(5): p. 2201-5.
143. MacLeod, R.J., N. Chattopadhyay, and E.M. Brown, *PTHrP stimulated by the Ca^{2+}-sensing receptor requires MAP kinase activation.* Am J Physiol Endocrinol Metab, 2003. **284**(2): p. E435-42.

144. Yamaguchi, T., et al., *Activation of p42/44 and p38 mitogen-activated protein kinases by extracellular Ca^{2+}-sensing receptor agonists induces mitogenic responses in the mouse osteoblastic MC3T3-E1 cell line.* Biochem Biophys Res Commun, 2000. **279**(2): p. 363-8.
145. Tfelt-Hansen, J., et al., *Ca^{2+}-sensing receptor stimulates PTHrP release by pathways dependent on PKC, p38 MAPK, JNK, and ERK1/2 in H-500 cells.* Am J Physiol Endocrinol Metab, 2003. **285**(2): p. E329-37.
146. Arthur, J.M., et al., *The Ca^{2+}-sensing receptor stimulates JNK in MDCK cells.* Biochem Biophys Res Commun, 2000. **275**(2): p. 538-41.
147. Jones, K.A., et al., *GABA(B) receptors function as a heteromeric assembly of the subunits GABA(B)R1 and GABA(B)R2.* Nature, 1998. **396**(6712): p. 674-9.
148. Gama, L., S.G. Wilt, and G.E. Breitwieser, *Heterodimerization of Ca^{2+} sensing receptors with metabotropic glutamate receptors in neurons.* J Biol Chem, 2001. **276**(42): p. 39053-9.
149. Cheng, Z., et al., *Type B gamma-aminobutyric acid receptors modulate the function of the extracellular Ca^{2+}-sensing receptor and cell differentiation in murine growth plate chondrocytes.* Endocrinology, 2007. **148**(10): p. 4984-92.
150. Chang, W., et al., *Complex formation with the Type B gamma-aminobutyric acid receptor affects the expression and signal transduction of the extracellular Ca^{2+}-sensing receptor. Studies with HEK-293 cells and neurons.* J Biol Chem, 2007. **282**(34): p. 25030-40.
151. Kifor, O., et al., *The Ca^{2+}-sensing receptor is localized in caveolin-rich plasma membrane domains of bovine parathyroid cells.* J Biol Chem, 1998. **273**(34): p. 21708-13.
152. Kifor, O., et al., *Decreased expression of caveolin-1 and altered regulation of mitogen-activated protein kinase in cultured bovine parathyroid cells and human parathyroid adenomas.* J Clin Endocrinol Metab, 2003. **88**(9): p. 4455-64.
153. Awata, H., et al., *Interaction of the Ca^{2+}-sensing receptor and filamin, a potential scaffolding protein.* J Biol Chem, 2001. **276**(37): p. 34871-9.
154. Hjalm, G., et al., *Filamin-A binds to the carboxyl-terminal tail of the Ca^{2+}-sensing receptor, an interaction that participates in CaR-mediated activation of mitogen-activated protein kinase.* J Biol Chem, 2001. **276**(37): p. 34880-7.
155. Zhang, M. and G.E. Breitwieser, *High affinity interaction with filamin A protects against Ca^{2+}-sensing receptor degradation.* J Biol Chem, 2005. **280**(12): p. 11140-6.
156. McLatchie, L.M., et al., *RAMPs regulate the transport and ligand specificity of the calcitonin-receptor-like receptor.* Nature, 1998. **393**(6683): p. 333-9.
157. Bouschet, T., S. Martin, and J.M. Henley, *Receptor-activity-modifying proteins are required for forward trafficking of the Ca^{2+}-sensing receptor to the plasma membrane.* J Cell Sci, 2005. **118**(Pt 20): p. 4709-20.
158. Wellendorph, P. and H. Brauner-Osborne, *Molecular cloning, expression, and sequence analysis of GPRC6A, a novel family C G-protein-coupled receptor.* Gene, 2004. **335**: p. 37-46.
159. Wellendorph, P., et al., *Deorphanization of GPRC6A: a promiscuous L-alpha-amino acid receptor with preference for basic amino acids.* Mol Pharmacol, 2005. **67**(3): p. 589-97.
160. Kuang, D., et al., *Cloning and characterization of a family C orphan G-protein coupled receptor.* J Neurochem, 2005. **93**(2): p. 383-91.
161. Pi, M., et al., *GPRC6A null mice exhibit osteopenia, feminization and metabolic syndrome.* PLoS One, 2008. **3**(12): p. e3858.
162. Nakamura, E., et al., *Luminal amino acid-sensing cells in gastric mucosa.* Digestion, 2011. **83 Suppl 1**: p. 13-8.
163. Haid, D., P. Widmayer, and H. Breer, *Nutrient sensing receptors in gastric endocrine cells.* J Mol Histol, 2011. **42**(4): p. 355-64.

164. Bystrova, M.F., et al., *Functional expression of the extracellular-Ca^{2+}-sensing receptor in mouse taste cells.* J Cell Sci, 2010. **123**(Pt 6): p. 972-82.
165. Pi, M., et al., *Identification of a novel extracellular cation-sensing G-protein-coupled receptor.* J Biol Chem, 2005. **280**(48): p. 40201-9.
166. Pi, M., et al., *Impaired osteoblast function in GPRC6A null mice.* J Bone Miner Res, 2010. **25**(5): p. 1092-102.
167. Wellendorph, P., et al., *No evidence for a bone phenotype in GPRC6A knockout mice under normal physiological conditions.* J Mol Endocrinol, 2009. **42**(3): p. 215-23.
168. Pi, M., Y. Wu, and L.D. Quarles, *GPRC6A mediates responses to osteocalcin in beta-cells in vitro and pancreas in vivo.* J Bone Miner Res, 2011. **26**(7): p. 1680-3.
169. Ferron, M., et al., *Insulin signaling in osteoblasts integrates bone remodeling and energy metabolism.* Cell, 2010. **142**(2): p. 296-308.
170. Pi, M., A.L. Parrill, and L.D. Quarles, *GPRC6A mediates the non-genomic effects of steroids.* J Biol Chem, 2010. **285**(51): p. 39953-64.
171. Pi, M. and L.D. Quarles, *GPRC6A regulates prostate cancer progression.* Prostate, 2011.
172. Muff, R., et al., *An amylin receptor is revealed following co-transfection of a calcitonin receptor with receptor activity modifying proteins-1 or -3.* Endocrinology, 1999. **140**(6): p. 2924-7.
173. Christopoulos, G., et al., *Multiple amylin receptors arise from receptor activity-modifying protein interaction with the calcitonin receptor gene product.* Mol Pharmacol, 1999. **56**(1): p. 235-42.
174. Christopoulos, A., et al., *Novel receptor partners and function of receptor activity-modifying proteins.* J Biol Chem, 2003. **278**(5): p. 3293-7.
175. Harikumar, K.G., et al., *Molecular basis of association of receptor activity-modifying protein 3 with the family B G protein-coupled secretin receptor.* Biochemistry, 2009. **48**(49): p. 11773-85.
176. Parameswaran, N. and W.S. Spielman, *RAMPs: The past, present and future.* Trends Biochem Sci, 2006. **31**(11): p. 631-8.
177. Kuwasako, K., et al., *The function of extracellular cysteines in the human adrenomedullin receptor.* Hypertens Res, 2003. **26 Suppl**: p. S25-31.
178. Kusano, S., et al., *Crystal structure of the human receptor activity-modifying protein 1 extracellular domain.* Protein Sci, 2008. **17**(11): p. 1907-14.
179. Kusano, S., et al., *Structural basis for extracellular interactions between calcitonin receptor-like receptor and receptor activity-modifying protein 2 for adrenomedullin-specific binding.* Protein Sci, 2011.
180. Flahaut, M., B.C. Rossier, and D. Firsov, *Respective roles of calcitonin receptor-like receptor (CRLR) and receptor activity-modifying proteins (RAMP) in cell surface expression of CRLR/RAMP heterodimeric receptors.* J Biol Chem, 2002. **277**(17): p. 14731-7.
181. Flahaut, M., et al., *N-Glycosylation and conserved cysteine residues in RAMP3 play a critical role for the functional expression of CRLR/RAMP3 adrenomedullin receptor.* Biochemistry, 2003. **42**(34): p. 10333-41.
182. Husmann, K., et al., *Mouse receptor-activity-modifying proteins 1, -2 and -3: amino acid sequence, expression and function.* Mol Cell Endocrinol, 2000. **162**(1-2): p. 35-43.
183. Nagae, T., et al., *Rat receptor-activity-modifying proteins (RAMPs) for adrenomedullin/CGRP receptor: cloning and upregulation in obstructive nephropathy.* Biochem Biophys Res Commun, 2000. **270**(1): p. 89-93.
184. Hay, D.L., et al., *CL/RAMP2 and CL/RAMP3 produce pharmacologically distinct adrenomedullin receptors: a comparison of effects of adrenomedullin22-52, CGRP8-37 and BIBN4096BS.* Br J Pharmacol, 2003. **140**(3): p. 477-86.

185. Buhlmann, N., et al., *A receptor activity modifying protein (RAMP)2-dependent adrenomedullin receptor is a calcitonin gene-related peptide receptor when coexpressed with human RAMP1.* Endocrinology, 1999. **140**(6): p. 2883-90.
186. Kuwasako, K., et al., *Visualization of the calcitonin receptor-like receptor and its receptor activity-modifying proteins during internalization and recycling.* J Biol Chem, 2000. **275**(38): p. 29602-9.
187. Steiner, S., et al., *The function of conserved cysteine residues in the extracellular domain of human receptor-activity-modifying protein.* FEBS Lett, 2003. **555**(2): p. 285-90.
188. Simms, J., et al., *Characterization of the structure of RAMP1 by mutagenesis and molecular modeling.* Biophys J, 2006. **91**(2): p. 662-9.
189. Kuwasako, K., et al., *Functions of the extracellular histidine residues of receptor activity-modifying proteins vary within adrenomedullin receptors.* Biochem Biophys Res Commun, 2008. **377**(1): p. 109-13.
190. Hilairet, S., et al., *Protein-protein interaction and not glycosylation determines the binding selectivity of heterodimers between the calcitonin receptor-like receptor and the receptor activity-modifying proteins.* J Biol Chem, 2001. **276**(31): p. 29575-81.
191. Kuwasako, K., et al., *Functions of the cytoplasmic tails of the human receptor activity-modifying protein components of calcitonin gene-related peptide and adrenomedullin receptors.* J Biol Chem, 2006. **281**(11): p. 7205-13.
192. Udawela, M., et al., *A critical role for the short intracellular C terminus in receptor activity-modifying protein function.* Mol Pharmacol, 2006. **70**(5): p. 1750-60.
193. Hilairet, S., et al., *Agonist-promoted internalization of a ternary complex between calcitonin receptor-like receptor, receptor activity-modifying protein 1 (RAMP1), and beta-arrestin.* J Biol Chem, 2001. **276**(45): p. 42182-90.
194. Steiner, S., et al., *The transmembrane domain of receptor-activity-modifying protein 1 is essential for the functional expression of a calcitonin gene-related peptide receptor.* Biochemistry, 2002. **41**(38): p. 11398-404.
195. Aiyar, N., et al., *Receptor activity modifying proteins interaction with human and porcine calcitonin receptor-like receptor (CRLR) in HEK-293 cells.* Mol Cell Biochem, 2001. **224**(1-2): p. 123-33.
196. Fraser, N.J., et al., *The amino terminus of receptor activity modifying proteins is a critical determinant of glycosylation state and ligand binding of calcitonin receptor-like receptor.* Mol Pharmacol, 1999. **55**(6): p. 1054-9.
197. Hay, D.L., et al., *Pharmacological discrimination of calcitonin receptor: receptor activity-modifying protein complexes.* Mol Pharmacol, 2005. **67**(5): p. 1655-65.
198. Bailey, R.J., et al., *Pharmacological characterisation of rat amylin receptors: implications for the identification of amylin receptor subtypes.* Br J Pharmacol, 2011.
199. Kuwasako, K., et al., *Identification of the human receptor activity-modifying protein 1 domains responsible for agonist binding specificity.* J Biol Chem, 2003. **278**(25): p. 22623-30.
200. ter Haar, E., et al., *Crystal structure of the ectodomain complex of the CGRP receptor, a class-B GPCR, reveals the site of drug antagonism.* Structure, 2010. **18**(9): p. 1083-93.
201. Fitzsimmons, T.J., X. Zhao, and S.A. Wank, *The extracellular domain of receptor activity-modifying protein 1 is sufficient for calcitonin receptor-like receptor function.* J Biol Chem, 2003. **278**(16): p. 14313-20.
202. Kuwasako, K., et al., *The seven amino acids of human RAMP2 (86) and RAMP3 (59) are critical for agonist binding to human adrenomedullin receptors.* J Biol Chem, 2001. **276**(52): p. 49459-65.

203. Simms, J., et al., *Structure-function analysis of RAMP1 by alanine mutagenesis.* Biochemistry, 2009. **48**(1): p. 198-205.
204. Qi, T., et al., *Identification of N-terminal receptor activity-modifying protein residues important for calcitonin gene-related peptide, adrenomedullin, and amylin receptor function.* Mol Pharmacol, 2008. **74**(4): p. 1059-71.
205. Hay, D.L., et al., *Determinants of 1-piperidinecarboxamide, N-[2-[[5-amino-l-[[4-(4-pyridinyl)-l-piperazinyl]carbonyl]pentyl]amino]-1- [(3,5-dibromo-4-hydroxyphenyl)methyl]-2-oxoethyl]-4-(1,4-dihydro-2-oxo-3(2 H)-quinazolinyl) (BIBN4096BS) affinity for calcitonin gene-related peptide and amylin receptors--the role of receptor activity modifying protein 1.* Mol Pharmacol, 2006. **70**(6): p. 1984-91.
206. Qi, T., et al., *Structure-function analysis of amino acid 74 of human RAMP1 and RAMP3 and its role in peptide interactions with adrenomedullin and calcitonin gene-related peptide receptors.* Peptides, 2011. **32**(5): p. 1060-7.
207. Moore, E.L., et al., *Mapping the CGRP receptor ligand binding domain: tryptophan-84 of RAMP1 is critical for agonist and antagonist binding.* Biochem Biophys Res Commun, 2010. **394**(1): p. 141-5.
208. Archbold, J.K., et al., *Structural insights into RAMP modification of secretin family G protein-coupled receptors: implications for drug development.* Trends Pharmacol Sci, 2011. **32**(10): p. 591-600.
209. Bomberger, J.M., et al., *Novel function for receptor activity-modifying proteins (RAMPs) in post-endocytic receptor trafficking.* J Biol Chem, 2005. **280**(10): p. 9297-307.
210. Bomberger, J.M., et al., *Receptor activity-modifying protein (RAMP) isoform-specific regulation of adrenomedullin receptor trafficking by NHERF-1.* J Biol Chem, 2005. **280**(25): p. 23926-35.
211. Morfis, M., et al., *Receptor activity-modifying proteins differentially modulate the G protein-coupling efficiency of amylin receptors.* Endocrinology, 2008. **149**(11): p. 5423-31.
212. Prado, M.A., et al., *The role of the CGRP-receptor component protein (RCP) in adrenomedullin receptor signal transduction.* Peptides, 2001. **22**(11): p. 1773-81.
213. Sexton, P.M., et al., *Receptor activity modifying proteins.* Cell Signal, 2001. **13**(2): p. 73-83.
214. Ono, Y., et al., *Decreased gene expression of adrenomedullin receptor in mouse lungs during sepsis.* Biochem Biophys Res Commun, 2000. **271**(1): p. 197-202.
215. Chakravarty, P., et al., *CGRP and adrenomedullin binding correlates with transcript levels for calcitonin receptor-like receptor (CRLR) and receptor activity modifying proteins (RAMPs) in rat tissues.* Br J Pharmacol, 2000. **130**(1): p. 189-95.
216. Tsujikawa, K., et al., *Hypertension and dysregulated proinflammatory cytokine production in receptor activity-modifying protein 1-deficient mice.* Proc Natl Acad Sci U S A, 2007. **104**(42): p. 16702-7.
217. Dackor, R., et al., *Receptor activity-modifying proteins 2 and 3 have distinct physiological functions from embryogenesis to old age.* J Biol Chem, 2007. **282**(25): p. 18094-9.
218. Dackor, R.T., et al., *Hydrops foetalis, cardiovascular defects, and embryonic lethality in mice lacking the calcitonin receptor-like receptor gene.* Mol Cell Biol, 2006. **26**(7): p. 2511-8.
219. Caron, K.M. and O. Smithies, *Extreme hydrops foetalis and cardiovascular abnormalities in mice lacking a functional Adrenomedullin gene.* Proc Natl Acad Sci U S A, 2001. **98**(2): p. 615-9.
220. Barick, C.J., et al., *Loss of receptor activity-modifying protein 3 exacerbates cardiac hypertrophy and transition to heart failure in a sex-dependent manner.* J Mol Cell Cardiol, 2011.
221. Kadmiel, M., et al., *Research resource: Haploinsufficiency of receptor activity-modifying protein-2 (RAMP2) causes reduced fertility, hyperprolactinemia, skeletal abnormalities, and endocrine dysfunction in mice.* Mol Endocrinol, 2011. **25**(7): p. 1244-53.

222. Piston, D.W. and G.J. Kremers, *Fluorescent protein FRET: the good, the bad and the ugly.* Trends Biochem Sci, 2007. **32**(9): p. 407-14.
223. van Rheenen, J., M. Langeslag, and K. Jalink, *Correcting confocal acquisition to optimize imaging of fluorescence resonance energy transfer by sensitized emission.* Biophys J, 2004. **86**(4): p. 2517-29.
224. Hoppe, A., K. Christensen, and J.A. Swanson, *Fluorescence resonance energy transfer-based stoichiometry in living cells.* Biophys J, 2002. **83**(6): p. 3652-64.
225. Mathis, G., *Rare earth cryptates and homogeneous fluoroimmunoassays with human sera.* Clin Chem, 1993. **39**(9): p. 1953-9.
226. Mathis, G., *Probing molecular interactions with homogeneous techniques based on rare earth cryptates and fluorescence energy transfer.* Clin Chem, 1995. **41**(9): p. 1391-7.
227. Angers, S., et al., *Detection of beta 2-adrenergic receptor dimerization in living cells using bioluminescence resonance energy transfer (BRET).* Proc Natl Acad Sci U S A, 2000. **97**(7): p. 3684-9.
228. Hynes, T.R., et al., *Visualization of G protein betagamma dimers using bimolecular fluorescence complementation demonstrates roles for both beta and gamma in subcellular targeting.* J Biol Chem, 2004. **279**(29): p. 30279-86.
229. Vidi, P.A., et al., *Ligand-dependent oligomerization of dopamine D(2) and adenosine A(2A) receptors in living neuronal cells.* Mol Pharmacol, 2008. **74**(3): p. 544-51.
230. Clayton, A.H., et al., *Dual-channel photobleaching FRET microscopy for improved resolution of protein association states in living cells.* Eur Biophys J, 2005. **34**(1): p. 82-90.
231. Hellwig, D., et al., *Acceptor-photobleaching FRET analysis of core kinetochore and NAC proteins in living human cells.* Eur Biophys J, 2009. **38**(6): p. 781-91.
232. Patterson, G.H., D.W. Piston, and B.G. Barisas, *Forster distances between green fluorescent protein pairs.* Anal Biochem, 2000. **284**(2): p. 438-40.
233. Stryer, L., *Fluorescence energy transfer as a spectroscopic ruler.* Annu Rev Biochem, 1978. **47**: p. 819-46.
234. Chen, H., et al., *Measurement of FRET efficiency and ratio of donor to acceptor concentration in living cells.* Biophys J, 2006. **91**(5): p. L39-41.
235. Miyawaki, A., et al., *Fluorescent indicators for Ca^{2+} based on green fluorescent proteins and calmodulin.* Nature, 1997. **388**(6645): p. 882-7.
236. Rizzo, M.A., et al., *An improved cyan fluorescent protein variant useful for FRET.* Nat Biotechnol, 2004. **22**(4): p. 445-9.
237. Heikal, A.A., et al., *Molecular spectroscopy and dynamics of intrinsically fluorescent proteins: coral red (dsRed) and yellow (Citrine).* Proc Natl Acad Sci U S A, 2000. **97**(22): p. 11996-2001.
238. Shaner, N.C., P.A. Steinbach, and R.Y. Tsien, *A guide to choosing fluorescent proteins.* Nat Methods, 2005. **2**(12): p. 905-9.
239. Hachet-Haas, M., et al., *FRET and colocalization analyzer--a method to validate measurements of sensitized emission FRET acquired by confocal microscopy and available as an ImageJ Plug-in.* Microsc Res Tech, 2006. **69**(12): p. 941-56.
240. Carriba, P., et al., *Detection of heteromerization of more than two proteins by sequential BRET-FRET.* Nat Methods, 2008. **5**(8): p. 727-33.
241. Malkani, N. and J.A. Schmid, *Some secrets of fluorescent proteins: distinct bleaching in various mounting fluids and photoactivation of cyan fluorescent proteins at YFP-excitation.* PLoS One, 2011. **6**(4): p. e18586.
242. Samama, P., et al., *A mutation-induced activated state of the beta 2-adrenergic receptor. Extending the ternary complex model.* J Biol Chem, 1993. **268**(7): p. 4625-36.

243. Gama, L., L.M. Baxendale-Cox, and G.E. Breitwieser, *Ca^{2+}-sensing receptors in intestinal epithelium.* Am J Physiol, 1997. **273**(4 Pt 1): p. C1168-75.
244. McNeil, L., et al., *Functional Ca^{2+}-sensing receptor expression in ovarian surface epithelial cells.* Am J Obstet Gynecol, 1998. **178**(2): p. 305-13.
245. Huang, C., M.E. Handlogten, and R.T. Miller, *Parallel activation of phosphatidylinositol 4-kinase and phospholipase C by the extracellular Ca^{2+}-sensing receptor.* J Biol Chem, 2002. **277**(23): p. 20293-300.
246. Handlogten, M.E., et al., *The Ca^{2+}-sensing receptor activates cytosolic phospholipase A2 via a Gqalpha -dependent ERK-independent pathway.* J Biol Chem, 2001. **276**(17): p. 13941-8.
247. Yano, S., et al., *Ca^{2+}-sensing receptor activation stimulates parathyroid hormone-related protein secretion in prostate cancer cells: role of epidermal growth factor receptor transactivation.* Bone, 2004. **35**(3): p. 664-72.
248. Cornish, J., et al., *Shared pathways of osteoblast mitogenesis induced by amylin, adrenomedullin, and IGF-1.* Biochem Biophys Res Commun, 2004. **318**(1): p. 240-6.
249. DeLapp, N.W., et al., *Determination of [35S]guanosine-5'-O-(3-thio)triphosphate binding mediated by cholinergic muscarinic receptors in membranes from Chinese hamster ovary cells and rat striatum using an anti-G protein scintillation proximity assay.* J Pharmacol Exp Ther, 1999. **289**(2): p. 946-55.
250. Mannoury la Cour, C., et al., *Dopamine D1 receptor coupling to Gs/olf and Gq in rat striatum and cortex: a scintillation proximity assay (SPA)/antibody-capture characterization of benzazepine agonists.* Neuropharmacology, 2007. **52**(3): p. 1003-14.
251. Cussac, D., et al., *Differential activation of Gq/11 and Gi(3) proteins at 5-hydroxytryptamine(2C) receptors revealed by antibody capture assays: influence of receptor reserve and relationship to agonist-directed trafficking.* Mol Pharmacol, 2002. **62**(3): p. 578-89.
252. Dupuis, D.S., et al., *Actions of novel agonists, antagonists and antipsychotic agents at recombinant rat 5-HT6 receptors: a comparative study of coupling to G alpha s.* Eur J Pharmacol, 2008. **588**(2-3): p. 170-7.
253. Mannoury La Cour, C., et al., *An immunocapture/scintillation proximity analysis of G alpha q/11 activation by native serotonin (5-HT)2A receptors in rat cortex: blockade by clozapine and mirtazapine.* Synapse, 2009. **63**(2): p. 95-105.
254. Cussac, D., V. Pasteau, and M.J. Millan, *Characterisation of Gs activation by dopamine D1 receptors using an antibody capture assay: antagonist properties of clozapine.* Eur J Pharmacol, 2004. **485**(1-3): p. 111-7.
255. Thomas, D., et al., *A comparison of fluorescent Ca^{2+} indicator properties and their use in measuring elementary and global Ca^{2+} signals.* Cell Ca^{2+}, 2000. **28**(4): p. 213-23.
256. Gee, K.R., et al., *Chemical and physiological characterization of fluo-4 Ca($^{2+}$)-indicator dyes.* Cell Ca^{2+}, 2000. **27**(2): p. 97-106.
257. Minta, A., J.P. Kao, and R.Y. Tsien, *Fluorescent indicators for cytosolic Ca^{2+} based on rhodamine and fluorescein chromophores.* J Biol Chem, 1989. **264**(14): p. 8171-8.
258. Grynkiewicz, G., M. Poenie, and R.Y. Tsien, *A new generation of Ca^{2+} indicators with greatly improved fluorescence properties.* J Biol Chem, 1985. **260**(6): p. 3440-50.
259. Paredes, R.M., et al., *Chemical Ca^{2+} indicators.* Methods, 2008. **46**(3): p. 143-51.
260. Porter, A.C., et al., *M1 muscarinic receptor signaling in mouse hippocampus and cortex.* Brain Res, 2002. **944**(1-2): p. 82-9.
261. Odagaki, Y. and R. Toyoshima, *Muscarinic acetylcholine receptor-mediated activation of G(q) in rat brain membranes determined by guanosine-5'-O-(3-[(35)S]thio)triphosphate ([(35)S]GTPgammaS) binding using an anti-G protein scintillation proximity assay.* J Neural Transm, 2011.

262. Tilakaratne, N., et al., *Amylin receptor phenotypes derived from human calcitonin receptor/RAMP coexpression exhibit pharmacological differences dependent on receptor isoform and host cell environment.* J Pharmacol Exp Ther, 2000. **294**(1): p. 61-72.
263. Rajagopal, S., et al., *Beta-arrestin- but not G protein-mediated signaling by the "decoy" receptor CXCR7.* Proc Natl Acad Sci U S A, 2010. **107**(2): p. 628-32.
264. Awumey, E.M., et al., *Ca($^{2+}$) mobilization through dorsal root ganglion Ca($^{2+}$)-sensing receptor stably expressed in HEK293 cells.* Am J Physiol Cell Physiol, 2007. **292**(5): p. C1895-905.
265. Yamauchi, M., et al., *Involvement of Ca^{2+}-sensing receptor in osteoblastic differentiation of mouse MC3T3-E1 cells.* Am J Physiol Endocrinol Metab, 2005. **288**(3): p. E608-16.
266. Tu, C.L., W. Chang, and D.D. Bikle, *The extracellular Ca^{2+}-sensing receptor is required for Ca^{2+}-induced differentiation in human keratinocytes.* J Biol Chem, 2001. **276**(44): p. 41079-85.
267. Ayoub, M.A., et al., *Monitoring of ligand-independent dimerization and ligand-induced conformational changes of melatonin receptors in living cells by bioluminescence resonance energy transfer.* J Biol Chem, 2002. **277**(24): p. 21522-8.
268. Issafras, H., et al., *Constitutive agonist-independent CCR5 oligomerization and antibody-mediated clustering occurring at physiological levels of receptors.* J Biol Chem, 2002. **277**(38): p. 34666-73.
269. Hay, D.L., et al., *Determinants of 1-piperidinecarboxamide, N-[2-[[5-amino-l-[[4-(4-pyridinyl)-l-piperazinyl]carbonyl]pentyl]amino]-1-[(3,5-d ibromo-4-hydroxyphenyl)methyl]-2-oxoethyl]-4-(1,4-dihydro-2-oxo-3(2H)-quinazoliny l) (BIBN4096BS) affinity for calcitonin gene-related peptide and amylin receptors--the role of receptor activity modifying protein 1.* Mol Pharmacol, 2006. **70**(6): p. 1984-91.
270. Takhshid, M.A., et al., *Characterization and effects on cAMP accumulation of adrenomedullin and calcitonin gene-related peptide (CGRP) receptors in dissociated rat spinal cord cell culture.* Br J Pharmacol, 2006. **148**(4): p. 459-68.
271. Lavreysen, H., et al., *[3H]R214127: a novel high-affinity radioligand for the mGlu1 receptor reveals a common binding site shared by multiple allosteric antagonists.* Mol Pharmacol, 2003. **63**(5): p. 1082-93.
272. He, Y., et al., *Involvement of Ca^{2+}-sensing receptor in inhibition of lipolysis through intracellular cAMP and Ca^{2+} pathways in human adipocytes.* Biochem Biophys Res Commun, 2011. **404**(1): p. 393-9.
273. Kwak, J.O., et al., *The extracellular Ca^{2+} sensing receptor is expressed in mouse mesangial cells and modulates cell proliferation.* Exp Mol Med, 2005. **37**(5): p. 457-65.
274. Xing, W., et al., *The functional expression of Ca^{2+}-sensing receptors in BRL cells and related signal transduction pathway responsible for intracellular Ca^{2+} elevation.* Mol Cell Biochem, 2010. **343**(1-2): p. 13-9.
275. Jung, S.Y., et al., *Ca^{2+} sensing receptor forms complex with and is up-regulated by caveolin-1 in cultured human osteosarcoma (Saos-2) cells.* Exp Mol Med, 2005. **37**(2): p. 91-100.
276. Tjernberg, A., et al., *DMSO-related effects in protein characterization.* J Biomol Screen, 2006. **11**(2): p. 131-7.
277. Lee, S.B., et al., *Antibody-based bio-nanotube membranes for enantiomeric drug separations.* Science, 2002. **296**(5576): p. 2198-200.
278. Koth, C.M., et al., *Molecular basis for negative regulation of the glucagon receptor.* Proc Natl Acad Sci U S A, 2012. **109**(36): p. 14393-8.
279. Davey, A.E., et al., *Positive and negative allosteric modulators promote biased signaling at the Ca^{2+}-sensing receptor.* Endocrinology, 2012. **153**(3): p. 1232-41.

280. Janicic, N., et al., *Mapping of the Ca^{2+}-sensing receptor gene (CASR) to human chromosome 3q13.3-21 by fluorescence in situ hybridization, and localization to rat chromosome 11 and mouse chromosome 16.* Mamm Genome, 1995. **6**(11): p. 798-801.
281. Pearce, S.H., et al., *Ca^{2+}-sensing receptor mutations in familial benign hypercalcemia and neonatal hyperparathyroidism.* J Clin Invest, 1995. **96**(6): p. 2683-92.
282. Mithal, A., et al., *The reduced responsiveness of cultured bovine parathyroid cells to extracellular Ca^{2+} is associated with marked reduction in the expression of extracellular $Ca(^{2+})$-sensing receptor messenger ribonucleic acid and protein.* Endocrinology, 1995. **136**(7): p. 3087-92.
283. Brown, A.J., et al., *Loss of Ca^{2+} responsiveness in cultured bovine parathyroid cells is associated with decreased Ca^{2+} receptor expression.* Biochem Biophys Res Commun, 1995. **212**(3): p. 861-7.
284. Ritter, C.S., et al., *Parathyroid cells cultured in collagen matrix retain Ca^{2+} responsiveness: importance of three-dimensional tissue architecture.* J Bone Miner Res, 2004. **19**(3): p. 491-8.
285. Carrillo-Lopez, N., et al., *Simultaneous changes in the Ca^{2+}-sensing receptor and the vitamin D receptor under the influence of Ca^{2+} and calcitriol.* Nephrol Dial Transplant, 2008. **23**(11): p. 3479-84.
286. Brown, A.J., et al., *Rat Ca^{2+}-sensing receptor is regulated by vitamin D but not by Ca^{2+}.* Am J Physiol, 1996. **270**(3 Pt 2): p. F454-60.
287. Rogers, K.V., et al., *Ca^{2+} receptor messenger ribonucleic acid levels in the parathyroid glands and kidney of vitamin D-deficient rats are not regulated by plasma Ca^{2+} or 1,25-dihydroxyvitamin D3.* Endocrinology, 1995. **136**(2): p. 499-504.
288. Canaff, L. and G.N. Hendy, *Human Ca^{2+}-sensing receptor gene. Vitamin D response elements in promoters P1 and P2 confer transcriptional responsiveness to 1,25-dihydroxyvitamin D.* J Biol Chem, 2002. **277**(33): p. 30337-50.
289. Canadillas, S., et al., *Ca^{2+}-sensing receptor expression and parathyroid hormone secretion in hyperplastic parathyroid glands from humans.* J Am Soc Nephrol, 2005. **16**(7): p. 2190-7.
290. Mathias, R.S., et al., *Reduced expression of the renal Ca^{2+}-sensing receptor in rats with experimental chronic renal insufficiency.* J Am Soc Nephrol, 1998. **9**(11): p. 2067-74.
291. Mizobuchi, M., et al., *Calcimimetic compound upregulates decreased Ca^{2+}-sensing receptor expression level in parathyroid glands of rats with chronic renal insufficiency.* J Am Soc Nephrol, 2004. **15**(10): p. 2579-87.
292. Chattopadhyay, N., et al., *Ontogeny of the extracellular Ca^{2+}-sensing receptor in rat kidney.* Am J Physiol, 1996. **271**(3 Pt 2): p. F736-43.
293. Chattopadhyay, N., et al., *Ca^{2+}-sensing receptor in the rat hippocampus: a developmental study.* Brain Res Dev Brain Res, 1997. **100**(1): p. 13-21.
294. Canaff, L. and G.N. Hendy, *Ca^{2+}-sensing receptor gene transcription is up-regulated by the proinflammatory cytokine, interleukin-1beta. Role of the NF-kappaB PATHWAY and kappaB elements.* J Biol Chem, 2005. **280**(14): p. 14177-88.
295. Nielsen, P.K., et al., *Inhibition of PTH secretion by interleukin-1 beta in bovine parathyroid glands in vitro is associated with an up-regulation of the Ca^{2+}-sensing receptor mRNA.* Biochem Biophys Res Commun, 1997. **238**(3): p. 880-5.
296. Derst, C., et al., *Genomic structure and chromosome mapping of human and mouse RAMP genes.* Cytogenet Cell Genet, 2000. **90**(1-2): p. 115-8.
297. Cueille, C., et al., *Increased myocardial expression of RAMP1 and RAMP3 in rats with chronic heart failure.* Biochem Biophys Res Commun, 2002. **294**(2): p. 340-6.
298. Tadokoro, K., et al., *Altered gene expression of adrenomedullin and its receptor system and molecular forms of tissue adrenomedullin in left ventricular hypertrophy induced by malignant hypertension.* Regul Pept, 2003. **112**(1-3): p. 71-8.

299. Pan Ch, S., et al., *Potentiated response to adrenomedullin in myocardia and aortas in spontaneously hypertensive rat.* Basic Res Cardiol, 2006. **101**(3): p. 193-203.
300. Cao, Y.N., et al., *Chronic salt loading upregulates expression of adrenomedullin and its receptors in adrenal glands and kidneys of the rat.* Hypertension, 2003. **42**(3): p. 369-72.
301. Nishikimi, T., et al., *Role of increased circulating and renal adrenomedullin in rats with malignant hypertension.* Am J Physiol Regul Integr Comp Physiol, 2001. **281**(6): p. R2079-87.
302. Qing, X., J. Svaren, and I.M. Keith, *mRNA expression of novel CGRP1 receptors and their activity-modifying proteins in hypoxic rat lung.* Am J Physiol Lung Cell Mol Physiol, 2001. **280**(3): p. L547-54.
303. Dong, Y.L., et al., *Expression of calcitonin gene-related peptide receptor components, calcitonin receptor-like receptor and receptor activity modifying protein 1, in the rat placenta during pregnancy and their cellular localization.* Mol Hum Reprod, 2003. **9**(8): p. 481-90.
304. Thota, C., et al., *Changes in the expression of calcitonin receptor-like receptor, receptor activity-modifying protein (RAMP) 1, RAMP2, and RAMP3 in rat uterus during pregnancy, labor, and by steroid hormone treatments.* Biol Reprod, 2003. **69**(4): p. 1432-7.
305. Watanabe, H., et al., *The estrogen-responsive adrenomedullin and receptor-modifying protein 3 gene identified by DNA microarray analysis are directly regulated by estrogen receptor.* J Mol Endocrinol, 2006. **36**(1): p. 81-9.
306. Uzan, B., M.C. de Vernejoul, and M. Cressent, *RAMPs and CRLR expressions in osteoblastic cells after dexamethasone treatment.* Biochem Biophys Res Commun, 2004. **321**(4): p. 802-8.
307. Cornish, J., et al., *Adrenomedullin is a potent stimulator of osteoblastic activity in vitro and in vivo.* Am J Physiol, 1997. **273**(6 Pt 1): p. E1113-20.
308. Livak, K.J. and T.D. Schmittgen, *Analysis of relative gene expression data using real-time quantitative PCR and the 2(-Delta Delta C(T)) Method.* Methods, 2001. **25**(4): p. 402-8.
309. Bilbe, G., et al., *PCR phenotyping of cytokines, growth factors and their receptors and bone matrix proteins in human osteoblast-like cell lines.* Bone, 1996. **19**(5): p. 437-45.
310. Mulkins, M.A., et al., *1,25-Dihydroxyvitamin D3 increases bone alkaline phosphatase isoenzyme levels in human osteogenic sarcoma cells.* J Biol Chem, 1983. **258**(10): p. 6219-25.
311. Lazaretti-Castro, M., et al., *1,25-Dihydroxyvitamin D3 stimulates growth and inhibits calcitonin secretion in a human C cell carcinoma cell line.* Braz J Med Biol Res, 1995. **28**(9): p. 1013-8.
312. Silver, I.A., R.J. Murrills, and D.J. Etherington, *Microelectrode studies on the acid microenvironment beneath adherent macrophages and osteoclasts.* Exp Cell Res, 1988. **175**(2): p. 266-76.
313. Yamaguchi, T., et al., *Expression of extracellular Ca^{2+}-sensing receptor in human osteoblastic MG-63 cell line.* Am J Physiol Cell Physiol, 2001. **280**(2): p. C382-93.
314. Yamaguchi, T., et al., *Expression of extracellular Ca^{2+} (Ca2 + o)-sensing receptor in the clonal osteoblast-like cell lines, UMR-106 and SAOS-2.* Biochem Biophys Res Commun, 1998. **243**(3): p. 753-7.
315. Chang, W., et al., *Expression and signal transduction of Ca^{2+}-sensing receptors in cartilage and bone.* Endocrinology, 1999. **140**(12): p. 5883-93.
316. Pi, M., T.K. Hinson, and L. Quarles, *Failure to detect the extracellular Ca^{2+}-sensing receptor (CasR) in human osteoblast cell lines.* J Bone Miner Res, 1999. **14**(8): p. 1310-9.
317. Quarles, L.D., et al., *A distinct cation-sensing mechanism in MC3T3-E1 osteoblasts functionally related to the Ca^{2+} receptor.* J Bone Miner Res, 1997. **12**(3): p. 393-402.
318. Pi, M., et al., *Sensing of extracellular cations in CasR-deficient osteoblasts. Evidence for a novel cation-sensing mechanism.* J Biol Chem, 2000. **275**(5): p. 3256-63.
319. Pautke, C., et al., *Characterization of osteosarcoma cell lines MG-63, Saos-2 and U-2 OS in comparison to human osteoblasts.* Anticancer Res, 2004. **24**(6): p. 3743-8.

320. Orriss, I.R., et al., *Osteoblast responses to nucleotides increase during differentiation.* Bone, 2006. **39**(2): p. 300-9.
321. Orriss, I.R., et al., *Inhibition of osteoblast function in vitro by aminobisphosphonates.* J Cell Biochem, 2009. **106**(1): p. 109-18.
322. Phelps, E., et al., *Parathyroid hormone induces receptor activity modifying protein-3 (RAMP3) expression primarily via 3',5'-cyclic adenosine monophosphate signaling in osteoblasts.* Calcif Tissue Int, 2005. **77**(2): p. 96-103.
323. Kawase, T., K. Okuda, and D.M. Burns, *Immature human osteoblastic MG63 cells predominantly express a subtype 1-like CGRP receptor that inactivates extracellular signal response kinase by a cAMP-dependent mechanism.* Eur J Pharmacol, 2003. **470**(3): p. 125-37.
324. Frendo, J.L., et al., *Calcitonin receptor mRNA expression in TT cells: effect of dexamethasone.* Mol Cell Endocrinol, 1998. **139**(1-2): p. 37-43.
325. Pidasheva, S., et al., *Ca^{2+}-sensing receptor dimerizes in the endoplasmic reticulum: biochemical and biophysical characterization of CASR mutants retained intracellularly.* Hum Mol Genet, 2006. **15**(14): p. 2200-9.
326. Galperin, E., V.V. Verkhusha, and A. Sorkin, *Three-chromophore FRET microscopy to analyze multiprotein interactions in living cells.* Nat Methods, 2004. **1**(3): p. 209-17.
327. Canals, M., J.F. Lopez-Gimenez, and G. Milligan, *Cell surface delivery and structural re-organization by pharmacological chaperones of an oligomerization-defective alpha(1b)-adrenoceptor mutant demonstrates membrane targeting of GPCR oligomers.* Biochem J, 2009. **417**(1): p. 161-72.
328. Heroux, M., et al., *Functional calcitonin gene-related peptide receptors are formed by the asymmetric assembly of a calcitonin receptor-like receptor homo-oligomer and a monomer of receptor activity-modifying protein-1.* J Biol Chem, 2007. **282**(43): p. 31610-20.
329. Jordan, B.A., et al., *Oligomerization of opioid receptors with beta 2-adrenergic receptors: a role in trafficking and mitogen-activated protein kinase activation.* Proc Natl Acad Sci U S A, 2001. **98**(1): p. 343-8.
330. Lee, S.P., et al., *Dopamine D1 and D2 receptor Co-activation generates a novel phospholipase C-mediated Ca^{2+} signal.* J Biol Chem, 2004. **279**(34): p. 35671-8.
331. Fribourg, M., et al., *Decoding the signaling of a GPCR heteromeric complex reveals a unifying mechanism of action of antipsychotic drugs.* Cell, 2011. **147**(5): p. 1011-23.
332. Thomsen, A.R., M. Hvidtfeldt, and H. Brauner-Osborne, *Biased agonism of the Ca^{2+}-sensing receptor.* Cell Ca^{2+}, 2011.
333. Olesen, J., et al., *Calcitonin gene-related peptide receptor antagonist BIBN 4096 BS for the acute treatment of migraine.* N Engl J Med, 2004. **350**(11): p. 1104-10.
334. Leung, G., et al., *Cellular Dielectric Spectroscopy: A Label-Free Technology for Drug Discovery.* Journal of the Association for Laboratory Automation, 2005. **10**(4): p. 258-269.
335. Hipolito, U.V., et al., *Chronic ethanol consumption reduces adrenomedullin-induced relaxation in the isolated rat aorta.* Alcohol, 2011. **45**(8): p. 805-14.
336. Zhao, Y., et al., *Differential expression of components of the cardiomyocyte adrenomedullin/intermedin receptor system following blood pressure reduction in nitric oxide-deficient hypertension.* J Pharmacol Exp Ther, 2006. **316**(3): p. 1269-81.
337. Kaafarani, I., et al., *Targeting adrenomedullin receptors with systemic delivery of neutralizing antibodies inhibits tumor angiogenesis and suppresses growth of human tumor xenografts in mice.* FASEB J, 2009. **23**(10): p. 3424-35.
338. Fernandez-Sauze, S., et al., *Effects of adrenomedullin on endothelial cells in the multistep process of angiogenesis: involvement of CRLR/RAMP2 and CRLR/RAMP3 receptors.* Int J Cancer, 2004. **108**(6): p. 797-804.